DISSERTATION

THE ADVENTURES OF *LACTOBACILLUS ACIDOPHILUS*: EVALUATING A RECOMBINANT PROBIOTIC ROTAVIRUS VACCINE FROM HOST AND MICROBIAL PERSPECTIVES

Submitted by

Darby L. Gilfillan

Department of Microbiology, Immunology, and Pathology

In partial fulfillment of the requirements

For the Degree of Doctor of Philosophy

Colorado State University

Fort Collins, Colorado

Summer 2024

Doctoral Committee:

Advisor: Allison Vilander
Co-Advisor: Gregg Dean

Zaid Abdo
Mike Wilkins

ABSTRACT

THE ADVENTURES OF *LACTOBACILLUS ACIDOPHILUS*: EVALUATING A RECOMBINANT PROBIOTIC ROTAVIRUS VACCINE FROM HOST AND MICROBIAL PERSPECTIVES

Rotavirus is an enteric infection of global importance causing diarrheal-associated illness that can be fatal in young children and the elderly. There is a gap in vaccine efficacy between high- and lower-middle-income countries (LMIC) with LMIC often experiencing diminished vaccine-conferred protection. Rotaviruses, whether attenuated vaccine strains or primary pathogens, do not exist in isolation within the host's gastrointestinal tract. Other actors present within the microbiome can inhibit or augment vaccine efficacy by influencing the vaccine itself or the mucosal immune response. Understanding and exploiting interactions between host and microbe is a promising frontier for mucosal vaccinology. This dissertation will explore the probiotic *Lactobacillus acidophilus* (LA) as a vaccine platform for a microbiome-minded, next-generation approach to rotavirus immunization. We developed and confirmed a novel recombinant LA (rLA) vaccine expressing rotavirus antigens of the VP8* domain from the rotavirus EDIM VP4 capsid protein along with the adjuvants FimH and FliC. Rotavirus naïve adult BALB/cJ mice were orally immunized followed by murine rotavirus strain EC_{WT} viral challenge. Antirotavirus serum IgG and antigen-specific antibody-secreting cell responses were detected in rLA-vaccinated mice. A day after the oral rotavirus challenge, fecal antigen shedding was significantly decreased in the rLA group. These results demonstrate the potential of rLA platforms to generate protective mucosal immunity. Additionally, metagenomic and metatranscriptomic analyses of exogenous probiotic administration within the murine small intestine revealed differences between LA genome expression and the whole metatranscriptome in recombinant- versus wild-type LA-vaccinated mice. LA genome expression in rLA-vaccinated mice had decreased carbohydrate metabolism and increased stress responses. We also detected antigen and adjuvant transcript expression only in mice exposed to the rLA platform. There was relative enrichment of probiotic

species in the wild-type group with overall increased α- and β-diversity in the buffer compared to probiotic groups. These results highlight the interactions between an exogenous probiotic and the host microbiome at an immune inductive site. Finally, we used an in vitro model to evaluate modulation of polyunsaturated fatty acid (PUFA) metabolism on host cell and (r)LA interactions. Both (r)LA and PUFA treatments significantly changed pathogen recognition receptor expression. (r)LA treatment mainly altered inflammatory cytokine expression while PUFA supplementation primarily influenced mucin expression. rLA strains adhered more to host cells than wild-type LA while the rLA strain expressing both antigens and adjuvants may better prevent *E. coli* adhesion. These results and methodologies provide a starting point for further investigation into PUFA metabolism as a mechanism for improving rLA immunogenicity and competition against other enteric pathogens.

ACKNOWLEDGEMENTS

First and foremost, I want to thank Dr. Allison Vilander and Dr. Gregg Dean for their incredible mentorship and support. To Allison, your work ethic is inspiring. I appreciate and admire how you approach research and your ability to truly listen. Still think you cheated during that one Villainous game, but I am willing to forgive and forget (maybe). To Gregg, thank you for supporting all your students in whatever they choose to do. You set the example for getting the maximum out of yourself and life, such as having the bravery to run 400m repeats on a dirt track. A big thank you to my committee members Dr. Zaid Abdo and Dr. Mike Wilkins for their time and advice during committee meetings. Specifically, thank you to Dr. Abdo for the exceptional research opportunities and for his mentorship when I was unable to find Terminal as an undergraduate student. I appreciate the entire Abdo lab, specifically Dr. Reed Woyda and Dr. Steven Lakin who both helped me navigate bioinformatics, and to Dr. Matt Hopken for his positivity and collaboration. Finally, thank you to Dr. Gregory Florant for giving me the chance and support when I first dipped my toes into research.

A wholehearted thank you to our collaborators who made the following research possible. I acknowledge the work and contributions of Dr. Meichen Pan, Dr. Yong Jun Goh, Dr. Sarah O' Flaherty, and Dr. Rodolphe Barrangou at North Carolina State University, Dr. Ningguo Feng and Dr. Harry Greenberg at Stanford University, and Dr. Nurul Islam, Dr. John Belisle, and Barb Graham at Colorado State University.

I appreciate all the people I have met at Colorado State. Thank you to the Vilander-Dean lab, where I was fortunate to be surrounded by incredible individuals and scientists, including Alora LaVoy, Callie Lang, Dr. Ben Curtis, Kayl Ecton, Kenzie Fletcher, Christian Cherry, Janahan Loganathan, and Sophie and Paris Kiehl. Thank you to past lab members, including Dr. Bridget Fox, Kim Shelton, and Dr. Ben Swartzwelter. Bridget taught me everything I know and in whom I am fortunate to have a life-long friend. A shout-out to Callie and Kim for the lunch and coffee runs, and to Alora for supplying the best caramel.

Thank you to Dr. Joe Westrich during my graduate school rotations for his unforgettable kindness when my family was going through a challenging time. I greatly appreciate the support Dr. Andrew West provided from year one of this journey.

I am thankful for the best cohort you could ask for, especially Fitz, G-Ma Karbs Katherine, Jules, and Kayl for being a constant source of encouragement. I am lucky to have friends like Laura, Hope, Mary, and Raegan with whom I can always confide in, rely on, and laugh with. I want to acknowledge my aunt Sue, who shares her passion for science, and uncle Char who came to every race I had in New Mexico during my undergraduate degree and who continues to cheer me on. Thank you to my cousin Ginger who is inspiring in her creativity and to my uncle Dickie, aunt Lola, and aunt Cheryl for the weekend brunches that are unrivaled.

Finally, thank you…

…to my dad Tom, who always runs the extra mile while reminding us that "time is now."

…to my mom Lynn, who inspires by example in her truly selfless caring for others.

…to my brother Tommy, who easily makes others laugh and forges his own path.

…to my sister Laney, who is never afraid to give her all or be true to herself.

…to my partner Max, who finds and shares joy in the little things, like winning pick-up basketball games.

…to the family dogs Bue & Sherman, who are always excited for runs, snuggles, and fetch.

TABLE OF CONTENTS

LIST OF TABLES

LIST OF FIGURES

CHAPTER 1: LITERATURE REVIEW

1.1. Introduction

There is abundant interest in how the microbiome influences vaccination as a Google Scholar search of these two keywords generates over 150,000 results. Bacteria, viruses, fungi, helminths, protozoa and archaea all contribute to the host intestinal microbiome (1). The interaction between these diverse components of the microbiome in response to enteric infection is termed "transkingdom control" (2). Next-generation sequencing has revealed novel interactions between host and microbe during both infection and vaccination (3). Microbes can both worsen and ameliorate intestinal disease. For instance, resident bacteria can augment enteric infection while translocation of specific bacteria can contribute to inflammatory diseases of the gut (4, 5). Conversely, supplementing with probiotic species has been shown in some instances to improve vaccine responses (6). The following mini review will try answering the question "can host microbiome diversity inform next-generation rotavirus vaccine development?". In doing so, it will discuss how the intestinal bacteriome and virome are currently known to influence rotavirus infection and vaccination, describe the limitations to this current understanding, and suggest potential future approaches for the microbiome-minded development of rotavirus vaccines. Understanding the microbiome's impact on immune responses may improve vaccine efficacy and human health.

1.1.1. Background on Rotavirus Vaccination

Rotavirus is a double-stranded RNA enteric virus transmitted via the fecal-oral route that replicates within mature enterocytes and enteroendocrine cells in the small intestine. Infection primarily causes acute gastroenteritis characterized by diarrhea and vomiting which can ultimately lead to dehydration and death (7). Rotavirus generally infects children under five years of age and the elderly over 70 (8). There are currently four World Health Organization prequalified oral, live-attenuated rotavirus vaccines (Rotarix®, RotaTeq®, Rotavac®, and Rotasiil®) and it is recommended to include rotavirus in national immunization programs (9). By 2022, over a hundred and twenty countries had done so, thus reducing the burden of

disease globally (8, 10). However, current rotavirus vaccines are less efficacious in lower-middle-income countries (LMIC) as compared to high-income countries (11, 12). Vaccination only prevents 35-58% of severe rotavirus cases in countries experiencing high childhood mortality but over 90% in low mortality areas in the first two years of life (12, 13). Reasons for this discrepancy are multifactorial with commonly attributable causes including interference by maternally derived antibodies, environmental enteric dysfunction, and the impact of intestinal microbiome on host immunity (14). The microbiome impacts host vaccine-induced immunity and protection from enteric infection, including rotavirus, through local and systemic mechanisms as reviewed by de Jong et al. (2020) (15). Briefly, these include direct interaction between microbe and host at sites where microbiomes are present (skin and respiratory, reproductive, and gastrointestinal tracts) or immune cell sensing of microbial by-products and signaling cascades originating from the microbiome (15, 16).

1.1.2. Bacteriome-Immune System Regulation

Stacking up to human cells at a ratio of 1:1, gut bacteria can influence enteric viral infection in myriad ways including stabilizing virions, preventing viral attachment, and attenuating the host's immune responses (5, 17, 18). For example, Toll-like receptor (TLR) 5 tolerance of the commensal bacteriome microbe-associated molecular pattern (MAMP) flagellin is mediated through microbial expression of "silent" flagellins. These weak TLR5 activators are more prominent among non-urbanized groups (19, 20). Inactivated influenza and polio vaccines that are considered non-adjuvanted may receive an adjuvant-like benefit from similar sensing of flagellin by TLR5 (21, 22). Additionally, norovirus infection of human B-cells is augmented by intestinal bacteria that express HBGA types, such as Enterobacter cloacae (23). Bile acid metabolites produced by bacteria like *Clostridium scindens* initiate INF-λ production to inhibit norovirus replication (6, 24). The intimate relationship between microbiome and the host immune system undeniably impacts infection and vaccination outcomes.

1.1.3. Influence of Bacteriome Diversity on Rotavirus Immunity

There is variability in correlates of successful vaccination (e.g. seroconversion and vaccine shedding) and the bacteriome partly due to inherent intra- and inter-population microbial diversity (25). Infants from Navrongo, Ghana that successfully seroconverted after oral rotavirus vaccination (anti-rotavirus IgA titers ≥20 IU/mL) had a greater enterobacteria than Bacteroidetes abundance. As hypothesized by the authors, the more immunogenic lipopolysaccharide (LPS) expressed by enterobacteria possibly contributed to this successful seroconversion (26). However, Kim et al. (2022) found no difference in the bacterial diversity between responders and non-responders in the same region of Ghana (27). The bacteriome of Ghanian vaccine responders has been reported to significantly resemble that of infants from the Netherlands, a high-income country with low rotavirus disease burden where children are assumed to be rotavirus vaccine responders (26). In a separate study, there was a collective difference found between the bacteriome of a Pakistani cohort (including responders and non-responders) and Dutch infants (28). Notably, the abundance of gram-negative bacteria, which contain LPS in their outer membrane (29), correlated with improved vaccine responses in the Pakistani cohort. (28). There were no differences identified between the bacteriome of responders and non-responders in Zimbabwean or Indian children; however, the presence of additional enteropathogens, particularly bacterial, in the Indian cohort was positively associated with seroconversion (30, 31). In certain populations, a less diverse bacteriome is associated with better vaccine responses, including India, Malawi, and Qatar (32, 33). Even gnotobiotic pigs that received a “healthy” human fecal microbiota transplant (FMT), derived from a Nicaraguan infant that successfully seroconverted after rotavirus vaccination with a microbiome having a high α-diversity, exhibited decreased α-diversity after vaccination and rotavirus challenge. These pigs also generated stronger anti-rotavirus T-cell responses, and greater protection from viral shedding upon challenge compared to pigs with an “unhealthy” (no seroconversion and low α-diversity) human FMT (34). This review is inherently limited as the studies described here used Rotarix® and evaluated vaccine response by seroconversion primarily. A concrete correlative between bacteriome composition and rotavirus vaccine-induced immunity remains undetermined.

1.1.4. Species-Specific Impact on Rotavirus Immunity

There are limited bacterial species identified that alter host immune response to rotavirus vaccination and infection. C57BL/6 Rag1-KO mice (lack B- and T-cells and become persistently rotavirus infected) naturally harboring *Candidatus arthromitus* are unsusceptible to rotavirus infection. This protection, at least partially, is conferrable through FMT to immunocompetent and other immunocompromised C57BL/6 hosts (35). Conversely, *Akkermansia muciniphila* does not appear to similarly ameliorate rotavirus infection and has been associated with rotavirus susceptibility and non-seroconversion in mice and humans (35-38). The anti-inflammatory microbe *Faecalibacterium prausnitzii* induces specific DP8α, double-positive CD4CD8αα (39), Treg cells in individuals with a secretor phenotype (functional *FUT2* gene regulating mucus histo-blood group antigen expression) and existing anti-rotavirus IgA or neutralizing antibodies (40). This microbe could alter vaccine responses in secretor phenotype hosts with pre-existing rotavirus immunity. Secretor status itself can also mediate protection against rotavirus and other enteric infections (41, 42). Certain bacteria associate significantly with seroconversion status over the course of the immunization schedule. Taxa within the Enterobacteriaceae family were correlated with seroconversion at the initial rotavirus vaccine dose, *Streptococcus* and *Lactobacillus fermentum* at the middle dose, and the Enterobacteriaceae family plus *Rothia mucilaginosa* for the final dose in a Ghanian cohort (27). In Qatar, the phyla Verrucomicrobia and Bacteroidetes were dominant in children receiving two doses over one dose (43). More longitudinal studies are needed to help unravel the relationship between immune response during vaccination and taxonomic composition of the bacteriome (20). Few bacterial species that directly influence vaccine performance have been identified and further functional characterization of the bacteriome is needed (44).

1.1.5. Applying Antibiotics to Understand the Bacteriome

Antibiotics, though an unrealistic approach to improving vaccine responses at a global scale, are an effective method for isolating how the bacteriome alters rotavirus vaccine response. Narrow spectrum

antibiotics can induce anti-rotavirus IgA boosting in adults seven days after rotavirus vaccination, coupled with increased antigen shedding (45). This antibiotic exposure induced an abundance of the Proteobacteria phyla – which have "pathogenic potential" – prior to vaccination, and the Enterobacteriaceae and Prevotellaceae families were associated with increased rotavirus vaccine shedding at days zero and seven, respectively (45). Another multi-center study of antibiotic exposure and vaccine response from countries representing South America, Africa, the Middle East, and Asia showed minimal seropositivity across the entire cohort (30%); however, 40% more infants exposed to antibiotics by seven days after the final rotavirus dose were seropositive compared to not exposed (46). There was no similar significant impact of antibiotics on serological responses in infants from the United States in a separate study, but the relatively high seroconversion rate within this population could mask any potential influence of antibiotic administration (47, 48). Length of bacteriome disruption is immunologically relevant as longer antibiotic treatment prior to vaccination can improve rotavirus-specific antibody titers and antibody-secreting cell numbers than a shorter antibiotic course in C57BL/6 mice (49). In a different study, mice of the same strain continuously exposed to antibiotics had comparable immune responses as mice never exposed when immunized with five common infant vaccines excluding rotavirus (e.g. BCG and PCV13) (21). However, early-life antibiotic treatment (which alters bacteriome development) reduced antigen-specific IgG, but improved recall of T-cell cytokines, compared to non-antibiotic exposed murine pups (21). The authors hypothesized a dysbiotic microbiome develops following antibiotic completion in early-life, including less Bacteriodetes and eventual overabundance of *Akkermansia*, as an FMT from control mice rescued antigen-specific antibody responses in antibiotic-exposed mice (21). Antibiotics offer a mechanism to measure how the immune system responds when changing the bacteriome's composition in a relatively targeted way. This approach can help elucidate which communities and potential species are directly correlative to vaccine immune outcomes.

1.1.6. The Promise of Probiotics

Probiotics are exogenously consumed live microbes that provide some benefit to the host (50). Species including *Lactobacillus* and *Bifidobacterium* can interact with and activate the host immune system via their MAMPs, assist mucosal barrier function, and can outcompete deleterious microbes (51, 52). Lactic acid bacteria (LAB) specifically can endogenously secrete antimicrobial compounds (53). Supplementation with probiotics can reduce the severity of live rotavirus infection (54); however, such benefits were not seen in Canadian or American cohorts, countries that traditionally experience less rotavirus disease burden (55). LAB including *Lactobacillus* species have a promising track record for improving rotavirus vaccine-induced immune responses by acting as an adjuvant for the currently available live-attenuated vaccines (56-58). Relatedly, next-generation *Lactobacillus*-based platforms are under investigation as alternative rotavirus vaccines (59, 60). Probiotics including LAB can adhere to the small intestine and directly interact with microfold cells to be taken up into Peyer's patches and the gut associated lymphoid tissue for antigen exposure and mucosal immune activation (53, 61). There is a demand for developing such next-generation vaccines that can reach mucosal surfaces to generate protective mucosal immune responses at the site where rotavirus infection occurs (62, 63). Parentally delivered vaccines often generate a lackluster mucosal immunity and live-attenuated virus vaccines specifically are at risk for reversion to virulence and recombination with wild viral strains (64-66). Probiotic-based rotavirus vaccines could avoid these and other common issues with live-attenuated vaccines, including the need for cold-chain storage and requirement of trained personnel for administration – which can be costly or unavailable in LMIC (7, 67). Next-generation mucosal vaccine strategies are reviewed elsewhere (68).

1.1.7. Background on the Virome

The virome is underexplored compared to the bacteriome but similarly contributes to host immunity and response to enteric infections (69, 70). The human virome contains RNA and DNA eukaryotic viruses and bacteriophages. Said bacteriophages are collectively referred to as the phageome which is staggeringly diverse and constitutes a majority of the virome (71). Eukaryotic viral diversity increases with age while

the inverse is observed with phage diversity, which is highest early in life (71, 72). Some eukaryotic viruses (including *Anelloviridae*, *Adenoviridae*, *Caliciviridae* and *Picornaviridae*) and phages from the *Caudovirales* order are commonly identified within the first few months of infancy seemingly across populations (72-74). Breastfeeding can impact the infant virome, as *Lactobacillus* and *Bifidobacterium* species are more abundant in breastfed than formula-fed infants which corresponds to an increase in phages specific for the respective bacterium. African cohorts have demonstrated a higher abundance of viruses capable of infecting human cells (69, 75). TLR3 and 7 recognition of the resident virome alleviates intestinal inflammation by inducing anti-inflammatory cytokine production (76). Anti-inflammatory responses were also generated by simply introducing inactivated rotavirus to the virome. Like the bacteriome, the enteric virome interacts with the host immune system and influences response to vaccination.

1.1.8. Rotavirus Immunity and the Virome

Diversity of the viromes' composition can impact rotavirus vaccine efficacy. Rotavirus tends to co-exist, and co-infect, with other viruses including adenovirus and norovirus (77). Kim et al. determined phage abundance changes per dose of vaccination and at the initial dose, with phage diversity inversely correlated with seroconversion in Ghanian infants. Seven viral families were present consistently before and during dosing, including *Picornaviridae*, *Parvoviridae*, *Reoviridae*, *Astroviridae*, *Anelloviridae*, *Adenoviridae* and *Caliciviridae* (27). Only *Reovridiae* and *Astroviridae* increased in abundance over the immunization schedule, and increased rotavirus vaccine *Reoviridae* reads detected at dose one was positively associated with improved anti-rotavirus IgA titers. *Enterovirus B* and *Cosavirus A* abundance at dose one was associated with non-seroconversion, and this abundance of "competing" enteroviruses apart from poliovirus may inhibit rotavirus seroconversion (27). Similarly, the β-diversity of viromes between healthy and diarrheal infants with rotavirus in regions across China were significantly different (78). Even in Australia where the rotavirus vaccine performs well, enteric viruses detected before vaccination were associated with decreased vaccine shedding (79). Finally, the murine astrovirus strain STL5 present in the virome of an immunodeficient mouse model (*Rag2*$^{-/-}$ *Il2rg*$^{-/-}$) prevented infection from both murine

norovirus and rotavirus by increasing INF-λ expression. This INF over-expression was isolated in the gut (colon and small intestine) and this protective member of the virome was transferrable via FMT to other immunodeficient mice (*Rag1*$^{-/-}$) (80). Further sequencing of the virome and detecting novel virus and phage sequences is necessary for improving the comprehensiveness of current databases and our understanding of how the virome adapts during rotavirus vaccination and infection. Figure 1.1 summarizes the described microbiome-immune system interactions.

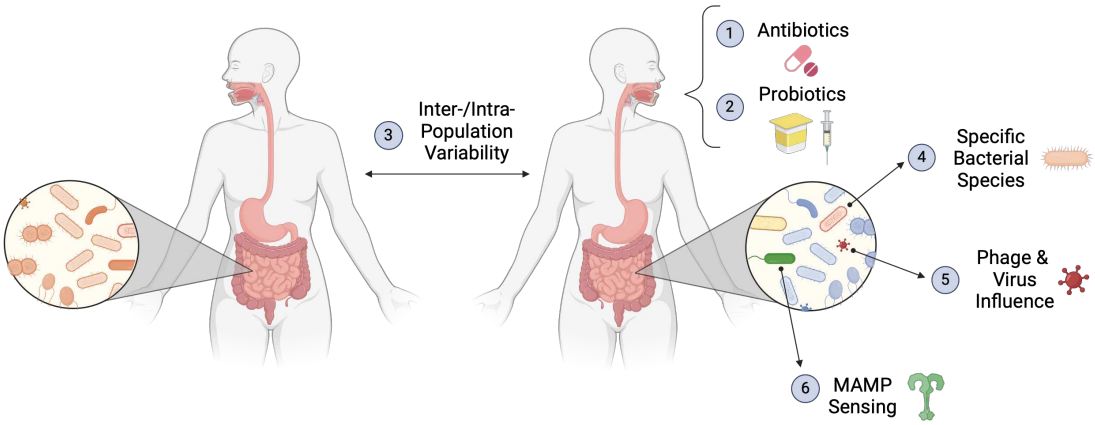

Figure 1.1. Variables that contribute to the holistic microbiome's impact on rotavirus vaccine performance across populations. (1) Antibiotic treatment attenuates (either improves or suppresses) immune responses to rotavirus among other vaccines traditionally administered in childhood (21, 49). (**2**) Probiotics including lactic acid bacteria offer an aduvant strategy to current rotavirus vaccines and are promising orally-delivered novel vaccine platforms. (**3**) There is a high level of bacteriome diversity within and between populations which often lacks consistent correlation to rotavirus vaccine outcomes. (**4-6**) There are specific mechanisms by which the micobiome – both bacterial and viral – can impact vaccine-induced immunity. These include (**4**) modulation of rotavirus-specific immune responses by certain bacterial species (e.g. *Candidatus arthromitus*-conferred rotavirus protection) (35). **(5)** Viruses and phages can change in relative abundance over the course of the rotavirus immunization schedule which correlates with seroconversion following rotavirus vaccination (27). The virome can also directly curb enteric infection through mechanisms like inducing INF-γ overproduction (80). (**6**) Host immune sensing of bacterial microbe-associated molecular patterns including Toll-like receptor 5 recognition of flagellin can either increase tolerance to activation, or provide an adjuvant-like benefit for vaccines (19, 22). Created with BioRender.com.

1.1.9. Limitations

Humans are complex systems with inherent variability that makes drawing indelible connections between the microbiome and rotavirus vaccine performance feel like an uphill battle. These include but are not limited to the role of maternal immunity, prior rotavirus infection, nutrition, vaccine regimen,

geography, sociopolitical events, and socioeconomic status (62, 81). For instance, maternal antibodies passed via the placenta and breastmilk can interfere with rotavirus vaccine efficacy in infants (82). Conversely, the breastmilk bacteriome impacts infection as infants with mothers having an abundance of *Staphylococcus* and *Streptococcus* tended to have negative or asymptomatic rotavirus infection (83). Immunization status and prior infection also muddies the waters. Although it is recommended to co-administer rotavirus and poliovirus vaccines to maximize resources in LMIC, there is some evidence this reduces rotavirus vaccine efficacy at the initial dose (84, 85). Additionally, rotavirus infection early in life prior to vaccination has been associated with improved vaccine responses and protection from further infections (86). Even animal microbiome studies using genetically identical mice with controlled environments can be complicated by variables including pellet composition, vendor, and housing conditions (87).

Tangentially, the specific sequencing methodology used to measure the microbiome can generate variability between studies. Each step of the sequencing process from nucleic acid extraction to data analysis introduces possible bias (88). Potentially biologically relevant niches within the microbiome can go unaccounted for, including the mycobiome which remains largely uncharacterized (89, 90). Certain human populations are also under-represented in sequencing data. This limits our understanding of global microbiome communities and how the variables of being human impact our microbes and our immunity in turn (91). Sequencing of 16S rRNA variable regions is a tried and true approach for basic taxonomic classification of the microbiome; yet, it fails to capture functional potential, species-level diversity, or metabolic differences and similarities amidst microbes (92, 93). Long-read sequencing and "meta-omics" analyses could help fill these gaps (44, 94-96). However, standardizing and integrating sequencing protocols and datasets generated from independent researchers remains a pertinent challenge (97). These limitations collectively highlight the difficulties with identifying microbiome-immune correlates of rotavirus vaccine-induced protection.

1.1.10. Discussion and Future Directions

Given its relevance, next-generation vaccines along with current vaccine adjuvant strategies for rotavirus and other enteric diseases must either collaborate with or circumvent the resident microbiome to provide sufficient protection. Looking at the future of microbiomics for novel rotavirus vaccines, it is necessary to view the human microbiome from an ecological perspective where perturbations to the microbiome ecology may include enteric infection and vaccination (98). We can accomplish this by first understanding redundancy among beneficial microbes. Commensals in the microbiome provide metabolic redundancy capable of protecting against enteric bacterial infection. This microbial strategy protects against enteric infections through diminishing pathogen metabolic niches by having overlapping metabolic needs to the pathogen (98). Second, by ascertaining which metabolites produced by the microbiome are biologically relevant during infection. Then, altering concentrations of these metabolites for a desired, beneficial health outcome (99). Third, by considering the resident microbiome at the site of infection. Enteric viruses each elicit unique host immune responses; for example, genes regulated by proinflammatory cytokines (IL-1β and TNF-α) are enriched during rotavirus infection (100). Developing vaccines that are tailored to similarly mimic natural infection could in turn meaningfully interact with the rotavirus-specific microbial niche to improve immunogenicity. Understanding the ecology of the microbiome could help advance microbiome-informed solutions for improved efficacy of rotavirus vaccines.

The rotavirus field could also benefit from microbiome-related vaccinology research in similar fields, including influenza. Probiotics have been used to improve and induce influenza-specific immune responses in humans and animal models (101, 102). Using a multi-omics approach, antibiotic administration decreased IgG1 antibody titers after influenza vaccination in individuals with low, but not high, pre-existing immunity (103). To understand if the microbiome mediated this response, antibiotic administration seemingly disrupted “foundational communities” in the microbiome that in turn impaired IgG1 responses and induced secondary bile-acid-mediated inflammation, though by lateral mechanisms. Applying the same cross-sectional study design from such influenza studies to rotavirus research could provide a more nuanced evaluation of how host, microbiome, immunity, and metabolome intersect when responding or failing to

respond to vaccination. This cross-sectional design is potentially more important with an enteric versus respiratory infection where the gastrointestinal microbiome and associated immune system interact intimately with the pathogen.

To answer the question "can host microbiome diversity inform next-generation rotavirus vaccine development?": someday. The microbiome has a decided impact on host immunity, and vice versa, with the potential to inform better next-generation rotavirus vaccines. However, the host microbiome and immunity are similarly complex, making specific, and actionable applications to vaccine development using the microbiome difficult. This pursuit is a worthy frontier for mucosal vaccinology.

1.2. A Tail of Murine Rotaviruses

Rotavirus is a non-enveloped double-stranded RNA virus with an 11 segment genome encoding six viral and six non-structural proteins (7). The term '*rota*' is from the Latin word for "wheel" given the virus' resemblance to a wheel and spokes (7). Rotaviruses are present throughout the animal kingdom with high genetic diversity among human rotaviruses (104). A diversity of murine rotavirus strains similarly exists and have been studied since the mid-1900's. The historical background of identifying and classifying murine rotavirus strains specifically is relevant as the following Chapters in this dissertation include murine rotavirus infection along with the development of a recombinant probiotic vaccine expressing murine rotavirus antigens.

Rotavirus was once an enigma. Symptoms related to an "epizootic of intestinal disease" in mice were seemingly first described in 1934 and initially not determined to be viral in nature. Instead, *Salmonella* was thought to be the culprit (105). The etiological agent responsible for the "epidemic diarrheal disease of suckling mice" was first thoroughly investigated in a four-part mini-series of papers published during the 1940's (106-109). These were primarily spearheaded by Dr. F. Sargent Cheever. This research was pertinent given mouse mortality from an infection causing dehydration and diarrhea that was financially devastating to laboratories conducting animal studies. The perpetrator remained elusive after *Salmonella* infection and diet were ruled out. The infectious agent was determined to infect intestinal epithelial cells

(107). There were cytoplasmic inclusions imaged by Laidlaw stain; however, no distinctive conclusions could be drawn between clinical symptoms and presence of inclusions (109). One mouse strain from Carworth Farms were proven highly susceptible to the disease with moderate seasonality to the condition evidenced among these highly susceptible mice. The data consistently indicated evidence of maternally derived protection from infection between litters as first litters were the most susceptible to infection compared to latter litters, which experienced reduced disease burden (108). These series of studies confirmed the infectious agent was not bacterial and that uninfected, unexposed mice did not have detectable inclusions or infectious feces. Later studies confirmed that infection occurred approximately within two weeks of life and further established the role of maternal protective immunity. Based on filtered diarrheal content remaining infectious, the agent was suspected to be viral (110, 111). Infectious feces were deemed capable of rapidly infecting neighboring mice (110, 111). Ultimately, the viral etiological agent of epizootic diarrhea of infant mice (EDIM) was officially unmasked in a 1963 *Science* publication (112). Electron micrographs showed viral particle association with the endoplasmic reticulum within epithelial cells of the small intestine. Human rotavirus was identified a decade later (7). Monkey and cattle rotaviruses were also uncovered in the 1960's and for other species, including birds and bats, rotaviruses were discovered in the 21st century (113). A more detailed historical review of animal and human rotaviruses are provided elsewhere (114).

The original EDIM murine rotavirus strain generated by Kraft et al. (1957) was the lone murine isolate when it was published in 1963 (110, 112, 115). Since then, there are many murine rotavirus strains identified and used in cell culture and murine models, including EW, EHP, EB, EC, EL, and YR-1. In an effort to avoid confusion with the diversity of strains, Burns et al. (1995) encouraged a uniform naming system. As the authors pointed out, nearly all of the aforementioned rotavirus strains could be considered "EDIM" as they cause epizootic diarrhea of infant mice (115). The authors suggested names for newly discovered strains begin with "E" to represent "EDIM" and any following letters stand for who and/or where the strain originated. Therefore, EW stands for EDIM ("E") isolated by Wolf ("W"). The EW rotavirus strain underwent many passages through suckling mice and was originally generated by Wolf et

al. (1981) (116), and is a direct descendent from the original EDIM strain (117, 118). EB was an isolate from a suckling mouse with diarrhea at the National Institutes of Health while EHP was isolated by H.B. Periera from a sick suckling mouse with diarrhea in Rio de Janiero, Brazil (117). All three of these wild-type strains are capable of being cell-culture adapted (117). The EL, or EDIM-Liverpool, strain was generated by Dr. T. Flewett with the WHO Collaborative Centre for Research on Rotaviruses from murine intestinal homogenate (115). EC is the EDIM-Cambridge strain, also generated from intestinal homogenate by T. Flewett (115). The term "EC_{WT}" to describe EDIM-Cambridge wild-type (the EC_{WT} strain is used in Chapter 2 of this dissertation) was seemingly first coined in 1997 (119). The EC and EL strains can also be tissue-culture adapted though EL replicates poorly (115). A relatively new murine rotavirus strain, EMcN, was originally obtained from a BALB/c mouse colony with mild diarrhea at the Children's Hospital in Cincinnati, OH, USA. This strain is uniquely able to induce more constant and elevated amounts of shedding in C57BL/6 and BALB/c adult mice than EDIM; however, EMcN induces less shedding in infant mice compared to EDIM (120). One additional strain from Tajiama et al. (1984) has been mentioned in the literature but to the author's knowledge it has not otherwise been widely characterized (121). The Japanese murine epizootic diarrhea of newborn mice rotavirus strain YR-1 was first noticed in 1974 and has high homology with other EDIM-like strains (122).

Strains that are closely related to EDIM including EW have similar VP4, the protease sensitive spike protein determining the P serotype, amino acid sequences while strains that are more distantly related (EL and EC) exhibit more differences (Figure 1.2) (7, 123). The phylogenetic relationship between murine rotavirus strains and among rotaviruses of different species is described elsewhere (120, 124). Most murine rotavirus strains are currently considered to be a P16 and a G3 (determined by the VP7 glycoprotein) serotype, except EHP, which is P20G3. Serotype is determined by neutralizing antibody specificity to VP4 and VP7 (125).

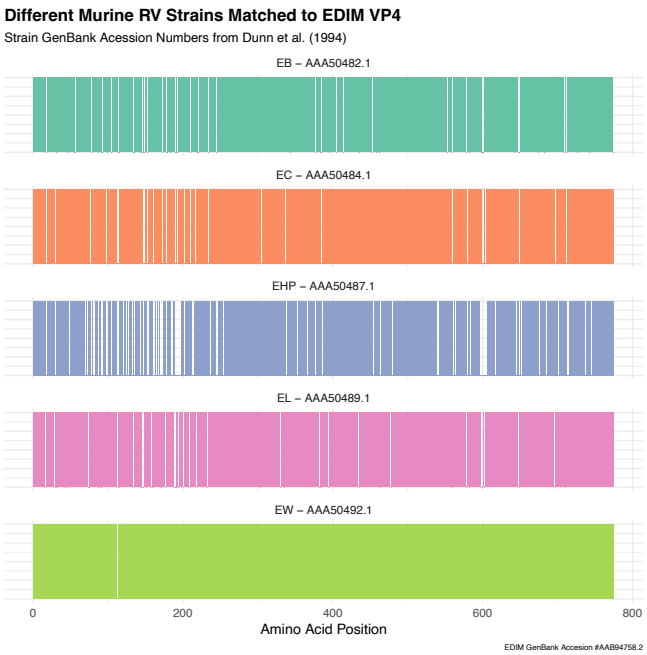

Figure 1.2. Similarities and differences between the VP4 spike protein of different murine rotavirus strains as compared to the EDIM strain (124). The amino acid sequence of the VP4 structural protein for each of the murine rotaviruses (EW, EL, EHP, EC, and EB) described in Dunn et al. (1984) were aligned to the VP4 EDIM sequence (GenBank accession AAB94758.2) to determine if there was a match. Matches are represented by a line (e.g. pink line for EL) and mismatches by a space. The EDIM strain was chosen as the sequence to which all others would be aligned as the VP8* antigen (amino acids 26-231) used in the recombinant *Lactobacillus acidophilus* probiotic vaccine described in Chapter 2 was designed from EDIM. This figure demonstrates similarities between genetically related and distinct murine rotavirus strains' spike protein which determines the P serotype. Figure was generated by aligning sequences in Geneious Prime v.2019.2.3 for MacOS (https://www.geneious.com). Data visualization was performed in R (v.4.3.1) (126) and RStudio (v.2023.06.1+524) (127) with the ggplot2 package (128).

1.3. Brief B-cell Mediated Rotavirus Immunity

The following section reviews B-cell mediated immunity both broadly and as it relates to rotavirus infection. This topic reflects the investigation in this dissertation of rotavirus antigen-specific antibody-secreting cell (ASC) responses for protection against viral challenge after immunization with a probiotic rotavirus vaccine. B-cell populations are imperative for clearing primary rotavirus infection and developing lasting, protective immunity against future infection (129-131). For example, Franco & Greenberg (1995) determined that B-cells are helpful in clearing primary infection and essential in preventing rotavirus reinfection in mice. They demonstrated that J_HM knock-out mice which lack B-cells are neither able to completely clear a second round of rotavirus infection nor able to develop virus-

specific antibodies in sera or feces (132). Following rotavirus exposure, plasmacytoid dendritic cells (pDCs) specifically help activate B-cells via type I IFN to generate anti-rotavirus IgA and IgG (133). Additionally, during rotavirus infection, viral replication in enteroendocrine cells is seemingly necessary to activate dendritic cell (DC) migration to Peyer's patches (134). BALB/c and C57BL/6 mice exhibit type 2 and type 1 helper T (Th) cell immune responses, respectively. The former is characterized by antibody production and the latter by macrophage activation via INF-γ (135). Th1- versus 2-type driven responses to identical immunogenic stimuli often contrast (136). Therefore, mouse strain can mediate protective immunity to rotavirus infection. For instance, C57BL/6 mice have been demonstrated to shed little when infected with EDIM rotavirus (120). A simplified schematic of B-cell activation and trafficking to gut mucosal tissues during rotavirus infection is provided in Figure 1.3.

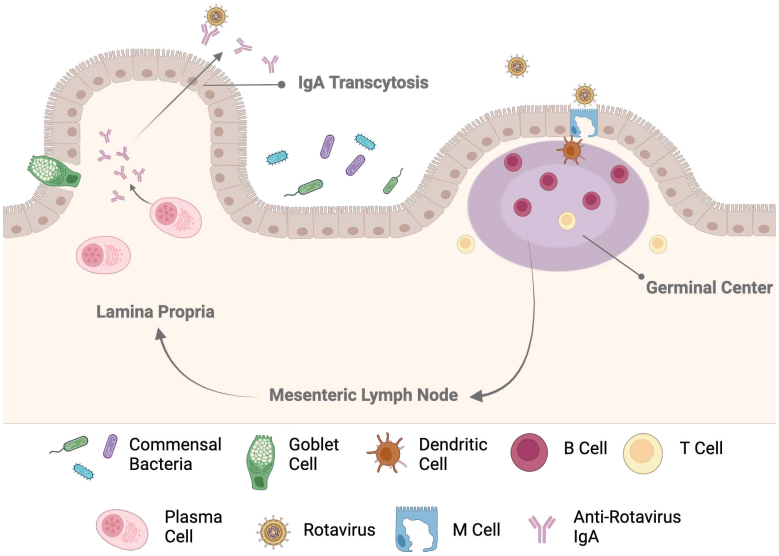

Figure 1.3. Activation of mucosal immune system in the intestine during rotavirus infection. Luminal sampling of rotavirus antigen by antigen presenting cells, including dendritic cells, through M cells activate naïve B-cells within the Peyer's patch. Selected B-cells undergo expansion, class switch recombination, and rounds of somatic hypermutation for affinity maturation in the germinal center to produce rotavirus-specific IgA (137). In short, activated B-cells become either IgA secreting plasma cells, long-lived plasma cells, or memory B-cells (138). Antibody-secreting plasma cells enter mesenteric lymph nodes and are trafficked back to the lamina propria to generate secretory IgA (139, 140). Memory B-cells often reside in resident tissues where rotavirus antigen encounter is more likely to occur, and are activated upon antigen recall to expand into virus-specific antibody-secreting plasma cells (141). Transcytosis of immunoglobulins is a highly regulated process described elsewhere (142). Rotavirus-specific IgA in part reaches the intestinal lumen via J-chain expression (140). Figure adapted from Blutt and Connor (2013) (140) and Park et al. (2023) (139). Created with BioRender.com.

Immune cells surveil throughout the body with some cell populations demonstrating tissue preferences (143). Binding between the lymphocyte-expressed $\alpha_4\beta_7$ integrin and the mucosal addressin cell adhesion molecule 1 (MAdCAM-1) expressed by gut mucosal tissues (e.g. mesenteric lymph nodes and high endothelial venules of Peyer's patches) helps guide lymphocytes, including T cells and ASC B blasts, in a tissue-specific manner back to the gut (144). Mature antigen-primed intestinal DC vitamin A metabolism induces $\alpha_4\beta_7$ integrin expression in activated T cells originating from the GALT along with honing and augmenting IgA secretion of mucosal B-cells (145, 146). $\alpha_4\beta_7$ integrin knockout mice exhibit reduced stool anti-rotavirus IgA along with reduced rotavirus-specific IgA ASC in the MLN 25 days following infection. The $\alpha_4\beta_7$ integrin is also seemingly necessary for resolving rotavirus infection since only purified $\alpha_4\beta_7^{high}$ memory (IgD^-) $B220^+$ B-cells from *IgA* $^{-/-}$ deficient mice could prevent rotavirus infection when transferred to Rag-1 chronically rotavirus-infected mice (147). Additionally, only $\alpha_4\beta_7^{high}$ memory (IgD^-) $B220^+$ splenocytes transferred to the same strain of chronically infected mice significantly cleared rotavirus infection and induced detectable ASC IgA cells in spleen, bone marrow, and lamina propria where IgA dominated over IgG secreting cells (148). Rotavirus specifically appears to infect intestinal versus circulating B-cells more along with preferentially infecting memory B-cells previously exposed to antigen (149). Route of infection or vaccine delivery is relevant as oral challenge and not intraperitoneal with a heterologous rotavirus strain in mice generated mucosal immunity, including virus-specific ASC B-cells in Peyer's patches, mesenteric lymph nodes, and the lamina propria (148). Memory B-cells are not largely persistent and seemingly require natural boosting through reinfection of enteric bugs to maintain IgA memory in the mucosa, as reviewed elsewhere (150).

IgA is the most abundant antibody in the gastrointestinal tract and production of secretory IgA in the lumen modulates immune function at the intestinal epithelium by preventing bacterial adhesion to the mucus and mitigating excessive immune responses from bacterial stimuli (151). IgA is a correlate of rotavirus protection; however, a decisive immune correlate of protection with clinical relevance is debated (140, 152). Finding a broad immune correlate of protection outside of rotavirus-specific IgA in human populations, potentially based on B-cell populations and integrin expression, is promising but remains a

challenge (153). Secretory IgA is one of the inherent intestinal defense mechanisms and can complex with pathogens invading from the lumen (154). Mucosal IgA is responsible for helping clear rotavirus infection and providing heterotypic protection. Virus specific IgA can prevent rotavirus infection and diarrhea within the mucosa through various mechanisms including interruption of virus attachment and cell entry along with neutralizing specific viral antigens and transcytosis to the lumen (155). IgA helps resolve primary rotavirus infection and prevent reinfection as *IgA*$^{-/-}$ knockout mice from either a C57BL/6 or BALB/c background shed virus longer after initial infection than their wild-type counterparts and are susceptible to numerous rotavirus infections (156). Administration of certain lactic acid bacteria species help generate anti-rotavirus gut IgA responses to inhibit rotavirus-induced diarrhea following rotavirus infection (155).

1.4. Foray into Fatty Acids

Fatty acid-derived metabolites generated by the microbiome influences general host health and specifically the immune system (157). The following overview provides a foundation for understanding the potential for dietary fatty acids to modulate next-generation probiotic rotavirus vaccine efficacy and host interactions. Fatty acids are a type of lipid that can be further categorized into either saturated fatty acids, monounsaturated fatty acids, or polyunsaturated fatty acids (PUFA) based on presence and number of double bonds (158). Dietary PUFAs are essential for biological maintenance, such as regulating nerve, eye, brain, and cardiovascular health – to name a few (158). PUFAs are incorporated and subsequently released from cell membranes, including those of immune cells (157, 159). PUFA content influences membrane functionality and the relative availability of different fatty acids with distinct immunomodulatory properties (159, 160). Overconsumption of omega-6 compared to omega-3 PUFA can lead to certain health conditions including inflammation in the gut and obesity, and Western diets are characterized by an elevated omega-6 to omega-3 ratio (160, 161). High-fat diets are generally thought to induce inflammation via various mechanisms, including increased cell permeability and bacterial activation of Toll-like receptor 4 inducing downstream proinflammatory cytokine secretion (160, 162). Certain PUFAs can ameliorate inflammation

in part by decreasing adhesion molecule expression (e.g. VCAM-1) which mediates interactions between endothelial cells and leukocytes arriving at a site of inflammation (Figure 1.4) (159).

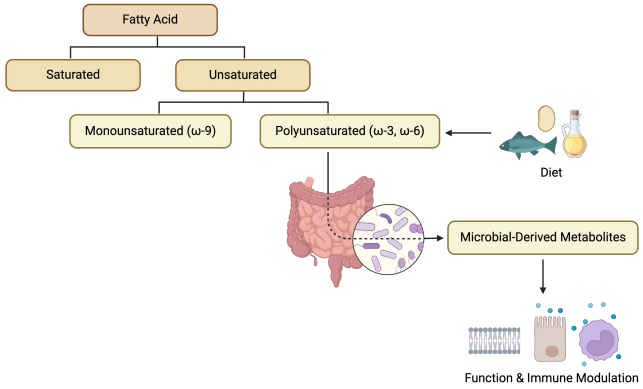

Figure 1.4. Simplified representation of how dietary fatty acids impact host health. Fatty acids can be further broken down into additional categories, including PUFAs. PUFAs are derived from dietary sources including fish and soybean oils. PUFA consumption in general, along with the microbial-derived metabolites, can impact immunological and functional responses at the epithelium among enterocytes and immune cells. This includes cytokine and chemokine secretion along with lipid membrane content and mobility. Figure adapted from Shibata et al. (2018) (157) and Shah et al. (2022) (158). Figure created with BioRender.com. PUFA: polyunsaturated fatty acids.

Diet and dietary changes, such as increases in fat or glucose, intrinsically influence composition of the gut microbiome which can in turn impact host health (163). For instance, the human commensal *Ruminococcus hominiciens*, which oversees cellulose degradation, is far more common in the microbiomes of rural than urban populations. Urban groups tend to follow a Western diet with less fiber (164). High-fat diets can also alter overall microbiome diversity and increase the relative abundance of microbes classified as detrimental versus beneficial (160). For example, diets rich in either saturated or polyunsaturated lipids can alter the relative abundance of different bacteria in mice, including an enrichment of lactic acid bacteria with a polyunsaturated lipid-rich diet (163). These diet-induced differences in microbiome structure resulted in weight gain and increased TLR activation causing white adipose tissue inflammation in mice fed lard which is saturated lipid-heavy (163). Exogenous administration of microbial-derived metabolites of fatty acid metabolism, such as conjugated linoleic acid, can relieve inflammatory conditions including colitis (157). Such microbial-derived lipid metabolites are present in specific pathogen free mice with an intact microbiome but undetectable in germ-free mice (157). PUFAs are considered essential as they must

be derived from diet and, as detailed above, are imperative for human health. The world could face a shortage of these essential lipids; for example, omega-3 docosahexaenoic acid which contributes to neurological development and function. PUFA produced by bacteria are attracting attention as a method to fill the projected gap as synthetically introducing the required double bonds is challenging (158, 165). The biological importance of diet-derived lipids and host microbes is intertwined.

1.5. Review of Rotavirus Vaccines

Accessibility to healthcare varies around the world which can in turn impact vaccine administration and coverage. For example, there is approximately one doctor for every 4,500 patients in Kenya while the United States has between three and four doctors per thousand patients, according to *The Economist* (166). This shortage of healthcare professionals is compounded by limited availability of teachers, and a curriculum that can be lacking (166). Sub-Saharan Africa specifically carries 80% of the global rotavirus-associated mortality (167). Variables external to rotavirus vaccine efficacy that contribute to diarrheal disease burden in these regions include limited use of and access to oral rehydration therapy, safe drinking water, and sanitation, and access is variable within and between countries (167). Consistently vaccinating children, even with a vaccine just over 50% effective, does reduce rotavirus-related deaths and health care costs. However, children remain highly at-risk for moderate-to-severe rotavirus infection and can suffer developmental repercussions even in countries with national rotavirus vaccine programs (167).

Efficacy is an obvious and important factor when choosing a rotavirus vaccine. Outside of vaccine performance, cost, safety, predicted dosage waste, ease of use and storage, political investment, and staffing are additional variables that are considered when electing a rotavirus vaccine for adoption into a national immunization program (168, 169). Administering rotavirus vaccines at birth is an attractive approach to potentially improve rotavirus vaccine-induced immune responses and vaccine coverage in resource-poor settings (82, 170, 171). Combining norovirus and rotavirus in one vaccine could also provide protection for multiple enteric pathogens simultaneously and affordably (172). Next-generation vaccines are also necessary to help improve vaccine efficacy and coverage (167). The benefits associated with probiotic-

based next-generation vaccines are discussed elsewhere in Chapter 1 and the remaining Chapters of this dissertation. These include but are not limited to affordability, lack of cold-chain storage, and independence from specialized administration while inducing mucosal immunity (173, 174). Specifications for the currently available rotavirus vaccines are listed in Figure 1.5.

	ROTASIIL®	RotaTeq®	Rotarix®	Rotavac®
Formulation	Pentavalent (Bovine, Human)	Pentavalent (Bovine, Human)	Monovalent	Monovalent
Presentation	Lyophilized, thermostable lyophilized, liquid. Oral administration.	Liquid. Oral administration.	Liquid. Oral administration.	Liquid. Oral administration
Dosage	3 doses	3 doses	2 doses	3 doses
Storage	**Lyophilized:** 2-8 °C, diluent stored dry and cool. **Rotasiil-thermo:** ≤ 25 °C in conditioned rooms, 1 week at 37 °C for transport. Diluent stored cool and dry. **ROTASIIL-liquid:** 2-8 °C protected from light	2-8 °C protected from light. 2-year shelf-life.	2-8 °C protected from light. 2-year shelf-life.	-20 °C for five years, 2-8 °C for 6 months after thawing. **Rotavac 5D:** 2-8 °C for 24 months.
Price per Dose	$0.90 (lyophilized) $1. (-thermo) $0.85 (-liquid)	$3.20	$2.54	$0.85 $1.15 (-5D)

Figure 1.5. Characteristics of the currently available global rotavirus vaccines. Dosage, storage, cost, and formulation all influence the decision to include one vaccine over another in a national immunization program. Table adapted from the Rotavirus vaccines: WHO position paper – July 2021 (9) and Varghese et al. (2022) (168). Created with BioRender.com.

There are international resources available to provide improved rotavirus vaccine access. GAVI, the Vaccine Alliance was initially funded in 2000 and helps provide vaccine subsidies for low-income countries with self-financing of immunization programs being the ultimate goal for participating nations (https://www.gavi.org/programmes-impact/our-support). Nicaragua was the first GAVI-eligible country to include rotavirus in their national immunization program in 2006 (175). GAVI, the Vaccine Alliance is not without criticism, primarily surrounding its somewhat ineffective approaches to holistic health system support and insufficiently addressing equal access to immunizations within countries (176, 177). GAVI has seemed most efficacious in closing the distance between low- and high-income countries for vaccine access generally (177, 178). 12.3 million additional rotavirus vaccinations are estimated to be attributable to GAVI

support between 2000 and 2016 (179). In addition to GAVI, The Rotavirus Accelerated Vaccine Introduction Network (RAVIN) project was carried out from 2016 – 2020. RAVIN was centered around providing an evidence-based and country-owned approach to supporting nations in selecting and implementing a rotavirus vaccine in their immunization programs and sustaining that immunization program. The purpose of RAVIN was to try closing the gap between availability of vaccines in the market and the number of countries implementing these vaccines in their immunization programs (180). RAVIN incorporated eight GAVI-eligible countries, including Afghanistan, Myanmar, Benin, and Nepal. Five of the eight eventually introduced a rotavirus vaccine nationally. RAVIN helped countries navigate GAVI applications, connect country leadership with local and external experts and support, and assisted in identifying country-specific needs. RAVIN experienced many challenges, including the national and regional political influence on vaccine introduction and public health outbreaks altering vaccine prioritization, such as COVID-19 administration over rotavirus. Supply shortages for specific vaccines also happened; for example, in 2018 with RotaTeq® and Rotarix®. These delays can be challenging for countries who were planning on using the now out-of-stock vaccines. In 2018 two more vaccines fortuitously entered the market: Rotavac® and Rotasill®. When handling vaccine shortages countries must decide if they should delay and wait for their first-choice vaccine to become available or transition to an available vaccine. This switch requires much consideration, such as deciding to build alternative infrastructure for a different vaccine formulation than originally planned (169). Wastage estimates are also important, meaning the consideration of how many doses will be wasted when using an alternative, higher-dose container. Similar programs to RAVIN can help improve rotavirus vaccine coverage globally.

Weighing all variables when considering the right rotavirus vaccine is applicable to countries of all economic classifications. In middle-income countries (MIC) – which do not qualify for GAVI support – cost is predominantly prohibitory along with potential safety risks (181). It was determined between 2020-2029 that introduction of rotavirus vaccines in MIC will be cost-effective (U.S. dollars per disability-adjusted life-year averted) in a majority (77%) of the countries evaluated. Additionally, rotavirus vaccines will have a demonstrable benefit-risk payoff (181). Benefit-risk analyses indicate the health benefit of

rotavirus vaccination outweighs potential risk (e.g. intussusception). The income classifications, including LMIC, used for countries are determined according to Gross National Income per capita by The World Bank (https://www.worldbank.org/en/home). This dissertation implements the term LMIC but there are notable limitations with its use worth recognizing. As reviewed by Lencucha et al. (2022), the term LMIC restricts the representation of complex variables for a country or countries to just national income. Its overuse in the literature can ingrain a sense of colonialism and an "us" versus "them" narrative, while potentially embedding racism and other prejudices further (182). The author of this dissertation does not claim to know an improved alternative but tries to recognize the impact of the words that are used.

CHAPTER 2: LACTOBACILLUS ACIDOPHILUS EXPRESSING MURINE ROTAVIRUS VP8 AND MUCOSAL ADJUVANTS INDUCE VIRUS-SPECIFIC IMMUNE RESPONSES

2.1. Introduction

Diarrheal illness is the fourth leading cause of death in children under five years of age worldwide (183). It is estimated that rotavirus infection killed approximately 128,000 children in 2016 and accounted for 19.11% of all diarrhea-associated deaths in 2019 (8, 184). The World Health Organization recommends including a rotavirus vaccine in all global vaccination protocols and, currently, 124 countries have introduced rotavirus into their national immunization programs (184, 185). There are currently four vaccines (Rotarix®, RotaTeq®, Rotavac®, and Rotasiil®) that are preapproved internationally, all of which are formulated as orally delivered attenuated live-virus vaccines (9). However, these current rotavirus vaccines have limited efficacy (50–60%) in lower-middle-income countries (LMIC) with a low sociodemographic index and high childhood mortality (8, 11, 82). This discrepancy in vaccine efficacy leaves millions of children at risk for rotavirus infection and diarrheal illness (186), and the cause of the decreased response to the attenuated live-rotavirus vaccines is poorly understood. Factors such as mal/undernutrition, impact of the intestinal microbiome, coinfection with enteric pathogens, environmental enteric dysfunction, and maternal antibody interference are believed to play a role (82, 187, 188). Attenuated vaccines also have inherent risks, including reversion to virulence, recombination with circulating viruses, and decreased safety in immune-suppressed populations. Additionally, they require cold-chain storage and specialized personnel/training for administration (174). Intussusception has also been a historic risk of live attenuated rotavirus vaccines (189). It is therefore recognized that a new generation of vaccines is needed to overcome these many obstacles and provide improved protection for more people.

B-cells and IgA have been identified as key to mucosal protection against rotavirus infection in humans and animal models (131, 190). Mucosal immunization by orally delivered vaccines is the most effective means of inducing mucosal IgA; however, there is a paucity of oral vaccine platforms that have been proven to be safe and immunogenic (156, 191, 192). Probiotic-based vaccines have promise as a

mucosal immunization platform (193). Probiotics are generally regarded as safe (GRAS) as they are often commensal residents of the human microbiome, and offer logistical advantages to both orally and parentally delivered vaccines due to low production cost, storage sans cold chain, and ease of administration (189, 194, 195). To date, *Lactobacillus* spp. have primarily been used as an adjuvant strategy for the current rotavirus vaccines, but the application of *Lactobacillus* as a vaccine platform itself is an emerging next-generation approach (56, 57, 196, 197). The immune system can also be altered by probiotics which can interact with the mucosa-associated lymphoid tissue directly at immune inductive sites to generate both local mucosal and systemic immune responses (51, 56, 57, 150, 197). *Lactobacillus* spp. specifically exhibit endogenous innate immune-modulating mechanisms including Toll-like receptor (TLR) activation by the cell wall components lipoteichoic acid and peptidoglycan, direct interaction with dendritic cells, and generation of antimicrobial compounds like lactic acid (194, 198, 199). *L. casei* expressing porcine VP4 antigen demonstrated proof of concept for *Lactobacillus* spp. as next-generation rotavirus-vaccine vectors, as they induced antigen-specific serum IgG and mucosal IgA, with serum antibodies capable of rotavirus neutralization (59, 200).

We have previously demonstrated the feasibility of using *Lactobacillus acidophilus* (LA) as a vaccine candidate by developing recombinant LA (rLA) strains for the mucosal pathogen HIV-1-expressing MPER and Gag epitopes along with IL-1β or the TLR5 ligand *Salmonella enterica* serovar Typhimurium flagellin (FliC) as adjuvants (199, 201, 202). Oral immunization with these rLA-generated antigen-specific serum IgG, mucosal IgA, and B-cells in mucosal tissues (female reproductive tract and large intestine). These responses were improved by the adjuvants IL-1β and FliC. We have also established that rLA vaccination neither colonizes the intestine nor permanently disrupts the resident host microbiome (201).

To evaluate the potential of our rLA platform as a next-generation rotavirus vaccine, we constructed an rLA rotavirus vaccine strain expressing peptide and protein viral antigens from the VP8 capsid protein (203). The VP8 capsid protein was selected as the vaccine epitope since some rotavirus-neutralizing antibodies are directed to this protein and the VP8Pep epitope is highly conserved among type-A rotaviruses (204, 205). We also included two immune-stimulating adjuvants, FliC and *E. coli* type-I pilus microfold

cell-targeting adhesin protein FimH (202, 206). Adjuvants are essential for mucosal vaccines to overcome the immunotolerant nature of the gut due to high antigen exposure (207). Here, we present vaccine-strain construction and validation. The immunogenicity of the vaccine was evaluated using a murine in vivo rotavirus challenge model to assess antirotavirus immune responses and protection against a homotypic murine rotavirus.

2.2. Materials and Methods

2.2.1. rLA Vaccine Strain Construction

(r)LA strains are described in Table 2.1. NCK56 is a control strain of the human isolate *Lactobacillus acidophilus* NCFM that has plasmid-conferred erythromycin resistance (201, 208, 209). VP8-1 and N-terminal FimH integration downstream of the *lba0889* (*enolase*) gene was performed using the *upp*-based counterselective gene-replacement system, as previously described by Douglas et al. (210). Detailed methods are provided in Supplementary File S2.1. The VP8Pep epitope was integrated into the *slpA* gene, as previously described (206, 211). The FliC plasmid pTRK1034 was transformed into exponential cultures of NCK2783 by electroporation, as previously described (210, 212, 213). *E. coli* and LA strains used to construct the rLA strains are listed in Supplementary Table S2.1 (214). The antigen amino acid sequences and their expression profiles are listed in Supplementary Table S2.2. The primers and plasmids used during cloning are listed in Supplementary Table S2.3 and Supplementary Table S2.4, respectively.

Table 2.1. Wild-type *Lactobacillus acidophilus* (LA) and recombinant LA (rLA) strains used for oral immunization in this study. Erythromycin: Erm.

Strain	Components	Resistance	Reference
NCK56	Wild-type lab LA NCFM strain	Erm	(208)
GAD84	LA-expressing VP8Pep within SlpA and chromosomal VP8-1 downstream of *enolase*	None	This study
GAD85	LA-expressing VP8Pep within SlpA, pFliC, and chromosomal VP8-1 and FimH downstream of *enolase*	Erm	This study

2.2.2. Bacterial Growth Conditions

LA strains were grown anaerobically overnight at 37 °C in MRS media (BD Difco, Franklin Lakes, NJ, USA) supplemented with 5 μg/mL erythromycin when growing antibiotic-resistant strains. The rLA strain GAD85 (Table 2.1) was grown overnight and then diluted 1:10 to exponential growth. All cultures were washed twice in PBS (Corning, Corning, NY, USA). Colony forming units (CFU) were calculated based on the optical density at 600 nm as previously described (206).

2.2.3. Confirmation of rLA Antigen and Adjuvant Surface Expression by Flow Cytometry

Resuspended in 100 μL PBS + 1% BSA (Equitech-Bio, Kerrville, TX, USA) + 1:1000 kathon CG/ICP (Supelco, Bellefonte, PA, USA) staining buffer with primary and secondary antibodies was 1×10^7 CFU of (r)LA, as listed in Supplementary Table S5. Samples were analyzed on a Gallios flow cytometer (Beckman Coulter, Indianapolis, IN, USA). Analyses were performed in FlowJo (v.10.8.1, Ashland, OR, USA) with gating based on NCK56 and secondary antibody-only controls.

2.2.4. Confirmation of Cytosolic Accumulation of VP8-1 Antigen by SDS-PAGE Western Blot

Pelleted exponential phase cultures were treated with 75 μg/mL lysozyme (Sigma-Aldrich, St. Louis, MO, USA), resuspended in PBS, and incubated for one hour at 37 °C. VP8-1 expressed by *E. coli* and purified by his-tag was included as a positive control. The sample and loading dye (Pierce, Appleton, WI, USA) were incubated at 95 °C for five min and run on a Mini-Protean TGX gel (Bio-Rad, Hercules, CA, USA) in Tris–Glycine–SDS buffer at 200 V. A Precision Plus WesternC ladder (Bio-Rad) was also included. The gel was transferred onto a PVDF membrane and stored overnight at 4 °C in a blocking buffer made of 1% milk + PBST (PBS and 0.05% Tween20) + 1:1000 kathon. The PVDF was incubated with polyclonal mouse anti-VP8 antibody (provided by Dr. Harry Greenberg from Stanford University, Palo Alto, CA, USA) and diluted 1:1000 in blocking buffer. PVDF was washed and incubated with antimouse IgG (clone 7076; Cell Signaling, Danvers, MA, USA) diluted 1:2000 and StrepTactin (Bio-Rad) diluted 1:5000 in the blocking buffer. PVDF was washed and incubated with equal parts of the Clarity Western

ECL (Bio-Rad). The membrane was imaged on a Bio-Rad Chemi-Doc XRS+, and lanes were analyzed using Image Lab software (v.6.1; Bio-Rad).

2.2.5. Animal Ethics and Murine Oral Immunization

All research involving animals was approved by and in accordance with guidelines set by the Institutional Animal Care and Use Committee of Colorado State University (IACUC #18-1234A). An equal number of male and female rotavirus naïve BALB/cJ mice were obtained from Jackson Laboratories (Bar Harbor, ME, USA). The mice were maintained in specific pathogen-free conditions, housed socially in single-sex groups in commercially available individually ventilated cages, and provided with autoclaved bedding and enrichment. Animals were fed ad libitum commercially irradiated rodent chow (Teklad Global, Envigo, Indianapolis, IN, USA) and tap water filtered via reverse osmosis in autoclaved water bottles. The animals were tracked and monitored daily for any signs of stress or illness. For oral delivery of wild-type LA and rLA strains, washed bacterial cultures were resuspended to 5×10^9 CFU in 200 µL of buffer made of soybean trypsin inhibitor (Sigma-Aldrich) and sodium bicarbonate ($NaHCO_3$) (213). The experimental design is as described in Table 2.2. The mice were immunized with either the control or the experimental strains for three sequential days every other week (Figure 2.1, publication license provided in Supplementary File S2.2). Negative control mice did not receive any intervention. The mice were euthanized by CO_2 then exsanguination, and tissues were collected at necropsy. 303 550 8369

Table 2.2. Study design describing treatments used in vaccination and challenge experiments.

Group	N per Treatment	Treatment	Challenged with Rotavirus
Negative Control	7	No Intervention	No
Buffer	8	Bacterial Resuspension Media	Yes
NCK56	8	Wild-type LA Control	Yes
GAD84	8	Dual-Antigen rLA	No
GAD85	8	Dual-Antigen and Dual-Adjuvant rLA	Yes

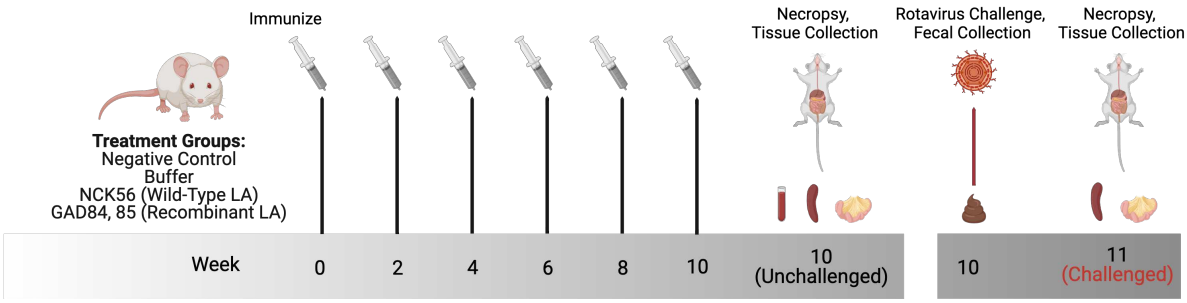

Figure 2.1. Experimental design. To evaluate host response to the vaccination, mice were vaccinated by oral gavage every two weeks with either buffer ($n = 8$), the wild-type *Lactobacillus acidophilus* (LA) strain (NCK56; $n = 8$), dual-antigen recombinant *Lactobacillus acidophilus* (rLA) strain (GAD84; $n = 8$), or dual-antigen/dual-adjuvant rLA strain (GAD85; $n = 8$). Negative control ($n = 7$) mice received no intervention. Mice were administered a sixth vaccination dose a day before the necropsy. Spleen, mesenteric lymph node (MLN), and sera were collected at necropsy. To determine host response to the challenge, mice were orally dosed with either buffer ($n = 8$), NCK56 ($n = 8$), or GAD85 ($n = 8$) for eight weeks before infection with EC_{WT} two weeks after the final immunization. Fecal samples were collected daily for six days following infection with spleens and MLN collected at necropsy on day seven. Figure created with BioRender.com.

2.2.6. Murine Rotavirus Challenge

To generate the wild-type murine rotavirus EDIM-Cambridge (EC_{WT}) used for murine infection, 50 µL (400·infectious dose 50; ID_{50}) of virus stock (obtained from Dr. Mary Estes at Baylor College of Medicine in Houston, Texas USA) was orally given to 5-day old neonates. Neonates were euthanized 48 hours after infection by isoflurane overdose and decapitation. The intestines were collected and tissues pooled, homogenized by bead beating, and diluted in DMEM (Corning) + 1% pen/strep (Hyclone, Logan, UT, USA). Neonates were challenged with serial dilutions of viral stock and screened for the virus in their feces by antigen ELISA to calculate ID_{50} using the Reed and Muench Calculator (215). Adult mice were orally challenged with a 1×10^5 ID_{50} of EC_{WT} two weeks after the last vaccination (Figure 2.1). Fecal samples were collected directly before infection, then daily for six days postinfection to detect rotavirus antigen shedding. Mice were euthanized by CO_2 and then exsanguination seven days after infection. Tissues were collected at necropsy. Fecal pellets were homogenized in PBS + 2X protease inhibitor (ProteaseArrest, G Biosciences, St. Louis, MO, USA), and fecal supernatants were stored at −80 °C following centrifugation for analysis.

2.2.7. Tissue Collection, Cell Isolation, and Antibody-Secreting Cell (ASC) FluoroSpot Assay

The spleen and mesenteric lymph node (MLN) were collected in RPMI (Corning), supplemented with 2% L-glutamine (CellGro, Lincoln, NE, USA), 1% HEPES (Caisson Labs, Smithfield, UT, USA), 1% pen/strep (Hyclone), and 0.1% gentamicin (Sigma-Aldrich). Tissues were processed into single-cell suspensions. The spleen was mechanically disrupted using a GentleMACS dissociator (Miltenyi Biotec, Auburn, CA, USA); then, red blood cells were lysed with 7.2 pH ACK lysis buffer (0.15 mol/L NH_4Cl, 0.001 mol/L $KHCO_3$, and 0.0001 mol/L Na_2EDTA in water). The MLN was mechanically disrupted through a 40 µm cell strainer. Both tissues were centrifuged and then filtered through a 40 µm filter cap tube (Corning). Live cells were counted using a Cellometer Auto2000 (Nexcelom Bioscience, Lawrence MA, USA). Cells were plated in culture medium of RPMI supplemented with 2% L-glutamine, 2% MEM essential amino acids (Cytiva, Marlborough, MA, USA), 1% pen/strep, 1% HEPES, 1% sodium pyruvate (Cytiva), 1% MEM nonessential amino acids (Cytiva), 5% FBS (Hyclone), 0.1% 2-mercaptoethanol (Thermo Fisher, Waltham, MA, USA), and 0.9% 1 g/L NaOH (Sigma-Aldrich). All media were filter sterilized. Peyer's patches (PP), large intestine (LI), and female reproductive tract (FRT) samples were collected and processed as previously described (199, 206).

Mouse IgG/IgA double-color FluoroSpot assays (Cellular Technology Limited; CTL, Shaker Heights, OH, USA) were performed following the manufacturer's instructions. Plates were coated with 2 µg/mL of either VP8-biotin peptide (MASLIYRQLL-biotin, Bio-Synthesis Inc., Lewisville, TX, USA) or VP8-1 (Colorado State University, Fort Collins, CO, USA)-coating antigen. Cell suspensions in culture media from the spleen and MLN collected on the day of the necropsy were added to wells in duplicate at 250,000 cells/well. Plates were developed using 5–10 µL of antimurine IgA (FITC) and IgG (Biotin). Plates were dried overnight, and spots were counted and analyzed using a CTL ImmunoSpot analyzer and associated software (v.7.0.26.0; CTL). To identify $CD45^+CD19^+$ B-cells, 50,000 cells from each tissue on the day of isolation were washed with staining buffer, blocked with antimouse CD16/32 (clone 93; Biolegend, San Diego, CA, USA), and labeled with a cocktail of 7-AAD viability staining solution (Biolegend), FITC antimouse CD45 (clone 30-F11; Biolegend), and Pacific Blue antimouse CD19 (clone

6D5; Biolegend). Flow cytometry was performed using a Gallios flow cytometer (Beckman Coulter, Indianapolis, IN, USA). Analysis was performed using FlowJo (v.10.8.1). Gates were set using fluorescence minus one (FMO) controls after gating for live cells. $CD45^{+}CD19^{+}$ B-cell percentages determined from flow cytometry analysis were used to calculate the antigen-specific secreting cells per 1×10^6 B-cells based on the following calculation:

$$\text{spots per well} \cdot \left(\frac{(1 \cdot 10^6)}{\text{cells per well} \cdot \%\ \text{B} - \text{cells determined by flow cytometry}}\right.$$

2.2.8. Fecal Antigen Shedding ELISA

Plates were coated with rotavirus polyclonal antibody (Thermo Fisher, PA1-7241) diluted 1:4000 in a 9.6 pH sodium carbonate/bicarbonate buffer (0.015 mol/L Na_2CO_3, 0.035 mol/L $NaHCO_3$) and incubated overnight at 4 °C. All wash steps were performed five times using PBST unless stated otherwise. Plates were washed and blocked with 250 µL/well of 5% milk + PBS + 1% kathon for three hours, then washed. Undiluted 50 µL/well of homogenized fecal samples were added in duplicate. For plates that included a standard curve to calculate the relative amount of rotavirus antigen shed in murine feces, homogenized intestines of murine neonates infected with EC_{WT} were serially diluted to a 1:1024 dilution in 1% milk + PBS + 0.2% kathon sample diluent. Adult fecal samples were diluted to ensure optical density would fall within this standard curve. Samples were incubated for two hours and plates were washed before adding 50 µL/well of rotavirus NCDV polyclonal antibody HRP (Thermo Fisher, PA1-73015) diluted 1:500 in sample diluent. Plates were incubated for one hour and, after seven washes, 50 µL/well of room temperature (RT) TMB (SeraCare, Milford, MA, USA) were added. The reaction was stopped after 15 min by adding an equal volume of 1 mol/L hydrochloric acid (HCL Thermo Fisher Science Education). The plates were read at a 450–570 nm wavelength on a BioTek (Winooski, VT, USA) Synergy H1 Multimode Reader.

2.2.9. Tissue-Culture-Adapted Murine RV (ETD) Propagation

The MA104 cell line was obtained from ATCC (CRL-2378.1^{TM}) and cultured in complete M199 media (Sigma-Aldrich) supplemented with heat-inactivated 10% fetal calf serum (FCS; heated to 56 °C for 30 min), 1% L-glutamine, and pen/strep (Corning). Incomplete M199 media was only supplemented with 1% L-glutamine and pen/strep without FCS. Cells were passaged using 0.05% 1X trypsin-EDTA (Gibco, Grand Island, New York, USA). Unless specified otherwise, all culturing and incubating conditions were performed at 37 °C and 5% CO_2; 200 µL of murine ETD rotavirus, a tissue-culture adapted EDIM strain (118), was diluted in incomplete M199 media for an MOI of approximately 0.01. The virus was activated by incubating for 20 min with 2.5 µg/mL of trypsin type IX (Sigma-Aldrich). Confluent MA104 cells were washed in incomplete M199 media. Activated virus was diluted 1 to 5 with incomplete M199 media and incubated for 50 min with the cells. Fifteen mL of incomplete M199 media and 0.5 µg of trypsin/mL were added to the flask, and the infected cells were incubated for 3–4 days until complete cell death. The virus was aliquoted and stored at −80 °C.

2.2.10. ETD Immunoperoxidase Focus Reduction Neutralization Assay

The cell-culture-propagated ETD virus was activated with 5 µg/mL of trypsin type IX for 20 min in incomplete M199 media. The virus was diluted in incomplete M199 media to a titer that would form 200–300 foci. In a dilution plate, murine sera were diluted 1:4 in incomplete M199, then serially diluted 1:2 across the plate. Equal volumes of diluted virus and murine sera (60 µL/well total volume) were incubated for one hour in a separate plate. A 96-well plate confluent with MA104 cells was washed twice with incomplete M199 media and 50 µL/well of the virus and sera mixture was incubated for one hour with the MA104 cells. Inoculants were removed, the plate was washed twice with PBS, and 100 µL per well of incomplete M199 media without trypsin was added. The plate was cultured for 16 hours, then washed once with PBS. Cells were fixed with 70 µL/well of 10% formalin (37% formaldehyde (Sigma-Aldrich) diluted 1:10 in PBS). The formalin was removed, and the cells were permeabilized with 70 µL/well of 1% Triton-X (diluted in PBS), incubated for three min at RT, and then washed twice with PBS. Seventy µL/well of

rabbit antirotavirus hyperimmune serum diluted in PBS + 0.5% BSA was added, and the plates were incubated for one hour at RT. The plate was washed twice with PBS and 70 µL/well of peroxidase-conjugated goat antirabbit IgG (Kirkegaard and Perry Lab, Gaithersberg, MD, USA) in PBS + 0.5% BSA, and the plate was incubated for one hour at RT. The plates were washed with PBS before adding 70 µL/well of AEC substrate (Vector Lab AEC peroxidase substrate kit, Newark, CA, USA). After the color developed for 5–10 min, the reaction was stopped by washing twice with PBS. Foci indicating ETD-infected cells were counted with a microscope.

2.2.11. ETD-Infected MA104 Cell-Based Antibody ELISA

The virus was activated with 5 µg/mL of trypsin type IX in incomplete M199, then diluted in incomplete M199 media to a titer that would form 200–300 foci. Confluent MA104 cells were washed in incomplete M199 media. Fifty µL/well of diluted virus were added and the plate was incubated for one hour. The virus was removed, plates were washed twice with incomplete M199 media, and then, 100 µL/well of incomplete M199 media were added. The plates were incubated overnight, washed once with PBS, and then cells were fixed with 90 µL/well of 10% formalin for 30 min at RT. Formalin was removed and 90 µL/well of 1% Triton-X (diluted in PBS) were added to permeabilize the cells. Murine sera samples were serially diluted starting at a 1:12.5 dilution in PBS plus 0.2% BSA and 100 µL/well added and incubated for one hour at RT. The plates were washed and 90 µL/well peroxidase-conjugated goat antimouse IgG (Kirkegaard and Perry Lab) in PBS + 0.2% BSA were added to each well and incubated for one hour at RT. The plates were washed with PBS before adding 70 µL/well of AEC substrate. After the color developed for 5–10 min, the reaction was stopped by washing twice with PBS. Positive foci were observed with a microscope with the last titer (1:200 across experimental samples) positive for virus staining considered the titer of the serum sample.

2.2.12. Statistical Analyses

Unless stated otherwise, statistical analyses were performed on macOS in R (v.4.2.2) (216) and RStudio (v.2022.12.0+353) (217) with data visualization performed using the ggplot2 package (218). To analyze serum antibody titers, a Fisher's exact test for categorical data was performed to compare the proportions of detectable antirotavirus IgG present across all groups. Titers less than 50 were deemed "not present" and titers equal to or greater than 50 were deemed "present". A two-way ANOVA followed by Tukey's HSD to correct for multiple pairwise comparisons was performed for each tissue (spleen, MLN) individually for the ASC assay analyses. The relative amount of EC_{WT} antigen shed in murine feces six days after infection was calculated from a power trendline formula generated in Excel (v.16.73) from the OD values (450–570 nm absorbance) of standard curves from plates run simultaneously. To evaluate differences in the relative amount of EC_{WT} antigen shed between treatment groups, a Shapiro–Wilk test and a Kruskal–Wallis test were performed, then a Dunn's test for multiple comparisons with Benjamini–Hochburg adjustment per day postinfection to generate adjusted *p*-values. Mice were considered positive for fecal EC_{WT} antigen shedding when raw OD values exceeded a cutoff calculated as the mean plus three times the standard deviation of OD values at day zero across all groups.

2.3. Results

2.3.1. rLA Expresses Rotavirus Antigens and Mucosal Adjuvants

The truncated VP8* protein antigen (VP8-1; amino acids 26-231, Supplementary Table S2.2) from the EDIM murine rotavirus strain (GenBank accession AAB94758.2) was double-crossed into the LA genome behind the highly expressed *enolase* gene (219, 220). Cytoplasmic VP8-1 accumulation in rLA was confirmed by Western blot (Figure 2.2A). The VP8* peptide antigen (VP8Pep; amino acids 1–10, Supplementary Table S2.2) was double-crossed into the surface-layer protein SlpA, as previously described (206).VP8Pep surface expression was confirmed by flow cytometry (Figure 2.2B). The N-terminal binding domain of the FimH adjuvant was double-crossed into the LA genome in tandem with VP8-1. The FliC adjuvant was expressed from the pTRK1034 plasmid (213). The surface expression of both adjuvants was confirmed by flow cytometry (Figure 2.2C,D).

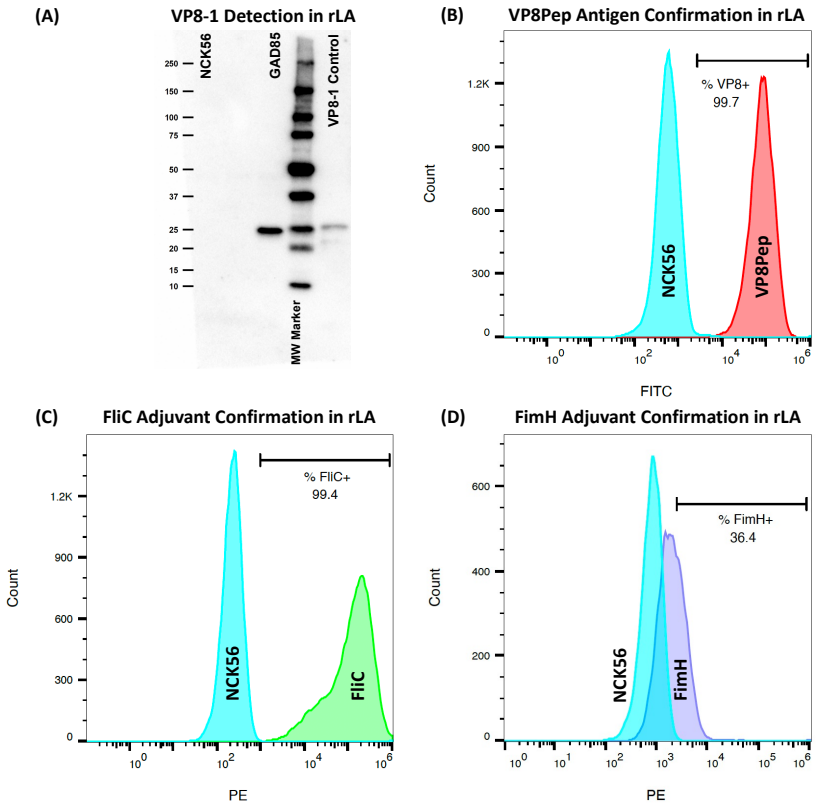

Figure 2.2. Rotavirus rLA vaccine-strain confirmation. Western blot (**A**) of VP8-1 antigen protein (25 kDa, as measured by the molecular weight marker) exclusively present in GAD85 lysate corresponding to the *E. coli* expressed positive VP8-1 control. No detectable band was observed in the NCK56 lysate negative control. The uncropped Western blot for GAD85 is provided in Supplementary Figure S2.1 and the densitometry readings are in Supplementary Table S2.6. Flow cytometry histograms confirming surface expression of (**B**) VP8Pep, (**C**) FliC, and (**D**) FimH for rLA constructs compared to the NCK56 control (blue peaks). Confirmation of dual-antigen expression for the rLA strain GAD84 is provided in Supplementary Figure S2.2A (uncropped Western blot) and Figure S2.2B (flow cytometry histograms) with the densitometry readings in Supplementary Table S2.7. VP8-1: 206 amino acid rotavirus protein antigen, VP8Pep: VP8 10 amino acid rotavirus peptide antigen, FliC: flagellin adjuvant, FimH: adhesion adjuvant.

2.3.2. rLA Vaccination Induces Antirotavirus Serum IgG

Mice received six oral immunizations of either control (negative control, buffer, or NCK56) or rLA strains (GAD84 or GAD85) every other week for ten weeks (Figure 2.1) with the last dose given 24 hours before necropsy. Serum was used to measure anti-ETD rotavirus IgG via cell-based ELISA. Mice in both rLA-vaccinated groups had detectable rotavirus-specific IgG while all the control groups did not have a detectable antirotavirus antibody (Figure 2.3; *p*-value based on a Fisher's Exact Test comparing proportions across all groups: 0.017). A higher percentage of mice (50%) vaccinated with the GAD85 strain had detectable antirotavirus serum IgG compared to mice vaccinated with GAD84 (12.4%); the rLA

nonadjuvanted control strain expressing rotavirus antigens exclusively. One mouse from the GAD85 group exhibited high serum neutralization to ETD with a titer of 800; all other mice across groups had no detectable serum neutralization with titers <400 (Supplementary Table S2.8). rLA antigen-specific (VP8-1, VP8Pep) fecal ELISAs were also performed, and no fecal IgA was detected. The serum results indicate that rLA vaccination induces a rotavirus-specific antibody response, which is moderately augmented by adjuvants, and there is some potential for eliciting neutralizing antibodies by probiotic vaccination.

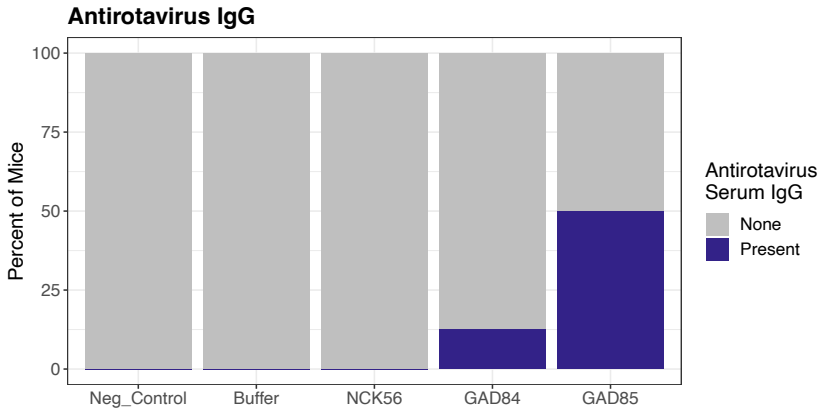

Figure 2.3. Antirotavirus serum IgG titers in the following vaccination. Mice in the negative control, buffer, and NCK56 groups did not have a detectable serum antibody response to the ETD rotavirus strain. A higher percent of mice vaccinated with the rLA strain expressing both antigens and adjuvants (GAD85) had an antiviral IgG response present compared to the rLA strain only expressing antigens (GAD84).

2.3.3. Rotavirus Challenge after Vaccination Boosted Antigen-Specific Immunity

There were no antigen-specific (VP8-1 or VP8Pep) ASC responses detected after vaccination in the control or rLA-immunized mice as measured by FluoroSpot. Total IgA and IgG ASCs for the spleen and MLN are provided in Supplementary Figure S2.3A,B, respectively. To evaluate the impact of the rotavirus challenge on antibody-secreting $CD45^{+}CD19^{+}$ B-cell populations, the mice were orally dosed with either buffer, NCK56, or GAD85 every other week over eight weeks. Two weeks after the final dose, all groups were challenged with 1×10^5 ID_{50} of EC_{WT} rotavirus. Fecal samples were collected daily for six days after infection and tissues for ASC assays were collected at necropsy seven days post rotavirus challenge. Antigen-specific (VP8-1, VP8Pep) cells per 100,000 antibody-secreting (IgA, IgG) $CD45^{+}CD19^{+}$ B-cells were measured in the spleen (Figure 2.4A) and MLN (Figure 2.4B). Insignificant

(adjusted *p*-value: <0.05) comparisons between groups share a common letter. GAD85-vaccinated mice had significantly more antigen-specific splenic antibody-secreting B-cells compared to the buffer and NCK56 control groups for both VP8-1-specific IgA and IgG and VP8Pep IgA (Figure 2.4A; all adjusted *p*-values were <0.05). More VP8Pep IgG-secreting cells were detectable in GAD85 compared to the control groups, but the difference was not significant (all adjusted *p*-values: > 0.05).

GAD85-vaccinated mice generated a VP8-1-specific IgG response in the MLN, which was significantly increased compared to both controls (all adjusted *p*-values: <0.05). The remaining comparisons were found not to be significant between all groups (all adjusted *p*-values: > 0.05). The NCK56 group had detectable but insignificant antigen-specific responses in the spleen and MLN compared to GAD85, and the buffer group had no detectable antigen-specific B-cell responses in either tissue (all adjusted *p*-values: > 0.05). No significant differences were detected between the NCK56 and buffer groups in either tissue (all adjusted *p*-values: > 0.05). Adjusted *p*-values for the spleen and MLN are provided in Supplementary Tables S2.9 and S2.10, respectively. Antigen-specific secreting B-cell populations were boosted after the EC_{WT} viral challenge, and rLA vaccination was able to generate B-cell responses specific to both antigens. The full-length protein was the sole antigen with specific B-cell responses across tissues.

The rotavirus antigen shedding curve and antigen-specific ASC responses in spleen and MLN are provided in Supplementary Figure S2.4 for a separate treatment of mice given three instead of five GAD85 oral immunizations at zero, two, and six weeks before rotavirus challenge at 10 weeks. Despite detectable antigen-specific ASC (Supplementary Figure S2.4A), there was no delay in rotavirus antigen shed (days one-six raw OD values were above the day zero value; Supplementary S2.4B) potentially hinting at the necessity for more rLA doses. Antigen-specific ASC were evaluated in the PP, LI, and FRT by FluoroSpot for mice vaccinated orally with buffer, NCK56, and GAD85 after rotavirus challenge (Supplementary Figure S2.5). There was excessive cellular debris when performing the FluoroSpot assay for these tissues. Multiple wells were therefore discarded during the image analysis quality control step and plates were analyzed with a laxer definition of what constituted a spot to account for the excessive debris. The data should be interpreted with a meteor-sized grain of salt. Briefly, there is mild indication we could plausibly

induce antigen-specific immune responses in additional mucosal tissues (LI, FRT) along with immune inductive sites (PP) using an rLA platform.

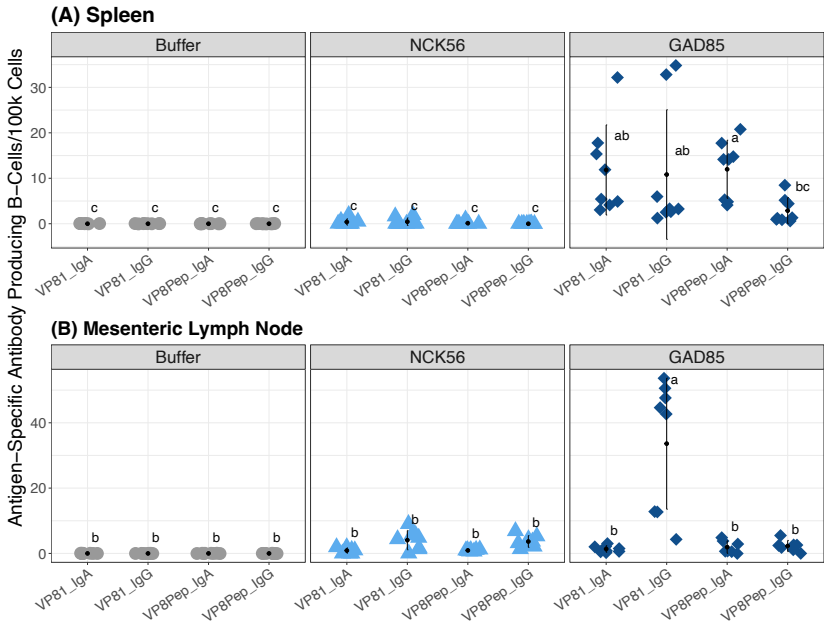

Figure 2.4. Antigen-specific antibody-producing cells per 100,000 CD45+CD19+ B-cells as measured by FluoroSpot in the (A) spleen and (B) MLN. Insignificant comparisons between groups share a common letter (a, b, or c). GAD85 had significantly more antigen-specific B-cell responses compared to both controls in the (**A**) spleen. The VP8Pep-specific IgG trended higher in the GAD85 group, but this difference was not significant. VP8-1-specific IgG was the only antigen-specific response significantly increased in GAD85-vaccinated mice compared to both control groups in the (**B**) MLN. All other responses were not significantly different between groups. The buffer and NCK56 did not differ significantly from one another across tissues. Significant adjusted *p*-values are <0.05 and insignificant are > 0.05 based on a two-way ANOVA followed by Tukey's HSD. MLN: mesenteric lymph node.

2.3.4. rLA Vaccination Delays Rotavirus Shedding

The relative amount of rotavirus antigen shed in feces was quantified by ELISA for six days following the EC_{WT} viral challenge (Figure 2.5A). A Shapiro–Wilk test determined that the data were not normally distributed, and a Kruskal–Wallis test indicated significant differences were detectable between groups (*p*-values: <0.0001; *p*-values provided in Supplementary Table S2.11). Mice vaccinated with GAD85 shed significantly less virus a day following infection compared to both control groups (adjusted *p*-values: 0.029 for buffer and 0.0002 for NCK56) with a 4864 average relative amount of EC_{WT} antigen for GAD85-vaccinated mice, with 147,075 and 429,761 averages for the buffer and NCK56 groups, respectively. Averages rounded to the nearest whole number are provided in Supplementary Table S2.12

and adjusted *p*-values in Supplementary Table S2.13. The percentage of mice positive for EC_{WT} antigen shedding (Figure 2.5B) was determined based on a cutoff three times the standard deviation plus the mean of day zero OD values across groups. Twenty-five percent of GAD85-vaccinated animals were deemed positive for rotavirus antigen shedding on day one postinfection, while 100% in both of the control groups were positive. These results suggest that rLA vaccination can provide some reduction of EC_{WT} rotavirus shedding in vivo.

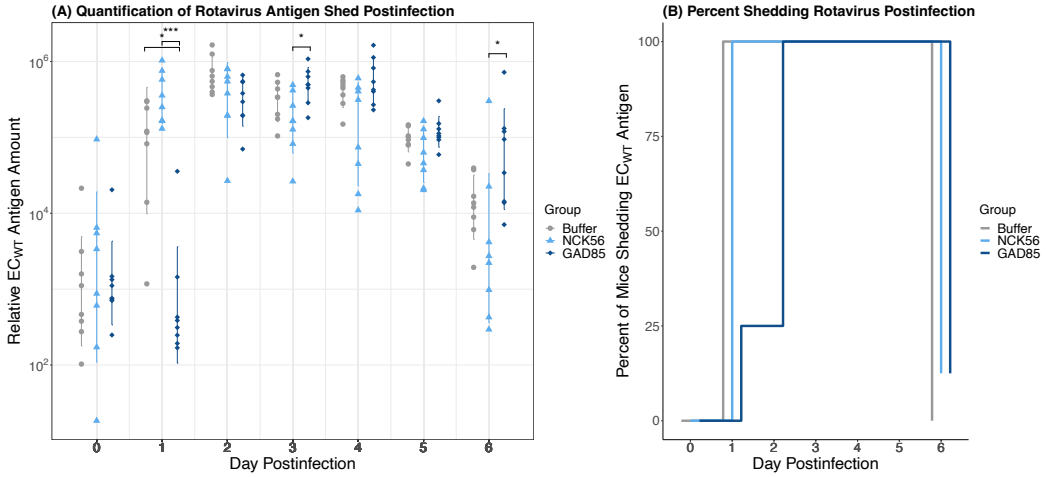

Figure 2.5. Rotavirus ECWT fecal shedding following oral rotavirus challenge. (**A**) Relative amount of EC_{WT} rotavirus antigen shed in fecal samples for six days after viral infection as quantified by ELISA using a standard curve. There is a significant, one-day delay in antigen shedding in the GAD85 group compared to the buffer and NCK56 groups. Statistical analyses were performed on untransformed data, and the y-axis is visualized on a log-10 transformed scale. (**B**) All mice from the buffer and NCK56 groups were positive for antigen shedding by day one, with only 25% of the GAD85 group shedding virus. One hundred percent of mice across groups were shedding virus by day two; 87.5–100% of mice were negative for viral shedding by day six across groups. Adjusted *p*-value: '***' <0.001, '*' <0.05 based on a Dunn's test with Benjamini–Hochburg adjustment.

2.4. Discussion

There is a clear and significant need for next-generation alternatives to the currently available attenuated live human rotavirus vaccines that can address the relatively low efficacy in LMIC (195, 205). The probiotic strain *Lactobacillus acidophilus* is an attractive vaccine candidate due to its safety profile, ability to tolerate the acidic stomach environment, and endogenous interaction with the mucosal immune system (51, 199). In this study, we constructed a novel recombinant LA rotavirus vaccine that expresses two rotavirus antigens and two exogenous adjuvants, then assessed immunogenicity and efficacy after oral

immunization and viral challenge. This is the first rLA rotavirus platform, to the authors' knowledge, that delivers multiple viral antigens and mucosal adjuvants in combination.

Vaccination with rLA-induced VP8 antigen-specific ASC and whole rotavirus-specific IgG immune responses. A greater percentage of GAD85-immunized mice were seropositive for rotavirus compared to mice in the GAD84 nonadjuvanted control group. This suggests that the adjuvants FliC and FimH are potentially important for rLA immunogenicity, resembling the established role of adjuvants described for other mucosal vaccines (199, 221). Although antigen-specific ASCs were not detected in the control or the rLA groups following vaccination, mice vaccinated with GAD85 exhibited ASC responses specific to both the rotavirus VP8 peptide and protein antigens in systemic (spleen) and local (MLN) lymphoid tissues seven days after viral challenge with EC_{WT}. This indicates that memory B-cells were primed during vaccination and the immune response was activated after rotavirus infection. It was surprising that antigen-specific ASC responses were not detected after vaccination alone. It has been demonstrated that the detection of rotavirus-specific memory B-cells in tissues like the spleen may require ongoing antigen stimulation (190). We have previously shown that recombinant probiotics are cleared from the gastrointestinal tract by 72 hours postdelivery (222). Therefore, rotavirus antigen would no longer be present in tissues two weeks after the final full vaccination, making it likely the levels of rotavirus-specific ASC in the spleen and MLN would be low and possibly below the level of detection of the FluoroSpot assay. The levels of ASC we detected after the challenge are comparable to those seen in other animal models (223, 224). Additionally, antigen-specific fecal IgA was not detected by ELISA. It should be noted that these results were difficult to interpret due to the high background and limited sample availability. BALB/c mice are known to have abundant polyreactive IgA antibodies, which can obscure the detection of vaccine-induced antigen-specific responses (225). The presence of the antigen-specific IgA B-cells, indicating IgA induction, on FluoroSpot is a reasonable proxy for fecal IgA detection by ELISA. Additional studies are required to phenotypically characterize rotavirus-specific B-cell populations in lymphoid tissues and effector sites, particularly the intestinal lamina propria (150, 190).

In this study, mice were immunized with an rLA vaccine expressing antigens from the VP8* capsid protein sequence from the EDIM rotavirus strain (G3[P16] genotype) and were challenged with the homotypic yet different EC_{WT} strain (G3[P16]) (119, 226). We saw a one-day delay of fecal viral antigen shedding in the GAD85-immunized group, indicating the potential of our rLA construct to generate modest, though neither complete nor robust, protective immune responses against other homotypic rotaviruses. Current rotavirus vaccines are generally protective against both monotypic and heterotypic circulating rotavirus strains yet offer slightly less protection for partially or fully heterotypic strains (227, 228). It is likely that alternative or combination antigens other than VP8* alone may prove more immunogenic and ultimately protective. This is supported by the early closure of a clinical trial evaluating the efficacy of a P2-VP8 subunit injectable vaccine that did not provide improved protection against severe rotavirus diarrhea compared to the currently approved oral vaccines (ClinicalTrials.gov ID NCT04010448) (229-231). Although supplementation with wild-type probiotic strains including LA NCFM has been shown to delay rotavirus shedding in animal models and human infants (54, 232), this was not observed in the analogous NCK56 group. This may be due to the timing of vaccination since mice in this study received their final dose of the NCK56 wild-type control strain two weeks before the challenge.

A limitation of our study is an inability to assess protection from clinical disease, as we used an adult murine model. Adult mice do not display clinical symptoms of rotavirus infection (e.g., presence and prolonged duration of diarrhea and pathology characteristic of rotavirus) (56). We were therefore restricted to using rotaviral antigen shedding as a proxy for measuring rLA-induced protection from disease. Nevertheless, BALB/c mice are a conventional small-animal model of rotavirus infection, as neonates have been studied since 1947 and the adult model was established in 1990 (106, 233). Studying adaptive immunity is critical for vaccine development and can be more readily evaluated in adult mice as neonates must be infected within approximately 10 days of birth to observe clinical disease (233). Assessing the rLA rotavirus vaccine's potential to abate morbidity and mortality is necessary. To this end, using a neonatal pig model is a logical next step in our vaccine development, as they show clinical symptoms and can be infected with human rotavirus strains (56, 191).

2.5. Conclusions

This study highlights the promise of engineering the probiotic *Lactobacillus acidophilus* as a next-generation rotavirus vaccine to help overcome barriers against mucosal immunization. Future studies using relevant animal models will determine if this oral vaccine approach can address the reduced effectiveness observed in LMIC with current rotavirus vaccines (8).

CHAPTER 3: METAGENOMIC AND METATRANSCRIPTOMIC CHANGES AT AN IMMUNE INDUCTIVE SITE FOLLOWING VACCINATION WITH *LACTOBACILLUS ACIDOPHILUS*

3.1. Overview

Probiotic species including lactic acid bacteria (LAB) are enticing as next-generation, orally-delivered vaccine platforms for activating the gut-associated lymphoid tissue (GALT) to generate protective mucosal immunity against rotavirus (67). Effective probiotic-based vaccines should not adversely disrupt the resident microbiome while still interacting with immune inductive sites such as Peyer's patches for effective GALT activation. Multi-omics technologies provide a high-throughput approach to investigate such vaccine-microbiome interactions. Here, C57BL/6J mice were administered a novel recombinant *Lactobacillus acidophilus* (rLA; GAD85 strain) vaccine platform expressing two rotavirus antigens along with both FliC and FimH as adjuvants (60, 206). Control groups included mice administered wild-type *Lactobacillus acidophilus* (LA; NCK56 strain) or buffer only. Groups were vaccinated by oral administration both 24-hours and one-hour prior to sample collection. DNA and RNA were extracted from a small intestinal slice which included a Peyer's patch and any resident microbiome for metagenomic and metatranscriptomic analyses. Chapter 3 describes a multi-omics evaluation of responses between the host microbiome and exogenous rLA to potentially improve future next-generation vaccine development.

3.2. Introduction

The mucosal immune system is dynamic and contributes to host response to enteric infection and mucosal vaccination. The mucosa-associated lymphoid tissue (MALT) includes the nasopharynx-associated lymphoid tissue, the bronchus-associated lymphoid tissue, and the GALT, the latter of which comprises most of the MALT (234) . Peyer's patches are critical immune inductive sites within the broader GALT that interact with the intestinal microbiome to sample antigen from the gastrointestinal tract (GI) to identify friends from foes (137). This direct sampling of the intestinal lumen is unique to the GALT which is not reliant on afferent lymphatics (235). Peyer's patches are exposed to antigen from the GI tract via microfold (M) cells embedded within the overlying follicle-associated epithelium (FAE). M cells can

sample the lumen through phagocytosis which can be mediated by bacterial binding to proteins on the cell surface such as glycoprotein-2 (GP2) which is responsible for fimbrial FimH adhesion-expressing bacterial uptake (235). Communication and antigen trafficking between M cells, the FAE and Peyer's patches are facilitated by antigen presenting cells (APC) including dendritic cells (DCs). The traditionally protective mucus layer is relatively thin around M cells due to few mucus-producing goblet cells within the FAE, permitting accessibility to contents of the gut lumen which also leaves M cells vulnerable to pathogen invasion (234). Given their uniquely intimate relationship, the resident microbiome is key in developing mucosal immunity via the onslaught of antigen exposure due to the density of microbes present in the GI tract (236). For example, antibiotic exposure disrupting the resident microbiome can prove deleterious to early immune system development, including B-cell and secretory IgA production (237). Dysbiosis – abnormal perturbation of the microbiome – can promote deleterious physiological outcomes including diabetes and forms of cancer (238). The host immune system and resident microbiome communicate to regulate enteric pathogens and intestinal homeostasis (4-6).

For effective mucosal immunization, an orally-delivered probiotic vaccine platform would need to directly interact with and express relevant antigen at inductive sites like Peyer's patches to generate vaccine-specific and potentially protective immune responses including antigen-specific ASC (239). LAB are enticing vaccine candidates for this reason since they can interact with innate immune cells' pathogen recognition receptors (PRRs) via expression of microbe-associate molecular patterns (MAMPs) including lipoteichoic acid and the muramyl dipeptide of peptidoglycan (199). Specifically, the LA NCFM surface-layer protein SlpA interacts with DCs through DC expression of the PRR DC-specific intercellular adhesion molecule 3-grabbing nonintegrin (DC-SIGN) (240). Additionally, commensal probiotic bacteria can adhere to the intestinal mucosa to outcompete pathogens while also stimulating mucin expression to prevent pathogen colonization (241). Probiotics can also induce host heat shock protein expression for reducing apoptotic and stress responses within the intestine (242, 243). *Lactobacillus*-based vaccines are notably capable of generating mucosal immune responses to a variety of pathogens that infect within and outside of the GALT (59, 102, 200, 244). *Lactobacillus* spp. have historic precedence for innate enteric disease

prevention and are also genetically malleable for expressing cytoplasmic, secreted, or surface-displayed exogenous antigen to generate adaptive immune responses (245, 246).

The term "multi-omics" encompasses analyses that integrate some combination of high-throughput methodologies that can include metagenomics, metatranscriptomics, metabolomics, lipidomics, and proteomics. High-throughput technologies have evolved from 16S rRNA sequencing just before the turn of the century to single-cell sequencing about two decades later (238). The amount of microbiome-related metatranscriptomics projects alone has increased dramatically over the past couple of decades (247). Meta-omics as a field has expanded rapidly to a US $1.7 billion market since 2010 (248) – and for convincing reasons. Multi-omics permits a functional, interweaved, culture-independent, and somewhat unbiased understanding of host-microbiome relationships in healthy and diseased states. There is specific interest in applying meta-omics analyses to studies involving probiotic species given the relevance of these beneficial microbiome commensals to human health (249). Specifically, meta-omics can help our understanding of ecological niches and reveal inherent genetic diversity among common probiotics like LAB, of transcriptional regulation at the species and community levels, and the impact of microbial metabolic endotype on the host (249).

In Chapter 2, we demonstrated that an orally delivered rLA rotavirus vaccine platform provides moderate protection and induces vaccine-specific immune responses in an adult murine challenge model. We have also established previously that our selected adjuvants (e.g. FimH) can help traffic rLA to immune inductive sites (206), and that $CD11c^+$ DCs are required for effective rLA-induced mucosal immunogenicity (250). However, we lack cross-sectional understanding of how our probiotic vaccine and the resident microbiome reciprocally respond after oral delivery into the GALT. In this study, we sought to apply a subset of the aforementioned 'omics techniques in a novel system for multidimensional evaluation of interactions between the resident microbiome and an oral recombinant probiotic vaccine at an immune inductive site. This interaction is particularly relevant as the rLA strain GAD85 expresses exogenous mucosal adjuvants and viral antigens along with the endogenous MAMPs described above, together capable of activating the host innate and adaptive immune system (199, 250). Therefore, in the subsequent Chapter

3 we performed metatranscriptomic and metagenomic analyses on sequencing data from excised Peyer's patches containing digestive content inclusive of the resident microbiome following two immunizations within 24-hours with one of three treatments: buffer, wild-type LA strain NCK56, and rLA strain GAD85.

3.3. Materials and Methods

3.3.1. Animal Ethics Statement

This study was carried out in accordance with the ARRIVE guidelines (https://arriveguidelines.org) and the Guide for the Care and Use of Laboratory Animals of the National Institutes of Health. All protocols involving animals were approved by the Institutional Animal Care and Use Committee of Colorado State University (IACUC protocol #18-1234A). Animals were kept in specific pathogen free conditions and monitored daily for clinical signs of illness or stress. They were provided autoclaved bedding, enrichment and irradiated rodent chow (Teklad Global, Envigo, Indianapolis, IN, USA). Mice were housed in individually ventilated cages with eight-hour light/dark cycles. Animals had access to food and water ad libitum.

3.3.2. Experimental Design

Eighteen, 6–8-week-old, C57BL/6J mice (Jackson Labs, USA) were assigned equally male and female to each treatment group (Table 3.1). Mice in the experimental group received the rLA rotavirus probiotic vaccine construct GAD85. GAD85 expresses two rotavirus antigens from the VP8* domain of the VP4 capsid protein from the murine rotavirus EDIM strain. The expressed antigens are a pseudo full-length 206 amino acid protein (VP8-1) and a ten amino acid peptide (VP8Pep); their amino acid sequences are provided in Supplementary Table S2.2 (203). The rotavirus antigens are expressed in combination with two adjuvants, Toll-like receptor (TLR) 4 ligand FimH and TLR5 ligand FliC. Methodology for the construction of GAD85 is as previously described (60). The positive control group received a wild-type LA strain (NCK56) which neither expresses antigens nor adjuvants. NCK56 is a descendent of the LA NCFM

human intestinal isolate and has plasmid-conferred erythromycin (Erm) resistance (60). The negative control group received only the buffer used to resuspend the probiotic strains.

Table 3.1. Treatment groups. Male and female C57BL/6J mice were assigned evenly per treatment group for a total of $n = 6$ per treatment. However, during the study, a female buffer-treatment mouse was lost due to natural causes. The *Lactobacillus acidophilus* (LA) treatment groups either received a wild-type positive control LA or a recombinant LA probiotic vaccine construct.

Treatment	Description	Male	Female
Buffer	Bacterial Resuspension Buffer	3	2
NCK56	Wild-type Lab Strain of *Lactobacillus acidophilus*	3	3
GAD85	Recombinant *Lactobacillus acidophilus* Vaccine Expressing Dual-Rotavirus Antigens and Dual-Mucosal Adjuvants	3	3
Total		9	8

3.3.3. Animal Immunization and Sample Collection

The GAD85 and NCK56 strains were grown overnight in MRS broth (BD Diagnostics, Sparks, MD, USA) supplemented with 5 μg/ml Erm (Teknova, Hollister, CA, USA). Overnight cultures were grown to exponential and washed twice in PBS (Corning). GAD85 and NCK56 strains were individually resuspended to a concentration of 5 x 10^9 CFU per 200 μl of soybean trypsin inhibitor (Sigma-Aldrich, Inc., St. Louis, MO, USA) buffer containing 100 μm sodium bicarbonate ($NaHCO_3$). All mice were immunized by oral gavage with 200 μl of either buffer alone, NCK56, or GAD85 both 24-hours and one-hour prior to sample collection. Mice were euthanized by CO_2 overdose and exsanguination 1-hour after the final dose (Figure 3.1). The entire small intestine was initially collected in RPMI (Cytiva, Marlborough, MA, USA) media supplemented with 1% pen/strep (Hyclone, Logan, UT, USA), and 0.1% gentamicin (Sigma-Aldrich). A section of ileum containing a single Peyer's patch most proximal to the cecum along with any digestive content present was cut using a sterile razor blade and added to 10X the tissue weight in DNA/RNA Shield (Zymo Research, Irvine, CA, USA). Tissue slices were stored at **-80 °C** until nucleic acid extraction.

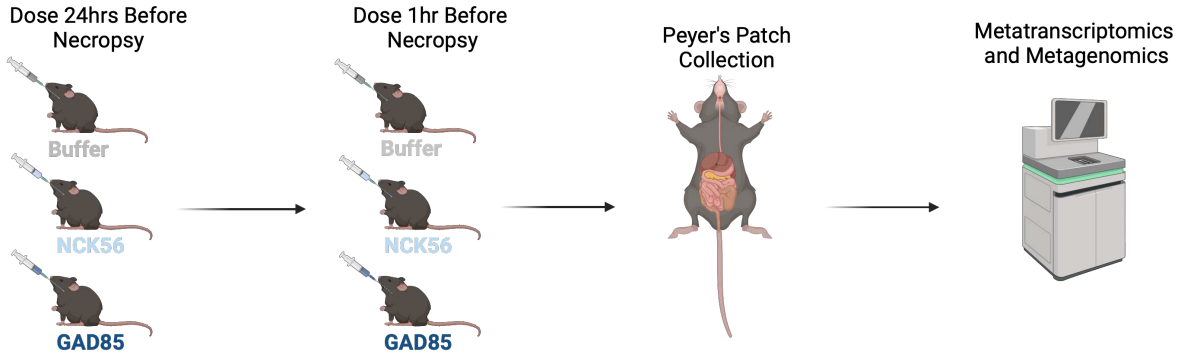

Figure 3.1. Experimental design. C57BL/6J Mice were immunized by oral gavage with either buffer (grey; n = 5), the wild-type LA strain NCK56 (light blue; n = 6) or the rLA vaccine strain GAD85 (dark blue; n = 6) 24-hours and one-hour prior to necropsy. At the time of necropsy, a singular Peyer's patch was excised from the small intestine to evaluate host-microbe interactions at an immune inductive site. All digestive content associated with the small intestinal tissue was retained. DNA and RNA was extracted from the Peyer's patch tissue for metagenomic and metatranscriptomic sequencing, respectively.

3.3.4. Nucleic Acid Extraction and Sequencing

DNA and RNA was extracted from the murine small intestinal tissue slices containing a Peyer's patch and digestive content using the Zymo *Quick*-DNA/RNA Miniprep Plus Kit (Zymo) following manufacturer's instructions. Briefly, samples were homogenized by bead beating for 60 seconds in 2mm tubes (Zymo) using an MP Bio FastPrep-24 high-speed homogenizer (MP Biomedicals, Santa Ana, CA, USA). The suggested DNase I step was completed. Samples were eluted in 100 µl of nuclease-free water that was included with the kit. DNA and RNA quantification was completed using a Qubit 4 fluorometer (ThermoFisher Scientific, Waltham, MA, USA) following manufacturers' instructions for the 1x dsDNA High Sensitivity Assay (ThermoFisher Scientific) and RNA Broad Range Assay (Thermo Fisher Scientific), respectively. Extracted nucleic acid was stored at -80 °C and shipped on dry ice for sequencing. Novogene (Novogene Corporation Inc., Sacramento, CA, USA) performed metagenomic sequencing with a target sequencing depth of 6Gb (20M, 2 x 150 paired-end reads) per-sample. Metatranscriptomic (Novogene Co., Ltd., Chaoyang District, Beijing, China) sequencing was performed with a target sequencing depth of 12Gb (40M, 2 x 150 paired-end reads) per-sample. All sequencing was performed on an Illumina NovaSeq 6000 (Illumina, San Diego, CA, USA).

3.3.5. Quality Control of Sequencing Data

All subsequent analyses were performed on MacOS. Statistical analyses and data visualization were performed in R (v.4.3.1) (126) and RStudio (v.2023.06.1+524) (127) unless stated otherwise. Quality of raw, paired-end shotgun metagenomic and metatranscriptomic 2 x 150bp reads provided by Novogene were evaluated with FastQC (v0.11.9) (251). Sequencing adapters were removed and the resulting sequences were quality trimmed using trimmomatic v.0.39 (252) with the parameters: ILLUMINACLIP:adapters:2:30:10 SLIDINGWINDOW:4:15 AVGQUAL: 20 MINLEN:70 (252). Adapter sequences are provided in Supplementary Table S3.1.

3.3.6. Metagenome Assembled Genomes (MAGs)

An average of 1506918.4 reads were trimmed. DNA reads mapping to the C57BL/6J host genome (GCF_000001635.27_GRCm39_genomic.fna) were separated from non-host reads using Burrows-Wheeler Aligner MEM (BWA; v. 0.7.17-r1188) (253). Reads that did not map to the host were presumed to be primarily microbial. Host-unmapped files were sorted and processed with samtools (v.1.12) (254), bedtools (v.2.30.0) (255), and seqtk (v.1.3-r106) (256). *De novo* assembly of contigs across samples was performed using the de Bruijn graph algorithm assembler metaSPAdes (v. 3.15.5) (257) with the default 21, 33, 55 kmers setting to maximize the number of contigs recovered for metagenome assembled genomes (MAGs). Quality of assemblies from metaSPAdes was evaluated using metaQuast (v. 5.0.2) (258) with option -f. In preparation to align the trimmed, quality-filtered microbial paired-end reads back to the contig scaffold produced by metaSPAdes, disordered samples were reordered using the bbmap (v. 38.79) (259) Repair_Align.sh script. Sample reads were then aligned to their respective sample contig scaffolds using BWA MEM (v. 0.7.17-r1188) (253), while samtools (v.1.12) (254) was used to create and index the resulting bam files. MAG contigs were binned using Metabat2 (v. 2.15) (260) with option -m 1500 and binning quality was evaluated with CheckM (v. 1.2.1) (261) lineage_wf. Kraken2 (v. 2.1.2) (262) was used for taxonomical identification of MAGs using the Kraken-specific database. GAD85 sample four used the --only-assembler metaSPAdes option due to a common issue that can prevent samples from running (https://github.com/ablab/spades/issues/152). Merged paired-end, non-host metatranscriptomic reads per

sample were mapped back to sample-matched MAGs with a 50% minimum completeness and <5% contamination as evaluated by CheckM (v. 1.2.1) (261) from the bin_stats _ext.tsv output using BWA MEM to quantify number of metatranscriptomic reads mapped per sample MAG.

3.3.7. Metatranscriptomic Functional Analyses

RNA reads were again aligned to the C57BL/6J reference genome (GCF_000001635.27_GRCm39_genomic.fna) using the BWA MEM (v.0.7.17-r1188) to separate reads mapping to the murine host genome from unmapped reads that were presumed to be microbial. The unmapped reads were analyzed with the simple annotation of Metatranscriptomes by sequence analysis 2 (SAMSA2) pipeline (v.2.2.0) (263) without using SortMeRNA (264). SAMSA2 (263) performed functional annotations of the reads. The R scripts included with SAMSA2 were used to analyze fold-change differences in identified proteins with their default settings. The R scripts are available on the SAMSA2 GitHub (https://github.com/transcript/samsa2).

3.3.8. VP8-1 Protein Antigen Transcript Detection

The R1/R2 merged metatranscriptomic reads per sample from the PEAR (265) output of the SAMSA2 pipeline (v.2.2.0) (263) were converted to FASTA format using seqtk (1.3-r106). Using these merged reads, a custom database was then generated per sample in Geneious Prime v.2019.2.3 for MacOS (https://www.geneious.com). The VP8-1 amino acid sequence (Supplementary Table S2.2) was aligned to each of these custom sample databases for antigen detection from metatranscriptomic reads in the buffer-, NCK56- and GAD85-vaccinated samples. The read pile-up per amino acid position of the antigen was visualized using the ggplot2 (128) R package for the samples where antigen was detected.

3.3.9. Metatranscriptomics α- and β-Diversity Quantification

Kraken2 (v. 2.1.2) (262) was used for phylogenic analysis of non-host metatranscriptomic reads. Unmapped reads were annotated with Kraken2 and the resulting .tax files were converted to .txt files using

the kreport2mpa.py script prior to statistical analyses and visualization. Bracken (266) may be used for follow-up analysis to potentially improve species-level identification and abundance estimates, but the database was not structured to perform this analysis. Bracken is not required but recommended (267). Custom R scripts developed by the Dr. Zaid Abdo lab (https://github.com/Abdo-Lab) to analyze α- and β-diversity, statistical analyses, and for data visualization as described previously (201, 268). The α-diversity metrics included inverse Simpson, richness, and Shannon diversity, along with individual sample species bar plots (269). The β-diversity was measured using Principal Coordinates Analysis (PCoA) and log-fold change analyses. Briefly, rarified richness was calculated using the vegan R package (270) and Shannon diversity with the phyloseq package (271). After normalizing with cumulative sum scaling (CSS), PCoA plots were visualized with vegan (270) using Bray-Curtis dissimilarity with 95% confidence ellipsoids. The metagenomeSeq package (272) was used for determining significant log fold-changes between groups with FDR-adjusted *p*-values using the eBayes function from the limma (273) package. The ggplot2 package (128) was used for data visualization.

3.3.10. *Lactobacillus acidophilus* NCFM Gene Expression Analysis

The annotated LA NCFM genome (backbone from which the GAD85 and NCK56 strains were constructed) GFF3 file was downloaded from NCBI (accession CP000033.3) and converted to the GTF format using the AGAT agat_convert_sp_gff2gtf.pl script (v1.0.0) (274), then indexed using STAR (v.2.7.10b) (275) genomeGenerate. STAR was also used to align metatranscriptomic reads across samples that failed to map to the C57BL/6 host genome to the indexed LA NCFM genome. The resulting SAM files were converted to BAM format using Samtools sort (v.1.7) (254) and HTSeq-count (v.2.0.3) (276) was used to determine the number of reads mapping to each identified gene per sample with options -i gene_id --additional-attr product. The DESeq2 (277), EnhancedVolcano (278), and ggplot2 (128) R packages were used for calculating differential gene expression and data visualization. pCutoff was set to 0.05 using adjusted *p*-values and the FCcutoff set to 1 (absolute value) when using the EnhancedVolcano package.

The LA genome available on NCBI was used instead of annotating the 91.36% MAG as the MAG was only specific at the genus level of *Lactobacillus*.

3.4. Results

3.4.1. Rotavirus Antigen Transcript is Detected in rLA-Vaccinated Mice

Control (buffer, NCK56) and GAD85-exposed metatranscriptomic reads were converted into individual custom Geneious databases per mouse sample. The rLA VP8-1 antigen amino acid sequence (Supplementary Table S2.2) was aligned to each of the individual sample databases. The pile up of reads where a match between database and the antigen that was detected is represented in Figure 3.2 for buffer samples 1-3 (teal, yellow, pale purple), NCK56 sample 4 (fuchsia), and GAD85 samples 1-6 (red, blue, orange, green, pink, and grey). There was a maximum of 668 reads across all GAD85 samples for an amino acid (position 48); however, there was a maximum of only three reads per any amino acid for samples in either control group (NCK56 and buffer). There were 84,137 total reads mapping to the antigen amino acid sequence across all GAD85 samples and 247 total reads between the control groups combined. These results demonstrate that the murine rotavirus EDIM VP8-1 epitope was only robustly detected in the small intestinal microbiome of mice exposed to the recombinant vaccine (GAD85), and that antigen expression is successfully detected at a mucosal site where immune induction occurs.

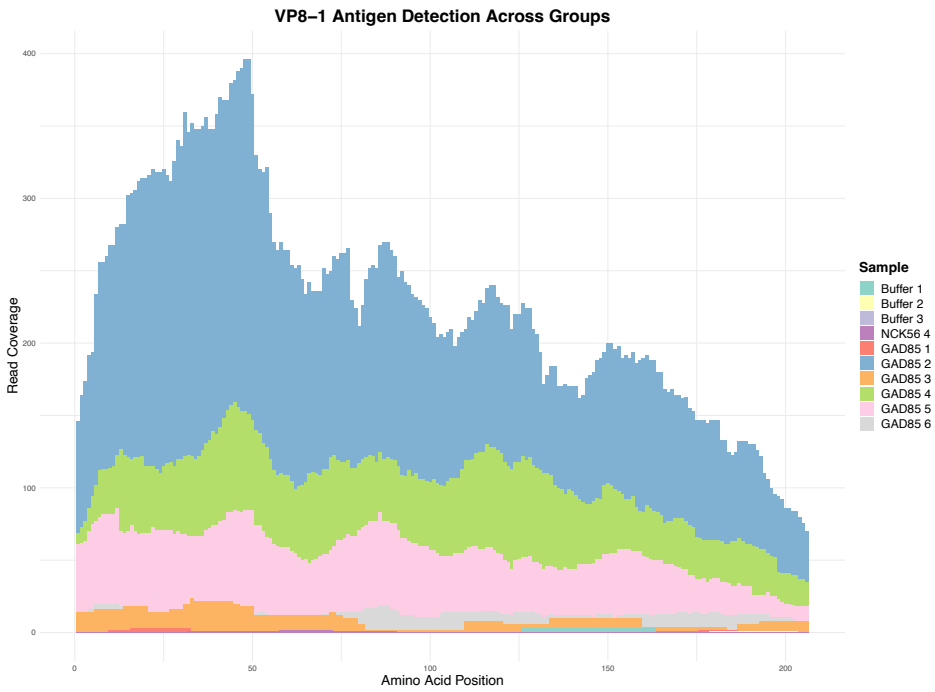

Figure 3.2. Read pile-up of VP8-1 rotavirus antigen transcripts. The 206 amino acid antigen sequence was mapped back to custom Geneious databases made per sample from the merged R1/R2 metatranscriptomic reads to detect antigen expression. The VP8-1 rotavirus antigen amino was only detected in GAD85-vaccinated mice, as demonstrated by the pile-up of reads. The amino acid position of the antigen is along the x-axis and the number of reads per sample matching to that amino acid is represented by the y-axis.

3.4.2. Differential Gene Expression from the LA NCFM Genome Between LA-Vaccinated Samples

Differential gene expression of the LA NCFM genome was determined by mapping the presumed microbial metatranscriptomic sequencing reads from NCK56- and GAD85-exposed samples to an indexed NCBI LA NCFM genome (accession CP000033.3). There are 64 identified genes that differ significantly (adjusted *p*-value of <0.05) between mice orally immunized twice before necropsy with either the recombinant or wild-type probiotic (Figure 3.3). Genes above a logFC of |1| and an adjusted *p*-value <0.005 appear red in Figure 3.3. The significant genes, log fold-change (logFC) values, and adjusted *p*-values are provided in Supplementary Table S3.2.

Significantly upregulated genes in GAD85-vaccinated mice compared to the NCK56 group are related generally to environmental stress responses. Environmental stressors can include bile exposure and dramatic changes in temperature and pH, conditions often encountered in the mammalian GI tract (279). There is a significant overexpression of the class I heat shock proteins (HSP) DnaK (logFC: 0.83, adjusted

p-value: 0.041), DnaJ (logFC: 0.93, adjusted *p*-value: 0.011), and GrpE (logFC: 1.23, adjusted *p*-value: 0.002) which form a chaperone complex to reconstruct denatured proteins (280, 281). These HSPs are regulated by the DNA-binding protein HrcA, an autorepressor which was also upregulated (logFC: 1.58 and adjusted *p*-value: <0.0001) in GAD85-vaccinated mice. HrcA is most likely inactive due to successful HSP expression and HrcA must be bound to GroEL to be conformationally capable of binding and repressing (280). The Clp-ATPase ClpE, responsible for degrading destructed proteins and also HrcA-dependent in *Lactobacillus acidophilus*, is also overexpressed (logFC: 1.42 and adjusted *p*-value: 0.002) (282). NusA (logFC: 1.03, adjusted *p*-value: 0.001) and the ribosome binding factor A RbfA (logFC: 1.25, *p*-value: <0.0001) are cold-shock response proteins (283). RbfA regulates a cold-sensitive mutation to help permit cell growth (284, 285). Ribosome maturation factor RimP (logFC: 1.38, adjusted *p*-value: 0.005) is under the same operon as RbfA and is similarly upregulated to RbfA (286). Additionally, the rLA group exhibited an overexpression of genes related to pyrimidine synthesis/metabolism, including aspartate carbamoyltransferase (PyrB; logFC: 2.59, adjusted *p*-value: 0.0002), bifunctional protein PyR (logFC: 1.53, adjusted *p*-value: 0.001) and dihydroorotase (logFC: 1.76, adjusted *p*-value: 0.0046). This could be in response to exposure to air after growing in anaerobic conditions (287).

Genes significantly downregulated in GAD85 compared to NCK56 are related to carbohydrate metabolism, including the PTS system cellobiose-specific EIIB (logFC: -1.13, adjusted *p*-value: 0.002), glucose-specific EIIA (logFC: -1.12, adjusted *p*-value: 0.012), and maltose-specific EIICB (logFC: -1.46, *p*-value: 0.027). 6-phospho-beta-glucosidase (logFC: 1.15, adjusted *p*-value: <0.0001) and enolase (logFC: -2.33, adjusted *p*-value: <0.0001) also contribute to metabolism and are downregulated as well (288-291). Genes related to translation and ribosome structure were downregulated in the GAD85 group, including Glutamyl-tRNA(Gln) amidotransferase subunit A (logFC: -1.53, adjusted *p*-value: <0.0001), Aspartyl/glutamyl-tRNA(Asn/Gln) amidotransferase subunit B (logFC: -1.22, adjusted *p*-value: <0.0001), and Proline--tRNA ligase (logFC: -0.93, adjusted *p*-value: <0.0001) (292). Additionally, the ABC transporter glutamine-binding protein GlnH (logFC: -0.73, adjusted *p*-value: 0.0009), the glutamine transport ATP-binding protein GlnQ (logFC: -0.73, adjusted *p*-value: 0.014) , and the putative glutamine

ABC transport system permease proteins GlnM (logFC: -1.31, adjusted *p*-value: <0.0001) and GlnP (logFC: -0.86, adjusted *p*-value: 0.011) were downregulated, potentially indicating amino acid metabolism/acquisition is deprioritized. Our results may indicate prioritization of certain biological processes (e.g. heat shock response, pyrimidine synthesis) over others (carbohydrate metabolism) in rLA when transitioning environments coupled with potential niche metabolic demands of expressing antigens and adjuvants.

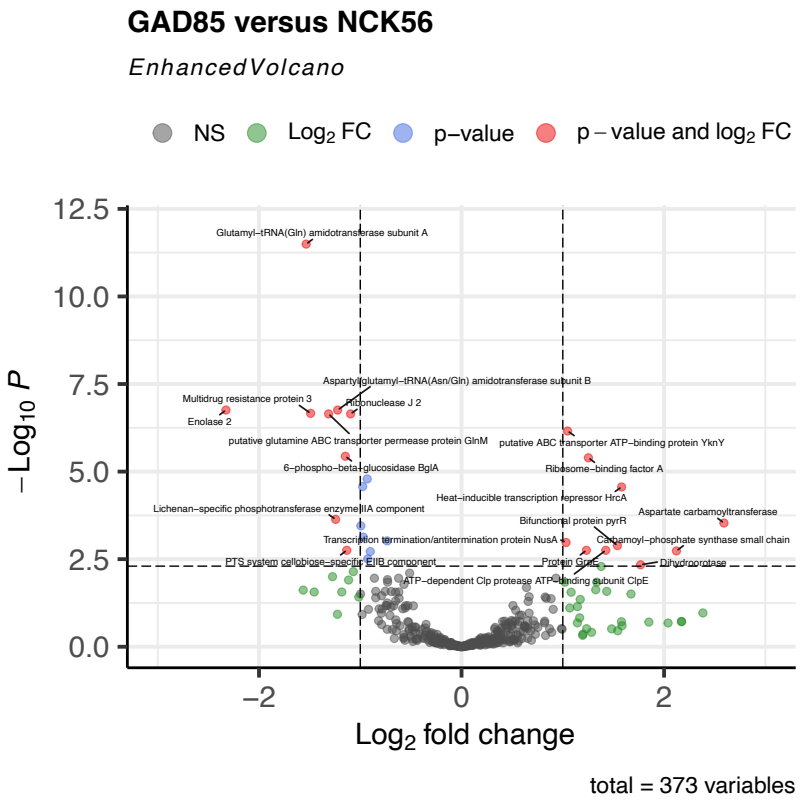

Figure 3.3. Volcano plot of differentially expressed genes in mice vaccinated with the rLA probiotic strain GAD85 as compared to the wild-type control NCK56-vaccinated mice. The red, green, and blue points represent differences in magnitude and significance of the identified genes, where red indicates genes above both the logFC (|1|) and adjusted *p*-value (0.005) thresholds. Blue and green points are only above either the adjusted *p*-value or logFC thresholds, respectively, and grey points are non-significant by either parameter. rLA: recombinant *Lactobacillus acidophilus*, logFC: log fold-change.

3.4.3. Adjuvants are Detected in the Metatranscriptome of rLA-Vaccinated Mice

The holistic metatranscriptome was characterized by the SAMSA2 (263) pipeline. There are 30 significant (adjusted *p*-values <0.05) transcripts differentially expressed between the metatranscriptomes

of mice immunized with either NCK56 or GAD85 (Supplementary Table S3.3). Additionally, there are 1707 significant transcripts (adjusted *p*-values <0.05) expressed differentially between the NCK56 and buffer groups, and 408 transcripts between GAD85 and buffer (top-30 significant genes are provided per comparison in Supplementary Tables S3.4 and S3.5, respectively). Such disparity in significant transcripts identified could reflect that NCK56 and GAD85 share the same genomic backbone (LA NCFM). Thus, given the dominance of LA in these microbiomes, the entire metatranscriptome will inherently have less differences when the two probiotic-exposed groups are compared than when either is compared to the buffer group.

The FliC (flagellin) adjuvant is expressed on a plasmid exclusively by the rLA construct and was also significantly more expressed in the GAD85 group as compared to NCK56 (Figure 3.4A; logFC: 13.89, adjusted *p*-value: <0.0001). Additionally, "flagellin, Partial" was detected significantly more in GAD85 than NCK56, potentially due to truncated reads mapping to FliC (logFC: 10.91, adjusted *p*-value: <0.0001). FliC was also significantly overexpressed in GAD85 when compared to buffer (logFC: 11.35, adjusted *p*-value: <0.0001); however, was not detected in NCK56 when compared to buffer as expected. The other mucosal adjuvant expressed by rLA, TLR4 agonist *E. coli* FimH, was expressed significantly more in the GAD85 samples than NCK56, both as the fimbrial protein (logFC: 4.81, adjusted *p*-value: 0.0009; Supplementary Table S3.3) and fimbrial protein FimH (logFC: 6.51, adjusted *p*-value: 0.02). The S-layer (surface-layer) protein is over-expressed in both GAD85 (Figure 3.4B,C; logFC: 11.04, adjusted *p*-value: <0.0001) and NCK56 (logFC: 11.88, adjusted *p*-value: <0.0001) when each was compared to the buffer group individually. Additionally, mucus binding protein was over-expressed in both NCK56 (logFC; 1.15, adjusted *p*-value: <0.0001) and GAD85 (logFC; 3.41, adjusted *p*-value: 0.036) when compared to buffer. These results demonstrate that adjuvant expression from rLA can be successfully detected at a mucosal inductive site using a metatranscriptomic sequencing approach. Additionally, they collectively highlight the impact of exogenous LA on the resident metatranscriptome.

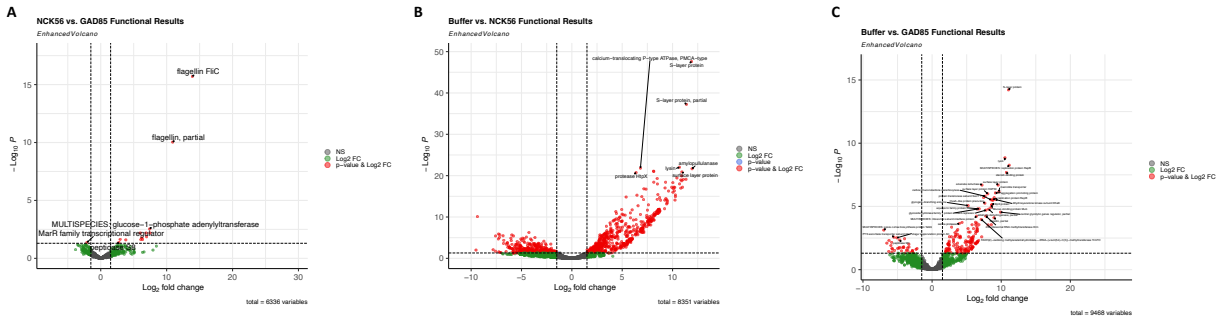

Figure 3.4. Volcano plots comparing differential putative protein expression of the whole metatranscriptome from buffer-, NCK56-, and GAD85-vaccinated mice using the SAMSA2 pipeline with default thresholds (1.5 logFC and 0.05 adjusted p-value) (263). Significantly differentially expressed transcripts are in red and transcripts of interest are labeled. LogFC: log fold-change.

3.4.4. MAG Assembly is Limited to Dominant Species

Metagenome assembled genome (MAGs) contigs were first assembled using metaSPAdes (257) with default settings of 21, 33, 55 kmers. The only contig assembled with moderate genome completeness across samples was the *Lactobacillus acidophilus* NCFM strain with an average of 43% completeness across samples (Figure 3.5A; dark pink). The LA NCFM genome was not assembled in any of the buffer group samples (zoomed-in plot in Figure 3.5A) which was exposed to neither the wild-type nor recombinant LA probiotic. The assembled MAGs were binned using metaBAT2 (260). After binning, there was no strain-level and the only bins with high genome completeness (defined as > 50% and <5% contamination) were identified either at the genus *Lactobacillus* (Figure 3.5B; deep purple) or *Bacteriodales* order (Figure 3.5B; grey) levels in a majority of the GAD85 samples and one NCK56 sample. The black dots on Figure 3.5B represent the percent of metatranscriptomic reads per sample that were able to map to the corresponding bin. Therefore, more metatranscriptomic reads can map to a bin that has higher genome completeness (e.g. GAD85 Sample 2, Bin 1 at > 90% genome completeness). These results indicate that given the dominance of murine host reads during sequencing – thus limiting the amount of presumed microbial data – MAG contig assembly was restricted to detecting the dominant exogenous LA NCFM species with strain specificity notably lost upon binning.

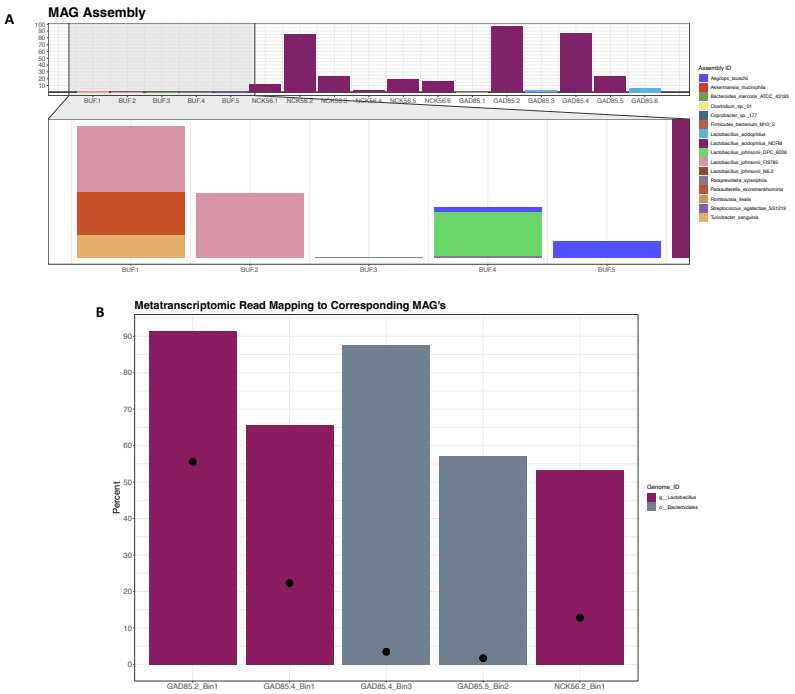

Figure 3.5. The (A) MAG assembled contigs and resulting (B) bins with the quantity of metatranscriptomic reads that successfully mapped. (**A**) *Lactobacillus acidophilus* NCFM was the only contig with high genome completeness. As represented by the zoomed-in buffer samples, no *Lactobacillus acidophilus* contigs were generated in samples not exposed to the probiotic in any form. Only the (**B**) *Lactobacillus* genus binned at a high genome completeness, and more metatranscriptomic reads per sample can map to the MAG when the genome is more complete. MAG: metagenome assembled genome.

3.4.5. Exogenous LA Dominates and Restructures the Resident Microbiome

Metatranscriptomic reads were taxonomically classified by Kraken2 and then LogFC in bacterial abundance determined as described above. The LogFC and significant adjusted *p*-values for comparisons between NCK56-GAD85, buffer-NCK56, and buffer-GAD85 are provided in Supplementary Tables S3.6-S3.8, respectively. Differential abundance of the identified virus OTU's are provided in Supplementary Table S3.9. *Lactobacillus acidophilus* (OTU 192) was significantly (adjusted *p*-value: <0.0001) less abundant in the GAD85 group as compared to NCK56 with a -3.87-log fold-change (logFC). *Lactobacillus acidophilus* was significantly more abundant in the NCK56 (logFC: 13.3, adjusted *p*-value: <0.0001) and GAD85 (logFC: 9.46, adjusted *p*-value: <0.0001) groups when independently compared to the buffer group. This was expected as the buffer group was not exposed to the probiotic in any form, either wild-type or recombinant vaccine strain. *Akkermansia muciniphila* (OTU 3030) is a probiotic microbe known to associate tightly with the intestinal mucosa and can augment rotavirus infection (293, 294). This microbe

was significantly less abundant in GAD85 than NCK56 (LogFC: -1.80 and adjusted *p*-value: 0.001). It was also significantly more abundant in NCK56 when compared to buffer (LogFC: 3.02 and adjusted *p*-value: <0.0001) but not significantly more abundant when GAD85 was compared to buffer. Three additional *Lactobacillus* species were commonly enriched in both probiotic-exposed groups (rLA and LA) when compared to buffer; however, NCK56 had more *Lactobacillus* species generally enriched (Table 3.2). Species that were similarly enriched include *Lactobacillus helveticus* (OTU 3331), *Lactobacillus amylovorus* (OTU 206) and *Lactobacillus kefiranofaciens* (OTU 3329). There were three *Lactobacillus* species that were just enriched in NCK56 when compared to buffer, including *Lactobacillus amylolyticus* (OTU 196)*, Lactobacillus gallinarum* (OTU 207), and *Lactobacillus acetotolerans* (OTU 198). Other common probiotic species including *Enterococcus faecalis* (OTU 252) enriched in GAD85 when compared to buffer (LogFC: 4.08 and adjusted *p*-value: <0.0001) and NCK56 (LogFC: 3.81 and adjusted *p*-value: <0.0001). *Enterococcus durans* (OTU 253) was enriched in GAD85 compared to NCK56 and less abundant in NCK56 compared to buffer. However, *Enterococcus gilvus* (OTU 254) was significantly less abundant in GAD85 compared to buffer (LogFC: -2.34 and adjusted *p*-value: 0.0031). These *Enterococcus* species have probiotic properties that can help alleviate diarrhea (293, 294). We predict *Bacillus anthracis* is a misidentification as these reads were phylogenetically characterized from metatranscriptomic data. Detecting the *Candidatus arthromitus* sp. SFB-rat-Yit was surprising given this segmented filamentous bacterium (SFB) is traditionally detected in mice sourced from Taconic Farms as the mice used in this study were from Jackson Labs; however, presence of SFB in the murine microbiome can depend on specific vendor site (295). These results confirm LA is detected within the small intestine microbiome of mice when administered the probiotic (wild-type or recombinant). Additionally, this exogenous LA seemingly rapidly restructures the relative abundance of microbes present in the surrounding community.

Table 3.2. *Lactobacillus* species enriched in GAD85 and/or NCK56 as compared to the buffer group.

	NCK56		GAD85	
Bacteria	**LogFC**	**Adjusted *p*-value**	**LogFC**	**Adjusted *p*-value**
Lactobacillus helveticus (OTU 3331)	6.52	<0.0001	5.02	<0.0001
Lactobacillus amylovorus (OTU 206)	4.57	<0.0001	6.16	<0.0001
Lactobacillus kefiranofaciens (OTU 3329)	2.69	<0.0001	2.38	0.0005
Lactobacillus amylolyticus (OTU 196)	1.62	<0.0001	N/A	N/A
Lactobacillus gallinarum (OTU 207)	2,25	<0.0001	N/A	N/A
Lactobacillus acetotolerans (OTU 198)	1.77	0.0001	N/A	N/A

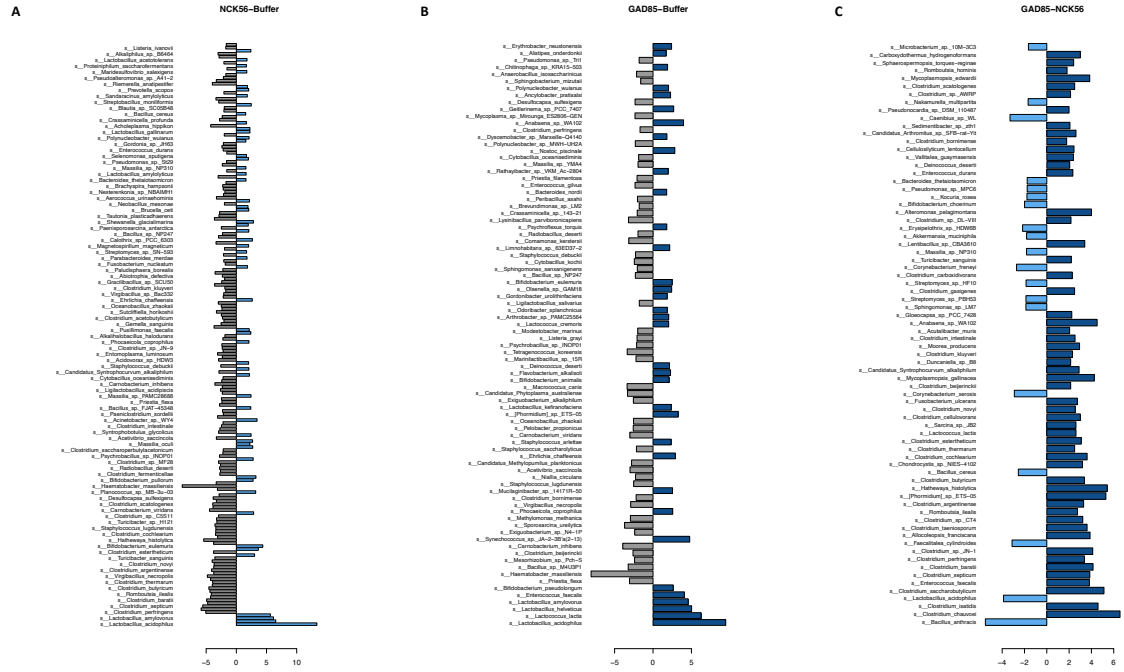

Figure 3.6. LogFC charts indicating the significant (adjusted *p*-value <0.005, LogFC > 2), differentially abundant bacteria between groups and the magnitude of this difference. (**A**) represents the NCK56-vaccinated group compared to the buffer group, (**B**) GAD85 to buffer, (**C**) and GAD85 to NCK56. Bacteria that are more abundant in the buffer group are represented by grey bars, the NCK56 group by light blue, and the GAD85 group by dark blue. LogFC: log fold-change.

3.4.6. Exogenous LA Induces α-Diversity Differences

There was a significant difference (adjusted *p*-values: <0.05) between treatment groups for bacterial richness, inverse Simpson and Shannon α-diversity metrics as determined by ANOVA (Table 3.3), reflecting the intra-sample microbiome diversity. A Tukey's honest significant difference test for multiple comparisons was applied to determine specific differences between groups using the default settings for the TukeyHSD function in R. The upper and lower limits and adjusted *p*-values are provided in Supplementary Table S3.10 for InvSimpson, Richness, and Shannon.

Table 3.3. ANOVA results for comparisons between different groups (adjusted *p*-values: <0.05) for three α-diversity metrics.

	Richness	Shannon	Inverse Simpson
Between Groups	0.0037	0.0013	0.0144

NCK56 consistently had the lowest α-diversity, buffer the highest, and GAD85 a relatively intermediate level of α-diversity between the control groups according to Inverse Simpson, Richness, and Shannon diversity metrics (Figure 3.7A). The buffer negative control group was significantly more diverse from the NCK56 group according to all three α-diversity metrics from the NCK56 group (adjusted *p*-values: <0.05). Inverse Simpson (1/Simpson's Index) diversity measures the probability of two randomly selected species being the same and tends to weigh dominant species more heavily. Shannon diversity represents the information contained within a sample and the predictability of sampling. It can favor rare over common species. Richness is the number of species present (296). These three metrics are not perfect representations of α-diversity but are well-established ecological diversity measurements commonly applied to microbiome research (297). The increased α-diversity in the buffer group is potentially due to the dominance of LA in both LA-exposed groups (NCK56 and GAD85), leaving minimal species diversity outside LA. There were no significant differences in α-diversity of the viruses detected between treatment groups (ANOVA results provided in Supplementary Table S3.11). Figure 3.7B represents the relative abundance of the top-20 most abundant species present in each sample after normalization as bar plots. Buffer samples are primarily dominated by *Lactobacillus johnsonii* and *Romboutsia ileali. Lactobacillus acidophilus* NCFM is the most abundant species for all NCK56 and a majority of GAD85 samples, as LA NCFM is the backbone of both the control NCK56 and recombinant GAD85 strains. Across all groups, the most dominant species were also binned during MAG assembly (*L. johnsonii* and *L. acidophilus* NCFM). *Muribaculum intestinale* is a mouse microbiome-specific anaerobe that has been characterized relatively recently (298). As reflected in the α-diversity metrics, buffer samples have the most species represented in the relative abundance plots, followed by GAD85 then NCK56, the latter of which appears the most homogenous. The dominant viral family is *Autogrphiviridae* which characterized by bacteriophages (299) (Supplementary Figure S3.1). The

second and third most dominant families are common to the virome, including *Siphoviridae* and *Myoviridae*. These results collectively indicate there is more variability within samples of the buffer and GAD85 group than within the NCK56 group and that administration of LA is detectable and immediately dominates the bacteriome.

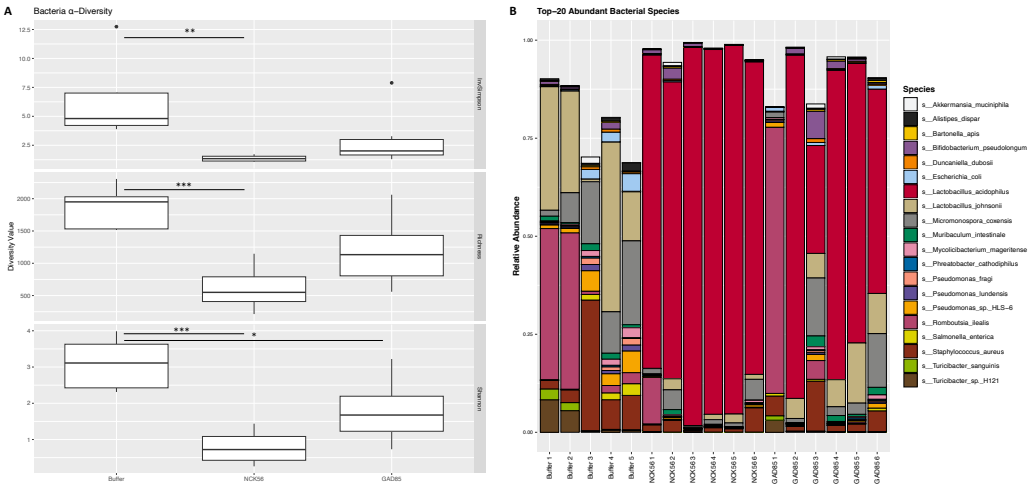

Figure 3.7. Boxplots representing (A) α-diversity metrics and (B) relative abundance bar plots per sample. There is a significant difference between only NCK56 and buffer groups for inverse Simpson (adjusted *p*-value: 0.0086) and richness (adjusted *p*-value: 0.0007) as measured by Tukey's honest significant difference after ANOVA (Table 3.3). For Shannon diversity, there was a significant difference between the NCK56 and buffer groups (adjusted *p*-value: 0.003) and between the GAD85 and buffer groups (adjusted *p*-value: <0.0289). The y-axes between the α-diversity boxplots are disconnected. (**B**) Relative abundance bar plots of the 20 topmost abundant species are provided for each sample in the buffer-, NCK56- and GAD85-vaccinated groups.

3.4.7. Exogenous LA Induces ß-Diversity Differences

The ß-diversity of the bacteriome composition between the buffer (grey) and NCK56 (light blue) groups are significantly different from one another as the 95% confidence elipsoides in the PCoA ordination plot do not overlap (Figure 3.8). However, the GAD85 group ellipsoid encomapses both control groups, indicating there is no significant difference in bacteriome composition between GAD85 and either of the controls (buffer or NCK56). Axis one accounts for nearly half of data distribution (46.9%) and axis 2 approximately a quarter (21.8%). As demonstrated by the distribution of GAD85 samples, they cluster moderately closer to the NCK56 samples. This again reinforces that GAD85 induces a somehwhat intermediate microbiome between that of the buffer and wild-type LA groups. Additionally, these results

demonstrate oral probiotic administration shifts the collective resident bacteriome structure immediately; specifically, after only two oral vaccinations within 24-hours.

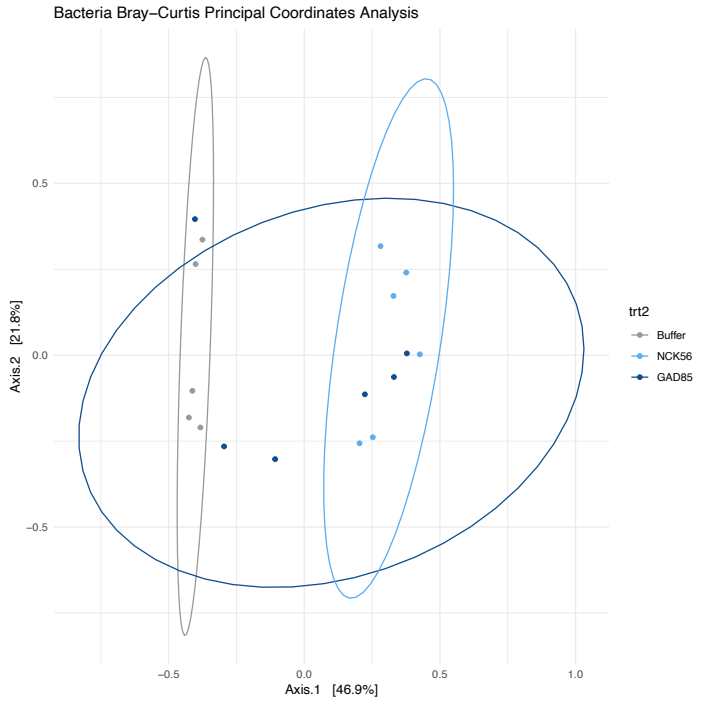

Figure 3.8. PCoA ordination plot representing inter-sample microbiome diversity was calculated after CSS and using Bray-Curtis dissimilarity. The 95% confidence ellipsoids do not overlap for the buffer and NCK56 groups indicating a significant difference, while no significant difference is seen between GAD85 and both buffer or NCK56.

3.5. Discussion

Exogenous probiotics and probiotic-based vaccines can help generate innate and adaptive immunity against enteric infections like rotavirus (243, 300). Such probiotic vaccines need to interact with the host microbiome during oral delivery. Therefore, to inform improved vaccine design, it is important to understand how the microbiome responds to vaccination and in turn how the probiotic platform itself adjusts to the host environment. In Chapter 2, we described the development and relative efficacy of an rLA vaccine candidate (GAD85) expressing two rotavirus antigens from the VP8* capsid protein along with two adjuvants (FliC, FimH) using a murine challenge model. In this Chapter, we successfully applied a multi-omics (metatranscriptomics and metagenomics) evaluation of interactions between this novel rLA vaccine and the resident intestinal microbiome at an immune inductive site – a Peyer's patch. This study was unique

in its evaluation of the immediate microbiome response to short-term probiotic exposure as mice were vaccinated twice within 24 hours of necropsy. Such a study design is useful in that exogenous probiotics do not permanently colonize the intestine (301); therefore, the immediate impact of an rLA vaccine is relevant to understand. However, the results are potentially not translatable to the long-term impact of a multi-series probiotic vaccine course. Another benefit of our study design was assessing the microbiome within the upper GI tract (ileum) as the microbiome is often characterized from stool samples. However, the stool microbiome in both mice and humans is found to poorly represent the microbiome of either the upper or lower GI tract (302). Even the intestinal mucosa and lumen can differ in microbiome composition (302).

The changes we observed in the composition of the microbiome, like the dominance of LA and moderate attenuation of α- and β-diversity (Figures 3.7 and 3.8), are most likely a rapid yet transient response to exogenous probiotic exposure. For example, there was no difference in α- or β-diversity of the fecal microbiome between Danish infants who received daily probiotics for six months and placebo groups either before or after treatment. Similar to our observation of increased *Lactobacillus acidophilus* abundance in probiotic-vaccinated groups (Figure 3.6), they also detected relative enrichment of *Lactobacillus* in the probiotic group (303). Individuals given a probiotic yogurt regimen had an immediate enrichment in oral microbiome diversity, where we observed a decrease in diversity with LA-exposed groups, but the α-diversity did not ultimately change over time. They also detected modest persistence of the *Lactobacillus* probiotic strains (304). A longitudinal study would be required to discern any permanent impact of GAD85 administration on the small intestinal microbiome, but prior work from our group with a different rLA strain determined no lasting impact on microbiome structure while simultaneously activating the GALT to generate antigen-specific immune responses (201). This is beneficial as an exogenous vaccine should not have off target effects on the host microbiome like permanently changing the community structure. Additionally, colonization has not necessarily been tagged as the mechanism of action for the beneficial side-effects of probiotics (303).

MAGs provide a powerful tool for discovering novel and complete genomes in both microbial rich and sparse samples (305). We were able to assemble the LA NCFM genome only in mice that were exposed to the probiotic, but the resulting binned MAGs' completeness and specificity was lackluster across samples. The density of LA present in most of our samples could have limited our ability to recover high-quality (high genome completeness with low contamination) MAGs. An abundance of a specific population relative to the rest of the community, compounded with any potential strain "heterogeneity" among the specific detected species, has been demonstrated to impede high-quality MAG assembly (306). Potentially depleting host nucleic acid, or separating the microbiome content from tissue before extraction, could have improved the quality and quantity of microbial-mapped reads in this study. It is also important when thinking of future directions informed by the results presented here to ensure all MAG's are compliant with minimal information about a metagenome assembled genome (MIMAG) proposed by the Genomic Standard Consortium (307).

The difference in LA genome expression between mice vaccinated with NCK56 or GAD85 (Figure 3.3) could indicate mechanisms by which the recombinant LA vaccine vector uniquely adapts to changing environments. Such external hurdles include stationery and exponential growth, resuspension prior to oral vaccination in a sodium bicarbonate buffer, and introduction to and association with the host and endogenous microbes. All these environments have unique temperatures, pH's, physical barriers, and the presence of host immune mediators and the impact of other gut bacteria. In an impressive study with a germ free 129S6/SvEv murine model, Goh et al. (2021) determined gene expression from wild-type LA NCFM changes dramatically when adapting to different growth phases in MRS broth, PBS exposure, and transit along the host GI tract from small intestine through the cecum to the large intestine (308). They determined the LA NCFM transcriptome is "niche-specific", differing between the ileum, cecum, and large intestine, with the LA NCFM cecal and large intestinal transcriptomes having slightly more resemblance (308). Goh et al. (2021) found many of the genes within the LA ileal transcriptome were related to amino acid metabolism, transcription, and replication. Similarly, we found differential regulation of transcriptional regulation and amino acid metabolism genes in the ileal rLA transcriptome when compared to LA. Goh et

al. (2021) also found the classic stress genes (DnaJ, DnaK, and GrpE) in the LA transcriptome during growth in MRS broth but not when LA was in the ileum; conversely, we found these stress response genes upregulated in the rLA transcriptome within the ileum compared to wild-type LA. Differing from Goh et al. (2021), we worked in a murine model with an intact microbiome and used recombinant and wild-type LA strains. Some of the carbohydrate metabolism differences we see between the transcriptomes of the probiotic groups (cellobiose, glucose, and maltose) may reflect nutrient availability on account of the rodent chow consumed by the mice and GAD85 versus NCK56 consuming these available energy sources differently (309, 310). Notably, the differences between the GAD85 and NCK56 transcriptome may also be accounted for by antigen and adjuvant expression from the rLA strain. Surface layer proteins including SlpA are metabolically intensive and LA NCFM expresses SlpA aggressively when transiting the gut (308, 311). Since VP8Pep is expressed by SlpA on the surface of GAD85, this rotavirus antigen display could be driving gene expression uniquely in the rLA compared to wild-type LA due to differing energy demands. The SlpA signal peptide has been demonstrated to put exogenous protein expression into overdrive in recombinant bacteria compared to other signal peptides (311).

The primary distinction between the entire microbial metatranscriptomes of GAD85- and NCK56-vaccinated mice was the successful detection of FliC and FimH adjuvant expression at a Peyer's patch (Figure 3.4). Both adjuvants were overexpressed in GAD85 samples as expected since GAD85 was the exclusive strain expressing antigens or adjuvants. Many of the identified proteins that were significantly upregulated in the metatranscriptome of the (r)LA groups when compared to buffer could indicate probiotic interaction with the murine small intestine. For example, S-layer and mucus binding transcripts were overexpressed in both probiotic groups compared to buffer, and these are well-characterized proteins that help LA interact with and adhere to host intestinal epithelial cells (312, 313). The glutamine ABC transport protein GlnH that was significantly downregulated from the LA transcriptome of GAD85 compared to NCK56 is also capable of modulating probiotic adherence (312, 313).

Our future directions include measuring and correlating immunological outcomes of rLA administration, including but not limited to antigen-specific antibody and antibody-secreting cellular

responses, with ‘omics techniques. Additional techniques may include multiplexed cytokine analysis, microscopy, and flow cytometry (314). These and similar techniques would permit augmented interrogation of probiotic vaccine-induced protective immune responses, help identify signs of efficacious immunization, and determine possible avenues for future vaccine development (315, 316). Such an approach would require a longitudinal study design to evaluate host-microbe-immune responses over time. Also, measuring the transcriptome of (r)LA prior to introduction to the murine intestine could provide a useful control (308). The power of applying a meta-omics approach with immunological outcomes to determine correlates of differential vaccine response was demonstrated with the live-attenuated BCG vaccine, which has a high variability in efficacy. In a large human cohort, the authors determined hyper-individual correlates of vaccine response using high-throughput methods by establishing an endophenotype to link epigenetics (genome and environmental interaction) with immune outcomes (316). To do this, parallel genome-wide and epigenome-wide association studies were coupled with immune cell phenotyping, chromatin availability, and cytokine response to varied microbial stimuli. Applying a similar cross-sectional design could further our understanding of our novel rLA platform and vaccine-induced host responses. Regarding other future directions, terminal sera was also collected during the study presented in this Chapter and the murine metabolome was evaluated using liquid chromatography mass spectrometry. These data are beyond the scope of Chapter 3; however, once integrated with transcriptome data, the results demonstrated significant upregulation of polyunsaturated fatty acid metabolism. These results informed the study design of Chapter 4. Studies on the metabolomics of LAB have indicated the impact of environment on LAB function, such as exposure to air (287).

There are limitations that need addressing. Primarily, this study was initially intended to be a pilot, proof-of-concept project demonstrating successful use of multi-omics analysis with a novel LA-based vaccine. Therefore, we had a limited sample size ($n = 6$), reduced further by the unexpected loss of a mouse in the negative control group ($n = 5$). Additionally, there was somewhat of an outlier in the rLA vaccine group that did not have any detectable LA (GAD85 sample 1; Figure 3.7B). When this outlier was removed, the same comparisons remained significant among α-diversity metrics along with the same β-diversity

trends of only the buffer and NCK56 ellipsoids separating as when the outlier was included. The viral family bar plots (Supplementary Figure S3.1) do not show this same outlier. Given the extent to which analyses were performed with the MAG assembly, and the similarity in conclusions drawn from the results with or without the sample, it seems reasonable to have included GAD85 sample 1 in the analyses presented. Additionally, our recombinant LA vaccine expresses the FliC adjuvant from an Erm-resistant plasmid and the wild-type LA also has plasmid-conferred Erm resistance. As this platform moves forward it remains front of mind to remove plasmids and integrate all antigens and adjuvants into the *Lactobacillus* genome. This reduces the reliance on antibiotics in maintaining probiotic vaccine strains and relieves the potential spread of antibiotic resistance among microbes. Genome integration is also imperative when developing genetically modified organisms for human health (317). Finally, the difference in potential mouse models should be considered. C57BL/6 and BALB/c have distinct immune repertoires, including differences in microbial cross-reactive IgA, TLR-expression profiles of DCs, and T helper cell phenotype (136, 225, 318). Therefore, evaluating host-microbiome interactions could change depending on the mouse strain used. As is the case for any animal model, acknowledging the limitations with generalizing conclusions drawn from using a murine microbiome is warranted. Every host houses a unique microbial community that may exclude the biologically relevant microbes of a different species (298). However, C57BL/6 mice are a conventional animal model for microbiome research (319).

3.6. Conclusions

Using a multi-omics approach, our results confirm that an rLA vaccine can reach and express exogenous antigen and adjuvants at an immune inductive site (Peyer's patch). We determined orally delivered exogenous (r)LA induces distinct structural and metatranscriptional changes in the resident microbiome and that the probiotic vaccine adapts uniquely to the host environment. These results can help elucidate interactions occurring between a recombinant *Lactobacillus* vaccine platform and the microbiome at an immune inductive site which may better inform future probiotic vaccine strategies.

CHAPTER 4: POLYUNSATURATED FATTY ACID AND *LACTOBACILLUS ACIDOPHILUS* STRAIN MODULATION OF HOST CELL RESPONSES IN VITRO

4.1. Introduction

Polyunsaturated fatty acid (PUFA) consumption and metabolism is relevant to human health. Diets rich in omega-6 PUFAs, including the standard Western diet, are correlated with increased incidence of obesity and inflammatory conditions (320). Omega-6 PUFAs include linoleic acid (LNA) and arachidonic acid (AA) (320). Conversely, omega-3 PUFAs including α-linolenic acid (A-LNA) and its derivatives docosahexaenoic and eicosapentaenoic are often regarded as anti-inflammatory in nature. Omega-3 PUFAs are being studied as potential treatments for inflammatory bowel disease and similar conditions via PUFA-induced inflammation resolution (321, 322). Docosahexaenoic and eicosapentaenoic are also important for maintaining membrane fluidity and their metabolism generates resolvins and protectins (323). Increased or reduced availability of omega-6 versus omega-3 fatty acids influence their respective incorporation into phospholipid bilayers of immune and other cells, potentially impacting cell function and signaling (324). LNA and A-LNA provide the building blocks for AA and are considered essential PUFAs as they are not synthesized natively by the body and must instead be consumed through diet (325). Common dietary sources of LNA include soybean and corn oils while linseed, olive, and sesame oils are good sources of A-LNA (326). Alternative omega-3 fatty acids are frequently derived from certain fish oils (324). AA is either freely available or released from cell phospholipid membranes as the precursor for eicosanoids which include prostaglandins and leukotrienes. Eicosanoids are notorious for their primarily proinflammatory effects including fever, increased cellular permeability, and production of proinflammatory cytokines like tumor necrosis factor-α (TNF-α) (159). Diet-derived PUFA can influence the immune response against enteric pathogens such as rotavirus (325). For example, diarrhea symptoms and viral shedding in neonatal BALB/c mice following rotavirus infection were worse when fed diets rich in polyunsaturated than monosaturated or unsaturated fatty acids. The effect of PUFA is not identical across enteric infections (325).

The intestinal epithelium is protected by mucins to mediate interaction with commensal and pathogenic microbes. Mucins are glycoproteins broadly characterized by their hefty *O*-linked glycan

content which bind water. There are two types of mucins in the small and large intestine: transmembrane and gel-forming. MUC2 is the dominant gel-forming mucin produced primarily by goblet cells along the intestine to form flat net-like structures (327). Goblet cells are located mainly in crypts along the small intestine with some on the villi intermingled with enterocytes. The mucus layer is thin and penetrable in the small intestine and not strictly adhered; therefore, MUC2 is regularly cleaved and attaches to existing MUC2 for transport downstream. Conversely, the colonic mucus is two layers thick, with the inner layer adhered strongly to the epithelium and relatively impenetrable to bacteria (327). MUC2 production is energy demanding and highly controlled. Mucin release from goblet cells occurs in low pH, high calcium environments created by bicarbonate (HCO_3^-) release from the cystic fibrosis transmembrane conductance regulator in enterocytes. Mucin expression occurs at both a constitutive level and can happen in a mass release – called compound exocytosis – induced by certain stimuli. MUC2 also modulates host immune responses in the intestine. Defensins and other antimicrobial peptides produced by Paneth cells are contained and transported in MUC2 sheets, along with secretory IgA, which all modulate immune tolerance at the epithelium. Exposure to the bacterially-derived muramyl dipeptide (MDP), a piece of peptidoglycan shared between gram positive and negative bacteria, can also induce defensin secretion from Paneth cells (328). Recognition of MDP by nucleotide-oligomerization domain containing 2 (NOD2) generally helps regulate intestinal mucosal inflammation (328). Additionally, Toll-like receptor (TLR) recognition of pathogen-associated molecular patterns, such as TLR5 with flagellin, can stimulate MUC2 compound exocytosis from sentinel goblet cells in the colon sentinel goblet cells (329). Finally, goblet cells secreting mucin can sample luminal antigens via goblet cell-associated antigen passages and converse with dendritic cells in the lamina propria (327).

The milieu of intestinal bacteria can influence intestinal host functionality, immune response, and general health via direct interaction with the intestine or through microbial-derived metabolites. Certain commensal bacteria feast on glycans attached to MUC2 and reside within the mucosa. In turn, short-chain fatty acid microbial byproducts, such as butyrate, provide energy stores for intestinal epithelial cells and act as substrates for host cell reactions (329). Intestinal bacteria have also evolved to take advantage of

changing nutrient availability in the intestine. For example, the colonic mutualist *Bacteroides thetaiotaomicron* can adhere to and digest shed mucus and epithelial cells or undigested food particles, exhibiting impressive niche versatility in the host diet polysaccharides it can digest (330). Probiotic species like *Lactobacillus* and *Bifidobacteria* can prevent infection by enteropathogens, including different pathogenic strains of *E. coli*, from colonizing by impairment of pathogen adhesion, antimicrobials including fatty acid byproducts, and activating the host immune system (326). Microbial-derived metabolites of LNA (HYA. HYB, HYC, KetoA, KetoB, KetoC, conjugated LNA) and A-LNA (αHYA-C and αKetoA-C, conjugated A-LNA) can either augment or buffer against obesity (320). A high fat-diet results in more omega-6 than omega-3 fatty acid microbial-derived metabolites in C57BL/6J mice. Supplementing the high-fat diet with the microbial-derived LNA metabolite HYA reduced inflammation and weight gain while improving glucose regulation, and a high-fat diet supplemented with LNA has greater relative abundance of the *Lactobacillus* genus than a high-fat diet alone (320). A fecal microbiota transplant of an older microbiome (from two year old C57Bl/6JRj mice) decreased brain PUFA and liver omega-3 PUFAs significantly in germ-free C3H/HeN mice (331). Finally, lactic acid bacteria (LAB)-derived metabolites can regulate β-oxidation and in turn boost host metabolism (332).

In Chapters 2 and 3, we evaluated probiotic and host interactions from distinct perspectives. In Chapter 2, we used an in vivo challenge model for assessing vaccine-induced protection and immune responses. In Chapter 3, we applied a next-generation sequencing omics-based approach to understand host-vaccine interactions in the gut-associated lymphoid tissue. In the following Chapter, we expand on conclusions generated from Chapter 3 to explore PUFA and bacterial co-culture modulation of *Lactobacillus acidophilus* (LA) and human host cell interactions using an in vitro model. The human colon carcinoma cell line Caco-2 is a well-established intestinal epithelium model developed in the 1970's for measuring transport, absorption, and infection at the epithelium (333). We evaluated cellular responses to bacterial exposure (recombinant and wild-type LA strains, *E. coli*) and PUFA (LNA, A-LNA, or AA) supplementation including mucin, inflammatory cytokine, and pathogen recognition receptor (PRR) expression (334, 335). We lack understanding of recombinant LA (rLA) interactions in a human model;

therefore, this approach could highlight mechanisms for improving immunogenicity of the probiotic vaccine and potential competition against other enteric pathogens. LA strains included the wild-type NCK56, dual-antigen rLA GAD84, and dual-antigen dual-adjuvant rLA GAD85.

4.2. Materials and Methods

4.2.1. Caco-2 Cell Culturing and Storage Conditions

The human colon adenocarcinoma cell line Caco-2 (ATCC HTB-37™) was cultured in complete DMEM media (C-DMEM; Corning, Corning, NY, USA) supplemented with 10% FBS (HyClone, Logan, UT, USA), 1% pen/strep (HyClone), and 1% L-glutamine (Caisson, Colorado Springs, CO, USA). Incomplete DMEM (I/C DMEM) was only supplemented with L-glutamine. All materials used for cell culture were warmed for approximately 20 min in a 37 °C water bath before use and incubations were performed at 37 °C and 5% CO_2 unless stated otherwise.

Cryogenic vials (Cryovials; Corning) of Caco-2 cells stored in liquid nitrogen were thawed for approximately two minutes in a 37 °C water bath. Thawed cells were gently resuspended, then added to 9 mL of warmed C-DMEM. The cryovial was rinsed with 500 µl of the media to collect any leftover cells. Cells were centrifuged at 120 g for 6 min and the supernatant carefully removed. Cells were slowly resuspended with 1 ml of C-DMEM then added to a T75 flask for expansion. Cells were frozen back for liquid nitrogen storage by pelleting cells by centrifugation for 6 min at 120 g after passaging. After removing the supernatant, the cell pellet was resuspended in 10% DMSO/C-DMEM and 1 ml aliquots were made per cryovial. Cryovials were stored in CoolCell™ LX containers (Corning) 24 hours at -80 °C before moving to liquid nitrogen.

Cells were passaged by aspirating old media and washing once with 1XPBS. Cells were dissociated from the flask by incubating with 2 mL of 0.05% trypsin protease solution (Hyclone) for 10 min. The trypsin and detached cells were diluted in 10 mL of DMEM (Corning) and repeat pipetted to ensure a single-cell suspension. Cells were counted by mixing 10 µl of the single-cell suspension with 10 µl of ViaStain

APOI staining solution (Nexcelom Bioscience, Lawrence, MA, USA) and counted on a Cellometer Auto2000 (Nexcelom Bioscience). Twenty mL of fresh DMEM was added to a new flask, or the old flask was washed once with 1XPBS, and the cells were seeded at a density of 5e5 cells per T75 flask or 5e9 per T225 flask. Cells were grown until 90-100% confluent before the next passage.

Passages 50-70 were used for experiments. Cells were seeded at a density of 5e4 per well with 1 ml/well of C-DMEM in a Bio-One Cellstar 24-well plate (Greiner, Kremsmünster, Austria). Each side of the plate was tapped multiple times to evenly disperse cells across the well. Cells were incubated for four days until approximately 95-100% confluent before supplementing with PUFA and/or performing co-culture experiments. Cells were washed once with 1 ml/well of warmed I/C DMEM 24-hours prior to bacterial co-culture by slowly aspirating old media using p1000 pipette and dispensing new media down the side of the well with a serological pipette set to the "slow" setting (336). Wells were washed in sets of three to avoid drying.

4.2.2. Bacterial Growth Conditions

NCK56 (wild-type LA), GAD84 (dual-rotavirus antigen recombinant LA), and GAD85 (dual-rotavirus antigen, dual-mucosal adjuvant recombinant LA) were constructed as previously described (60). (r)LA cultures were grown anaerobically at 37 °C overnight in MRS (BD Difco, Franklin Lakes, NJ, USA) supplemented with 5 μg/mL erythromycin (Erm; Teknova) if resistant. GAD85 was diluted 1:10 and grown to exponential for two and a half hours. The *Escherichia coli* (ATCC 31616; EC) strain was grown in TSB (BD Difco) aerobically at 37 °C. Overnight and exponential bacterial cultures were washed twice with 1XPBS. After the final wash, colony forming units (CFU) were quantified using an optical density of 600 nm as described previously (206). If exclusively co-culturing with (r)LA, 1e8 CFU of culture was added per well. If co-culturing with (r)LA and EC, 5e7 CFU of both (r)LA and EC per well was added. Freezer stocks of either *Lactobacilli* or *E. coli* cultures were made in 500 μl aliquots of overnight cultures in 10% DMSO/culture media and stored at -80 °C until use.

4.2.3. Mycoplasma Species Testing

Caco-2 cells were tested for mycoplasma contamination after initial thawing from liquid nitrogen using the eMyco plus Mycoplasma PCR Detection Kit (LiliF Diagnostics, Seongnam, Kyonggi-do, South Korea). 5e4 cells were washed twice with 1XPBS and resuspended in 100 µl of 1XPBS and then the boiling method was used following manufacturer's instructions. PCR was performed on a Bio-Rad (Bio-Rad). PCR products were run on a 2% agarose gel. The gel was visualized on a Bio-Rad Chemi-Doc XRS+ and lanes were analyzed using Image Lab software (Bio-Rad; v.6.1) Gel provided in Supplementary Figure S4.1.

4.2.4. Polyunsaturated Fatty Acid (PUFA) Supplementation

Confluent 24-well plates of Caco-2 cells were washed then incubated overnight in fresh I/C DMEM supplemented with either 500 µM linoleic acid (LNA; Cayman Chemical Company, Ann Arbor, MI, USA), 500 µM α-linolenic acid (A-LNA, Cayman), or 125 µM arachidonic acid (AA; Cayman), unless stated otherwise. PUFA's were stored at -20 °C until use.

4.2.5. Cytotoxicity Assay

Confluent 24-well plates of Caco-2 cells were incubated overnight with two-fold serial dilutions of PUFA (either LNA, A-LNA, or AA) starting from 1000 µM in DMEM. Directly prior to the assay, an alamarBlue (resazurin) working solution was made by further diluting a master stock (alamarBlue diluted 1:50 in 1xPBS) 1:10 in warm DMEM. The protocol and resazurin were kindly provided by Dr. Rushika Perrera. After aspirating the PUFA-supplemented media, 500 µl/well of the alamarBlue working solution was added to the plate. Control wells were included on each plate; specifically, cells treated with 1% cold Triton-X100 (Sigma Aldrich, St. Louis, MO, USA) in 1XPBS to ensure cell death along with cells that were left untreated (neither supplemented with PUFA nor treated with Triton-X100). The plate was incubated between 2-4 hours until a color change from blue to pink/purple occurred. 100 µl/well was

transferred to a clear 96-well polystyrene plate (Greiner) then read at 560 nm excitation and 590 nm emission on a BioTek (Winooski, VT, USA) Synergy H1 Multimode Reader. Each PUFA concentration was run in duplicate, and the optical densities (OD) were averaged together.

4.2.6. RNA Extraction and Quantitative Real-Time PCR

Caco-2 cell monolayers were co-cultured with (r)LA for an hour and a half. RNA was extracted directly from the 24-well plate using the Quick-RNA Purification Kit (Zymo, Irvine, CA, USA) following manufacturer's instructions. The suggested DNA digestion step was performed, and all centrifugation steps were completed at 13,000 rcf on a tabletop centrifuge at room temperature (RT). RNA was eluted in 100 µl of nuclease-free water. RNA was quantified using the Qubit RNA Broad Range Assay (Thermo Fisher Scientific) and RNA quality was determined using the Qubit RNA IQ Assay (Thermo Fisher Scientific), both following the manufacturer's instructions using a Qubit 4 Fluorometer (Thermo Fisher Scientific). RNA quality averaged 8.1. RNA was stored at -80 °C until use. The optimal amount of RNA per RT-qPCR reaction was determined to be 40 ng and the RNA was diluted to 10 ng/5 µl in nuclease-free water prior to RT-qPCR. Extracted RNA was evaluated by RT-qPCR for gene expression using the Applied Biosystems TaqMan™ RNA to Ct One Step Kit (Thermo Scientific) with the respective Taqman™ Gene Expression Assay for GAPDH (Hs99999905_m1), TNF-α (Hs00174128_m1), Tlr5 (Hs00152825_m1), and MUC2 (Hs00159374_m1). RT-qPCR was performed in a 96-well skirted white PCR plate (Bio-Rad) following manufacturer's instructions for a 50 µl reaction. Samples were run in duplicate and randomized among plates. A no template water control was included per transcript on each plate. Plates were spun at 140g for 1 min at RT prior to running on a Bio-Rad CFX96 Touch Real Time PCR Detection System (Bio-Rad), which passed all three criteria for quality-control using the CFX Qualification Plate (Bio-Rad). Fold-change in gene expression was quantified following the $2^{-\Delta\Delta CT}$ method as previously described (250, 337) relative the untreated Caco-2 cell negative control samples and normalization to the housekeeping gene GAPDH.

4.2.7. Adhesion Assay with Flow Cytometry

After washing, bacterial cultures were normalized to the sample with the lowest concentration and then incubated with 5 µl/mL of 5M Cell Trace Violet (CTV; ThermoFisher) for 30 min while protected from light. 10 mL per sample of 10% FBS/PBS (Hyclone) was added to interrupt the reaction and cultures were then centrifuged. Samples were incubated with 1 mL of 10% FBS/PBS twice for five minutes. Cultures were resuspended after the final incubation in 1 ml of 1XPBS. When co-culturing (r)LA strains with EC, only the EC culture was CTV-stained. Caco-2 cell monolayers were co-cultured with CTV-labeled bacteria for an hour and a half. Treatments were run in triplicate. Monolayers were washed slowly twice with warm I/C DMEM and once with warm 1XPBS to remove unbound bacteria. 500 µl of RT 1XPBS was added after the final wash to each well. Cells were then scraped thoroughly from the culture surface with pipette tip and the well was rinsed repeatedly. Using trypsin or Triton-X100 to remove cells resulted in clumping that could have prevented samples from running successfully on the cytometer. The 500 µl of 1XPBS containing cells and bacteria was spun down for 5 min at 3700 RPM. Samples were then washed twice in 600 µl of PBS + 1% BSA (Equitech-Bio, Kerrville, TX, USA). After the final wash, samples were resuspended in 90 µl of RT 1XPBS in preparation for flow cytometry analysis. Samples were run on a Beckman Coulter Gallios Flow Cytometer (Beckman Coulter, Brea, CA, USA). Flow gating was based on unstained bacteria, CTV-stained bacteria, and cell-only controls. Flow analysis was performed in FlowJo™ Software v.10.8.1 for Windows (BD Life Sciences). Experiments are as described in Figure 4.1.

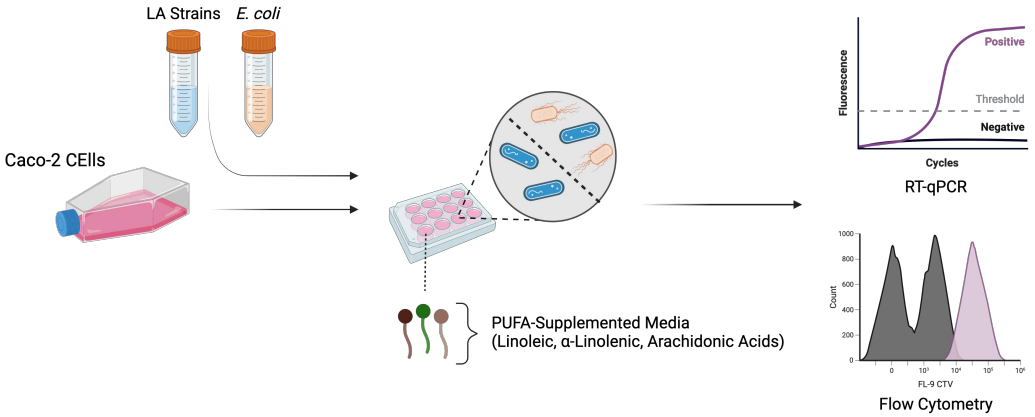

Figure 4.1. Experimental design using the assays developed for Chapter 4. Confluent Caco-2 cells in 24-well plates were cultured overnight in cell culture media supplemented with one of three polyunsaturated

fatty acids (PUFA), either linoleic acid, α-linolenic acid, or arachidonic acid. Cells were co-cultured with just *Lactobacillus acidophilus* (LA; wild-type NCK56 or recombinant strains GAD84 or GAD85) or with LA and *E. coli* (EC). RT-qPCR was performed to evaluate expression of TLR5, TNF-α, and MUC2 transcripts following co-culturing with LA species. Flow cytometry analysis of Cell Trace Violet (CTV)-stained bacteria was implemented to determine LA and EC adhesion to the Caco-2 cells. Created with BioRender.com.

4.2.8. Statistics

The cytotoxicity data is log10 transformed and the RT-qPCR data is log2 transformed. For the RT-qPCR data, a two-way ANOVA with a Tukey-Kramer test of multiple comparisons was performed. For the CTV adhesion assay results, an ordinary one-way ANOVA was performed with a Tukey-Kramer test for multiple comparisons. Further, a Brown-Forsythe test was used for evaluating differences in variance between groups. All data were analyzed and visualized in GraphPad Prism 10.0.3 for MacOS, GraphPad Software, Boston, Massachusetts USA, www.graphpad.com.

4.3. Results

4.3.1. Determination of Optimal PUFA Concentration

In developing the assays presented in this Chapter, the optimal concentration of PUFA was determined to avoid cell death using an alamarBlue cytotoxicity assay. Briefly, the resazurin substrate is an oxidation-reduction indicator that changes colors when cells are metabolically active (338). The cytotoxicity assay results are provided for Caco-2 cells supplemented overnight with concentrations of LNA (Figure 4.2A), A-LNA (Figure 4.2B), and AA (Figure 4.2C) ranging from 1000 μM to 15.65 μM. As demonstrated by the experimental lines aligning with the "Untreated" control cell value LNA (green) and A-LNA (blue) did not impair cellular metabolism at any concentration. LNA mildly reduces cell metabolism at a concentration of 15.65 μM which could be a result of cells drying out slightly. AA (tan) negatively impacts cell metabolism at a concentration higher than 250 μM as the line dips to the "Dead" control cell value (indicating minimal to no cellular activity). Therefore, 500 μM of A-LNA and LNA were used for the experiments, to reduce the amount of reagent needed, and 125 μM of AA to ensure cell viability.

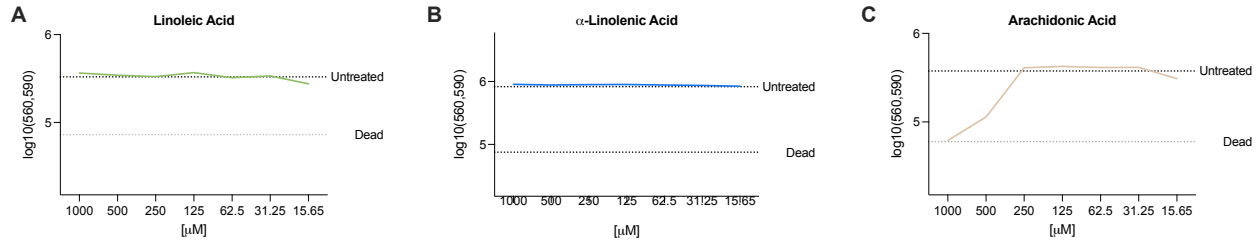

Figure 4.2. AlamarBlue cytotoxicity assay determining the non-cytotoxic optimal concentration for supplementing Caco-2 cell culture media with either of the following PUFA: (A) LNA, (B) A-LNA, or (C) AA. The black dotted lines marked "Untreated" indicate the wells where cells were neither supplemented with PUFA nor treated with 1% Triton-X100 and should be actively respiring. The gray line marked "Dead" indicates the wells that were treated with cold 1% Triton-X100 to kill cells as an internal control where cells are not respiring. PUFA: polyunsaturated fatty acids, LNA: linoleic acid, A-LNA: α-linolenic acid, AA: arachidonic acid.

4.3.2. LA and PUFA Treatment Distinctly Attenuate Cellular Responses

Caco-2 cell monolayers were either cultured in media alone (not supplemented) or media supplemented with one of three PUFA (LNA, A-LNA, AA). Cells were then co-cultured with the wild-type LA (NCK56), dual-antigen rLA (GAD84), or the dual-antigen and dual-adjuvant rLA (GAD85) and RNA was extracted to evaluate TLR5 (Figure 4.3A), TNF-α (Figure 4.3B), and MUC2 (Figure 4.3C) gene expression by RT-qPCR. GAD84 expresses two rotavirus antigens from the VP8* domain of the VP4 capsid protein (203). GAD85 expresses these two antigens in combination with the TLR5 ligand *Salmonella enterica* flagellin (FliC) and *E. coli* TLR4 agonist fimbriae adhesion (FimH) adjuvants (206). The Gene Expression Assays™ used to evaluate gene expression have been used in the literature with the same cell line (339-341). Transcripts were chosen to help determine if (r)LA activates TLR5 in vivo, evaluate host cell inflammatory responses (TNF-α), and investigate mucin expression (MUC2) as a potential mechanism by which different probiotic strains may be adhering or failing to adhere to human cells. TLR4 (Hs00152939_m1) was an initial transcript of interest since GAD85 expresses a TLR4 agonist, but TLR4 expression was largely not detectable during optimization (data not shown) and thus not pursued further. Both PUFA supplementation (p-value: <0.0001 as measured by ANOVA) and bacterial treatment (p-value: 0.0057) significantly changed general TLR5 expression. Bacterial treatment significantly changed TNF-α expression (p-value: <0.0001) with no significant overall impact of PUFA treatment (p-value: > 0.05).

PUFA supplementation significantly changed MUC2 (p-value: <0.0001) expression; however, bacterial treatment did not have an overall significant impact (p-value: > 0.05). ANOVA tables are provided in Supplementary Table S4.1.

In cells treated with A-LNA, NCK56 induced a significantly higher expression of TLR5 than GAD85 (all adjusted p-values: <0.05; Figure 4.3A). LNA supplementation significantly decreased TLR5 expression in cells treated with NCK56, GAD84, and GAD85 as compared to cells that were only co-cultured with the respective LA species but not supplemented with any PUFA (adjusted p-value: <0.01). AA supplementation significantly decreased TLR5 expression compared to non-supplemented cells when co-cultured with GAD85 (adjusted p-value: <0.05). AA-supplemented cells co-cultured with NCK56 and GAD84 exhibited a similar trend but the difference in TLR5 expression was not significant (all adjusted p-values: > 0.05).

All bacterial treatments (NCK56, GAD84, and GAD85) increased TNF-α expression across all PUFA supplementations (non-supplemented, LNA, A-LNA, and AA; Figure 4.3B). There was significantly increased TNF-α expression in cells co-cultured with NCK56 as compared to GAD84 across all PUFA treatments (all adjusted p-values: <0.05). Similarly, GAD85 induced significantly increased expression of TNF-α than GAD84 across all PUFA treatments (all adjusted p-values: <0.05). TNF-α expression trended higher in GAD85-exposed cells than NCK56 regardless of PUFA treatment, but this difference was only significant in cells supplemented with A-LNA and AA (all adjusted p-values: <0.05). Additionally, AA supplementation induced the most significant difference in TNF-α expression between GAD85 and both GAD84 (adjusted p-value: <0.0001) and NCK56 (adjusted p-value: 0.0084).

LNA supplementation significantly increased MUC2 expression as compared to all other PUFA treatments (no supplementation, A-LNA, and AA) for NCK56-, GAD84-, and GAD85-exposed cells (all adjusted p-values: <0.05; Figure 4.3C). Conversely, A-LNA supplementation significantly decreased MUC2 expression as compared to all other PUFA treatments across all bacterial treatments (all adjusted p-values: <0.05). AA supplementation significantly decreased MUC2 expression as compared to all other PUFA treatments for GAD84 co-cultured cells (all adjusted p-values: <0.05). AA treatment only

significantly decreased MUC2 expression as compared to LNA and non-supplemented cells for NCK56 and GAD85 co-cultured treatments (all adjusted *p*-values: <0.05).

Adjusted *p*-values for TLR5, TNF-α, and MUC2 are provided in Supplementary Tables S4.2-S4.4, respectively. These data collectively demonstrate bacterial co-culture in combination with PUFA treatment differentially induce gene expression related to microbial recognition, inflammation, and intestinal barrier integrity.

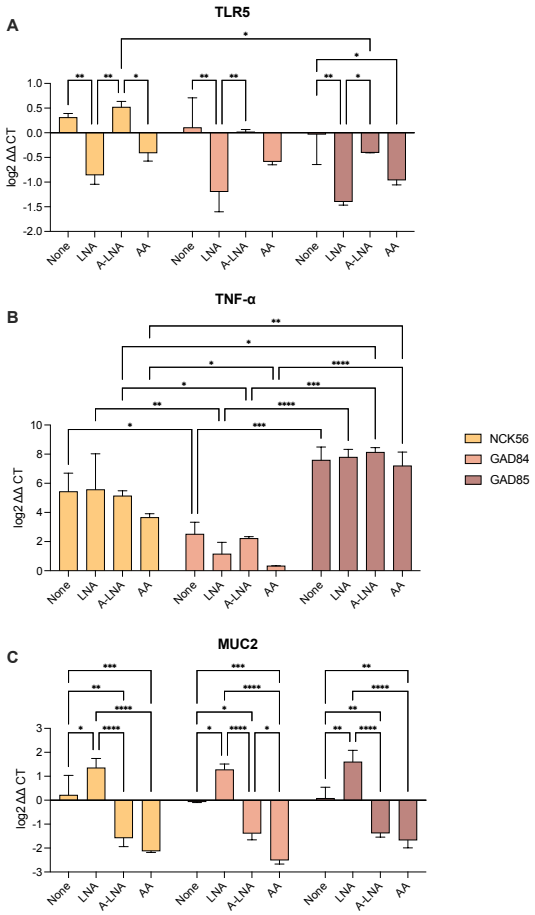

Figure 4.3. Differential gene expression of (A) TLR5, (B) TNF-α, and (C) MUC2 following co-culture of either NCK56 (yellow), GAD84 (orange), or GAD85 (brown) with PUFA-treated (None, LNA, A-LNA, or AA) Caco-2 cells. Gene expression was evaluated by RT-qPCR by normalizing to the GAPDH housekeeping gene with fold-change determined relative to untreated Caco-2 cell controls. (**A**) TLR5 expression was altered by both PUFA and bacterial treatments. (**B**) TNF-α and (**C**) MUC2 expression were attenuated primarily by mainly PUFA treatment or bacterial treatment, respectively. Two-way ANOVA with Tukey's adjusted *p*-value: '****' <0.0001, '***' <0.001, '**' <0.01, '*' <0.05. None: no PUFA supplementation, LNA: linoleic acid, A-LNA: α-linolenic acid, AA: arachidonic acid.

4.3.3. LA Adhesion is Dependent on Strain and PUFA Treatment

Caco-2 cell monolayers were co-cultured with (r)LA. Bacterial adhesion to cells in vitro was determined by percent of CTV-positive events by flow cytometry. Confirmation of successful CTV staining for NCK56 (Figure 4.4A), GAD84 (Figure 4.4B), and GAD85 (Figure 4.4C).

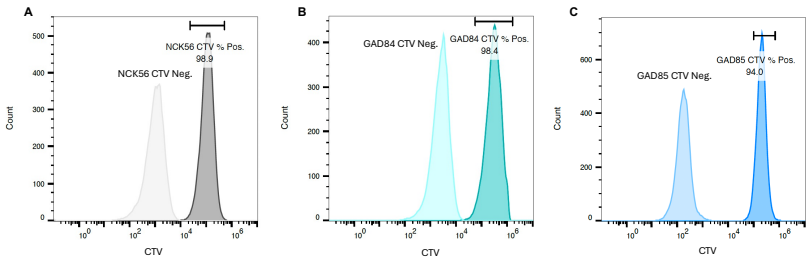

Figure 4.4. Histograms confirming successful Cell Trace violet (CTV) staining of (r)LA cultures by flow cytometry. The dark peaks indicate the CTV-stained positive controls in the CTV (FL-9) channel for (**A**) NCK56, (**B**) GAD84, (**C**) GAD85. The unstained, negative bacteria controls are represented by the light peaks.

Caco-2 cell culture media was either not supplemented (Figure 4.5A) or supplemented with one of three PUFA: LNA (Figure 4.5B), A-LNA (Figure 4.5C), or AA (Figure 4.5D). Replicates within treatments were reproducible as the Brown-Forsythe test was insignificant (*p*-values: > 0.05) for all treatments (Figure 4.5A-D), indicating the standard deviations were not significantly different among groups. GAD85, which expresses two rotavirus antigens along with two mucosal adjuvants, adhered significantly more (adjusted *p*-value: <0.05) to human cells in vitro than NCK56 across all treatments, regardless of PUFA supplementation status. GAD85 also adhered significantly more than GAD84 across all treatments apart from cells treated with arachidonic acid, where the difference between GAD84 and GAD85 was insignificant (adjusted *p*-value: > 0.05; Figure 4.5D). GAD84 adhered significantly more than NCK56 when cells were supplemented with either LNA, A-LNA, or AA (Figure 4.5B-D). However, there was no significant difference (adjusted *p*-value: > 0.05) between NCK56 and GAD84 when cells were not supplemented with PUFA (Figure 4.5A). These results demonstrate that the rLA construct GAD85 expressing multiple rotavirus antigens and adjuvants is consistently capable of adhering to host cells more than either wild-type or other recombinant *Lactobacillus* strains. Additionally, these results hint at potential

exogenous treatments, like PUFA supplementation, that can further attenuate and potentially enhance adhesion and association of rLA strains with host cells.

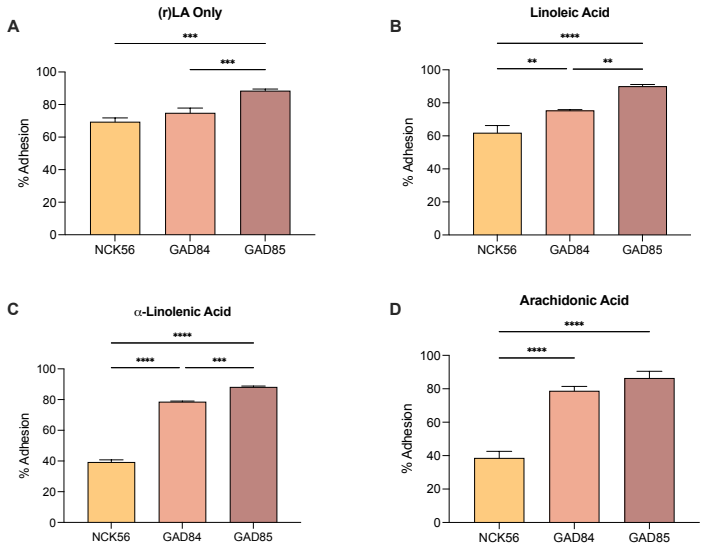

Figure 4.5. Percent of (r)LA adhering to Caco-2 cells as measured by flow cytometry. LA strains NCK56 (yellow), GAD84 (orange), or GAD85 (brown) adherence to cells either (**A**) not supplemented with any PUFA or supplemented with either (**B**) LNA, (**C**) A-LNA, or (**D**), AA. One-way ANOVA with Tukey's adjusted *p*-value: '****' <0.0001, '***' <0.001, '**' <0.01. LNA: linoleic acid, A-LNA: α-linolenic acid, AA: arachidonic acid.

4.3.4. Recombinant LA Prevents *E. coli* Adhesion

Caco-2 cell monolayers were co-cultured with both (r)LA and EC to simulate the presence of other enteric pathogens that exogenous probiotics encounter in the host intestinal environment. Percent of EC adhesion was measured by CTV positive events by flow cytometry. Confirmation of successful CTV staining of EC (Figure 4.6A). Replicates within treatments were reproducible as the Brown-Forsythe test was insignificant (*p*-value: 0.151), indicating the standard deviations were not significantly different among groups (Figure 4.6B). There was significantly less (adjusted *p*-value: <0.05) EC adherence to the Caco-2 cell monolayer when co-cultured with GAD85 (brown) compared to GAD84 (orange) and NCK56 (yellow). GAD84 had less EC detected compared to NCK56; however, this difference was not significant (adjusted *p*-value: > 0.05). These results demonstrate interference of EC interaction with human host cells in vitro by administration of the rLA GAD85 strain.

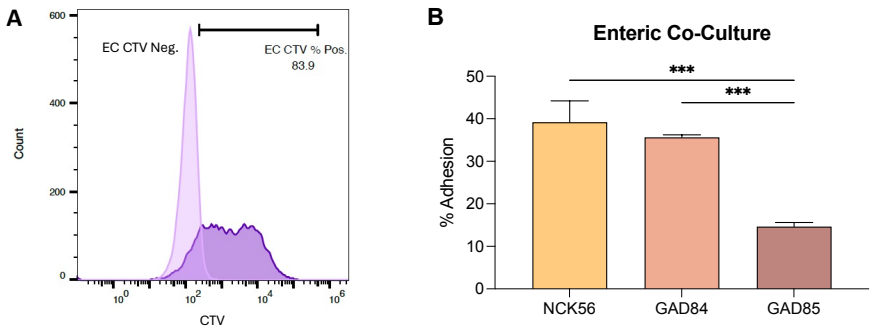

Figure 4.6. Co-culture of *E. coli* (EC) and (r)LA. (**A**) Flow cytometry histograms confirming CTV-staining of EC. CTV-stained bacteria are in dark purple compared to the light purple histogram of unstained cells. (**B**) Prevention of EC adhesion by different (r)LA strains. Percent of EC adhering to Caco-2 cells after co-culture with LA strains NCK56 (yellow), GAD84 (orange), or GAD85 (brown). One-way ANOVA with Tukey's adjusted *p*-value: '***' <0.001.

4.4. Discussion

The host intestinal microenvironment is complex, from the physical structure of the epithelium to the protective effect of commensal bacteria and the mucosal immune response to pathogens. Structural components like MUC2 are necessary for intestinal integrity by preventing translocation of bacteria and other potentially harmful substances from the lumen (327). The gut performs a balancing act of housing and supplying nutrients for diverse commensal microbes without allowing energy depletion from these microbes or invasion of pathogens (342). For example, commensal microbiome metabolites, including taurine, can regulate inflammasome signaling to maintain antimicrobial peptide induction and a "healthy" microbiome composition. Disruption of inflammasome signaling leads to dysbiosis within the microbiome which can induce inflammatory conditions in the gut (343). Dietary changes can alter the microbiome's composition and function. In a human cohort, animal- compared to plant-based diets changed the microbiome community structure more and increased bile acid microbial metabolism which can be inflammatory (344). High-fat diets worsened existing colitis in mice through a decrease in short-chain fatty acid (butyrate and retinoic acid) concentration and dendritic cell dysregulation in the colon (345). Enteric infections can take advantage of host fatty acids to augment infection and disease progression. In both in vivo and in vitro models, rotavirus infection increases prostaglandin (PGE_2) levels, which are AA derivatives. This PGE_2 attenuation potentially augments the infection through various mechanisms

including improved virus attachment and increased water secretion (346). For example, administering PGE_2 inhibitors (cyclooxygenases) at the start of rotavirus infection in vitro decreased viral internalization and yield, while supplementation with certain PUFAs increased viral yield in a time-specific manner (346). Additionally, rotavirus uses innate host lipid metabolism for viral lipid droplet formation (347). The omega-6 and omega-3 long-chain PUFAs are important for cell membrane function and cell signaling, and the ratio of omega-6 to omega-3 has immunomodulatory outcomes and an imbalance can lead to conditions like heart disease (348, 349).

Caco-2 is generally considered an inherently low to absent MUC2-producing cell line (350). However, co-culturing with exogenous probiotics has been shown to increase MUC2 expression in Caco-2 cells (351). Similarly, we saw differential MUC2 expression upon exposure to LA strains. The greatest increase in relative MUC2 expression was seen in LNA-supplemented cells (Figure 4.3C). Mucin can provide protection for LAB against the harmful effects of LNA, which could explain why we observed increased relative MUC2 expression during LNA supplementation and LA co-culture (352). Additionally, increases in MUC2 mRNA may not be reflected in actual protein accumulation (327). Therefore, MUC2 protein may be accumulating differently than what we can detect with gene expression alone. TNF-α and serum amyloid 2 protein can work in tandem to induce MUC2 expression in the face of bacterial infection at the epithelium (329). Whether the increased TNF-α expression we observed might eventually result in an increase of MUC2, would require a longitudinal analysis of cellular responses.

Some probiotic organisms are known to ameliorate inflammatory responses by disrupting production of inflammatory cytokines including TNF-α (335). Interestingly, we see upregulation of TNF-α in both wild-type and recombinant LA strains with the greatest increase seen in the rLA strain expressing both antigens and adjuvants (Figure 4.3B). TNF-α expression across all LA strains could be due to the innate immune-activating microbe-associated molecular patterns (MAMPs) of LA including the cell wall component lipoteichoic acid (LTA) and MDP. The LTA from various *Lactobacillus* spp. including LA can induce TNF-α expression to different extents in murine splenocytes (353). We have seen NOD2 signaling is important for generating rLA-specific mucosal immune responses in vivo and that rLA MDP activates

NOD2 in vitro (250, 354). The significant log-fold increase of TNF-α in the dual-antigen, dual-adjuvant rLA strain presented here aligns with prior studies where we demonstrated recombinant *Lactobacillus*-based vaccines can induce increased inflammatory cytokine expression (213). *Lactobacillus* spp. used as a rotavirus vaccine adjuvant in pigs also induced TNF-α expression (355). AA supplementation generated the most significant differences in relative TNF-α expression between NCK56, GAD84 and GAD85 co-cultured cells. These data demonstrate proinflammatory responses are induced by (r)LA exposure and these responses are seemingly attenuated tangentially by PUFA supplementation. There was no TLR5 expression detected in the GAD85 treatment for non-supplemented cells (Figure 4.3A). This was surprising given that GAD85 alone expresses the TLR5 agonist FliC which is an effective mucosal adjuvant, and Caco-2 cells have detectable TLR5 expression from initial seeding to day 21 post-seeding (356, 357). TLR5 is usually located on the basolateral side of the epithelium to prevent commensal bacterial flagellin from inducing inflammation, but TLR5 expression has been seen apically in Caco-2 cells three days post-confluence, which resembles when cells this Chapter were used prior to complete polarization (357, 358). LA-induced TLR5 expression in Caco-2 cells was dependent on PUFA treatment as TLR5 was significantly less expressed in LNA and AA treated cells across probiotic treatments, and there was significantly more relative TLR5 expression with NCK56 than GAD85 treatment in A-LNA-supplemented host cells. Caco-2 cell generation of proinflammatory responses is dependent on the stimuli (359). Our results may indicate TLR5 expression is potentially not inducible by rLA stimulation in this system or not measurable by the presented approach. Measuring gene expression of alternative transcripts such as IL-1β or IL-8, which are expressed from enterocytes in response to bacterial pathogens, could prove helpful in elucidating rLA impact on host cells outside of TLR5 expression exclusively (360, 361).

Lactobacillus species have been shown to endogenously contain various PUFA, including conjugated LNA isomers, A-LNA, docosahexaenoic acid and oleic acid. LNA and AA were not found (362). When grown in MRS supplemented with PUFA, *Lactobacillus* species can incorporate these free PUFA into their lipid content. Integrating PUFA only results in minor changes on the physical characteristics of the probiotic; for example, slightly decreased hydrophobicity (362). Like our results,

Kankaanpää et al. (2001) found adhesion to Caco-2 cells supplemented with different PUFA is strain- and PUFA-dependent (363). The authors determined supplementation with LNA, AA and A-LNA decreased *Lactobacillus* spp. adhesion relative to not supplemented controls. We observed this trend with the NCK56 group (Figure 4.5). Conversely, rLA strains generally adhered relatively similarly regardless of PUFA treatment to the not supplemented controls, with GAD85 significantly more adherent than the other rLA strain with LNA and A-LNA supplementation. The differences in adhesive capability we observed could be attributed to alterations in fatty acid content of epithelial cell membranes during PUFA supplementation as hypothesized by Kankaanpää et al. (2001) (363). Additionally, antigen and/or adjuvant expression may improve host cell adherence. For example, FliC and FimH expression in a uropathogenic *E. coli* strain improved adherence as compared to the FliC and FimH knockout strains (364). Also, LAB adherence to cells in vitro inherently differs by species (360). Caco-2 cells appear to express minimal GP2 endogenously, but expression can be induced by differentiation into M-cells via co-culturing with Raji B lymphocytes (36, 365). Therefore, it is unlikely GP2 is the mechanism of action for improved adhesion between rLA and host cells. *Lactobacillus* species can interrupt and attenuate *E. coli* adhesion in both in vivo and in vitro models (366, 367). We also observed inhibition of *E. coli* adherence to Caco-2 cells primarily by the rLA GAD85 strain (Figure 4.6B). This could be due to the increased adherence of recombinant than wild-type LA to cells (Figure 4.5A-D). Additional follow-up studies are required to be conclusive, but tentatively rLA is effective at preventing potential enteropathogens from adhering to host cells. This is relevant for a rotavirus probiotic-based vaccine as pathogenic *E. coli* is a common enteric infection in lower-middle-income countries (368).

Limitations include Caco-2 cells, although commonly used and generally accepted as representative of the intestinal mucosa (369, 370), offer a somewhat incomplete proxy for the intestinal epithelium. The gastrointestinal tract primarily includes enterocytes and goblet cells, the latter of which are responsible for mucin production (371). Caco-2 cells are capable of polarizing and mimicking enterocytes while the other common colon carcinoma cell line HT29 is undifferentiated but contains mucus-secreting cells in addition to absorptive cells. The related HT29-MTX cell line is differentiated with more goblet-like

cell properties (371), and the LS174T cell line potentially expresses more MUC2 (370). We did not use fully polarized Caco-2 cells in Transwell® filters as that system is primarily used to measure drug transport and membrane resistance (372). Caco-2 cells are mosaic while differentiating from 0 to 21 days post-seeding and can differentiate spontaneously upon confluence (333, 373). Further studies of (r)LA-cell interactions could therefore culture Caco-2 cells longer after seeding in plates for comparison. Additional future directions may include using an alternative cell model or human intestinal enteroids (HIE). HIEs are 3D recapitulations of the intestinal environment that can maintain segment-specific characteristics of cells along the intestine (374). HIEs support rotavirus replication and appear promising for evaluating metabolite influence on the epithelium and potentially microbiome in a physiologically representative system (375). No cell line or model is a perfect replica. We did not quantify any metabolite or protein concentrations and instead used mRNA expression and adhesion as proxies, which are limitations for drawing definitive conclusions regarding mechanisms behind rLA-cell interactions during fatty acid supplementation. We successfully determined PUFA concentration for cell viability (Figure 4.2), but another avenue for improvement is optimizing the PUFA concentration for bacterial viability (363). Future directions include potentially using the porcine IPEC-J2 cell line which was generated from small intestinal tissue and offers an effective in vitro model of rotavirus infection (376). We are using pigs as our next animal model for measuring in vivo rLA-induced immune responses and protection from viral challenge. The benefits of porcine versus murine models are described in Chapters 2 and 5. In the same vein, PUFA supplementation with rLA vaccination in a murine or other relevant animal model could permit measuring bacterial-derived metabolites of PUFA saturation and correlating with immune outcomes. Finally, overexpressing conjugated LNA in *Lactobacillus* species inhibits *Salmonella enterica* serovar Typhimurium and enterohaemorrhagic *E. coli* adhesion (377). Similarly developing a recombinant LA platform that can take advantage of biologically relevant microbial-derived metabolites to drive improved vaccine-induced immune responses could be worth investigating.

4.5. Conclusions

This Chapter was a preliminary investigation into attenuating host-LA interactions via PUFA supplementation. LA strains adhered distinctly to host cells and both PUFA supplementation and bacterial strain induced differential gene expression related to inflammation, pathogen recognition, and intestinal integrity. Future investigations are required to draw concrete conclusions about (r)LA-host cell interactions in the face of fatty acid supplementation. The studies presented here provide initial insight into and a methodology for evaluating PUFA metabolism on rLA efficacy in vitro.

CHAPTER 5: SUMMARY AND FUTURE DIRECTIONS

5.1. Concluding Remarks

Four rotavirus vaccines are currently approved for global use. However, rotavirus remains an enteric pathogen of concern as one of the leading causes of diarrheal-associated death in children under five (378). This is in part due to a discrepancy in vaccine efficacy between high-income and lower-middle-income countries (LMIC). The reasons underpinning this difference in vaccine performance are multifaceted, some of which include maternal antibody interference, enteric enteropathy, malnutrition, and differential access to healthcare and safe drinking water (14). As reviewed in Chapter 1, another contributing factor is the microbiome. Both the host immune system and resident microbiome are complex. Due to the high variability in microbiota composition between and within populations, establishing cause-and-effect relationships between microbes and vaccine-induced immune responses are difficult. Given these variables, there is a demand for alternative vaccines that may bridge the gap in rotavirus vaccine efficacy.

We have previously shown *Lactobacillus acidophilus* (LA) to be one such promising next-generation vaccine platform (201, 222). This commensal bacterium can be delivered orally to reach the gut-associated lymphoid tissue for effective mucosal immune activation, and it can tolerate expression of exogenous immunogenic components. Additionally, it does not require specialized administration or cold-chain storage making it ideal for use in resource-poor settings. In this dissertation we further investigated our novel recombinant LA (rLA) rotavirus vaccine platform from host and microbial perspectives. First, we developed two rLA vaccines expressing either VP8* antigens (10 amino-acid peptide VP8Pep and pseudo full-length protein VP8-1) from the murine EDIM rotavirus strain alone (rLA GAD84 strain) or in conjunction with the FimH and FliC adjuvants (rLA GAD85 strain). We evaluated rLA vaccine efficacy in vivo using an adult BALB/c murine rotavirus challenge model. Our results indicate that rLA can induce rotavirus-specific antibody responses that was further improved by adjuvant expression. Additionally, antigen-specific antibody-secreting cell (ASC) responses are generated in both systemic and local lymphoid

tissues. These ASC memory B-cell responses are seemingly primed by rLA vaccination and boosted by viral challenge. Additionally, rLA provides modest homotypic protection from viral challenge.

Next, we assessed immediate transcriptional (metatranscriptomics) and structural (metagenomics) changes within the small intestine microbiome following rLA vaccination in C567BL/6 mice. Our results demonstrate that LA is detectable at a mucosal inductive site (Peyer's patch) in probiotic-exposed groups. Further, rLA expresses relevant antigen (VP8-1) and adjuvant (FliC, FimH) transcripts. Our results highlight how the recombinant LA may adapt to the host environment distinctly from wild-type LA (e.g. overexpressing pyrimidine synthesis/metabolism genes). There is a differential and rapid, but likely temporary, change in the α- and β-diversity metrics resulting from oral probiotic administration. We also find metagenome assembled genomes have limited usefulness with our sequencing strategy, potentially due to the dominance of LA. Finally, we took an in vitro approach to dissecting rLA-cell interactions in response to polyunsaturated fatty acid (PUFA) metabolism in a human enterocyte cell line. We supplemented cells with either omega-6 (linoleic acid, arachidonic acid) or omega-3 (α-linolenic acid) PUFAs as they have distinct immunomodulatory properties, then co-cultured with different recombinant and wild-type LA strains. Both LA strain and PUFA supplementation generate distinct gene expression related to inflammation, pathogen recognition, and epithelial structure. rLA strains seemingly adhere better to cells across PUFA treatments compared to wild-type, and rLA expressing both antigens and adjuvants preliminarily prevents *E. coli* (a representative for other enteropathogens present in the microbiome) cellular adhesion best. More work is required to unravel the mechanism underlying these initially observed interactions.

Collectively, these results indicate the potential for a probiotic next-generation vaccine construct against rotavirus. We demonstrated the possibility for modest, but not complete, protection against live infection and the applicability of using multi-omics for informing future improved probiotic-based vaccine designs. We also established a methodology for further understanding of additional mechanisms by which rLA efficacy could be improved and out compete other enteric pathogens through dietary fatty acid metabolism.

5.2. Future Directions

Developing a probiotic vaccine platform that can generate protective mucosal immunity against rotavirus infection is no small feat but a worthwhile challenge. There are several future directions from which to build on the studies presented in this dissertation. As discussed in Chapter 2, using an alternative animal model to an adult murine model is necessary to understand protection from clinical disease conferred by rLA vaccination. A neonatal pig model will help fill this gap in our understanding as pigs develop clinical signs of rotavirus disease for a longer duration. Therefore, we can evaluate clinically-relevant amelioration of disease outcomes in conjunction with adaptive immunity resulting from rLA vaccination (191). Currently, immunization and challenge studies are in progress with gnotobiotic neonatal pigs. Using gnotobiotic pigs will also help further isolate the role of the microbiome in rLA-induced immunity as they can be transplanted with an exogenous microbial community of interest, such as "healthy" and dysbiotic human microbiomes. Despite being a well-established animal model, mice are genetically identical which is a factor limiting their translatability to humans. Pigs are genetically diverse and more closely represent humans immunologically, physically, and developmentally than rodents (379). Additionally, developing rLA vaccines that express human antigens is relevant for future rLA vaccine use in a human cohort. Confirmation of rLA strains expressing antigens from the human rotavirus VP7 outer capsid protein combined with the *Salmonella enterica* serovar Typhimurium FliC adjuvant are in progress (7). In the same vein, in vitro models of the human intestinal microenvironment could bridge animal to human applications of rLA. For example, "mini-gut" enteroid and organoid systems are effective models for enteric infection research as they include the relevant physiology and cell types of the human intestine (380).

In the future, as we have done for microbiome community structure (201), we could monitor the microbiome's transcriptional changes over the course of a full rLA immunization schedule. This may confirm which changes are transient versus persistent, and if every oral probiotic dose results in similar changes to what are described in this dissertation. It is also necessary to correspond 'omics results with

immune correlates of protection and immune cell population dynamics to provide a more cohesive picture of how the rLA vector and resident microbiome directly influence vaccine immunogenicity. For instance, single-cell transcriptomics of human-derived monocytes revealed some mechanisms driving immunogenicity behind BCG vaccination (381). Additionally, Hagan et al. (2019) found recall versus primary immune responses to influenza vaccination were resistant to the impact of microbiome perturbation (e.g. antibiotic administration) in adult human cohorts (103). Similar evaluation of such immune memory durability to microbiome shifts in the context of rotavirus vaccine-mediated immunity could be interesting in populations experiencing rotavirus re-infection coupled with a dysbiotic microbiome.

There is progress to be made in furthering a recombinant probiotic rotavirus vaccine. It will be an exciting adventure for *Lactobacillus acidophilus*.

REFERENCES

1. Desselberger U. The Mammalian Intestinal Microbiome: Composition, Interaction with the Immune System, Significance for Vaccine Efficacy, and Potential for Disease Therapy. Pathogens. 2018;7(3):57.
2. Pfeiffer JK, Virgin HW. Viral immunity. Transkingdom control of viral infection and immunity in the mammalian intestine. Science. 2016;351(6270).
3. Arnold JW, Roach J, Azcarate-Peril MA. Emerging Technologies for Gut Microbiome Research. Trends in Microbiology. 2016;24(11):887-901.
4. Vujkovic-Cvijin I, Welles HC, Ha CWY, Huq L, Mistry S, Brenchley JM, et al. The systemic anti-microbiota IgG repertoire can identify gut bacteria that translocate across gut barrier surfaces. Science Translational Medicine. 2022;14(658):eabl3927.
5. Karst SM. The influence of commensal bacteria on infection with enteric viruses. Nature Reviews Microbiology. 2016;14(4):197-204.
6. Zimmermann P, Curtis N. The influence of the intestinal microbiome on vaccine responses. Vaccine. 2018;36(30):4433-9.
7. Crawford SE, Ramani S, Tate JE, Parashar UD, Svensson L, Hagbom M, et al. Rotavirus infection. Nature Reviews Disease Primers. 2017;3(1):17083.
8. Du Y, Chen C, Zhang X, Yan D, Jiang D, Liu X, et al. Global burden and trends of rotavirus infection-associated deaths from 1990 to 2019: an observational trend study. Virology Journal. 2022;19(1):166.
9. WHO. Rotavirus Vaccines: WHO Position Paper - July 2021. Weekly Epidemiological Record. 2021;96(28):301-219.
10. WHO WHO. Immunization coverage. 2023.
11. Soares-Weiser K, Bergman H, Henschke N, Pitan F, Cunliffe N. Vaccines for preventing rotavirus diarrhoea: vaccines in use. Cochrane Database Syst Rev. 2019;3(3):Cd008521.
12. Ramakrishnan G, Ma JZ, Haque R, Petri WA. Rotavirus vaccine protection in low-income and middle-income countries. The Lancet Infectious Diseases. 2019;19(7):673-4.
13. Bergman H, Henschke N, Hungerford D, Pitan F, Ndwandwe D, Cunliffe N, et al. Vaccines for preventing rotavirus diarrhoea: vaccines in use. Cochrane Database Syst Rev. 2021;11(11):Cd008521.
14. Steele AD, Victor JC, Carey ME, Tate JE, Atherly DE, Pecenka C, et al. Experiences with rotavirus vaccines: can we improve rotavirus vaccine impact in developing countries? Hum Vaccin Immunother. 2019;15(6):1215-27.
15. de Jong SE, Olin A, Pulendran B. The Impact of the Microbiome on Immunity to Vaccination in Humans. Cell Host Microbe. 2020;28(2):169-79.
16. Dekaboruah E, Suryavanshi MV, Chettri D, Verma AK. Human microbiome: an academic update on human body site specific surveillance and its possible role. Archives of Microbiology. 2020;202(8):2147-67.
17. Walker AW, Hoyles L. Human microbiome myths and misconceptions. Nature Microbiology. 2023;8(8):1392-6.
18. Amimo JO, Raev SA, Chepngeno J, Mainga AO, Guo Y, Saif L, et al. Rotavirus Interactions With Host Intestinal Epithelial Cells. Frontiers in Immunology. 2021;12.
19. Clasen SJ, Bell MEW, Borbón A, Lee D-H, Henseler ZM, de la Cuesta-Zuluaga J, et al. Silent recognition of flagellins from human gut commensal bacteria by Toll-like receptor 5. Science Immunology. 2023;8(79):eabq7001.
20. Zimmermann P. The immunological interplay between vaccination and the intestinal microbiota. npj Vaccines. 2023;8(1):24.
21. Lynn MA, Tumes DJ, Choo JM, Sribnaia A, Blake SJ, Leong LEX, et al. Early-Life Antibiotic-Driven Dysbiosis Leads to Dysregulated Vaccine Immune Responses in Mice. Cell Host & Microbe. 2018;23(5):653-60.e5.

22. Oh JZ, Ravindran R, Chassaing B, Carvalho FA, Maddur MS, Bower M, et al. TLR5-mediated sensing of gut microbiota is necessary for antibody responses to seasonal influenza vaccination. Immunity. 2014;41(3):478-92.
23. Jones MK, Watanabe M, Zhu S, Graves CL, Keyes LR, Grau KR, et al. Enteric bacteria promote human and mouse norovirus infection of B cells. Science. 2014;346(6210):755-9.
24. Grau KR, Zhu S, Peterson ST, Helm EW, Philip D, Phillips M, et al. The intestinal regionalization of acute norovirus infection is regulated by the microbiota via bile acid-mediated priming of type III interferon. Nature Microbiology. 2020;5(1):84-92.
25. Lee B, Kader MA, Colgate ER, Carmolli M, Dickson DM, Diehl SA, et al. Oral rotavirus vaccine shedding as a marker of mucosal immunity. Scientific Reports. 2021;11(1):21760.
26. Harris VC, Armah G, Fuentes S, Korpela KE, Parashar U, Victor JC, et al. Significant Correlation Between the Infant Gut Microbiome and Rotavirus Vaccine Response in Rural Ghana. J Infect Dis. 2017;215(1):34-41.
27. Kim AH, Armah G, Dennis F, Wang L, Rodgers R, Droit L, et al. Enteric virome negatively affects seroconversion following oral rotavirus vaccination in a longitudinally sampled cohort of Ghanaian infants. Cell Host & Microbe. 2022;30(1):110-23.e5.
28. Harris V, Ali A, Fuentes S, Korpela K, Kazi M, Tate J, et al. Rotavirus vaccine response correlates with the infant gut microbiota composition in Pakistan. Gut Microbes. 2018;9(2):93-101.
29. Zhang G, Meredith TC, Kahne D. On the essentiality of lipopolysaccharide to Gram-negative bacteria. Current Opinion in Microbiology. 2013;16(6):779-85.
30. Robertson RC, Church JA, Edens TJ, Mutasa K, Min Geum H, Baharmand I, et al. The fecal microbiome and rotavirus vaccine immunogenicity in rural Zimbabwean infants. Vaccine. 2021;39(38):5391-400.
31. Parker EPK, Praharaj I, Zekavati A, Lazarus RP, Giri S, Operario DJ, et al. Influence of the intestinal microbiota on the immunogenicity of oral rotavirus vaccine given to infants in south India. Vaccine. 2018;36(2):264-72.
32. Parker EPK, Bronowski C, Sindhu KNC, Babji S, Benny B, Carmona-Vicente N, et al. Impact of maternal antibodies and microbiota development on the immunogenicity of oral rotavirus vaccine in African, Indian, and European infants. Nature Communications. 2021;12(1):7288.
33. Cunningham-Oakes E, Bronowski C, Chinyama E, Jere KC, Sindhu KNC, Kang G, et al. Increased bacterial taxonomic and functional diversity is associated with impaired rotavirus vaccine immunogenicity in infants from India and Malawi. BMC Microbiology. 2023;23(1):354.
34. Twitchell EL, Tin C, Wen K, Zhang H, Becker-Dreps S, Azcarate-Peril MA, et al. Modeling human enteric dysbiosis and rotavirus immunity in gnotobiotic pigs. Gut Pathogens. 2016;8(1):51.
35. Shi Z, Zou J, Zhang Z, Zhao X, Noriega J, Zhang B, et al. Segmented Filamentous Bacteria Prevent and Cure Rotavirus Infection. Cell. 2019;179(3):644-58.e13.
36. Rodríguez-Díaz J, García-Mantrana I, Vila-Vicent S, Gozalbo-Rovira R, Buesa J, Monedero V, et al. Relevance of secretor status genotype and microbiota composition in susceptibility to rotavirus and norovirus infections in humans. Scientific Reports. 2017;7(1):45559.
37. Fix J, Chandrashekhar K, Perez J, Bucardo F, Hudgens MG, Yuan L, et al. Association between Gut Microbiome Composition and Rotavirus Vaccine Response among Nicaraguan Infants. Am J Trop Med Hyg. 2020;102(1):213-9.
38. Engevik MA, Banks LD, Engevik KA, Chang-Graham AL, Perry JL, Hutchinson DS, et al. Rotavirus infection induces glycan availability to promote ileum-specific changes in the microbiome aiding rotavirus virulence. Gut Microbes. 2020;11(5):1324-47.
39. Sedwick C. A novel regulatory T cell population in the gut. PLoS Biology. 2014;12(4):e1001834.
40. Godefroy E, Barbé L, Le Moullac-Vaidye B, Rocher J, Breiman A, Leuillet S, et al. Microbiota-induced regulatory T cells associate with FUT2-dependent susceptibility to rotavirus gastroenteritis. Front Microbiol. 2023;14:1123803.
41. MacDonald J, Groome MJ, Mans J, Page N. FUT2 Secretor Status Influences Susceptibility to VP4 Strain-Specific Rotavirus Infections in South African Children. Pathogens. 2020;9(10):795.

42. Payne DC, Currier RL, Staat MA, Sahni LC, Selvarangan R, Halasa NB, et al. Epidemiologic Association Between FUT2 Secretor Status and Severe Rotavirus Gastroenteritis in Children in the United States. JAMA Pediatrics. 2015;169(11):1040-5.
43. Sohail MU, Al Khatib HA, Al Thani AA, Al Ansari K, Yassine HM, Al-Asmakh M. Microbiome profiling of rotavirus infected children suffering from acute gastroenteritis. Gut Pathogens. 2021;13(1):21.
44. Van Den Bossche T, Arntzen MØ, Becher D, Benndorf D, Eijsink VGH, Henry C, et al. The Metaproteomics Initiative: a coordinated approach for propelling the functional characterization of microbiomes. Microbiome. 2021;9(1):243.
45. Harris VC, Haak BW, Handley SA, Jiang B, Velasquez DE, Hykes BL, et al. Effect of Antibiotic-Mediated Microbiome Modulation on Rotavirus Vaccine Immunogenicity: A Human, Randomized-Control Proof-of-Concept Trial. Cell Host & Microbe. 2018;24(2):197-207.e4.
46. St Jean DT, Rogawski McQuade ET, Edwards JK, Thompson P, Thomas J, Becker-Dreps S. Effect of early life antibiotic use on serologic responses to oral rotavirus vaccine in the MAL-ED birth cohort study. Vaccine. 2022;40(18):2580-7.
47. Anderson EJ, Lopman B, Yi J, Libster R, Creech CB, El-Khorazaty J, et al. Effect of Concomitant Antibiotic and Vaccine Administration on Serologic Responses to Rotavirus Vaccine. Journal of the Pediatric Infectious Diseases Society. 2019;9(4):479-82.
48. Burke RM, Payne DC, McNeal M, Conrey SC, Burrell AR, Mattison CP, et al. Correlates of Rotavirus Vaccine Shedding and Seroconversion in a US Cohort of Healthy Infants. The Journal of Infectious Diseases. 2024:jiae055.
49. Uchiyama R, Chassaing B, Zhang B, Gewirtz AT. Antibiotic Treatment Suppresses Rotavirus Infection and Enhances Specific Humoral Immunity. The Journal of Infectious Diseases. 2014;210(2):171-82.
50. Hill C, Guarner F, Reid G, Gibson GR, Merenstein DJ, Pot B, et al. Expert consensus document. The International Scientific Association for Probiotics and Prebiotics consensus statement on the scope and appropriate use of the term probiotic. Nat Rev Gastroenterol Hepatol. 2014;11(8):506-14.
51. Bron PA, van Baarlen P, Kleerebezem M. Emerging molecular insights into the interaction between probiotics and the host intestinal mucosa. Nature Reviews Microbiology. 2012;10(1):66-78.
52. Hori T, Matsuda K, Oishi K. Probiotics: A Dietary Factor to Modulate the Gut Microbiome, Host Immune System, and Gut–Brain Interaction. Microorganisms. 2020;8(9):1401.
53. Gill HS. Probiotics to enhance anti-infective defences in the gastrointestinal tract. Best Practice & Research Clinical Gastroenterology. 2003;17(5):755-73.
54. Azagra-Boronat I, Massot-Cladera M, Knipping K, Garssen J, Ben Amor K, Knol J, et al. Strain-Specific Probiotic Properties of Bifidobacteria and Lactobacilli for the Prevention of Diarrhea Caused by Rotavirus in a Preclinical Model. Nutrients. 2020;12(2):498.
55. Freedman SB, Xie J, Nettel-Aguirre A, Pang X-L, Chui L, Williamson-Urquhart S, et al. A randomized trial evaluating virus-specific effects of a combination probiotic in children with acute gastroenteritis. Nature Communications. 2020;11(1):2533.
56. Parreno V, Bai M, Liu F, Jing J, Olney E, Li G, et al. Probiotic as Adjuvant Significantly Improves Protection of the Lanzhou Trivalent Rotavirus Vaccine against Heterologous Challenge in a Gnotobiotic Pig Model of Human Rotavirus Infection and Disease. Vaccines. 2022;10(9):1529.
57. Liu F, Wen K, Li G, Yang X, Kocher J, Bui T, et al. Dual Functions of Lactobacillus acidophilus NCFM as Protection Against Rotavirus Diarrhea. Journal of Pediatric Gastroenterology and Nutrition. 2014;58(2):169-76.
58. Kandasamy S, Chattha KS, Vlasova AN, Rajashekara G, Saif LJ. Lactobacilli and Bifidobacteria enhance mucosal B cell responses and differentially modulate systemic antibody responses to an oral human rotavirus vaccine in a neonatal gnotobiotic pig disease model. Gut Microbes. 2014;5(5):639-51.
59. Qiao X, Li G, Wang X, Li X, Liu M, Li Y. Recombinant porcine rotavirus VP4 and VP4-LTB expressed in Lactobacillus casei induced mucosal and systemic antibody responses in mice. BMC Microbiol. 2009;9:249.

60. Gilfillan D, Vilander AC, Pan M, Goh YJ, O'Flaherty S, Feng N, et al. Lactobacillus acidophilus Expressing Murine Rotavirus VP8 and Mucosal Adjuvants Induce Virus-Specific Immune Responses. Vaccines. 2023;11(12):1774.
61. Kobayashi N, Takahashi D, Takano S, Kimura S, Hase K. The Roles of Peyer's Patches and Microfold Cells in the Gut Immune System: Relevance to Autoimmune Diseases. Front Immunol. 2019;10:2345.
62. Carvalho MF, Gill D. Rotavirus vaccine efficacy: current status and areas for improvement. Human Vaccines & Immunotherapeutics. 2019;15(6):1237-50.
63. Holmgren J, Svennerholm A-M. Vaccines against mucosal infections. Current Opinion in Immunology. 2012;24(3):343-53.
64. Van der Weken H, Cox E, Devriendt B. Advances in Oral Subunit Vaccine Design. Vaccines. 2021;9(1):1.
65. Vilander AC, Dean GA. Adjuvant Strategies for Lactic Acid Bacterial Mucosal Vaccines. Vaccines. 2019;7(4):150.
66. Condit RC, Williamson A-L, Sheets R, Seligman SJ, Monath TP, Excler J-L, et al. Unique safety issues associated with virus-vectored vaccines: Potential for and theoretical consequences of recombination with wild type virus strains. Vaccine. 2016;34(51):6610-6.
67. Davitt CJH, Lavelle EC. Delivery strategies to enhance oral vaccination against enteric infections. Advanced Drug Delivery Reviews. 2015;91:52-69.
68. Rhee JH. Chapter 19 - Current and New Approaches for Mucosal Vaccine Delivery. In: Kiyono H, Pascual DW, editors. Mucosal Vaccines (Second Edition): Academic Press; 2020. p. 325-56.
69. Liang G, Bushman FD. The human virome: assembly, composition and host interactions. Nature Reviews Microbiology. 2021;19(8):514-27.
70. Seo S-U, Kweon M-N. Virome–host interactions in intestinal health and disease. Current Opinion in Virology. 2019;37:63-71.
71. Cao Z, Sugimura N, Burgermeister E, Ebert MP, Zuo T, Lan P. The gut virome: A new microbiome component in health and disease. eBioMedicine. 2022;81:104113.
72. Tan SK, Granados AC, Bouquet J, Hoy-Schulz YE, Green L, Federman S, et al. Metagenomic sequencing of stool samples in Bangladeshi infants: virome association with poliovirus shedding after oral poliovirus vaccination. Scientific Reports. 2020;10(1):15392.
73. Lim ES, Zhou Y, Zhao G, Bauer IK, Droit L, Ndao IM, et al. Early life dynamics of the human gut virome and bacterial microbiome in infants. Nature Medicine. 2015;21(10):1228-34.
74. Mogotsi MT, Mwangi PN, Bester PA, Mphahlele MJ, Seheri ML, O'Neill HG, et al. Metagenomic Analysis of the Enteric RNA Virome of Infants from the Oukasie Clinic, North West Province, South Africa, Reveals Diverse Eukaryotic Viruses. Viruses. 2020;12(11):1260.
75. Liang G, Zhao C, Zhang H, Mattei L, Sherrill-Mix S, Bittinger K, et al. The stepwise assembly of the neonatal virome is modulated by breastfeeding. Nature. 2020;581(7809):470-4.
76. Yang J-Y, Kim M-S, Kim E, Cheon JH, Lee Y-S, Kim Y, et al. Enteric viruses ameliorate gut inflammation via toll-like receptor 3 and toll-like receptor 7-mediated interferon-β production. Immunity. 2016;44(4):889-900.
77. do Socorro Fôro Ramos E, de Oliveira Ribeiro G, Villanova F, de Padua Milagres FA, Brustulin R, Araújo EL, et al. Composition of Eukaryotic Viruses and Bacteriophages in Individuals with Acute Gastroenteritis. Viruses [Internet]. 2021; 13(12).
78. Bao S, Wang H, Li W, Wu H, Lu C, Yong L, et al. Viral metagenomics of the gut virome of diarrheal children with Rotavirus A infection. Gut Microbes. 2023;15(1):2234653.
79. El-Heneidy A, Grimwood K, Lambert SB, Ware RS. Interference Between Enteric Viruses and Live-Attenuated Rotavirus Vaccine Virus in a Healthy Australian Birth Cohort. The Journal of Infectious Diseases. 2023.
80. Ingle H, Lee S, Ai T, Orvedahl A, Rodgers R, Zhao G, et al. Viral complementation of immunodeficiency confers protection against enteric pathogens via interferon-λ. Nature Microbiology. 2019;4(7):1120-8.

81. Gosselin V, Généreux M, Gagneur A, Petit G. Effectiveness of rotavirus vaccine in preventing severe gastroenteritis in young children according to socioeconomic status. Human Vaccines & Immunotherapeutics. 2016;12(10):2572-9.
82. Otero CE, Langel SN, Blasi M, Permar SR. Maternal antibody interference contributes to reduced rotavirus vaccine efficacy in developing countries. PLoS Pathog. 2020;16(11):e1009010.
83. Ramani S, Stewart CJ, Laucirica DR, Ajami NJ, Robertson B, Autran CA, et al. Human milk oligosaccharides, milk microbiome and infant gut microbiome modulate neonatal rotavirus infection. Nature Communications. 2018;9(1):5010.
84. Steele AD, De Vos B, Tumbo J, Reynders J, Scholtz F, Bos P, et al. Co-administration study in South African infants of a live-attenuated oral human rotavirus vaccine (RIX4414) and poliovirus vaccines. Vaccine. 2010;28(39):6542-8.
85. Cowley D, Sari RM, Handley A, Watts E, Bachtiar NS, At Thobari J, et al. Immunogenicity of four doses of oral poliovirus vaccine when co-administered with the human neonatal rotavirus vaccine (RV3-BB). Vaccine. 2019;37(49):7233-9.
86. Verkerke H, Sobuz S, Ma JZ, Petri SE, Reichman D, Qadri F, et al. Malnutrition Is Associated with Protection from Rotavirus Diarrhea: Evidence from a Longitudinal Birth Cohort Study in Bangladesh. Journal of Clinical Microbiology. 2016;54(10):2568-74.
87. McCoy KD, Geuking MB, Ronchi F. Gut Microbiome Standardization in Control and Experimental Mice. Curr Protoc Immunol. 2017;117:23.1.1-.1.13.
88. Poussin C, Sierro N, Boué S, Battey J, Scotti E, Belcastro V, et al. Interrogating the microbiome: experimental and computational considerations in support of study reproducibility. Drug Discovery Today. 2018;23(9):1644-57.
89. Angebault C, Payen M, Woerther PL, Rodriguez C, Botterel F. Combined bacterial and fungal targeted amplicon sequencing of respiratory samples: Does the DNA extraction method matter? PLoS One. 2020;15(4):e0232215.
90. Kong HH, Morris A. The emerging importance and challenges of the human mycobiome. Virulence. 2017;8(3):310-2.
91. Amato KR, Maurice CF, Guillemin K, Giles-Vernick T. Multidisciplinarity in microbiome research: a challenge and opportunity to rethink causation, variability, and scale. BioEssays. 2019;41(10):1900007.
92. Blakeley-Ruiz JA, Erickson AR, Cantarel BL, Xiong W, Adams R, Jansson JK, et al. Metaproteomics reveals persistent and phylum-redundant metabolic functional stability in adult human gut microbiomes of Crohn's remission patients despite temporal variations in microbial taxa, genomes, and proteomes. Microbiome. 2019;7(1):18.
93. Johnson JS, Spakowicz DJ, Hong B-Y, Petersen LM, Demkowicz P, Chen L, et al. Evaluation of 16S rRNA gene sequencing for species and strain-level microbiome analysis. Nature Communications. 2019;10(1):5029.
94. Noecker C, McNally CP, Eng A, Borenstein E. High-resolution characterization of the human microbiome. Translational Research. 2017;179:7-23.
95. Li Y, Jin Y, Zhang J, Pan H, Wu L, Liu D, et al. Recovery of human gut microbiota genomes with third-generation sequencing. Cell Death & Disease. 2021;12(6):569.
96. Zhang Y, Thompson KN, Branck T, Yan Y, Nguyen LH, Franzosa EA, et al. Metatranscriptomics for the Human Microbiome and Microbial Community Functional Profiling. Annu Rev Biomed Data Sci. 2021;4:279-311.
97. Cernava T, Rybakova D, Buscot F, Clavel T, McHardy AC, Meyer F, et al. Metadata harmonization–Standards are the key for a better usage of omics data for integrative microbiome analysis. Environmental Microbiome. 2022;17(1):33.
98. Spragge F, Bakkeren E, Jahn MT, B. N. Araujo E, Pearson CF, Wang X, et al. Microbiome diversity protects against pathogens by nutrient blocking. Science. 2023;382(6676):eadj3502.
99. Guo C-J. Modulating microbiome metabolites in vivo. Science. 2020;369(6500):153-.

100. Dallari S, Heaney T, Rosas-Villegas A, Neil JA, Wong S-Y, Brown JJ, et al. Enteric viruses evoke broad host immune responses resembling those elicited by the bacterial microbiome. Cell Host & Microbe. 2021;29(6):1014-29.e8.
101. Dhakal S, Klein SL. Host Factors Impact Vaccine Efficacy: Implications for Seasonal and Universal Influenza Vaccine Programs. Journal of Virology. 2019;93(21):10.1128/jvi.00797-19.
102. Mezhenskaya D, Isakova-Sivak I, Gupalova T, Bormotova E, Kuleshevich E, Kramskaya T, et al. A Live Probiotic Vaccine Prototype Based on Conserved Influenza a Virus Antigens Protect Mice against Lethal Influenza Virus Infection. Biomedicines. 2021;9(11):1515.
103. Hagan T, Cortese M, Rouphael N, Boudreau C, Linde C, Maddur MS, et al. Antibiotics-Driven Gut Microbiome Perturbation Alters Immunity to Vaccines in Humans. Cell. 2019;178(6):1313-28.e13.
104. Iturriza-Gómara M, Kang G, Gray J. Rotavirus genotyping: keeping up with an evolving population of human rotaviruses. Journal of Clinical Virology. 2004;31(4):259-65.
105. Syverton JT, Olitsky PK. BACTERIOLOGICAL STUDIES ON AN EPIZOOTIC OF INTESTINAL DISEASE IN SUCKLING AND NEWLY WEANED MICE. Journal of Experimental Medicine. 1934;60(3):385-94.
106. Cheever FS, Mueller JH. EPIDEMIC DIARRHEAL DISEASE OF SUCKLING MICE : I. MANIFESTATIONS, EPIDEMIOLOGY, AND ATTEMPTS TO TRANSMIT THE DISEASE. J Exp Med. 1947;85(4):405-16.
107. Pappenheimer AM, Enders JF. An epidemic diarrheal disease of suckling mice: II. Inclusions in the intestinal epithelial cells. The Journal of Experimental Medicine. 1947;85(4):417-22.
108. Cheever FS, Mueller JH. EPIDEMIC DIARRHEAL DISEASE OF SUCKLING MICE: III. THE EFFECT OF STRAIN, LITTER, AND SEASON UPON THE INCIDENCE OF THE DISEASE. The Journal of Experimental Medicine. 1948;88(3):309.
109. Pappenheimer AM, Cheever FS. Epidemic diarrheal disease of suckling mice: IV. Cytoplasmic inclusion bodies in intestinal epithelium in relation to the disease. The Journal of Experimental Medicine. 1948;88(3):317.
110. Kraft LM. Studies on the etiology and transmission of epidemic diarrhea of infant mice. The Journal of Experimental Medicine. 1957;106(5):743-55.
111. Kraft LM. Observations on the control and natural history of epidemic diarrhea of infant mice (EDIM). Yale J Biol Med. 1958;31(3):121-37.
112. Adams W, Kraft L. Epizootic diarrhea of infant mice: identification of the etiologic agent. Science. 1963;141(3578):359-60.
113. Desselberger U. Rotaviruses. Virus Research. 2014;190:75-96.
114. Flewett TH, Woode GN. The rotaviruses. Arch Virol. 1978;57(1):1-23.
115. Burns JW, Krishnaney AA, Vo PT, Rouse RV, Anderson LJ, Greenberg HB. Analyses of homologous rotavirus infection in the mouse model. Virology. 1995;207(1):143-53.
116. Wolf JL, Cukor G, Blacklow NR, Dambrauskas R, Trier JS. Susceptibility of mice to rotavirus infection: effects of age and administration of corticosteroids. Infection and Immunity. 1981;33(2):565-74.
117. Greenberg HB, Vo PT, Jones R. Cultivation and characterization of three strains of murine rotavirus. J Virol. 1986;57(2):585-90.
118. Feng N, Yasukawa LL, Sen A, Greenberg HB. Permissive replication of homologous murine rotavirus in the mouse intestine is primarily regulated by VP4 and NSP1. J Virol. 2013;87(15):8307-16.
119. O'Neal CM, Crawford SE, Estes MK, Conner ME. Rotavirus virus-like particles administered mucosally induce protective immunity. Journal of Virology. 1997;71(11):8707-17.
120. McNeal MM, Belli J, Basu M, Choi AHC, Ward RL. Discovery of a new strain of murine rotavirus that is consistently shed in large quantities after oral inoculation of adult mice. Virology. 2004;320(1):1-11.
121. Tajima T, Suzuki E, Ushijima H, Araki K, Kim B, Shinozaki T, et al. Isolation of murine rotavirus in cell cultures. Archives of virology. 1984;82:119-23.

122. USHIJIMA H, NISHIO O, MORIKAWA S, MUKOYAMA A. Characterization of VP4 and VP7 of a murine rotavirus (YR-1) isolated in Japan. Japanese Journal of Medical Science and Biology. 1995;48(5-6):237-47.
123. Hoshino Y, Kapikian AZ, editors. Classification of rotavirus VP4 and VP7 serotypes1996; Vienna: Springer Vienna.
124. Dunn SJ, Burns JW, Cross TL, Vo PT, Ward RL, Bremont M, et al. Comparison of VP4 and VP7 of Five Murine Rotavirus Strains. Virology. 1994;203(2):250-9.
125. Hoshino Y, Jones RW, Kapikian AZ. Characterization of Neutralization Specificities of Outer Capsid Spike Protein VP4 of Selected Murine, Lapine, and Human Rotavirus Strains. Virology. 2002;299(1):64-71.
126. R Core Team (2022). R: A language and environment for statistical computing. R Foundation for Statistical Computing, Vienna, Austria. URL https://www.R-project.org/.
127. RStudio Team (2020). RStudio: Integrated Development for R. RStudio, PBC, Boston, MA URL http://www.rstudio.com/.
128. H W. ggplot2: Elegant Graphics for Data Analysis. Springer-Verlag New York. ISBN 978-3-319-24277-4, https://ggplot2.tidyverse.org. (2016).
129. González AM, Nguyen TV, Azevedo MS, Jeong K, Agarib F, Iosef C, et al. Antibody responses to human rotavirus (HRV) in gnotobiotic pigs following a new prime/boost vaccine strategy using oral attenuated HRV priming and intranasal VP2/6 rotavirus-like particle (VLP) boosting with ISCOM. Clin Exp Immunol. 2004;135(3):361-72.
130. Wen X, Wen K, Cao D, Li G, Jones RW, Li J, et al. Inclusion of a universal tetanus toxoid CD4+ T cell epitope P2 significantly enhanced the immunogenicity of recombinant rotavirus ΔVP8* subunit parenteral vaccines. Vaccine. 2014;32(35):4420-7.
131. Blutt SE, Warfield KL, Lewis DE, Conner ME. Early response to rotavirus infection involves massive B cell activation. J Immunol. 2002;168(11):5716-21.
132. Franco MA, Greenberg HB. Role of B cells and cytotoxic T lymphocytes in clearance of and immunity to rotavirus infection in mice. J Virol. 1995;69(12):7800-6.
133. Deal EM, Lahl K, Narváez CF, Butcher EC, Greenberg HB. Plasmacytoid dendritic cells promote rotavirus-induced human and murine B cell responses. The Journal of clinical investigation. 2013;123(6):2464-74.
134. Lopez-Guerrero DV, Meza-Perez S, Ramirez-Pliego O, Santana-Calderon MA, Espino-Solis P, Gutierrez-Xicotencatl L, et al. Rotavirus Infection Activates Dendritic Cells from Peyer's Patches in Adult Mice. Journal of Virology. 2010;84(4):1856-66.
135. Mills CD, Kincaid K, Alt JM, Heilman MJ, Hill AM. M-1/M-2 Macrophages and the Th1/Th2 Paradigm1. The Journal of Immunology. 2000;164(12):6166-73.
136. Soudi S, Zavaran-Hosseini A, Muhammad Hassan Z, Soleimani M, Jamshidi Adegani F, Hashemi SM. Comparative study of the effect of LPS on the function of BALB/c and C57BL/6 peritoneal macrophages. Cell J. 2013;15(1):45-54.
137. Reboldi A, Cyster JG. Peyer's patches: organizing B-cell responses at the intestinal frontier. Immunol Rev. 2016;271(1):230-45.
138. Palm A-KE, Henry C. Remembrance of Things Past: Long-Term B Cell Memory After Infection and Vaccination. Frontiers in Immunology. 2019;10.
139. Park JI, Cho SW, Kang JH, Park TE. Intestinal Peyer's Patches: Structure, Function, and In Vitro Modeling. Tissue Eng Regen Med. 2023;20(3):341-53.
140. Blutt SE, Conner ME. The gastrointestinal frontier: IgA and viruses. Frontiers in immunology. 2013;4:402.
141. Spencer J, Sollid LM. The human intestinal B-cell response. Mucosal Immunology. 2016;9(5):1113-24.
142. Rojas R, Apodaca G. Immunoglobulin transport across polarized epithelial cells. Nature Reviews Molecular Cell Biology. 2002;3(12):944-56.

143. Yang XD, Sytwu HK, McDevitt HO, Michie SA. Involvement of beta 7 integrin and mucosal addressin cell adhesion molecule-1 (MAdCAM-1) in the development of diabetes in obese diabetic mice. Diabetes. 1997;46(10):1542-7.
144. Kuhbandner K, Hammer A, Haase S, Terbrack E, Hoffmann A, Schippers A, et al. MAdCAM-1-Mediated Intestinal Lymphocyte Homing Is Critical for the Development of Active Experimental Autoimmune Encephalomyelitis. Frontiers in Immunology. 2019;10.
145. Müller TM, Becker E, Wiendl M, Schulze LL, Voskens C, Völkl S, et al. Circulating Adaptive Immune Cells Expressing the Gut Homing Marker α4β7 Integrin Are Decreased in COVID-19. Frontiers in Immunology. 2021;12.
146. Mora JR, Iwata M, Eksteen B, Song S-Y, Junt T, Senman B, et al. Generation of Gut-Homing IgA-Secreting B Cells by Intestinal Dendritic Cells. Science. 2006;314(5802):1157-60.
147. Kuklin NA, Rott L, Feng N, Conner ME, Wagner N, Müller W, et al. Protective Intestinal Anti-Rotavirus B Cell Immunity Is Dependent on α4β7 Integrin Expression But Does Not Require IgA Antibody Production1. The Journal of Immunology. 2001;166(3):1894-902.
148. Williams MB, Rosé JR, Rott LS, Franco MA, Greenberg HB, Butcher EC. The Memory B Cell Subset Responsible for the Secretory IgA Response and Protective Humoral Immunity to Rotavirus Expresses the Intestinal Homing Receptor, α4β71. The Journal of Immunology. 1998;161(8):4227-35.
149. Narváez CF, Franco MA, Angel J, Morton JM, Greenberg HB. Rotavirus Differentially Infects and Polyclonally Stimulates Human B Cells Depending on Their Differentiation State and Tissue of Origin. Journal of Virology. 2010;84(9):4543-55.
150. Yuan L, Saif LJ. Induction of mucosal immune responses and protection against enteric viruses: rotavirus infection of gnotobiotic pigs as a model. Veterinary Immunology and Immunopathology. 2002;87(3):147-60.
151. Johansen FE, Kaetzel CS. Regulation of the polymeric immunoglobulin receptor and IgA transport: new advances in environmental factors that stimulate pIgR expression and its role in mucosal immunity. Mucosal Immunology. 2011;4(6):598-602.
152. Pasetti MF, Simon JK, Sztein MB, Levine MM. Immunology of gut mucosal vaccines. Immunological reviews. 2011;239(1):125-48.
153. Gonzalez AM, Jaimes MC, Cajiao I, Rojas OL, Cohen J, Pothier P, et al. Rotavirus-Specific B Cells Induced by Recent Infection in Adults and Children Predominantly Express the Intestinal Homing Receptor α4β7. Virology. 2003;305(1):93-105.
154. Borisova MA, Achasova KM, Morozova KN, Andreyeva EN, Litvinova EA, Ogienko AA, et al. Mucin-2 knockout is a model of intercellular junction defects, mitochondrial damage and ATP depletion in the intestinal epithelium. Scientific Reports. 2020;10(1):21135.
155. Qiao H, Duffy LC, Griffiths E, Dryja D, Leavens A, Rossman J, et al. Immune Responses in Rhesus Rotavirus-Challenged Balb/c Mice Treated with Bifidobacteria and Prebiotic Supplements. Pediatric Research. 2002;51(6):750-5.
156. Blutt SE, Miller AD, Salmon SL, Metzger DW, Conner ME. IgA is important for clearance and critical for protection from rotavirus infection. Mucosal Immunology. 2012;5(6):712-9.
157. Shibata N, Kunisawa J, Kiyono H. Dietary and Microbial Metabolites in the Regulation of Host Immunity. Frontiers in Microbiology. 2017;8.
158. Shah AM, Yang W, Mohamed H, Zhang Y, Song Y. Microbes: A Hidden Treasure of Polyunsaturated Fatty Acids. Frontiers in Nutrition. 2022;9.
159. Calder PC. Polyunsaturated fatty acids and inflammation. Prostaglandins, leukotrienes and essential fatty acids. 2006;75(3):197-202.
160. Bojková B, Winklewski PJ, Wszedybyl-Winklewska M. Dietary Fat and Cancer—Which Is Good, Which Is Bad, and the Body of Evidence. International Journal of Molecular Sciences. 2020;21(11):4114.
161. Oppedisano F, Macrì R, Gliozzi M, Musolino V, Carresi C, Maiuolo J, et al. The Anti-Inflammatory and Antioxidant Properties of n-3 PUFAs: Their Role in Cardiovascular Protection. Biomedicines. 2020;8(9):306.

162. Xu AA, Kennedy LK, Hoffman K, White DL, Kanwal F, El-Serag HB, et al. Dietary Fatty Acid Intake and the Colonic Gut Microbiota in Humans. Nutrients. 2022;14(13):2722.
163. Caesar R, Tremaroli V, Kovatcheva-Datchary P, Cani PD, Bäckhed F. Crosstalk between gut microbiota and dietary lipids aggravates WAT inflammation through TLR signaling. Cell metabolism. 2015;22(4):658-68.
164. Moraïs S, Winkler S, Zorea A, Levin L, Nagies FSP, Kapust N, et al. Cryptic diversity of cellulose-degrading gut bacteria in industrialized humans. Science. 2024;383(6688):eadj9223.
165. Colombo SM, Rodgers TFM, Diamond ML, Bazinet RP, Arts MT. Projected declines in global DHA availability for human consumption as a result of global warming. Ambio. 2020;49(4):865-80.
166. Chatbots for the bottom four billion: Could AI transform life in developing countries? The Economist. 2024(Jan 25th).
167. Steele AD, Armah GE, Mwenda JM, Kirkwood CD. The Full Impact of Rotavirus Vaccines in Africa Has Yet to Be Realized. Clinical Infectious Diseases. 2023;76(Supplement_1):S1-S4.
168. Varghese T, Kang G, Steele AD. Understanding Rotavirus Vaccine Efficacy and Effectiveness in Countries with High Child Mortality. Vaccines. 2022;10(3):346.
169. Jennings MC, Manchester C, Sauer M. Navigating country decisions in response to a global rotavirus vaccine shortage. Vaccine. 2020;38(46):7201-4.
170. Chan J, Nirwati H, Triasih R, Bogdanovic-Sakran N, Soenarto Y, Hakimi M, et al. Maternal antibodies to rotavirus: Could they interfere with live rotavirus vaccines in developing countries? Vaccine. 2011;29(6):1242-7.
171. Burnett E, Parashar U, Tate J. Rotavirus Vaccines: Effectiveness, Safety, and Future Directions. Pediatric Drugs. 2018;20(3):223-33.
172. Chen J, Grow S, Iturriza-Gómara M, Hausdorff WP, Fix A, Kirkwood CD. The Challenges and Opportunities of Next-Generation Rotavirus Vaccines: Summary of an Expert Meeting with Vaccine Developers. Viruses. 2022;14(11):2565.
173. Pandya A, Pulakkat S, Jadhav S, Patravale V. Probiotics as Edible Vaccines. In: Beri K, Deol PK, Sandhu SK, editors. Probiotic Research in Therapeutics: Volume 3: Probiotics and Gut Skin Axis–Inside Out and Outside In. Singapore: Springer Singapore; 2022. p. 269-93.
174. Yadav DK, Yadav N, Khurana SMP. Chapter 26 - Vaccines: Present Status and Applications. In: Verma AS, Singh A, editors. Animal Biotechnology. San Diego: Academic Press; 2014. p. 491-508.
175. Atherly DE, Lewis KDC, Tate J, Parashar UD, Rheingans RD. Projected health and economic impact of rotavirus vaccination in GAVI-eligible countries: 2011–2030. Vaccine. 2012;30:A7-A14.
176. Yamey G. Global vaccine initiative creates inequity, analysis concludes. BMJ: British Medical Journal. 2001;322(7289):754.
177. Storeng KT. The GAVI Alliance and the 'Gates approach' to health system strengthening. Global Public Health. 2014;9(8):865-79.
178. Gandhi G. Charting the evolution of approaches employed by the Global Alliance for Vaccines and Immunizations (GAVI) to address inequities in access to immunization: a systematic qualitative review of GAVI policies, strategies and resource allocation mechanisms through an equity lens (1999–2014). BMC Public Health. 2015;15(1):1198.
179. Ikilezi G, Augusto OJ, Dieleman JL, Sherr K, Lim SS. Effect of donor funding for immunization from Gavi and other development assistance channels on vaccine coverage: Evidence from 120 low and middle income recipient countries. Vaccine. 2020;38(3):588-96.
180. Jennings MC, Sauer M, Manchester C, Soeters HM, Shimp L, Hyde TB, et al. Supporting evidence-based rotavirus vaccine introduction decision-making and implementation: Lessons from 8 Gavi-eligible countries. Vaccine. 2024;42(1):8-16.
181. Debellut F, Clark A, Pecenka C, Tate J, Baral R, Sanderson C, et al. Evaluating the potential economic and health impact of rotavirus vaccination in 63 middle-income countries not eligible for Gavi funding: a modelling study. The Lancet Global Health. 2021;9(7):e942-e56.
182. Lencucha R, Neupane S. The use, misuse and overuse of the 'low-income and middle-income countries' category. BMJ Glob Health. 2022;7(6).

183. Troeger C, Khalil IA, Rao PC, Cao S, Blacker BF, Ahmed T, et al. Rotavirus Vaccination and the Global Burden of Rotavirus Diarrhea Among Children Younger Than 5 Years. JAMA Pediatrics. 2018;172(10):958-65.
184. Burke RM, Tate JE, Parashar UD. Global Experience With Rotavirus Vaccines. J Infect Dis. 2021;224(12 Suppl 2):S792-s800.
185. International Vaccine Access Center (IVAC), Johns Hopkins Bloomberg School of Public Health. VIEW-hub, www.view-hub.org. Accessed: 10/30/2023.
186. O'Ryan M. Rotavirus Vaccines: a story of success with challenges ahead. F1000Res. 2017;6:1517.
187. Burnett E, Parashar U, Tate J. Rotavirus Vaccines: Effectiveness, Safety, and Future Directions. Paediatr Drugs. 2018;20(3):223-33.
188. Steele AD, Victor JC, Carey ME, Tate JE, Atherly DE, Pecenka C, et al. Experiences with rotavirus vaccines: can we improve rotavirus vaccine impact in developing countries? Human Vaccines & Immunotherapeutics. 2019;15(6):1215-27.
189. Mak TW, Saunders ME. 23 - Vaccines and Clinical Immunization. In: Mak TW, Saunders ME, editors. The Immune Response. Burlington: Academic Press; 2006. p. 695-749.
190. Moser CA, Offit PA. Distribution of rotavirus-specific memory B cells in gut-associated lymphoid tissue after primary immunization. Journal of General Virology. 2001;82(9):2271-4.
191. Saif L, Yuan L, Ward L, To T. Comparative studies of the pathogenesis, antibody immune responses, and homologous protection to porcine and human rotaviruses in gnotobiotic piglets. Adv Exp Med Biol. 1997;412:397-403.
192. Offit PA, Clark HF. Protection against rotavirus-induced gastroenteritis in a murine model by passively acquired gastrointestinal but not circulating antibodies. J Virol. 1985;54(1):58-64.
193. Ismail B. The Use of Probiotics as Vaccine Vectors to Prevent Viral Infections. In: Al Kassaa I, editor. New Insights on Antiviral Probiotics: From Research to Applications. Cham: Springer International Publishing; 2017. p. 47-60.
194. Vlasova AN, Kandasamy S, Chattha KS, Rajashekara G, Saif LJ. Comparison of probiotic lactobacilli and bifidobacteria effects, immune responses and rotavirus vaccines and infection in different host species. Vet Immunol Immunopathol. 2016;172:72-84.
195. Lycke N. Recent progress in mucosal vaccine development: potential and limitations. Nature Reviews Immunology. 2012;12(8):592-605.
196. Isolauri E, Joensuu J, Suomalainen H, Luomala M, Vesikari T. Improved immunogenicity of oral D x RRV reassortant rotavirus vaccine by Lactobacillus casei GG. Vaccine. 1995;13(3):310-2.
197. Zhang W, Azevedo MS, Wen K, Gonzalez A, Saif LJ, Li G, et al. Probiotic Lactobacillus acidophilus enhances the immunogenicity of an oral rotavirus vaccine in gnotobiotic pigs. Vaccine. 2008;26(29-30):3655-61.
198. Wells JM. Immunomodulatory mechanisms of lactobacilli. Microbial Cell Factories. 2011;10(1):S17.
199. Kajikawa A, Zhang L, LaVoy A, Bumgardner S, Klaenhammer TR, Dean GA. Mucosal Immunogenicity of Genetically Modified Lactobacillus acidophilus Expressing an HIV-1 Epitope within the Surface Layer Protein. PLoS One. 2015;10(10):e0141713.
200. Zhang H, Zhao H, Zhao Y, Sui L, Li F, Zhang H, et al. Auxotrophic Lactobacillus Expressing Porcine Rotavirus VP4 Constructed Using CRISPR-Cas9D10A System Induces Effective Immunity in Mice. Vaccines. 2022;10(9):1510.
201. Fox BE, Vilander AC, Gilfillan D, Dean GA, Abdo Z. Oral Vaccination Using a Probiotic Vaccine Platform Combined with Prebiotics Impacts Immune Response and the Microbiome. Vaccines (Basel). 2022;10(9).
202. Kajikawa A, Zhang L, Long J, Nordone S, Stoeker L, LaVoy A, et al. Construction and immunological evaluation of dual cell surface display of HIV-1 gag and Salmonella enterica serovar Typhimurium FliC in Lactobacillus acidophilus for vaccine delivery. Clin Vaccine Immunol. 2012;19(9):1374-81.

203. Xue M, Yu L, Che Y, Lin H, Zeng Y, Fang M, et al. Characterization and protective efficacy in an animal model of a novel truncated rotavirus VP8 subunit parenteral vaccine candidate. Vaccine. 2015;33(22):2606-13.
204. Kovacs-Nolan J, Yoo D, Mine Y. Fine mapping of sequential neutralization epitopes on the subunit protein VP8 of human rotavirus. Biochemical Journal. 2003;376(1):269-75.
205. Clarke E, Desselberger U. Correlates of protection against human rotavirus disease and the factors influencing protection in low-income settings. Mucosal Immunol. 2015;8(1):1-17.
206. Vilander AC, Shelton K, LaVoy A, Dean GA. Expression of E. coli FimH Enhances Trafficking of an Orally Delivered Lactobacillus acidophilus Vaccine to Immune Inductive Sites via Antigen-Presenting Cells. Vaccines. 2023;11(7):1162.
207. Rhee JH, Lee SE, Kim SY. Mucosal vaccine adjuvants update. Clin Exp Vaccine Res. 2012;1(1):50-63.
208. Barefoot SF, Klaenhammer TR. Detection and activity of lactacin B, a bacteriocin produced by Lactobacillus acidophilus. Applied and Environmental Microbiology. 1983;45(6):1808-15.
209. Sanders ME, Klaenhammer TR. Invited Review: The Scientific Basis of Lactobacillus acidophilus NCFM Functionality as a Probiotic. Journal of Dairy Science. 2001;84(2):319-31.
210. Douglas GL, Goh YJ, Klaenhammer TR. Integrative Food Grade Expression System for Lactic Acid Bacteria. In: Williams JA, editor. Strain Engineering: Methods and Protocols. Totowa, NJ: Humana Press; 2011. p. 373-87.
211. Goh YJ, Azcárate-Peril MA, O'Flaherty S, Durmaz E, Valence F, Jardin J, et al. Development and application of a upp-based counterselective gene replacement system for the study of the S-layer protein SlpX of Lactobacillus acidophilus NCFM. Appl Environ Microbiol. 2009;75(10):3093-105.
212. Walker DC, Aoyama K, Klaenhammer TR. Electrotransformation of lactobacillus acidophilus group A1. FEMS Microbiol Lett. 1996;138(2-3):233-7.
213. Kajikawa A, Nordone SK, Zhang L, Stoeker LL, LaVoy AS, Klaenhammer TR, et al. Dissimilar properties of two recombinant Lactobacillus acidophilus strains displaying Salmonella FliC with different anchoring motifs. Appl Environ Microbiol. 2011;77(18):6587-96.
214. Law J, Buist G, Haandrikman A, Kok J, Venema G, Leenhouts K. A system to generate chromosomal mutations in Lactococcus lactis which allows fast analysis of targeted genes. J Bacteriol. 1995;177(24):7011-8.
215. Reed & Muench Calculator. Created by Brett D. Lindenbach.
216. (2022). RCT. R: A language and environment for statistical computing. R Foundation for Statistical Computing, Vienna, Austria. URL https://www.R-project.org/.
217. (2020). RT. RStudio: Integrated Development for R. RStudio, PBC, Boston, MA URL http://www.rstudio.com/.
218. H W. ggplot2: Elegant Graphics for Data Analysis.: Springer-Verlag New York; 2016.
219. Douglas GL, Klaenhammer TR. Directed chromosomal integration and expression of the reporter gene gusA3 in Lactobacillus acidophilus NCFM. Appl Environ Microbiol. 2011;77(20):7365-71.
220. O'Flaherty S, Klaenhammer TR. Multivalent Chromosomal Expression of the Clostridium botulinum Serotype A Neurotoxin Heavy-Chain Antigen and the Bacillus anthracis Protective Antigen in Lactobacillus acidophilus. Appl Environ Microbiol. 2016;82(20):6091-101.
221. Li YJ, Ma GP, Li GW, Qiao XY, Ge JW, Tang LJ, et al. Oral vaccination with the porcine rotavirus VP4 outer capsid protein expressed by Lactococcus lactis induces specific antibody production. J Biomed Biotechnol. 2010;2010:708460.
222. Stoeker L, Nordone S, Gunderson S, Zhang L, Kajikawa A, LaVoy A, et al. Assessment of Lactobacillus gasseri as a Candidate Oral Vaccine Vector. Clinical and Vaccine Immunology. 2011;18(11):1834-44.
223. Yuan L, Iosef C, Azevedo MS, Kim Y, Qian Y, Geyer A, et al. Protective immunity and antibody-secreting cell responses elicited by combined oral attenuated Wa human rotavirus and intranasal Wa 2/6-VLPs with mutant Escherichia coli heat-labile toxin in gnotobiotic pigs. J Virol. 2001;75(19):9229-38.

224. Yuan L, Azevedo MSP, Gonzalez AM, Jeong K-i, Van Nguyen T, Lewis P, et al. Mucosal and systemic antibody responses and protection induced by a prime/boost rotavirus-DNA vaccine in a gnotobiotic pig model. Vaccine. 2005;23(30):3925-36.
225. Fransen F, Zagato E, Mazzini E, Fosso B, Manzari C, El Aidy S, et al. BALB/c and C57BL/6 Mice Differ in Polyreactive IgA Abundance, which Impacts the Generation of Antigen-Specific IgA and Microbiota Diversity. Immunity. 2015;43(3):527-40.
226. McNeal MM, Rae MN, Bean JA, Ward RL. Antibody-Dependent and -Independent Protection following Intranasal Immunization of Mice with Rotavirus Particles. Journal of Virology. 1999;73(9):7565-73.
227. Leshem E, Lopman B, Glass R, Gentsch J, Bányai K, Parashar U, et al. Distribution of rotavirus strains and strain-specific effectiveness of the rotavirus vaccine after its introduction: a systematic review and meta-analysis. The Lancet Infectious Diseases. 2014;14(9):847-56.
228. Amin AB, Tate JE, Waller LA, Lash TL, Lopman BA. Monovalent Rotavirus Vaccine Efficacy Against Different Rotavirus Genotypes: A Pooled Analysis of Phase II and III Trial Data. Clinical Infectious Diseases. 2022;76(3):e1150-e6.
229. PATH. PATH announces early closure of pivotal Phase 3 study of an injectable rotavirus vaccine candidate. 2022.
230. Groome MJ, Koen A, Fix A, Page N, Jose L, Madhi SA, et al. Safety and immunogenicity of a parenteral P2-VP8-P[8] subunit rotavirus vaccine in toddlers and infants in South Africa: a randomised, double-blind, placebo-controlled trial. Lancet Infect Dis. 2017;17(8):843-53.
231. Groome MJ, Fairlie L, Morrison J, Fix A, Koen A, Masenya M, et al. Safety and immunogenicity of a parenteral trivalent P2-VP8 subunit rotavirus vaccine: a multisite, randomised, double-blind, placebo-controlled trial. Lancet Infect Dis. 2020;20(7):851-63.
232. Park MS, Kwon B, Ku S, Ji GE. The Efficacy of Bifidobacterium longum BORI and Lactobacillus acidophilus AD031 Probiotic Treatment in Infants with Rotavirus Infection. Nutrients. 2017;9(8):887.
233. Ward RL, McNeal MM, Sheridan JF. Development of an adult mouse model for studies on protection against rotavirus. Journal of Virology. 1990;64(10):5070-5.
234. Brandtzaeg P. Chapter 31 - The Mucosal B Cell System. In: Mestecky J, Strober W, Russell MW, Kelsall BL, Cheroutre H, Lambrecht BN, editors. Mucosal Immunology (Fourth Edition). Boston: Academic Press; 2015. p. 623-81.
235. Kanaya T, Hase K, Takahashi D, Fukuda S, Hoshino K, Sasaki I, et al. The Ets transcription factor Spi-B is essential for the differentiation of intestinal microfold cells. Nature Immunology. 2012;13(8):729-36.
236. Knoop KA, Newberry RD. Goblet cells: multifaceted players in immunity at mucosal surfaces. Mucosal Immunology. 2018;11(6):1551-7.
237. Borbet TC, Pawline MB, Li J, Ho ML, Yin YS, Zhang X, et al. Disruption of the early-life microbiota alters Peyer's patch development and germinal center formation in gastrointestinal-associated lymphoid tissue. iScience. 2023;26(6):106810.
238. Lin S, Mukherjee S, Li J, Hou W, Pan C, Liu J. Mucosal immunity–mediated modulation of the gut microbiome by oral delivery of probiotics into Peyer’s patches. Science Advances. 2021;7(20):eabf0677.
239. Sun J, Zhou T-T, Le G-W, Shi Y-H. Association of Lactobacillus acidophilus with mice Peyer's patches. Nutrition. 2010;26(10):1008-13.
240. Konstantinov SR, Smidt H, de Vos WM, Bruijns SCM, Singh SK, Valence F, et al. S layer protein A of Lactobacillus acidophilus NCFM regulates immature dendritic cell and T cell functions. Proceedings of the National Academy of Sciences. 2008;105(49):19474-9.
241. Ohland CL, MacNaughton WK. Probiotic bacteria and intestinal epithelial barrier function. American journal of physiology-gastrointestinal and liver physiology. 2010;298(6):G807-G19.
242. Kumar D, Shepherd FK, Springer NL, Mwangi W, Marthaler DG. Rotavirus Infection in Swine: Genotypic Diversity, Immune Responses, and Role of Gut Microbiome in Rotavirus Immunity. Pathogens. 2022;11(10):1078.

243. Vlasova AN, Takanashi S, Miyazaki A, Rajashekara G, Saif LJ. How the gut microbiome regulates host immune responses to viral vaccines. Current Opinion in Virology. 2019;37:16-25.
244. Li R, Chowdhury MY, Kim JH, Kim TH, Pathinayake P, Koo WS, et al. Mucosally administered Lactobacillus surface-displayed influenza antigens (sM2 and HA2) with cholera toxin subunit A1 (CTA1) Induce broadly protective immune responses against divergent influenza subtypes. Vet Microbiol. 2015;179(3-4):250-63.
245. LeCureux JS, Dean GA. Lactobacillus Mucosal Vaccine Vectors: Immune Responses against Bacterial and Viral Antigens. mSphere. 2018;3(3).
246. Yu Q, Zhu L, Kang H, Yang Q. Mucosal Lactobacillus vectored vaccines. Human Vaccines & Immunotherapeutics. 2013;9(4):805-7.
247. Shakya M, Lo C-C, Chain PS. Advances and challenges in metatranscriptomic analysis. Frontiers in genetics. 2019;10:904.
248. Bokulich NA, Ziemski M, Robeson MS, Kaehler BD. Measuring the microbiome: Best practices for developing and benchmarking microbiomics methods. Computational and Structural Biotechnology Journal. 2020;18:4048-62.
249. Kwoji ID, Aiyegoro OA, Okpeku M, Adeleke MA. 'Multi-omics' data integration: applications in probiotics studies. npj Science of Food. 2023;7(1):25.
250. Fox BE, Vilander A, Abdo Z, Dean GA. NOD2 signaling in CD11c + cells is critical for humoral immune responses during oral vaccination and maintaining the gut microbiome. Sci Rep. 2022;12(1):8491.
251. FastQC. 2015.
252. Bolger AM, Lohse M, Usadel B. Trimmomatic: a flexible trimmer for Illumina sequence data. Bioinformatics. 2014;30(15):2114-20.
253. Li H, Durbin R. Fast and accurate short read alignment with Burrows–Wheeler transform. Bioinformatics. 2009;25(14):1754-60.
254. Danecek P, Bonfield JK, Liddle J, Marshall J, Ohan V, Pollard MO, et al. Twelve years of SAMtools and BCFtools. GigaScience. 2021;10(2).
255. Quinlan AR, Hall IM. BEDTools: a flexible suite of utilities for comparing genomic features. Bioinformatics. 2010;26(6):841-2.
256. https://github.com/lh3/seqtk.
257. Nurk S, Meleshko D, Korobeynikov A, Pevzner PA. metaSPAdes: a new versatile metagenomic assembler. Genome Res. 2017;27(5):824-34.
258. Mikheenko A, Saveliev V, Gurevich A. MetaQUAST: evaluation of metagenome assemblies. Bioinformatics. 2015;32(7):1088-90.
259. Bushnell B. BBMap: a fast, accurate, splice-aware aligner. Lawrence Berkeley National Lab.(LBNL), Berkeley, CA (United States); 2014.
260. Kang DD, Li F, Kirton E, Thomas A, Egan R, An H, et al. MetaBAT 2: an adaptive binning algorithm for robust and efficient genome reconstruction from metagenome assemblies. PeerJ. 2019;7:e7359.
261. Parks DH, Imelfort M, Skennerton CT, Hugenholtz P, Tyson GW. CheckM: assessing the quality of microbial genomes recovered from isolates, single cells, and metagenomes. Genome Res. 2015;25(7):1043-55.
262. Wood DE, Lu J, Langmead B. Improved metagenomic analysis with Kraken 2. Genome Biology. 2019;20(1):257.
263. Westreich ST, Treiber ML, Mills DA, Korf I, Lemay DG. SAMSA2: a standalone metatranscriptome analysis pipeline. BMC Bioinformatics. 2018;19(1):175.
264. Kopylova E, Noé L, Touzet H. SortMeRNA: fast and accurate filtering of ribosomal RNAs in metatranscriptomic data. Bioinformatics. 2012;28(24):3211-7.
265. Zhang J, Kobert K, Flouri T, Stamatakis A. PEAR: a fast and accurate Illumina Paired-End reAd mergeR. Bioinformatics. 2014;30(5):614-20.
266. Lu J, Breitwieser FP, Thielen P, Salzberg SL. Bracken: estimating species abundance in metagenomics data. PeerJ Computer Science. 2017;3:e104.

267. Schmeier S. 6. Taxonomic investigation. 2016-2020.
268. Radwan S, Gilfillan D, Eklund B, Radwan HM, El Menofy NG, Lee J, et al. A comparative study of the gut microbiome in Egyptian patients with Type I and Type II diabetes. PLoS One. 2020;15(9):e0238764.
269. Zorz J. Stacked Bar Plots in R. 05 Jun 2019.
270. Oksanen J SG, Blanchet F, Kindt R, Legendre P, Minchin P, O'Hara R, Solymos P, Stevens M, Szoecs E, Wagner H, Barbour M, Bedward M, Bolker B, Borcard D, Carvalho G, Chirico M, De Caceres M, Durand S, Evangelista H, FitzJohn R, Friendly M, Furneaux B, Hannigan G, Hill M, Lahti L, McGlinn D, Ouellette M, Ribeiro Cunha E, Smith T, Stier A, Ter Braak C, Weedon J. vegan: Community Ecology Package. R package version 2.6-5, https://github.com/vegandevs/vegan. 2023.
271. McMurdie PJ, Holmes S. phyloseq: an R package for reproducible interactive analysis and graphics of microbiome census data. PloS one. 2013;8(4):e61217.
272. Paulson JN ON, Braccia DJ, Wagner J, Talukder H, Pop M, Bravo HC. metagenomeSeq: Statistical analysis for sparse high-throughput sequncing. Bioconductor package,. 2013.
273. Ritchie ME, Phipson B, Wu D, Hu Y, Law CW, Shi W, et al. limma powers differential expression analyses for RNA-sequencing and microarray studies. Nucleic Acids Research. 2015;43(7):e47-e.
274. Dainat J. AGAT: Another Gff Analysis Toolkit to handle annotations in any GTF/GFF format.(Version v1.0.0). . Zenodo.
275. Dobin A, Davis CA, Schlesinger F, Drenkow J, Zaleski C, Jha S, et al. STAR: ultrafast universal RNA-seq aligner. Bioinformatics. 2013;29(1):15-21.
276. Putri GH, Anders S, Pyl PT, Pimanda JE, Zanini F. Analysing high-throughput sequencing data in Python with HTSeq 2.0. Bioinformatics. 2022;38(10):2943-5.
277. Love MI, Huber W, Anders S. Moderated estimation of fold change and dispersion for RNA-seq data with DESeq2. Genome Biology. 2014;15(12):550.
278. Blighe K RS, Lewis M EnhancedVolcano: Publication-ready volcano plots with enhanced colouring and labeling. R package version 1.18.0, https://github.com/kevinblighe/EnhancedVolcano. 2023.
279. Bucka-Kolendo J, Juszczuk-Kubiak E, Sokołowska B. Effect of High Hydrostatic Pressure on Stress-Related dnaK, hrcA, and ctsR Expression Patterns in Selected Lactobacilli Strains. Genes. 2021;12(11):1720.
280. Martirani L, Raniello R, Naclerio G, Ricca E, De Felice M. Identification of the DNA-binding protein, HrcA, of Streptococcus thermophilus. FEMS Microbiology Letters. 2001;198(2):177-82.
281. Siezen RJ, Kok J, Abee T, Schaafsma G. Lactic acid bacteria: genetics, metabolism and applications. Antonie Van Leeuwenhoek. 2002;82(1-4):1.
282. Suokko A, Poutanen M, Savijoki K, Kalkkinen N, Varmanen P. ClpL is essential for induction of thermotolerance and is potentially part of the HrcA regulon in Lactobacillus gasseri. Proteomics. 2008;8(5):1029-41.
283. Phadtare S, Alsina J, Inouye M. Cold-shock response and cold-shock proteins. Current Opinion in Microbiology. 1999;2(2):175-80.
284. Ricke SC, Dawoud TM, Kim SA, Park SH, Kwon YM. Chapter One - Salmonella Cold Stress Response: Mechanisms and Occurrence in Foods. In: Gadd GM, Sariaslani S, editors. Advances in Applied Microbiology. 104: Academic Press; 2018. p. 1-38.
285. Noller. CSDaHF. Suppression of a cold-sensitive mutation in 16S rRNA by overexpression of a novel ribosome-binding factor, RbfA. Genes Dev. 1995;9(5):626–37.
286. Nord S, Bylund GO, Lövgren JM, Wikström PM. The RimP Protein Is Important for Maturation of the 30S Ribosomal Subunit. Journal of Molecular Biology. 2009;386(3):742-53.
287. Dinarieva TY, Klimko AI, Kahnt J, Cherdyntseva TA, Netrusov AI. Adaptation of Lacticaseibacillus rhamnosus CM MSU 529 to Aerobic Growth: A Proteomic Approach. Microorganisms. 2023;11(2):313.
288. Andersen JM, Barrangou R, Hachem MA, Lahtinen SJ, Goh YJ, Svensson B, et al. Transcriptional analysis of prebiotic uptake and catabolism by Lactobacillus acidophilus NCFM. PLoS One. 2012;7(9):e44409.

289. Michlmayr H, Kneifel W. β-Glucosidase activities of lactic acid bacteria: mechanisms, impact on fermented food and human health. FEMS Microbiology Letters. 2014;352(1):1-10.
290. Bagon BB, Valeriano VDV, Oh JK, Pajarillo EAB, Lee JY, Kang D-K. Exoproteome Perspective on the Bile Stress Response of Lactobacillus johnsonii. Proteomes. 2021;9(1):10.
291. Yang Z, Xu M, Li Q, Wang T, Zhang B, Zhao H, et al. The beneficial effects of polysaccharide obtained from persimmon (Diospyros kaki L.) on the proliferation of Lactobacillus and gut microbiota. International Journal of Biological Macromolecules. 2021;182:1874-82.
292. Gómez-Gómez B, Pérez-Corona T, Mozzi F, Pescuma M, Madrid Y. Silac-based quantitative proteomic analysis of Lactobacillus reuteri CRL 1101 response to the presence of selenite and selenium nanoparticles. Journal of Proteomics. 2019;195:53-65.
293. Steyer A, Mičetić-Turk D, Fijan S. The Efficacy of Probiotics as Antiviral Agents for the Treatment of Rotavirus Gastrointestinal Infections in Children: An Updated Overview of Literature. Microorganisms. 2022;10(12):2392.
294. Krawczyk B, Wityk P, Gałęcka M, Michalik M. The Many Faces of Enterococcus spp.-Commensal, Probiotic and Opportunistic Pathogen. Microorganisms. 2021;9(9).
295. Farkas AM, Panea C, Goto Y, Nakato G, Galan-Diez M, Narushima S, et al. Induction of Th17 cells by segmented filamentous bacteria in the murine intestine. Journal of Immunological Methods. 2015;421:104-11.
296. Roswell M, Dushoff J, Winfree R. A conceptual guide to measuring species diversity. Oikos. 2021;130(3):321-38.
297. Hill TCJ, Walsh KA, Harris JA, Moffett BF. Using ecological diversity measures with bacterial communities. FEMS Microbiology Ecology. 2003;43(1):1-11.
298. Lagkouvardos I, Pukall R, Abt B, Foesel BU, Meier-Kolthoff JP, Kumar N, et al. The Mouse Intestinal Bacterial Collection (miBC) provides host-specific insight into cultured diversity and functional potential of the gut microbiota. Nature Microbiology. 2016;1(10):16131.
299. Boeckman J, Korn A, Yao G, Ravindran A, Gonzalez C, Gill J. Sheep in wolves' clothing: Temperate T7-like bacteriophages and the origins of the Autographiviridae. Virology. 2022;568:86-100.
300. Kazemifard N, Dehkohneh A, Baradaran Ghavami S. Probiotics and probiotic-based vaccines: A novel approach for improving vaccine efficacy. Frontiers in Medicine. 2022;9.
301. Grazul H, Kanda LL, Gondek D. Impact of probiotic supplements on microbiome diversity following antibiotic treatment of mice. Gut Microbes. 2016;7(2):101-14.
302. Zmora N, Zilberman-Schapira G, Suez J, Mor U, Dori-Bachash M, Bashiardes S, et al. Personalized gut mucosal colonization resistance to empiric probiotics is associated with unique host and microbiome features. Cell. 2018;174(6):1388-405. e21.
303. Laursen MF, Laursen RP, Larnkjær A, Michaelsen KF, Bahl MI, Licht TR. Administration of two probiotic strains during early childhood does not affect the endogenous gut microbiota composition despite probiotic proliferation. BMC Microbiology. 2017;17(1):175.
304. Dassi E, Ferretti P, Covello G, Speccher A, Migazzi A, Bosco B, et al. The short-term impact of probiotic consumption on the oral cavity microbiome. Scientific Reports. 2018;8(1):10476.
305. Parks DH, Rinke C, Chuvochina M, Chaumeil P-A, Woodcroft BJ, Evans PN, et al. Recovery of nearly 8,000 metagenome-assembled genomes substantially expands the tree of life. Nature Microbiology. 2017;2(11):1533-42.
306. Meziti A, Rodriguez-R LM, Hatt JK, Peña-Gonzalez A, Levy K, Konstantinidis KT. The Reliability of Metagenome-Assembled Genomes (MAGs) in Representing Natural Populations: Insights from Comparing MAGs against Isolate Genomes Derived from the Same Fecal Sample. Applied and Environmental Microbiology. 2021;87(6):e02593-20.
307. Ramos-Barbero MD, Martin-Cuadrado A-B, Viver T, Santos F, Martinez-Garcia M, Antón J. Recovering microbial genomes from metagenomes in hypersaline environments: The Good, the Bad and the Ugly. Systematic and Applied Microbiology. 2019;42(1):30-40.

308. Goh YJ, Barrangou R, Klaenhammer TR. In Vivo Transcriptome of Lactobacillus acidophilus and Colonization Impact on Murine Host Intestinal Gene Expression. mBio. 2021;12(1):10.1128/mbio.03399-20.
309. Parker KD, Albeke SE, Gigley JP, Goldstein AM, Ward NL. Microbiome Composition in Both Wild-Type and Disease Model Mice Is Heavily Influenced by Mouse Facility. Frontiers in Microbiology. 2018;9.
310. Cabral DJ, Penumutchu S, Reinhart EM, Zhang C, Korry BJ, Wurster JI, et al. Microbial metabolism modulates antibiotic susceptibility within the murine gut microbiome. Cell metabolism. 2019;30(4):800-23. e7.
311. Klotz C, Barrangou R. Engineering components of the Lactobacillus S-layer for biotherapeutic applications. Frontiers in Microbiology. 2018;9:2264.
312. Abriouel H, Pérez Montoro B, Casimiro-Soriguer CS, Pérez Pulido AJ, Knapp CW, Caballero Gómez N, et al. Insight into Potential Probiotic Markers Predicted in Lactobacillus pentosus MP-10 Genome Sequence. Front Microbiol. 2017;8:891.
313. Quinn C, Tomás-Cortázar J, Ofioritse O, Cosgrave J, Purcell C, McAloon C, et al. GlnH, a Novel Antigen That Offers Partial Protection against Verocytotoxigenic Escherichia coli Infection. Vaccines. 2023;11(1):175.
314. Wimmers F, Pulendran B. Emerging technologies for systems vaccinology — multi-omics integration and single-cell (epi)genomic profiling. Current Opinion in Immunology. 2020;65:57-64.
315. Lash GE, Pinto LA. Multiplex cytokine analysis technologies. Expert Rev Vaccines. 2010;9(10):1231-7.
316. Moorlag SJ, Folkman L, Ter Horst R, Krausgruber T, Barreca D, Schuster LC, et al. Multi-omics analysis of innate and adaptive responses to BCG vaccination reveals epigenetic cell states that predict trained immunity. Immunity. 2024;57(1):171-87. e14.
317. Raya Tonetti F, Arce L, Salva S, Alvarez S, Takahashi H, Kitazawa H, et al. Immunomodulatory Properties of Bacterium-Like Particles Obtained From Immunobiotic Lactobacilli: Prospects for Their Use as Mucosal Adjuvants. Frontiers in Immunology. 2020;11.
318. Liu T, Matsuguchi T, Tsuboi N, Yajima T, Yoshikai Y. Differences in Expression of Toll-Like Receptors and Their Reactivities in Dendritic Cells in BALB/c and C57BL/6 Mice. Infection and Immunity. 2002;70(12):6638-45.
319. Franklin CL, Ericsson AC. Microbiota and reproducibility of rodent models. Lab Animal. 2017;46(4):114-22.
320. Miyamoto J, Igarashi M, Watanabe K, Karaki S-i, Mukouyama H, Kishino S, et al. Gut microbiota confers host resistance to obesity by metabolizing dietary polyunsaturated fatty acids. Nature Communications. 2019;10(1):4007.
321. Lee Y, Choo J, Kim SJ, Heo G, Pothoulakis C, Kim YH, et al. Analysis of endogenous lipids during intestinal wound healing. PLoS One. 2017;12(8):e0183028.
322. Bento AF, Claudino RF, Dutra RC, Marcon R, Calixto JB. Omega-3 Fatty Acid-Derived Mediators 17(R)-Hydroxy Docosahexaenoic Acid, Aspirin-Triggered Resolvin D1 and Resolvin D2 Prevent Experimental Colitis in Mice. The Journal of Immunology. 2011;187(4):1957-69.
323. Zhu X, Bi Z, Yang C, Guo Y, Yuan J, Li L, et al. Effects of different doses of omega-3 polyunsaturated fatty acids on gut microbiota and immunity. Food Nutr Res. 2021;65.
324. Calder PC, Grimble RF. Polyunsaturated fatty acids, inflammation and immunity. European Journal of Clinical Nutrition. 2002;56(3):S14-S9.
325. Quin C, Gibson DL. Dietary Fatty Acids and Host–Microbial Crosstalk in Neonatal Enteric Infection. Nutrients. 2019;11(9):2064.
326. Peng M, Biswas D. Short chain and polyunsaturated fatty acids in host gut health and foodborne bacterial pathogen inhibition. Critical reviews in food science and nutrition. 2017;57(18):3987-4002.
327. Johansson MEV, Hansson GC. Immunological aspects of intestinal mucus and mucins. Nature Reviews Immunology. 2016;16(10):639-49.

328. Lebeer S, Vanderleyden J, De Keersmaecker SCJ. Host interactions of probiotic bacterial surface molecules: comparison with commensals and pathogens. Nature Reviews Microbiology. 2010;8(3):171-84.
329. Song C, Chai Z, Chen S, Zhang H, Zhang X, Zhou Y. Intestinal mucus components and secretion mechanisms: what we do and do not know. Experimental & Molecular Medicine. 2023;55(4):681-91.
330. Sonnenburg JL, Xu J, Leip DD, Chen C-H, Westover BP, Weatherford J, et al. Glycan Foraging in Vivo by an Intestine-Adapted Bacterial Symbiont. Science. 2005;307(5717):1955-9.
331. Albouery M, Buteau B, Grégoire S, Cherbuy C, Pais de Barros J-P, Martine L, et al. Age-Related Changes in the Gut Microbiota Modify Brain Lipid Composition. Frontiers in Cellular and Infection Microbiology. 2020;9.
332. Noguchi M, Shimizu M, Lu P, Takahashi Y, Yamauchi Y, Sato S, et al. Lactic acid bacteria-derived γ-linolenic acid metabolites are PPARδ ligands that reduce lipid accumulation in human intestinal organoids. J Biol Chem. 2022;298(11):102534.
333. Lea T. Caco-2 cell line. The Impact of Food Bioactives on Health: in vitro and ex vivo models. 2015:103-11.
334. Kawasaki T, Kawai T. Toll-Like Receptor Signaling Pathways. Frontiers in Immunology. 2014;5.
335. Vincenzi A, Goettert MI, Volken de Souza CF. An evaluation of the effects of probiotics on tumoral necrosis factor (TNF-α) signaling and gene expression. Cytokine & Growth Factor Reviews. 2021;57:27-38.
336. Taguchi R, Tanaka S, Joe G-H, Maseda H, Nomura N, Ohnishi J, et al. Mucin 3 is involved in intestinal epithelial cell apoptosis via N-(3-oxododecanoyl)-l-homoserine lactone-induced suppression of Akt phosphorylation. American Journal of Physiology-Cell Physiology. 2014;307(2):C162-C8.
337. Livak KJ, Schmittgen TD. Analysis of relative gene expression data using real-time quantitative PCR and the 2(-Delta Delta C(T)) Method. Methods. 2001;25(4):402-8.
338. O'brien J, Wilson I, Orton T, Pognan F. Investigation of the Alamar Blue (resazurin) fluorescent dye for the assessment of mammalian cell cytotoxicity. European journal of biochemistry. 2000;267(17):5421-6.
339. Magnusson C, Bengtsson AM, Liu M, Liu J, Ceder Y, Ehrnström R, et al. Regulation of cysteinyl leukotriene receptor 2 expression—a potential anti-tumor mechanism. PLoS One. 2011;6(12):e29060.
340. Rizzello CG, Coda R, Macías DS, Pinto D, Marzani B, Filannino P, et al. Lactic acid fermentation as a tool to enhance the functional features of Echinacea spp. Microbial Cell Factories. 2013;12(1):44.
341. Tribolet L, Alexander MR, Brice AM, Vuren PJv, Rootes CL, Mara K, et al. ILRUN Downregulates ACE2 Expression and Blocks Infection of Human Cells by SARS-CoV-2. Journal of Virology. 2021;95(15):10.1128/jvi.00327-21.
342. Zheng D, Liwinski T, Elinav E. Interaction between microbiota and immunity in health and disease. Cell Research. 2020;30(6):492-506.
343. Levy M, Thaiss CA, Zeevi D, Dohnalová L, Zilberman-Schapira G, Mahdi JA, et al. Microbiota-modulated metabolites shape the intestinal microenvironment by regulating NLRP6 inflammasome signaling. Cell. 2015;163(6):1428-43.
344. David LA, Maurice CF, Carmody RN, Gootenberg DB, Button JE, Wolfe BE, et al. Diet rapidly and reproducibly alters the human gut microbiome. Nature. 2014;505(7484):559-63.
345. Cheng L, Jin H, Qiang Y, Wu S, Yan C, Han M, et al. High fat diet exacerbates dextran sulfate sodium induced colitis through disturbing mucosal dendritic cell homeostasis. International Immunopharmacology. 2016;40:1-10.
346. Sander WJ, Kemp G, Hugo A, Pohl CH, O'Neill HG. Rotavirus-Mediated Prostaglandin E2 Production in MA104 Cells Promotes Virus Attachment and Internalisation, Resulting in an Increased Viral Load. Frontiers in Physiology. 2022;13.
347. Crawford SE, Desselberger U. Lipid droplets form complexes with viroplasms and are crucial for rotavirus replication. Current Opinion in Virology. 2016;19:11-5.
348. Ilag LL. Are Long-Chain Polyunsaturated Fatty Acids the Link between the Immune System and the Microbiome towards Modulating Cancer? Medicines. 2018;5(3):102.

349. Simopoulos AP. The importance of the ratio of omega-6/omega-3 essential fatty acids. Biomedicine & Pharmacotherapy. 2002;56(8):365-79.
350. van Klinken BJ-W, Oussoren E, Weenink J-J, Strous GJ, Büller HA, Dekker J, et al. The human intestinal cell lines Caco-2 and LS174T as models to study cell-type specific mucin expression. Glycoconjugate Journal. 1996;13(5):757-68.
351. Mattar A, Teitelbaum DH, Drongowski R, Yongyi F, Harmon C, Coran A. Probiotics up-regulate MUC-2 mucin gene expression in a Caco-2 cell-culture model. Pediatric Surgery International. 2002;18(7):586-90.
352. De Weirdt R, Coenen E, Vlaeminck B, Fievez V, Van den Abbeele P, Van de Wiele T. A simulated mucus layer protects Lactobacillus reuteri from the inhibitory effects of linoleic acid. Beneficial microbes. 2013;4(4):299-312.
353. Matsuguchi T, Takagi A, Matsuzaki T, Nagaoka M, Ishikawa K, Yokokura T, et al. Lipoteichoic Acids from Lactobacillus Strains Elicit Strong Tumor Necrosis Factor Alpha-Inducing Activities in Macrophages through Toll-Like Receptor 2. Clinical and Vaccine Immunology. 2003;10(2):259-66.
354. Bumgardner SA, Zhang L, LaVoy AS, Andre B, Frank CB, Kajikawa A, et al. Nod2 is required for antigen-specific humoral responses against antigens orally delivered using a recombinant Lactobacillus vaccine platform. PLoS One. 2018;13(5):e0196950.
355. Wang H, Gao K, Wen K, Allen IC, Li G, Zhang W, et al. Lactobacillus rhamnosus GG modulates innate signaling pathway and cytokine responses to rotavirus vaccine in intestinal mononuclear cells of gnotobiotic pigs transplanted with human gut microbiota. BMC Microbiology. 2016;16(1):109.
356. Skountzou I, Martin MdP, Wang B, Ye L, Koutsonanos D, Weldon W, et al. Salmonella flagellins are potent adjuvants for intranasally administered whole inactivated influenza vaccine. Vaccine. 2010;28(24):4103-12.
357. Batah J, Denève-Larrazet C, Jolivot P-A, Kuehne S, Collignon A, Marvaud J-C, et al. Clostridium difficile flagella predominantly activate TLR5-linked NF-κB pathway in epithelial cells. Anaerobe. 2016;38:116-24.
358. Devriese S, Van den Bossche L, Van Welden S, Holvoet T, Pinheiro I, Hindryckx P, et al. T84 monolayers are superior to Caco-2 as a model system of colonocytes. Histochemistry and Cell Biology. 2017;148(1):85-93.
359. Ferrero MC, Fossati CA, Rumbo M, Baldi PC. Brucella invasion of human intestinal epithelial cells elicits a weak proinflammatory response but a significant CCL20 secretion. FEMS Immunology & Medical Microbiology. 2012;66(1):45-57.
360. Morita H, He F, Fuse T, Ouwehand AC, Hashimoto H, Hosoda M, et al. Adhesion of lactic acid bacteria to caco-2 cells and their effect on cytokine secretion. Microbiol Immunol. 2002;46(4):293-7.
361. Roselli M, Finamore A, Britti MS, Mengheri E. Probiotic bacteria Bifidobacterium animalis MB5 and Lactobacillus rhamnosus GG protect intestinal Caco-2 cells from the inflammation-associated response induced by enterotoxigenic Escherichia coli K88. British Journal of Nutrition. 2006;95(6):1177-84.
362. Kankaanpää P, Yang B, Kallio H, Isolauri E, Salminen S. Effects of Polyunsaturated Fatty Acids in Growth Medium on Lipid Composition and on Physicochemical Surface Properties of Lactobacilli. Applied and Environmental Microbiology. 2004;70(1):129-36.
363. Kankaanpää PE, Salminen SJ, Isolauri E, Lee YK. The influence of polyunsaturated fatty acids on probiotic growth and adhesion. FEMS Microbiology Letters. 2001;194(2):149-53.
364. Vega-Hernández R, Ochoa SA, Valle-Rios R, Jaimes-Ortega GA, Arellano-Galindo J, Aparicio-Ozores G, et al. Flagella, Type I Fimbriae and Curli of Uropathogenic Escherichia coli Promote the Release of Proinflammatory Cytokines in a Coculture System. Microorganisms. 2021;9(11):2233.
365. Werner L, Paclik D, Fritz C, Reinhold D, Roggenbuck D, Sturm A. Identification of Pancreatic Glycoprotein 2 as an Endogenous Immunomodulator of Innate and Adaptive Immune Responses. The Journal of Immunology. 2012;189(6):2774-83.
366. Wang T, Sun H, Chen J, Luo L, Gu Y, Wang X, et al. Anti-Adhesion Effects of Lactobacillus Strains on Caco-2 Cells Against Escherichia Coli and Their Application in Ameliorating the Symptoms of

Dextran Sulfate Sodium-Induced Colitis in Mice. Probiotics and Antimicrobial Proteins. 2021;13(6):1632-43.
367. Mack DR, Michail S, Wei S, McDougall L, Hollingsworth MA. Probiotics inhibit enteropathogenic E. coli adherence in vitro by inducing intestinal mucin gene expression. Am J Physiol. 1999;276(4):G941-50.
368. Urbina D, Arzuza O, Young G, Parra E, Castro R, Puello M. Rotavirus type A and other enteric pathogens in stool samples from children with acute diarrhea on the Colombian northern coast. International Microbiology. 2003;6(1):27-32.
369. Navabi N, McGuckin MA, Lindén SK. Gastrointestinal cell lines form polarized epithelia with an adherent mucus layer when cultured in semi-wet interfaces with mechanical stimulation. PloS one. 2013;8(7):e68761.
370. Bu X-D, Li N, Tian X-Q, Huang P-L. Caco-2 and LS174T cell lines provide different models for studying mucin expression in colon cancer. Tissue and Cell. 2011;43(3):201-6.
371. Gagnon M, Zihler Berner A, Chervet N, Chassard C, Lacroix C. Comparison of the Caco-2, HT-29 and the mucus-secreting HT29-MTX intestinal cell models to investigate Salmonella adhesion and invasion. Journal of Microbiological Methods. 2013;94(3):274-9.
372. Pires CL, Praça C, Martins PAT, Batista de Carvalho ALM, Ferreira L, Marques MPM, et al. Re-Use of Caco-2 Monolayers in Permeability Assays-Validation Regarding Cell Monolayer Integrity. Pharmaceutics. 2021;13(10).
373. Sambuy Y, De Angelis I, Ranaldi G, Scarino ML, Stammati A, Zucco F. The Caco-2 cell line as a model of the intestinal barrier: influence of cell and culture-related factors on Caco-2 cell functional characteristics. Cell Biology and Toxicology. 2005;21(1):1-26.
374. Zou WY, Blutt SE, Crawford SE, Ettayebi K, Zeng X-L, Saxena K, et al. Human Intestinal Enteroids: New Models to Study Gastrointestinal Virus Infections. In: Turksen K, editor. Organoids: Stem Cells, Structure, and Function. New York, NY: Springer New York; 2019. p. 229-47.
375. Pearce SC, Weber GJ, van Sambeek DM, Soares JW, Racicot K, Breault DT. Intestinal enteroids recapitulate the effects of short-chain fatty acids on the intestinal epithelium. PloS one. 2020;15(4):e0230231.
376. Brosnahan AJ, Brown DR. Porcine IPEC-J2 intestinal epithelial cells in microbiological investigations. Veterinary Microbiology. 2012;156(3):229-37.
377. Peng M, Tabashsum Z, Patel P, Bernhardt C, Biswas D. Linoleic Acids Overproducing Lactobacillus casei Limits Growth, Survival, and Virulence of Salmonella Typhimurium and Enterohaemorrhagic Escherichia coli. Frontiers in Microbiology. 2018;9.
378. Prudden HJ, Hasso-Agopsowicz M, Black RE, Troeger C, Reiner RC, Breiman RF, et al. Meeting Report: WHO Workshop on modelling global mortality and aetiology estimates of enteric pathogens in children under five. Cape Town, 28–29th November 2018. Vaccine. 2020;38(31):4792-800.
379. Vlasova AN, Rajashekara G, Saif LJ. Interactions between human microbiome, diet, enteric viruses and immune system: Novel insights from gnotobiotic pig research. Drug Discovery Today: Disease Models. 2018;28:95-103.
380. Ranganathan S, Smith EM, Foulke-Abel JD, Barry EM. Research in a time of enteroids and organoids: how the human gut model has transformed the study of enteric bacterial pathogens. Gut Microbes. 2020;12(1):1795492.
381. Kong L, Moorlag SJ, Lefkovith A, Li B, Matzaraki V, van Emst L, et al. Single-cell transcriptomic profiles reveal changes associated with BCG-induced trained immunity and protective effects in circulating monocytes. Cell reports. 2021;37(7).

APPENDIX

Chapter 2 Supplementary Figures

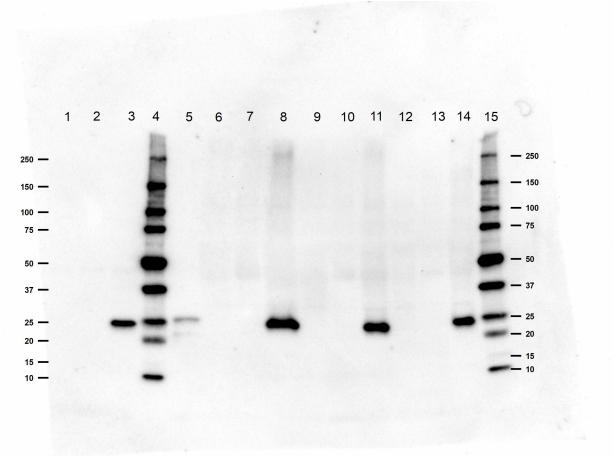

Figure S2.1. Uncropped western blot confirming VP8-1 rLA antigen cytoplasmic accumulation. Lanes 1: NCK56, 2: GAD80, 3: GAD85, 4: Precision Plus WesternC ladder (Bio-Rad, Hercules, CA, USA), 5: *E. coli* expressed VP8-1 positive control, 6: NCK56, 7: GAD80, 8: GAD85, 9: NCK56, 10: GAD80, 11: GAD85, 12: NCK56, 13: GAD80, 14: GAD85, 15: Precision Plus WesternC ladder (Bio-Rad).

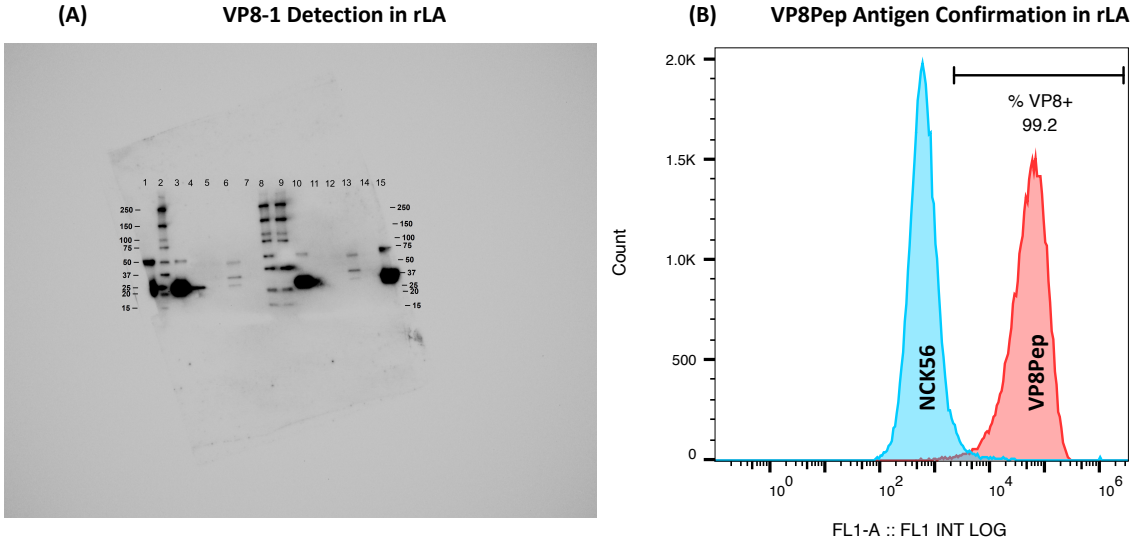

Figure S2.2. Uncropped western blot (A) confirming VP8-1 rLA antigen cytoplasmic accumulation in GAD84 with a 25 kDa band present in GAD84 lysates corresponding to the positive control. Western blot lanes 1: *E. coli* expressed VP8-1 positive control, 2: Precision Plus WesternC ladder (Bio-Rad), 3: *E. coli* expressed VP8-1 positive control, 4: GAD84, 5: NCK56, 6: GAD85, 7: NCK56, 8: Precision Plus WesternC ladder (Bio-Rad), 9: Precision Plus WesternC ladder (Bio-Rad), 10: *E. coli* expressed VP8-1 positive control, 11: GAD84, 12: NCK56, 13: GAD84, 14: NCK56, 15: *E. coli* expressed VP8-1 positive control. Flow cytometry histogram (B) confirming VP8Pep surface expression (red peak) in GAD84 as compared to the NCK56 negative control (blue peak).

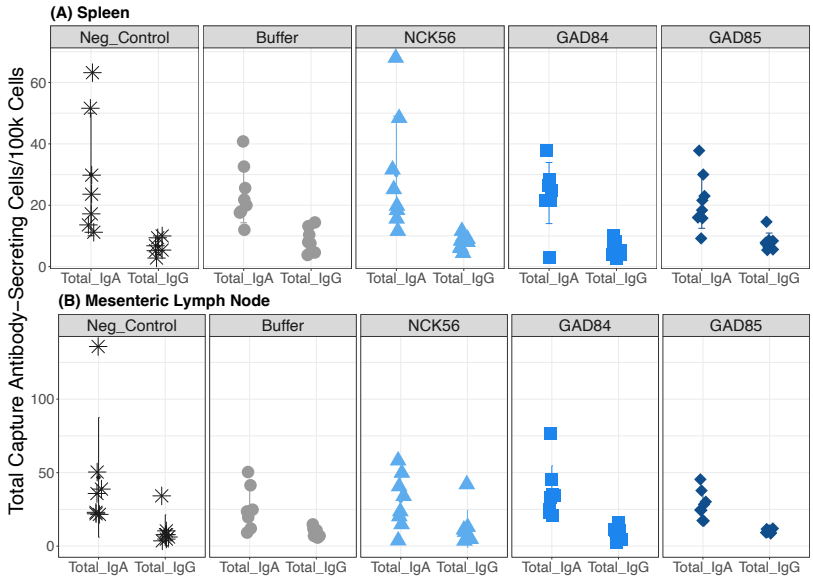

Figure S2.3. Total-capture IgA and IgG antibody-secreting cells per 100,000 cells as measured by FluoroSpot in the spleen (A) and MLN (B) post oral immunization. Mice were immunized every other week with either control (negative control, Buffer, NCK56) or recombinant probiotic vaccine strains (GAD84, GAD85). MLN; mesenteric lymph node, VP8-1: full-length rotavirus protein antigen, VP8Pep; 10 amino-acid length rotavirus peptide antigen, rLA; recombinant *Lactobacillus acidophilus.*

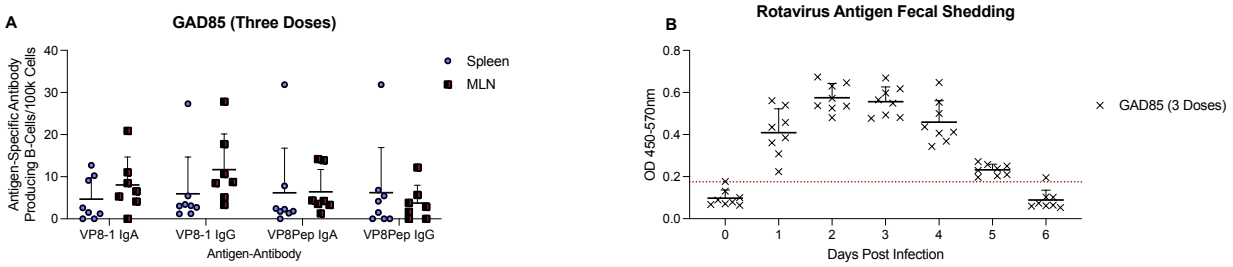

Figure S2.4. GAD85 treatment group receiving three oral vaccinations at 0, 2, and 6 weeks before challenge with the murine EC_{WT} rotavirus strain at 10 weeks. (A) Detectable antigen-specific (VP8-1, VP8Pep) ASC (IgA, IgG) responses after viral challenge in spleen (blue) and MLN (plum) as measured by FluoroSpot. Detectable is defined as > 0 antigen-specific antibody producing CD45+CD19+ B-cells per 100,000 cells. (B) Fecal rotavirus antigen shedding over six days as measured by ELISA following viral challenge demonstrating successful infection. ELISA plates were read at a 450–570 nm wavelength with the raw OD values per sample visualized (B). Despite detectable antigen-specific ASC (A), there was no delay in rotavirus antigen shed as the OD values for days 1-6 after infection are above the dotted line representing a cutoff three times the standard deviation plus the mean of day zero OD values (B). This could potentially indicate the necessity for more oral rLA doses. Data were anlayzed and visualized in GraphPad Prism 10.0.3 for MacOS, GraphPad Software, Boston, Massachusetts USA, www.graphpad.com. ASC: antibody-secreting cells, VP8-1: VP8* protein antigen, VP8pep: VP8* peptide antigen, MLN: mesenteric lymph node, OD: optical density.

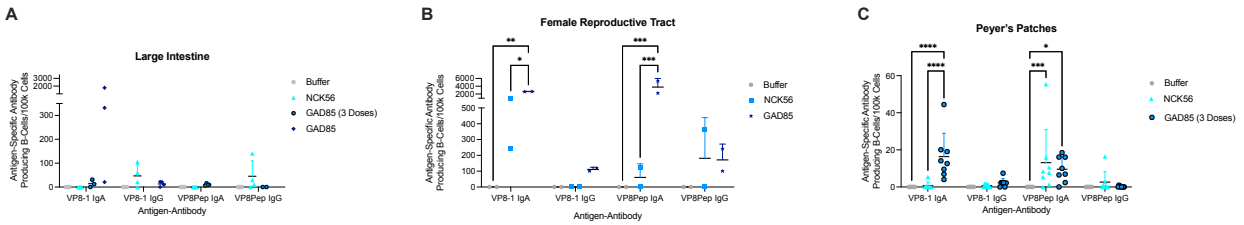

Figure S2.5. Antigen-specific (VP8-1, VP8Pep) ASC (IgA, IgG) responses in mice vaccinated with buffer (closed circles), NCK56 (triangles) or GAD85 (open circles, diamonds) over ten weeks before challenge with EC_{WT} murine rotavirus. ASC responses are provided for (A) LI, (B), FRT, and (C) PP as measured by FluoroSpot. A treatment of GAD85 mice received three instead of five immunizations. Groups randomly have missing values for certain antigen-antibody combinations across various tissues (e.g. VP8Pep-specific IgG in the LI for GAD85) because all the spots were removed during the imaging analysis quality control. These data are to be interpreted with extreme caution due to tissue debris interfering with the accuracy of the assay. They loosely indicate antigen-specific ASC responses may be inducible in diverse mucosal tissues (LI, FRT) and within immune inductive sites (PP) using an rLA platform. No ASC responses were seemingly detected in non-rLA groups. A two-way ANOVA with Tukey HSD for multiple comparisons was performed where possible. Data were analyzed and visualized in GraphPad Prism 10.0.3 for MacOS, GraphPad Software, Boston, Massachusetts USA, www.graphpad.com. Adjusted *p*-value: '****' <0.0001, '***' <0.001, '**' <0.01., '*' <0.05. ASC: antibody-secreting cells, VP8-1: VP8* protein antigen, VP8pep: VP8* peptide antigen, LI: large intestine, FRT: female reproductive tract, PP: Peyer's patches.

Chapter 2 Supplementary Tables

Table S2.1. List of *Lactobacillus acidophilus* (LA) and *E. coli* strains used for probiotic rotavirus vaccine construction.

Bacterial Strain	Plasmid	Resistance	Description	Reference
EC101		Kan	*E. coli* cloning host, *rep*A +	Law et al. 1995.
NCK1910	pTRK669	Cm	*L. acidophilus* NCFM with non-functional *upp*	Goh et al. 2009
GAD80	pTRK669	Cm	Recombinant *L. acidophilus* with VP8Pep surface display	Vilander et al. 2023
NCK2753			Recombinant *L. acidophilus* with VP8Pep surface display, FimH downstream of *lba0889*	This study
NCK2783			Recombinant *L. acidophilus* with VP8Pep surface display, VP8-1 and FimH downstream of *lba0889*	This study

Table S2.2. Amino acid sequences of antigens from the EDIM rotavirus strain included in the recombinant LA (rLA) vaccine constructs, including the pseudo full-length protein (VP8-1) and the 10 amino acid VP8 peptide (VP8Pep).

Antigen	Sequence	Expresion	Reference
VP8Pep	MASLIYRQLL	Surface (SlpA)	Xue et al. 2015

VP8-1	GAEKT QNVTVNPGPF AQTGYAPANW GPGETNDSTT VEPVLDGPYQ PIAFSPPPEY YILLSPTAPG VIAECTNTVN RWIAIIAIEP NVSPTNRTYT LFGITEQLTV ENSSVDKWKF IDFMKTPTTG SYVRYNILLS STKLCAVAKH TDNLYSYVGE TPTAGQAYYS SFNIFNLTAH CDFYIIPWSQ QSLCTQYVNN GLPPIQNTRN V	Cytoplasmic	Xue et al. 2015

Table S2.3. Primers used to perform cloning to construct the rLA platforms.

Primer	Sequence
AK_63	TTT TAA GCT TCA TCT GAG GAT AAA GTT GTT TGA T
AV_49	CAA GAA GCT GTC TAT AAA TCA AAC TGG CCA TAC CGG TGA ATT TTA CAT TT
AK_64	TTT TGG ATC CGA ATC GAA GTA TCA GAA GAT CC
AV_50	GCT TCT TGC AAA CAG TGA TAA TCA AAC
AV_06	TGG TCG ACA AGC AGG TCT TC
AV_09	CTG TAA AGG CAG ATG AAG TTG ATG
NEB_fimH_fwd	GTTGAAATTGTACTCGGTGCTTATCTCCGTTTCCTATCAG
NEB_fimH_rev	ATGTTGACCACGATTAATGCGGCTGAATTCAGGAGTTAATAATATG
upp_fwd	GGGCTGGCTTAACTATGC
upp_rev	CTTCCGGCTCGTATGTTG
repA-fwd	TCAGGTTATGACCATCTGTGC
repA-rev	CTCCGTCGCTATTGTAACCAG
889_fwd	GTTGTTGTTCCTGTAGGTAAGATTG
889_rev	CCACACTTTGAAGAAGGTTCTTG
FimH_flanking_fwd	CAACTGTTGGGAAGGGCGATAGCGATCAAGCTTCCGGC
FimH_flanking_rev	TAACGTTTAAATGCGGCTGAATTCAGGAGT

Table S2.4. Plasmids used to perform cloning to construct the rLA platforms.

Plasmid	Components	Resistance	Reference
pTRK669	Temperature-sensitive helper plasmid; RepA+	Cm	Goh et al. 2009
pTRK-AV04	FimH no tag	Ery	Vilander et al. 2023
pTRK-AV05	SlpA-VP8Pep		Vilander et al. 2023
pTRK1034	FliC	Ery	Kajikawa et al. 2011
pTRK1038	Integration plasmid containing 600bp upstream and 600bp downstream sequence flanking the *lba0889* (*enolase*) integration site	Ery	Douglas et al. 2011
pTRK1053	SlpA	Ery	Kajikawa et al. 2015
pTRK1209	pTRK1038 containing FimH cassette between the upstream and downstream sequence flanking the *lba0889* integration site	Ery	This study

pTRK1213	pTRK1038 containing VP8-1 between the upstream and downstream sequence flanking the integration site between *lba0889* and chromosomal FimH cassette	Ery	This study

Table S2.5. Antibodies and their dilutions used to perform flow cytometry to confirm antigen and adjuvant surface expression from rLA constructs.

Primary Antibody/Dilution	Manufacturer	Secondary Antibody/Dilution	Manufacturer
Rabbit anti-VP810AA Antibody (1:200)	Genscript (Piscataway, NJ, USA)	Donkey anti-rabbit FITC Clone Poly4064 (1:100)	BioLegend (San Diego, CA, USA)
Mouse anti-Salmonella FliC clone FLIC-1 (1:200)	BioLegend (San Diego, CA, USA)	Goat anti-mouse PE IgG1 (γ1) (1:100)	Invitrogen (Waltham, MA, USA)
Mouse anti-FimH mAB 824 (1:1000)	Gift from Dr. Svgeni V. Sorurenko (University of Washington, Seattle, WA)	Goat anti-mouse PE IgG1 (γ1) (1:100)	Invitrogen

Table S2.6. Densitometry readings of Western blot confirming rLA VP8-1 antigen cytoplasmic accumulation in Figure 2.5A.

Lane	Lane Label	Band No.	Mol. Wt. (kDa)	Relative Front	Adj. Volume (Int)	Volume (Int)	Band %	Lane %
1	NCK56	None						
3	GAD85	1	24.74	0.730205	7507172	8239161	100	85.33388
4	MW Marker	1	250.00	0.184751	1795332	4063306	2.788009	2.688764
4	MW Marker	2	150.00	0.27566	5630872	11930600	8.744301	8.433027
4	MW Marker	3	100.00	0.360704	5933023	11329488	9.213518	8.885541
4	MW Marker	4	75.00	0.419355	7025743	10856962	10.91043	10.52204
4	MW Marker	5	50.00	0.530792	19818658	23971139	30.77682	29.68124
4	MW Marker	6	37.00	0.618768	11725860	14261040	18.20934	17.56113
4	MW Marker	7	25.00	0.727273	5136016	7142555	7.975829	7.69191
4	MW Marker	8	20.00	0.788856	3016435	4420441	4.684286	4.517538
4	MW Marker	9	15.00	0.859481	35148	200158	0.054582	0.052639
4	MW Marker	10	10.00	0.912023	4277674	4649570	6.642891	6.406422
5	VP8-1 Control	1	25.64	0.718475	1735708	2055288	100	43.56453
15	15 (MW Marker)	1	250.00	0.173021	1165278	2391775	2.613637	2.517128
15	15 (MW Marker)	2	150.00	0.260997	1800349	3876198	4.038057	3.888951
15	15 (MW Marker)	3	100.00	0.346041	2291493	4555929	5.139658	4.949876

15	15 (MW Marker)	4	75.00	0.404692	4661344	7093719	10.45507	10.06901
15	15 (MW Marker)	5	50.00	0.516129	15137014	18084864	33.95126	32.69761
15	15 (MW Marker)	6	37.00	0.604106	9168930	11212038	20.56527	19.80589
15	15 (MW Marker)	7	25.00	0.706745	4406434	5829812	9.883322	9.51838
15	15 (MW Marker)	8	20.00	0.765396	2718344	3766201	6.097055	5.871921
15	15 (MW Marker)	9	15.00	0.83871	255664	639537	0.573436	0.552262
15	15 (MW Marker)	10	10.00	0.882698	2979692	3424552	6.68324	6.436461

Table S2.7. Densitometry readings of Western blot confirming rLA VP8-1 antigen cytoplasmic accumulation in Supplementary Figure S2.2A.

Lane	Lane Label	Band No.	Mol. Wt. (kDa)	Relative Front	Adj. Volume (Int)	Volume (Int)	Band %	Lane %
2	2 (MW Marker)	1	250.000	0.282	923168.000	923168.000	15.918	6.496
2	2 (MW Marker)	2	150.000	0.392	683604.000	683604.000	11.787	4.810
2	2 (MW Marker)	3	100.000	0.485	233172.000	233172.000	4.020	1.641
2	2 (MW Marker)	4	75.000	0.538	266560.000	266560.000	4.596	1.876
2	2 (MW Marker)	5	50.000	0.634	473348.000	473348.000	8.162	3.331
2	2 (MW Marker)	6	37.000	0.721	612272.000	612272.000	10.557	4.309
2	2 (MW Marker)	7	25.000	0.805	1572534.000	1572534.000	27.115	11.066
2	2 (MW Marker)	8	20.000	0.846	822732.000	822732.000	14.186	5.790
2	2 (MW Marker)	9	15.000	0.942	212194.000	212194.000	3.659	1.493
3	3 (VP8-1 Control)	1	51.011	0.629	247622.000	247622.000	1.440	0.963
3	3 (VP8-1 Control)	2	24.530	0.809	16945532.000	16945532.000	98.560	65.924
4	4 (GAD84)	1	24.605	0.808	1113670.000	1113670.000	100.000	11.068
5	5 (NCK56)	None						
6	6 (GAD84)	1	48.630	0.642	210324.000	210324.000	32.899	2.273
6	6 (GAD84)	2	33.583	0.742	233648.000	233648.000	36.547	2.525
6	6 (GAD84)	3	26.035	0.797	195330.000	195330.000	30.554	2.111

Table S2.8. Neutralization assay against tissue-culture-adapted EDIM (ETD) using unvaccinated control and vaccinated murine sera.

Sample Number	Normal Mice Sera	Negative Control	Buffer	NCK56	GAD84	GAD85
1	<400	<400	<400	<400	<400	<400
2	<400	<400	<400	<400	<400	<400
3	<400	<400	<400	<400	<400	<400
4	<400	<400	<400	<400	<400	<400

5	<400	<400	<400	<400	<400
6	<400	<400	<400	<400	<400
7	<400	<400	<400	<400	<400
8		<400	<400	<400	**800**

Table S2.9. Adjusted Tukey HSD p-values for VP8-1 and VP8Pep-specific IgA and IgG antibody-secreting cells (ASC) detected by FluoroSpot from single-cell splenic suspensions from mice vaccinated and then challenged with murine rotavirus.

Comparison (Spleen)	diff	lwr	upr	p.adj
NCK56:VP81_IgA-Buffer:VP81_IgA	0.39	-8.71	9.49	1.0000
GAD85:VP81_IgA-Buffer:VP81_IgA	11.83	2.73	20.93	0.0020
Buffer:VP81_IgG-Buffer:VP81_IgA	0.00	-9.10	9.10	1.0000
NCK56:VP81_IgG-Buffer:VP81_IgA	0.45	-8.65	9.55	1.0000
GAD85:VP81_IgG-Buffer:VP81_IgA	10.82	1.72	19.92	0.0072
Buffer:VP8Pep_IgA-Buffer:VP81_IgA	0.00	-9.10	9.10	1.0000
NCK56:VP8Pep_IgA-Buffer:VP81_IgA	0.12	-8.98	9.22	1.0000
GAD85:VP8Pep_IgA-Buffer:VP81_IgA	11.98	2.88	21.08	0.0016
Buffer:VP8Pep_IgG-Buffer:VP81_IgA	0.00	-9.10	9.10	1.0000
NCK56:VP8Pep_IgG-Buffer:VP81_IgA	0.00	-9.10	9.10	1.0000
GAD85:VP8Pep_IgG-Buffer:VP81_IgA	2.88	-6.23	11.98	0.9955
GAD85:VP81_IgA-NCK56:VP81_IgA	11.44	2.34	20.54	0.0033
Buffer:VP81_IgG-NCK56:VP81_IgA	-0.39	-9.49	8.71	1.0000
NCK56:VP81_IgG-NCK56:VP81_IgA	0.06	-9.04	9.16	1.0000
GAD85:VP81_IgG-NCK56:VP81_IgA	10.43	1.33	19.54	0.0114
Buffer:VP8Pep_IgA-NCK56:VP81_IgA	-0.39	-9.49	8.71	1.0000
NCK56:VP8Pep_IgA-NCK56:VP81_IgA	-0.26	-9.37	8.84	1.0000
GAD85:VP8Pep_IgA-NCK56:VP81_IgA	11.59	2.49	20.69	0.0027
Buffer:VP8Pep_IgG-NCK56:VP81_IgA	-0.39	-9.49	8.71	1.0000
NCK56:VP8Pep_IgG-NCK56:VP81_IgA	-0.39	-9.49	8.71	1.0000
GAD85:VP8Pep_IgG-NCK56:VP81_IgA	2.49	-6.61	11.59	0.9987
Buffer:VP81_IgG-GAD85:VP81_IgA	-11.83	-20.93	-2.73	0.0020
NCK56:VP81_IgG-GAD85:VP81_IgA	-11.38	-20.48	-2.28	0.0036
GAD85:VP81_IgG-GAD85:VP81_IgA	-1.01	-10.11	8.09	1.0000
Buffer:VP8Pep_IgA-GAD85:VP81_IgA	-11.83	-20.93	-2.73	0.0020
NCK56:VP8Pep_IgA-GAD85:VP81_IgA	-11.71	-20.81	-2.60	0.0023
GAD85:VP8Pep_IgA-GAD85:VP81_IgA	0.15	-8.95	9.25	1.0000
Buffer:VP8Pep_IgG-GAD85:VP81_IgA	-11.83	-20.93	-2.73	0.0020
NCK56:VP8Pep_IgG-GAD85:VP81_IgA	-11.83	-20.93	-2.73	0.0020
GAD85:VP8Pep_IgG-GAD85:VP81_IgA	-8.95	-18.05	0.15	0.0582
NCK56:VP81_IgG-Buffer:VP81_IgG	0.45	-8.65	9.55	1.0000

GAD85:VP81_IgG-Buffer:VP81_IgG	10.82	1.72	19.92	0.0072
Buffer:VP8Pep_IgA-Buffer:VP81_IgG	0.00	-9.10	9.10	1.0000
NCK56:VP8Pep_IgA-Buffer:VP81_IgG	0.12	-8.98	9.22	1.0000
GAD85:VP8Pep_IgA-Buffer:VP81_IgG	11.98	2.88	21.08	0.0016
Buffer:VP8Pep_IgG-Buffer:VP81_IgG	0.00	-9.10	9.10	1.0000
NCK56:VP8Pep_IgG-Buffer:VP81_IgG	0.00	-9.10	9.10	1.0000
GAD85:VP8Pep_IgG-Buffer:VP81_IgG	2.88	-6.23	11.98	0.9955
GAD85:VP81_IgG-NCK56:VP81_IgG	10.37	1.27	19.47	0.0123
Buffer:VP8Pep_IgA-NCK56:VP81_IgG	-0.45	-9.55	8.65	1.0000
NCK56:VP8Pep_IgA-NCK56:VP81_IgG	-0.33	-9.43	8.78	1.0000
GAD85:VP8Pep_IgA-NCK56:VP81_IgG	11.53	2.43	20.63	0.0029
Buffer:VP8Pep_IgG-NCK56:VP81_IgG	-0.45	-9.55	8.65	1.0000
NCK56:VP8Pep_IgG-NCK56:VP81_IgG	-0.45	-9.55	8.65	1.0000
GAD85:VP8Pep_IgG-NCK56:VP81_IgG	2.43	-6.67	11.53	0.9990
Buffer:VP8Pep_IgA-GAD85:VP81_IgG	-10.82	-19.92	-1.72	0.0072
NCK56:VP8Pep_IgA-GAD85:VP81_IgG	-10.70	-19.80	-1.60	0.0083
GAD85:VP8Pep_IgA-GAD85:VP81_IgG	1.16	-7.94	10.26	1.0000
Buffer:VP8Pep_IgG-GAD85:VP81_IgG	-10.82	-19.92	-1.72	0.0072
NCK56:VP8Pep_IgG-GAD85:VP81_IgG	-10.82	-19.92	-1.72	0.0072
GAD85:VP8Pep_IgG-GAD85:VP81_IgG	-7.95	-17.05	1.16	0.1478
NCK56:VP8Pep_IgA-Buffer:VP8Pep_IgA	0.12	-8.98	9.22	1.0000
GAD85:VP8Pep_IgA-Buffer:VP8Pep_IgA	11.98	2.88	21.08	0.0016
Buffer:VP8Pep_IgG-Buffer:VP8Pep_IgA	0.00	-9.10	9.10	1.0000
NCK56:VP8Pep_IgG-Buffer:VP8Pep_IgA	0.00	-9.10	9.10	1.0000
GAD85:VP8Pep_IgG-Buffer:VP8Pep_IgA	2.88	-6.23	11.98	0.9955
GAD85:VP8Pep_IgA-NCK56:VP8Pep_IgA	11.86	2.76	20.96	0.0019
Buffer:VP8Pep_IgG-NCK56:VP8Pep_IgA	-0.12	-9.22	8.98	1.0000
NCK56:VP8Pep_IgG-NCK56:VP8Pep_IgA	-0.12	-9.22	8.98	1.0000
GAD85:VP8Pep_IgG-NCK56:VP8Pep_IgA	2.75	-6.35	11.85	0.9969
Buffer:VP8Pep_IgG-GAD85:VP8Pep_IgA	-11.98	-21.08	-2.88	0.0016
NCK56:VP8Pep_IgG-GAD85:VP8Pep_IgA	-11.98	-21.08	-2.88	0.0016
GAD85:VP8Pep_IgG-GAD85:VP8Pep_IgA	-9.10	-18.20	0.00	0.0498
NCK56:VP8Pep_IgG-Buffer:VP8Pep_IgG	0.00	-9.10	9.10	1.0000
GAD85:VP8Pep_IgG-Buffer:VP8Pep_IgG	2.88	-6.23	11.98	0.9955
GAD85:VP8Pep_IgG-NCK56:VP8Pep_IgG	2.88	-6.23	11.98	0.9955

Table S2.10. Adjusted Tukey HSD p-values for VP8-1 and VP8Pep-specific IgA and IgG ASC detected by FluoroSpot from single-cell suspensions of the mesenteric lymph node (MLN) from mice vaccinated and then challenged with murine rotavirus.

Comparison (MLN)	diff	lwr	upr	p.adj

NCK56:VP81_IgA-Buffer:VP81_IgA	0.88	-9.21	10.98	1.0000
GAD85:VP81_IgA-Buffer:VP81_IgA	1.36	-8.73	11.46	1.0000
Buffer:VP81_IgG-Buffer:VP81_IgA	0.00	-10.10	10.10	1.0000
NCK56:VP81_IgG-Buffer:VP81_IgA	4.05	-6.05	14.15	0.9695
GAD85:VP81_IgG-Buffer:VP81_IgA	33.62	23.52	43.71	0.0000
Buffer:VP8Pep_IgA-Buffer:VP81_IgA	0.00	-10.10	10.10	1.0000
NCK56:VP8Pep_IgA-Buffer:VP81_IgA	0.92	-9.18	11.02	1.0000
GAD85:VP8Pep_IgA-Buffer:VP81_IgA	1.93	-8.52	12.38	1.0000
Buffer:VP8Pep_IgG-Buffer:VP81_IgA	0.00	-10.10	10.10	1.0000
NCK56:VP8Pep_IgG-Buffer:VP81_IgA	3.65	-6.45	13.75	0.9861
GAD85:VP8Pep_IgG-Buffer:VP81_IgA	2.27	-8.18	12.72	0.9999
GAD85:VP81_IgA-NCK56:VP81_IgA	0.48	-9.62	10.58	1.0000
Buffer:VP81_IgG-NCK56:VP81_IgA	-0.88	-10.98	9.21	1.0000
NCK56:VP81_IgG-NCK56:VP81_IgA	3.17	-6.93	13.26	0.9957
GAD85:VP81_IgG-NCK56:VP81_IgA	32.73	22.63	42.83	0.0000
Buffer:VP8Pep_IgA-NCK56:VP81_IgA	-0.88	-10.98	9.21	1.0000
NCK56:VP8Pep_IgA-NCK56:VP81_IgA	0.04	-10.06	10.13	1.0000
GAD85:VP8Pep_IgA-NCK56:VP81_IgA	1.05	-9.41	11.50	1.0000
Buffer:VP8Pep_IgG-NCK56:VP81_IgA	-0.88	-10.98	9.21	1.0000
NCK56:VP8Pep_IgG-NCK56:VP81_IgA	2.77	-7.33	12.86	0.9987
GAD85:VP8Pep_IgG-NCK56:VP81_IgA	1.39	-9.07	11.84	1.0000
Buffer:VP81_IgG-GAD85:VP81_IgA	-1.36	-11.46	8.73	1.0000
NCK56:VP81_IgG-GAD85:VP81_IgA	2.69	-7.41	12.78	0.9990
GAD85:VP81_IgG-GAD85:VP81_IgA	32.25	22.15	42.35	0.0000
Buffer:VP8Pep_IgA-GAD85:VP81_IgA	-1.36	-11.46	8.73	1.0000
NCK56:VP8Pep_IgA-GAD85:VP81_IgA	-0.44	-10.54	9.65	1.0000
GAD85:VP8Pep_IgA-GAD85:VP81_IgA	0.56	-9.89	11.02	1.0000
Buffer:VP8Pep_IgG-GAD85:VP81_IgA	-1.36	-11.46	8.73	1.0000
NCK56:VP8Pep_IgG-GAD85:VP81_IgA	2.29	-7.81	12.38	0.9998
GAD85:VP8Pep_IgG-GAD85:VP81_IgA	0.90	-9.55	11.36	1.0000
NCK56:VP81_IgG-Buffer:VP81_IgG	4.05	-6.05	14.15	0.9695
GAD85:VP81_IgG-Buffer:VP81_IgG	33.62	23.52	43.71	0.0000
Buffer:VP8Pep_IgA-Buffer:VP81_IgG	0.00	-10.10	10.10	1.0000
NCK56:VP8Pep_IgA-Buffer:VP81_IgG	0.92	-9.18	11.02	1.0000
GAD85:VP8Pep_IgA-Buffer:VP81_IgG	1.93	-8.52	12.38	1.0000
Buffer:VP8Pep_IgG-Buffer:VP81_IgG	0.00	-10.10	10.10	1.0000
NCK56:VP8Pep_IgG-Buffer:VP81_IgG	3.65	-6.45	13.75	0.9861
GAD85:VP8Pep_IgG-Buffer:VP81_IgG	2.27	-8.18	12.72	0.9999
GAD85:VP81_IgG-NCK56:VP81_IgG	29.57	19.47	39.66	0.0000
Buffer:VP8Pep_IgA-NCK56:VP81_IgG	-4.05	-14.15	6.05	0.9695

NCK56:VP8Pep_IgA-NCK56:VP81_IgG	-3.13	-13.23	6.97	0.9961
GAD85:VP8Pep_IgA-NCK56:VP81_IgG	-2.12	-12.57	8.33	0.9999
Buffer:VP8Pep_IgG-NCK56:VP81_IgG	-4.05	-14.15	6.05	0.9695
NCK56:VP8Pep_IgG-NCK56:VP81_IgG	-0.40	-10.50	9.70	1.0000
GAD85:VP8Pep_IgG-NCK56:VP81_IgG	-1.78	-12.23	8.67	1.0000
Buffer:VP8Pep_IgA-GAD85:VP81_IgG	-33.62	-43.71	-23.52	0.0000
NCK56:VP8Pep_IgA-GAD85:VP81_IgG	-32.69	-42.79	-22.60	0.0000
GAD85:VP8Pep_IgA-GAD85:VP81_IgG	-31.69	-42.14	-21.23	0.0000
Buffer:VP8Pep_IgG-GAD85:VP81_IgG	-33.62	-43.71	-23.52	0.0000
NCK56:VP8Pep_IgG-GAD85:VP81_IgG	-29.96	-40.06	-19.87	0.0000
GAD85:VP8Pep_IgG-GAD85:VP81_IgG	-31.35	-41.80	-20.89	0.0000
NCK56:VP8Pep_IgA-Buffer:VP8Pep_IgA	0.92	-9.18	11.02	1.0000
GAD85:VP8Pep_IgA-Buffer:VP8Pep_IgA	1.93	-8.52	12.38	1.0000
Buffer:VP8Pep_IgG-Buffer:VP8Pep_IgA	0.00	-10.10	10.10	1.0000
NCK56:VP8Pep_IgG-Buffer:VP8Pep_IgA	3.65	-6.45	13.75	0.9861
GAD85:VP8Pep_IgG-Buffer:VP8Pep_IgA	2.27	-8.18	12.72	0.9999
GAD85:VP8Pep_IgA-NCK56:VP8Pep_IgA	1.01	-9.44	11.46	1.0000
Buffer:VP8Pep_IgG-NCK56:VP8Pep_IgA	-0.92	-11.02	9.18	1.0000
NCK56:VP8Pep_IgG-NCK56:VP8Pep_IgA	2.73	-7.37	12.83	0.9988
GAD85:VP8Pep_IgG-NCK56:VP8Pep_IgA	1.35	-9.10	11.80	1.0000
Buffer:VP8Pep_IgG-GAD85:VP8Pep_IgA	-1.93	-12.38	8.52	1.0000
NCK56:VP8Pep_IgG-GAD85:VP8Pep_IgA	1.72	-8.73	12.17	1.0000
GAD85:VP8Pep_IgG-GAD85:VP8Pep_IgA	0.34	-10.45	11.13	1.0000
NCK56:VP8Pep_IgG-Buffer:VP8Pep_IgG	3.65	-6.45	13.75	0.9861
GAD85:VP8Pep_IgG-Buffer:VP8Pep_IgG	2.27	-8.18	12.72	0.9999
GAD85:VP8Pep_IgG-NCK56:VP8Pep_IgG	-1.38	-11.83	9.07	1.0000

Table S2.11. Shapiro–Wilk and Kruskal–Wallis test statistics and p-values for the relative amount of antigen shed in fecal samples for six days postinfection from vaccinated mice challenged with murine rotavirus.

Test	statistic	p
Shapiro-Wilk normality test	0.78	1.06E-14
Kruskal-Wallis chi-squared	95.41	2.27E-18

Table S2.12. Average relative amount of ECWT antigen shed across groups per day (one–six postinfection) rounded to the nearest whole number.

Day	Group	Avg. Relative Antigen
0	Buffer	3553
0	NCK56	13911
0	GAD85	3344

1	Buffer	147075
1	NCK56	429761
1	GAD85	4864
2	Buffer	760243
2	NCK56	446090
2	GAD85	360001
3	Buffer	349536
3	NCK56	216754
3	GAD85	544364
4	Buffer	431055
4	NCK56	240070
4	GAD85	681785
5	Buffer	99128
5	NCK56	72397
5	GAD85	131757
6	Buffer	17031
6	NCK56	41894
6	GAD85	141936

Table S2.13. Benjamini–Hochberg adjusted p-values from Dunn's Test of multiple comparisons between groups for relative antigen shed in fecal samples per day (one–six postinfection) from vaccinated mice challenged with murine rotavirus.

Day Post-Infection	group1	group2	n1	n2	statistic	p	p.adj	p.adj.signif
0	Buffer	NCK56	8	8	0.5835	0.5596	0.7908	ns
0	Buffer	GAD85	8	8	0.3183	0.7503	0.7908	ns
0	NCK56	GAD85	8	8	-0.2652	0.7908	0.7908	ns
1	Buffer	NCK56	8	8	1.5910	0.1116	0.1116	ns
1	Buffer	GAD85	8	8	-2.4395	0.0147	0.0294	*
1	NCK56	GAD85	8	8	-4.0305	0.0001	0.0002	***
2	Buffer	NCK56	8	8	-1.2924	0.1962	0.3924	ns
2	Buffer	GAD85	8	8	-2.0006	0.0454	0.1363	ns
2	NCK56	GAD85	8	8	-0.7082	0.4788	0.4788	ns
3	Buffer	NCK56	8	8	-1.4852	0.1375	0.1678	ns
3	Buffer	GAD85	8	8	1.3792	0.1678	0.1678	ns
3	NCK56	GAD85	8	8	2.8644	0.0042	0.0125	*
4	Buffer	NCK56	8	8	-1.5556	0.1198	0.2396	ns
4	Buffer	GAD85	8	8	0.4950	0.6206	0.6206	ns
4	NCK56	GAD85	8	8	2.0506	0.0403	0.1209	ns
5	Buffer	NCK56	8	8	-1.1139	0.2653	0.3960	ns
5	Buffer	GAD85	8	8	0.8487	0.3960	0.3960	ns

5	NCK56	GAD85	8	8	1.9626	0.0497	0.1491	ns
6	Buffer	NCK56	8	8	-1.2021	0.2293	0.2293	ns
6	Buffer	GAD85	8	8	1.5203	0.1284	0.2293	ns
6	NCK56	GAD85	8	8	2.7224	0.0065	0.0194	*

Chapter 2 Supplementary Files

File S2.1. rLA VP8-1 and FimH Integration Methods.

The full length VP8-1 and FimH were integrated consecutively into the chromosome of *Lactobacillus acidophilus* (LA) strain GAD80 using the previously developed *upp*-based counter selective gene replacement system (211) and the previously constructed chromosomal integration plasmid pTRK1038 (210) that contains 600 bp of upstream and 600 bp of downstream sequences flanking the immediate downstream of the highly expressed gene *lba0889* (*enolase*). The FimH integration cassette containing the FimH N-terminal binding domain, PrtP signal peptide, and Mub anchor motif (213) was amplified from pTRKAV-04 (206) with primers NEB_fimH_fwd and NEB_fimH_rev. The amplified FimH cassette was assembled with NotI digested pTRK1030 backbone using NEBuilder HiFi DNA Assembly mix (New England BioLabs, NEB, Ipswich, MA, USA) to generate FimH integration plasmid pTRK1209. The reaction mixture was then heat-shock transformed into cloning host *E. coli* EC101 for amplification. The transformants were plated on BHI agar plates supplemented with 40 μg/ml kanmycin and 150 μg/ml erythromycin (Erm) and incubated at 30°C. Resulting colonies were screened with primers upp_fwd and upp_rev for positive transformants and confirmed by Sanger sequencing. Plasmid pTRK1209 was then electroporated into GAD80 that also contains plasmid pTRK669 (provides repA in trans for the replication of pTRK1209 (211). Selection for single-crossover FimH recombinants was performed as previously described (211). Briefly, single-crossover recombinants were selected after growing the GAD80 transformants at 42 °C for 48 hr in MRS supplemented with 2.5 μg/ml Erm. Single-crossover plasmid integration was confirmed by screening with primers repA-fwd and repA-rev. The single-crossover recombinants were then grown at 37 °C for 48 hr without antibiotic pressure, to facilitate the double-crossover recombination event. The double-crossover recombinants were selected with 100 μg/mL 5-fluorouracil (Sigma-Aldrich, St. Louis, MO, USA). The chromosomal integration (double-crossover) mutants were confirmed by PCR using primers 889_fwd and 889_rev. The resulting strain expressing the FimH cassette was designated LA NCK2753. The full length VP8-1 integration follows similar procedures described above. The VP8-1 was obtained as a gene block (IDT technologies, Coralville, IA, USA) with overlap sequences for downstream assembly. The VP8-1 integration plasmid was constructed by inserting the VP8-1 fragment and 660 bp of FimH flanking sequence (amplified from pTRK1209 with primers FimH_flanking_fwd and FimH_flanking_rev) into NotI and PvuI double-digested pTRK1038. The resulting VP8-1 integration plasmid pTRK1213 was transformed into NCK2753 with pTRK669. The procedures to select for chromosomal VP8-1 integration mutants were described as above. The resulting strain expressing both VP8-1 and FimH cassette downstream of *lba0889* was designated LA NCK2783.

File S2.2. Biorender.com publication license for Figure 2.1.

49 Spadina Ave. Suite 200
Toronto ON M5V 2J1 Canada
www.biorender.com

Confirmation of Publication and Licensing Rights

November 8th, 2023
Science Suite Inc.

Subscription:	*Institution*
Agreement number:	*EY262MEGB2*
Journal name:	*MDPI Vaccines*

To whom this may concern,

This document is to confirm that Darby Gilfillan has been granted a license to use the BioRender content, including icons, templates and other original artwork, appearing in the attached completed graphic pursuant to BioRender's Academic License Terms. This license permits BioRender content to be sublicensed for use in journal publications.

All rights and ownership of BioRender content are reserved by BioRender. All completed graphics must be accompanied by the following citation: "Created with BioRender.com".

BioRender content included in the completed graphic is not licensed for any commercial uses beyond publication in a journal. For any commercial use of this figure, users may, if allowed, recreate it in BioRender under an Industry BioRender Plan.

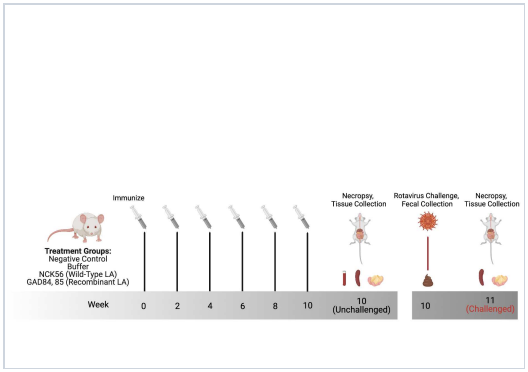

For any questions regarding this document, or other questions about publishing with BioRender refer to our BioRender Publication Guide, or contact BioRender Support at support@biorender.com.

Chapter 3 Supplementary Figures

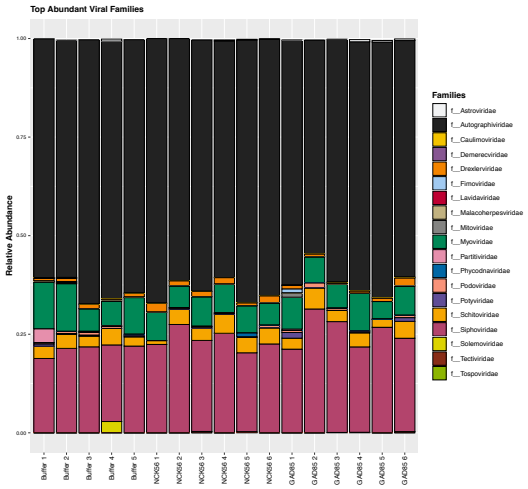

Figure S3.1. Relative abundance bar plots per sample of top 19 most abundant viral families. Many of the families are common to the virome, which is dominated by phages.

Chapter 3 Supplementary Tables

Table S3.1. Adapter sequences used for metatranscriptomic and metagenomic sequencing by Novogene™.

Adapter ID	Sequence
Adapter5	AGATCGGAAGAGCGTCGTGTAGGGAAAGAGTGTAGATCTCGGTGGTCGCCGTATCATT
Adapter3	GATCGGAAGAGCACACGTCTGAACTCCAGTCACGGATGACTATCTCGTATGCCGTCTTCTGCTTG

Table S3.2. LA NCFM genome log fold-change and adjusted *p*-values for differential transcript expression. Determined by mapping the presumed microbial metatranscriptomic sequencing reads from NCK56- and GAD85-exposed samples to an indexed NCBI LA NCFM genome.

NCK56-GAD85 LA Genome Transcript	log2FoldChange	padj
Glutamyl-tRNA(Gln) amidotransferase subunit A	-1.534169475	3.20E-12
Aspartyl/glutamyl-tRNA(Asn/Gln) amidotransferase subunit B	-1.223037673	1.75E-07
Enolase 2	-2.326210849	1.75E-07
Multidrug resistance protein 3	-1.490369088	2.17E-07
putative glutamine ABC transporter permease protein GlnM	-1.313259581	2.25E-07
Ribonuclease J 2	-1.095799547	2.25E-07
putative ABC transporter ATP-binding protein YknY	1.047115218	6.95E-07
6-phospho-beta-glucosidase BglA	-1.147391426	3.65E-06
Ribosome-binding factor A	1.252814863	4.04E-06
Proline--tRNA ligase	-0.93139828	1.62E-05
Diacylglycerol kinase	-0.976487173	2.67E-05
Heat-inducible transcription repressor HrcA	1.580820031	2.75E-05
Lichenan-specific phosphotransferase enzyme IIA component	-1.243262028	0.000231098
Aspartate carbamoyltransferase	2.591352877	0.000293554

Aspartate-semialdehyde dehydrogenase	-0.99427417	0.000353371
Putative peptide transport permease protein	-0.970140328	0.000743239
ABC transporter glutamine-binding protein GlnH	-0.734119822	0.000949434
Transcription termination/antitermination protein NusA	1.032071001	0.001055961
Bifunctional protein pyrR	1.539094192	0.001292845
Protein GrpE	1.233367101	0.001764532
PTS system cellobiose-specific EIIB component	-1.133409936	0.001764532
ATP-dependent Clp protease ATP-binding subunit ClpE	1.424166834	0.001764532
Carbamoyl-phosphate synthase small chain	2.121998406	0.001839602
CBS domain-containing protein YkuL	-0.90140455	0.001917712
ATP-dependent protease ATPase subunit ClpY	-0.925875912	0.003116998
Dihydroorotase	1.768056069	0.004567156
Ribosome maturation factor RimP	1.378564834	0.005098745
CCA-adding enzyme	-1.068505864	0.007172982
GTP-binding protein TypA/BipA	-0.51232544	0.007954217
Beta-glucoside kinase	-1.274197406	0.009983769
Peptide chain release factor 3	-0.621482046	0.011052435
Chaperone protein DnaJ	0.932622778	0.011052435
putative glutamine ABC transporter permease protein GlnP	-0.860618057	0.011052435
DNA polymerase III PolC-type	-0.731327549	0.012137744
PTS system glucose-specific EIIA component	-1.115229263	0.012462894
HTH-type transcriptional regulator ImmR	1.335216781	0.014329997
Toxin Doc	1.020844477	0.014329997
Glutamine transport ATP-binding protein GlnQ	-0.730078376	0.014329997
Putative zinc metalloprotease	-0.568443062	0.01658744
D-alanine--D-alanine ligase A	0.641182348	0.020362575
Aryl-phospho-beta-D-glucosidase BglH	1.325396153	0.023628016
Putative HMP/thiamine permease protein YkoE	-1.563343809	0.024132846
Carbamoyl-phosphate synthase large chain	1.433817585	0.026232113
Ribosomal protein L11 methyltransferase	-0.847130346	0.026232113
Energy-coupling factor transporter transmembrane protein EcfT	-0.754053781	0.026232113
Hydroxymethylglutaryl-CoA synthase	-0.693499048	0.026530912
Calcium-transporting ATPase 1	-1.182669332	0.027329692
Dipeptidase A	-0.619385589	0.027329692
PTS system maltose-specific EIICB component	-1.455089682	0.027329692
Lysozyme M1	1.082264679	0.027741333
Phosphatidate cytidylyltransferase	-0.652778017	0.027741333
Oligopeptide-binding protein AppA	-0.997241914	0.031179974
putative ribosomal protein YlxQ	1.673393289	0.031204879
Glutathione transport system permease protein GsiC	-0.789285103	0.035095087

HTH-type transcriptional repressor YvoA	0.667551132	0.037293593
4-hydroxy-tetrahydrodipicolinate reductase	-1.014452928	0.038037215
Translation initiation factor IF-1	0.826022273	0.038037215
tRNA pseudouridine synthase A	-0.84744129	0.039870449
DegV domain-containing protein	-0.616900164	0.041317795
Chaperone protein DnaK	0.836960539	0.041317795
30S ribosomal protein S18	0.884109488	0.042453176
putative D-methionine-binding lipoprotein MetQ	1.172225298	0.044514118
Chromosome partition protein Smc	-0.65165832	0.049393104

Table S3.3. NCK56 and GAD85 log fold-change and adjusted *p*-values for differential transcript expression between metatranscriptomes.

NCK56-GAD85 Transcripts	log2FoldChange	padj
flagellin FliC	13.89830643	1.97E-16
protective antigen	-11.11454437	1.97E-16
flagellin, partial	10.91158266	9.24E-11
sucrose phosphorylase	-4.09231351	0.000119201
fimbrial protein	4.182364154	0.000903132
MULTISPECIES: glucose-1-phosphate adenylyltransferase	7.42829663	0.002855463
V-type ATP synthase subunit I	7.488448725	0.006480526
V-type ATP synthase subunit D	6.886060582	0.006480526
DUF4422 domain-containing protein	5.995628748	0.006480526
MULTISPECIES: 6-phosphofructokinase	3.853860541	0.012083272
MULTISPECIES: glutamine-fructose-6-phosphate transaminase (isomerizing)	6.961672371	0.013579096
MULTISPECIES: glycogen/starch/alpha-glucan family phosphorylase	7.397802662	0.013897401
ATP synthase subunit A	6.22503536	0.017308587
fimbrial protein FimH	6.517406541	0.021520137
MULTISPECIES: thioredoxin	2.951611731	0.022739392
MULTISPECIES: DNA replication and repair protein RecF	3.302856853	0.022739392
MULTISPECIES: septation protein SpoVG	6.35243262	0.023319735
V-type ATP synthase subunit B	6.081585133	0.024027095
MULTISPECIES: glycogen/starch/alpha-glucan phosphorylase	9.22199318	0.024762694
MULTISPECIES: L-lactate dehydrogenase	3.81057797	0.025400811
transcription antiterminator	6.877926082	0.025400811
magnesium transporter MgtC	3.415931661	0.025926268
MULTISPECIES: phosphoribosylpyrophosphate synthetase	6.259894559	0.026658219
N(4)-(beta-N-acetylglucosaminyl)-L-asparaginase	5.154316307	0.032526326
peptidase S8	2.75902613	0.041640046
phosphopyruvate hydratase	-1.982360248	0.042139789
MarR family transcriptional regulator	-2.088889238	0.042139789

PTS mannose transporter subunit IIC	3.951361096	0.042139789
MULTISPECIES: peptide ABC transporter substrate-binding protein	5.180911536	0.042139789
MULTISPECIES: V-type ATP synthase subunit F	6.46646519	0.042601937

Table S3.4. Buffer and NCK56 log fold-change and adjusted *p*-values for differential transcript expression between metatranscriptomes.

Buffer-NCK56 Transcripts	log2FoldChange	padj
S-layer protein	11.883083	2.48E-48
surface protein	10.110541	1.41E-38
S-layer protein, partial	11.379127	5.63E-38
SlpX	13.313765	1.53E-34
23S ribosomal RNA methyltransferase Erm, partial	14.194687	4.87E-32
aldehyde dehydrogenase, partial	9.833302	1.11E-29
arsenate reductase	8.153071	2.52E-29
endoribonuclease YbeY	9.697133	5.10E-25
lysin	10.687342	9.35E-23
calcium-translocating P-type ATPase, PMCA-type	6.810049	1.53E-22
amylopullulanase	11.943322	2.10E-22
ribosomal-protein-alanine N-acetyltransferase RimI	8.116858	8.34E-22
homoserine O-succinyltransferase	8.134270	9.32E-22
surface layer protein	10.938266	1.25E-21
protease HtpX	6.380397	1.79E-21
50S ribosomal protein L31 type B	7.229966	2.09E-21
central glycolytic genes regulator, partial	10.902901	1.16E-20
DNA polymerase III subunit gamma/tau, partial	10.438318	3.65E-20
SPFH domain-containing protein	8.477689	4.92E-20
surface layer protein HAP50	9.284446	5.90E-20
Mannose-specific PTS system component IID	11.335831	7.63E-20
steroid-binding protein	11.069764	8.21E-20
peptidase M13, partial	10.829608	1.08E-19
adapter protein MecA, partial	10.587411	1.43E-19
glucan modification protein	10.921368	1.68E-19
aquaporin family protein	8.137176	3.84E-19
ATP--cob(I)alamin adenosyltransferase	9.308525	3.92E-19
tRNA (adenosine(37)-N6)-threonylcarbamoyltransferase complex transferase subunit TsaD	5.756990	4.96E-19
S-adenosylmethionine synthase	10.031807	4.96E-19

Table S3.5. Buffer and GAD85 log fold-change values and adjusted *p*-values for differential transcript expression between metatranscriptomes.

Buffer-GAD85 Transcripts	log2FoldChange	padj
S-layer protein	11.0482621	6.03E-15

SlpX	12.1143424	1.46E-11
surface protein	9.25381708	9.20E-10
flagellin FliC	11.3518479	9.20E-10
lysin	10.5445396	1.42E-09
MULTISPECIES: replication protein RepB	11.1607755	5.50E-09
steroid-binding protein	10.7357365	2.02E-08
arsenate reductase	7.21966367	2.05E-07
surface layer protein	9.556166	2.05E-07
ribose-phosphate diphosphokinase	7.46834883	3.24E-07
PTS-dependent dihydroxyacetone kinase phosphotransferase subunit DhaM	9.34323681	4.87E-07
50S ribosomal protein L31 type B	6.91662654	5.06E-07
S-layer protein, partial	9.14333978	5.68E-07
amylopullulanase	9.7647308	6.25E-07
macrolide transporter	9.6732532	6.90E-07
Serine protease DegP/HtrA do-like protein	8.86739788	8.50E-07
aggregation promoting protein	9.15252417	8.50E-07
glucan modification protein	9.41131714	9.23E-07
surface layer protein HAP50	8.0515953	1.01E-06
transcription antitermination protein BlgG	9.45243346	1.34E-06
carboxymuconolactone decarboxylase	7.6707844	1.57E-06
fibrinogen-binding protein	9.49865763	1.57E-06
antitermination protein BlgG	8.37401762	1.77E-06
S-adenosylmethionine synthase	8.98955316	2.01E-06
homoserine O-succinyltransferase	7.45761182	2.01E-06
dihydroxyacetone kinase subunit L	9.68580559	2.01E-06
Mannose-specific PTS system component IID	9.3490391	2.01E-06
dihydroxyacetone kinase subunit DhaK	9.17651322	2.86E-06
replication protein RepB	8.78535905	2.86E-06

Table S3.6. Log fold-change and adjusted *p*-values for differential abundance of significant bacteria between NCK56 and GAD85 bacteriomes. Provided at the genus and species level.

NCK56-GAD85 (Bact.)	logFC	adj.P.Val	genus	species
otu386	-5.506	0.000	g__Bacillus	s__Bacillus_anthracis
otu24	6.565	0.000	g__Clostridium	s__Clostridium_chauvoei
otu27	4.594	0.000	g__Clostridium	s__Clostridium_isatidis
otu192	-3.877	0.000	g__Lactobacillus	s__Lactobacillus_acidophilus
otu33	5.126	0.000	g__Clostridium	s__Clostridium_saccharobutylicum
otu252	3.819	0.000	g__Enterococcus	s__Enterococcus_faecalis
otu26	3.856	0.000	g__Clostridium	s__Clostridium_septicum
otu11	4.149	0.000	g__Clostridium	s__Clostridium_baratii

otu9	3.370	0.000	g__Clostridium	s__Clostridium_perfringens
otu17	4.119	0.000	g__Clostridium	s__Clostridium_sp._JN-1
otu559	-3.116	0.000	g__Faecalitalea	s__Faecalitalea_cylindroides
otu1294	3.878	0.000	g__Allocoleopsis	s__Allocoleopsis_franciscana
otu28	3.613	0.000	g__Clostridium	s__Clostridium_taeniosporum
otu12	3.224	0.000	g__Clostridium	s__Clostridium_sp._CT4
otu1	2.753	0.000	g__Romboutsia	s__Romboutsia_ilealis
otu35	3.302	0.000	g__Clostridium	s__Clostridium_argentinense
otu3694	5.298	0.000	g__Koinonema	s__[Phormidium]_sp._ETS-05
otu62	5.418	0.000	g__Hathewaya	s__Hathewaya_histolytica
otu10	3.373	0.000	g__Clostridium	s__Clostridium_butyricum
otu381	-2.551	0.000	g__Bacillus	s__Bacillus_cereus
otu1288	3.200	0.000	g__Chondrocystis	s__Chondrocystis_sp._NIES-4102
otu50	3.618	0.000	g__Clostridium	s__Clostridium_cochlearium
otu34	2.497	0.000	g__Clostridium	s__Clostridium_thermarum
otu42	3.085	0.000	g__Clostridium	s__Clostridium_estertheticum
otu3375	2.617	0.000	g__Lactococcus	s__Lactococcus_lactis
otu54	2.615	0.000	g__Sarcina	s__Sarcina_sp._JB2
otu38	3.004	0.000	g__Clostridium	s__Clostridium_cellulovorans
otu36	2.549	0.000	g__Clostridium	s__Clostridium_novyi
otu3009	2.745	0.000	g__Fusobacterium	s__Fusobacterium_ulcerans
otu702	-2.911	0.000	g__Corynebacterium	s__Corynebacterium_xerosis
otu37	2.142	0.000	g__Clostridium	s__Clostridium_beijerinckii
otu5108	4.262	0.000	g__Mycoplasmopsis	s__Mycoplasmopsis_gallinacea
otu164	2.898	0.000	g__Candidatus_Syntrophocurvum	s__Candidatus_Syntrophocurvum_alkaliphilum
otu2768	2.141	0.000	g__Duncaniella	s__Duncaniella_sp._B8
otu44	2.309	0.000	g__Clostridium	s__Clostridium_kluyveri
otu1293	2.937	0.000	g__Moorea	s__Moorea_producens
otu30	2.533	0.000	g__Clostridium	s__Clostridium_intestinale
otu68	2.047	0.001	g__Acutalibacter	s__Acutalibacter_muris
otu1271	4.515	0.001	g__Anabaena	s__Anabaena_sp._WA102
otu1289	2.242	0.001	g__Gloeocapsa	s__Gloeocapsa_sp._PCC_7428
otu2544	-1.874	0.001	g__Sphingomonas	s__Sphingomonas_sp._LM7
otu842	-1.870	0.001	g__Streptomyces	s__Streptomyces_sp._PBH53
otu25	2.491	0.001	g__Clostridium	s__Clostridium_gasigenes
otu843	-1.859	0.001	g__Streptomyces	s__Streptomyces_sp._HF10
otu40	2.283	0.001	g__Clostridium	s__Clostridium_carboxidivorans
otu4998	-2.711	0.001	g__Corynebacterium	s__Corynebacterium_freneyi
otu547	2.195	0.001	g__Turicibacter	s__Turicibacter_sanguinis
otu2235	-1.813	0.001	g__Massilia	s__Massilia_sp._NP310

otu473	3.406	0.001	g__Lentibacillus	s__Lentibacillus_sp._CBA3610
otu3030	-1.809	0.001	g__Akkermansia	s__Akkermansia_muciniphila
otu549	-2.168	0.001	g__Erysipelothrix	s__Erysipelothrix_sp._HDW6B
otu14	2.169	0.001	g__Clostridium	s__Clostridium_sp._DL-VIII
otu1936	4.000	0.001	g__Alteromonas	s__Alteromonas_pelagimontana
otu770	-1.994	0.001	g__Bifidobacterium	s__Bifidobacterium_choerinum
otu1049	-1.780	0.001	g__Kocuria	s__Kocuria_rosea
otu1413	-1.758	0.002	g__Pseudomonas	s__Pseudomonas_sp._MPC6
otu2782	-1.757	0.002	g__Bacteroides	s__Bacteroides_thetaiotaomicron
otu253	2.337	0.002	g__Enterococcus	s__Enterococcus_durans
otu5364	2.057	0.002	g__Deinococcus	s__Deinococcus_deserti
otu160	2.390	0.002	g__Vallitalea	s__Vallitalea_guaymasensis
otu110	2.439	0.002	g__Cellulosilyticum	s__Cellulosilyticum_lentocellum
otu32	1.781	0.002	g__Clostridium	s__Clostridium_bornimense
otu63	2.614	0.003	g__Candidatus_Arthromitus	s__Candidatus_Arthromitus_sp._SFB-rat-Yit
otu583	2.076	0.003	g__Sedimentibacter	s__Sedimentibacter_sp._zth1
otu4040	-3.298	0.003	g__Caenibius	s__Caenibius_sp._WL
otu5075	1.995	0.003	g__Pseudonocardia	s__Pseudonocardia_sp._DSM_110487
otu1214	-1.675	0.003	g__Nakamurella	s__Nakamurella_multipartita
otu22	2.130	0.004	g__Clostridium	s__Clostridium_sp._AWRP
otu47	2.499	0.004	g__Clostridium	s__Clostridium_scatologenes
otu1336	3.849	0.004	g__Mycoplasmopsis	s__Mycoplasmopsis_edwardii
otu3	1.821	0.004	g__Romboutsia	s__Romboutsia_hominis
otu1281	2.409	0.004	g__Sphaerospermopsis	s__Sphaerospermopsis_torques-reginae
otu180	3.006	0.004	g__Carboxydothermus	s__Carboxydothermus_hydrogenoformans
otu993	-1.648	0.004	g__Microbacterium	s__Microbacterium_sp._10M-3C3

Table S3.7. Log fold-change and adjusted *p*-values for the differential abundance of significant bacteria between NCK56 and buffer bacteriomes. Provided at the genus and species level.

NCK56-Buffer (Bact.)	logFC	adj.P.Val	genus	species
otu192	13.34246838	3.92E-243	g__Lactobacillus	s__Lactobacillus_acidophilus
otu3331	6.528046482	9.04E-56	g__Lactobacillus	s__Lactobacillus_helveticus
otu206	6.160544267	1.29E-51	g__Lactobacillus	s__Lactobacillus_amylovorus
otu386	5.645774283	2.95E-43	g__Bacillus	s__Bacillus_anthracis
otu9	-5.062575204	3.28E-32	g__Clostridium	s__Clostridium_perfringens
otu24	-5.837722104	5.69E-30	g__Clostridium	s__Clostridium_chauvoei
otu26	-5.566053491	3.30E-29	g__Clostridium	s__Clostridium_septicum
otu37	-4.749297187	2.44E-23	g__Clostridium	s__Clostridium_beijerinckii
otu11	-4.916701956	6.36E-23	g__Clostridium	s__Clostridium_baratii

otu27	-4.280946231	1.08E-22	g__Clostridium	s__Clostridium_isatidis
otu1	-4.14914686	7.05E-22	g__Romboutsia	s__Romboutsia_ilealis
otu54	-4.382974085	3.37E-20	g__Sarcina	s__Sarcina_sp._JB2
otu10	-4.559330043	5.44E-20	g__Clostridium	s__Clostridium_butyricum
otu32	-3.982742876	2.16E-19	g__Clostridium	s__Clostridium_bornimense
otu34	-3.922797276	6.45E-18	g__Clostridium	s__Clostridium_thermarum
otu28	-4.27136332	1.60E-17	g__Clostridium	s__Clostridium_taeniosporum
otu412	-4.80380278	1.01E-16	g__Virgibacillus	s__Virgibacillus_necropolis
otu12	-3.743591801	3.04E-15	g__Clostridium	s__Clostridium_sp._CT4
otu35	-4.096885863	6.75E-15	g__Clostridium	s__Clostridium_argentinense
otu33	-3.751351254	1.73E-13	g__Clostridium	s__Clostridium_saccharobutylicum
otu36	-3.687510473	8.71E-13	g__Clostridium	s__Clostridium_novyi
otu17	-4.014221486	1.56E-12	g__Clostridium	s__Clostridium_sp._JN-1
otu547	-3.560526625	2.85E-12	g__Turicibacter	s__Turicibacter_sanguinis
otu3030	3.02433219	4.38E-12	g__Akkermansia	s__Akkermansia_muciniphila
otu42	-3.762152752	7.31E-12	g__Clostridium	s__Clostridium_estertheticum
otu3375	3.638474944	1.42E-11	g__Lactococcus	s__Lactococcus_lactis
otu5751	4.383783384	3.72E-11	g__Bifidobacterium	s__Bifidobacterium_eulemuris
otu110	-3.758514679	5.75E-11	g__Cellulosilyticum	s__Cellulosilyticum_lentocellum
otu62	-5.409459501	1.13E-10	g__Hathewaya	s__Hathewaya_histolytica
otu333	-3.105007164	1.63E-10	g__Staphylococcus	s__Staphylococcus_saccharolyticus
otu50	-3.451391957	1.86E-10	g__Clostridium	s__Clostridium_cochlearium
otu40	-3.414918793	2.25E-10	g__Clostridium	s__Clostridium_carboxidivorans
otu330	-3.405161348	2.25E-10	g__Staphylococcus	s__Staphylococcus_lugdunensis
otu1294	-3.548173579	2.25E-10	g__Allocoleopsis	s__Allocoleopsis_franciscana
otu546	-3.228668833	4.65E-10	g__Turicibacter	s__Turicibacter_sp._H121
otu38	-3.28950907	1.08E-09	g__Clostridium	s__Clostridium_cellulovorans
otu13	-2.945105531	1.12E-09	g__Clostridium	s__Clostridium_sp._C5S11
otu770	2.864152252	3.79E-09	g__Bifidobacterium	s__Bifidobacterium_choerinum
otu311	-4.446682132	4.24E-09	g__Carnobacterium	s__Carnobacterium_viridans
otu552	-3.872036503	6.59E-09	g__Erysipelothrix	s__Erysipelothrix_rhusiopathiae
otu47	-3.910661454	8.82E-09	g__Clostridium	s__Clostridium_scatologenes
otu314	-3.309353368	1.15E-08	g__Marinilactibacillus	s__Marinilactibacillus_sp._15R
otu2695	-3.842258616	2.01E-08	g__Desulfocapsa	s__Desulfocapsa_sulfexigens
otu25	-2.866268805	1.56E-07	g__Clostridium	s__Clostridium_gasigenes
otu5745	3.210890019	1.79E-07	g__Planococcus	s__Planococcus_sp._MB-3u-03
otu269	-3.135515379	2.15E-07	g__Melissococcus	s__Melissococcus_plutonius
otu4068	-8.964012596	2.56E-07	g__Haematobacter	s__Haematobacter_massiliensis
otu2047	-3.339355538	2.65E-07	g__Methylomonas	s__Methylomonas_methanica
otu5092	2.77748786	2.76E-07	g__Bifidobacterium	s__Bifidobacterium_pullorum

otu4998	3.248400521	3.58E-07	g__Corynebacterium	s__Corynebacterium_freneyi
otu46	-2.751773587	7.91E-07	g__Clostridium	s__Clostridium_fermenticellae
otu513	-2.627131949	7.91E-07	g__Listeria	s__Listeria_grayi
otu462	-2.769918958	9.10E-07	g__Radiobacillus	s__Radiobacillus_deserti
otu561	-2.607198097	1.07E-06	g__Megamonas	s__Megamonas_hypermegale
otu18	-2.946940465	1.52E-06	g__Clostridium	s__Clostridium_sp._MF28
otu6106	2.794494101	1.97E-06	g__Mucilaginibacter	s__Mucilaginibacter_sp._14171R-50
otu456	-2.78754537	3.31E-06	g__Psychrobacillus	s__Psychrobacillus_sp._INOP01
otu519	-2.242018201	3.67E-06	g__Exiguobacterium	s__Exiguobacterium_sp._N4-1P
otu31	-2.171923789	4.03E-06	g__Clostridium	s__Clostridium_saccharoperbutylacetonicum
otu702	2.713450726	6.93E-06	g__Corynebacterium	s__Corynebacterium_xerosis
otu2242	2.247601747	6.93E-06	g__Massilia	s__Massilia_oculi
otu3329	2.693101442	7.44E-06	g__Lactobacillus	s__Lactobacillus_kefiranofaciens
otu69	-3.313405436	7.72E-06	g__Acetivibrio	s__Acetivibrio_saccincola
otu3475	2.452426047	1.05E-05	g__Bifidobacterium	s__Bifidobacterium_animalis
otu154	-2.932623891	1.27E-05	g__Syntrophobotulus	s__Syntrophobotulus_glycolicus
otu551	-2.736357153	1.32E-05	g__Erysipelothrix	s__Erysipelothrix_larvae
otu30	-2.458755306	1.46E-05	g__Clostridium	s__Clostridium_intestinale
otu3	-2.211706492	1.53E-05	g__Romboutsia	s__Romboutsia_hominis
otu5789	3.433234725	1.83E-05	g__Acinetobacter	s__Acinetobacter_sp._WY4
otu1322	-3.101712578	1.85E-05	g__Mycoplasma	s__Mycoplasma_sp._Mirounga_ES2806-GEN
otu4	-2.164902064	2.12E-05	g__Paeniclostridium	s__Paeniclostridium_sordellii
otu439	-2.292894156	2.17E-05	g__Niallia	s__Niallia_circulans
otu5289	2.401000351	2.59E-05	g__Bacillus	s__Bacillus_sp._FJAT-45348
otu160	-2.775811008	2.66E-05	g__Vallitalea	s__Vallitalea_guaymasensis
otu420	-2.397264838	2.80E-05	g__Priestia	s__Priestia_flexa
otu583	-2.462197605	2.80E-05	g__Sedimentibacter	s__Sedimentibacter_sp._zth1
otu5810	2.433773256	2.80E-05	g__Massilia	s__Massilia_sp._PAMC28688
otu3009	-2.326201035	2.80E-05	g__Fusobacterium	s__Fusobacterium_ulcerans
otu209	-2.631671834	3.12E-05	g__Ligilactobacillus	s__Ligilactobacillus_acidipiscis
otu438	-2.319821053	3.95E-05	g__Caldalkalibacillus	s__Caldalkalibacillus_thermarum
otu310	-3.561113018	3.98E-05	g__Carnobacterium	s__Carnobacterium_inhibens
otu48	-2.42077319	4.82E-05	g__Clostridium	s__Clostridium_formicaceticum
otu422	-2.206001082	4.92E-05	g__Cytobacillus	s__Cytobacillus_oceanisediminis
otu559	2.169915442	4.94E-05	g__Faecalitalea	s__Faecalitalea_cylindroides
otu164	-2.888207217	4.99E-05	g__Candidatus_Syntrophocurvum	s__Candidatus_Syntrophocurvum_alkaliphilum
otu2447	2.079728644	5.45E-05	g__Aureimonas	s__Aureimonas_sp._AU20
otu342	-2.579934753	8.03E-05	g__Staphylococcus	s__Staphylococcus_debuckii
otu4456	2.036344305	9.95E-05	g__Hymenobacter	s__Hymenobacter_sp._APR13
otu5498	-2.942675048	0.000112027	g__Acidovorax	s__Acidovorax_sp._HDW3

otu5376	-2.325456517	0.000116626	g__Candidatus_Riesia	s__Candidatus_Riesia_pediculischaeffi
otu1350	-3.104405254	0.000121085	g__Entomoplasma	s__Entomoplasma_luminosum
otu474	-2.198926085	0.000122317	g__Paenibacillus	s__Paenibacillus_sp._BIHB4019
otu15	-2.348952891	0.00013143	g__Clostridium	s__Clostridium_sp._JN-9
otu413	-2.401067166	0.00013503	g__Virgibacillus	s__Virgibacillus_phasianinus
otu2801	2.095737015	0.000159132	g__Phocaeicola	s__Phocaeicola_coprophilus
otu3018	-2.235673484	0.000160821	g__Leptotrichia	s__Leptotrichia_sp._oral_taxon_218
otu401	-1.895651107	0.000177056	g__Alkalihalobacillus	s__Alkalihalobacillus_halodurans
otu3681	2.408675862	0.000182031	g__Arcanobacterium	s__Arcanobacterium_sp._JY-X040
otu89	2.139212307	0.000202896	g__Pusillimonas_(ex_Kitahara_et_al._2021)	s__Pusillimonas_faecalis
otu356	-3.68939953	0.000210463	g__Macrococcus	s__Macrococcus_canis
otu522	-2.529910554	0.000242358	g__Gemella	s__Gemella_sanguinis
otu14	-2.061320462	0.000276861	g__Clostridium	s__Clostridium_sp._DL-VIII
otu41	-2.278456466	0.000283599	g__Clostridium	s__Clostridium_acetobutylicum
otu5417	-2.478270532	0.000336043	g__Hahella	s__Hahella_sp._KA22
otu453	-3.296597274	0.000337458	g__Sutcliffiella	s__Sutcliffiella_horikoshii
otu4722	-2.387668814	0.000342278	g__Vibrio	s__Vibrio_owensii
otu425	-2.502308827	0.000348114	g__Oceanobacillus	s__Oceanobacillus_zhaokaii
otu336	-2.993180696	0.000368852	g__Staphylococcus	s__Staphylococcus_muscae
otu5836	2.645862654	0.000368852	g__Ehrlichia	s__Ehrlichia_chaffeensis
otu539	-2.177983042	0.000405706	g__Alicyclobacillus	s__Alicyclobacillus_ferrooxydans
otu414	-2.09615254	0.00043591	g__Virgibacillus	s__Virgibacillus_sp._Bac332
otu29	-1.761966835	0.00043945	g__Clostridium	s__Clostridium_botulinum
otu44	-1.911703455	0.000450849	g__Clostridium	s__Clostridium_kluyveri
otu267	-3.594054081	0.000461408	g__Tetragenococcus	s__Tetragenococcus_koreensis
otu458	-2.427367298	0.000496389	g__Gracilibacillus	s__Gracilibacillus_sp._SCU50
otu4656	-1.934894397	0.000519606	g__Yersinia	s__Yersinia_intermedia
otu326	-2.315058249	0.000579206	g__Abiotrophia	s__Abiotrophia_defectiva
otu1925	-3.528312902	0.000596865	g__Parashewanella	s__Parashewanella_spongiae
otu3057	-2.240656481	0.000596865	g__Paludisphaera	s__Paludisphaera_borealis
otu4398	1.855224251	0.000608717	g__Psychroflexus	s__Psychroflexus_torquis
otu3010	-1.837209186	0.000620354	g__Fusobacterium	s__Fusobacterium_nucleatum
otu323	-2.08424826	0.0006231	g__Aerococcus	s__Aerococcus_sanguinicola
otu2823	1.772825948	0.000639097	g__Parabacteroides	s__Parabacteroides_merdae
otu446	-2.122307511	0.000651397	g__Peribacillus	s__Peribacillus_asahii
otu840	1.697420029	0.000836583	g__Streptomyces	s__Streptomyces_sp._SN-593
otu2058	-1.96000721	0.000855207	g__Gallaecimonas	s__Gallaecimonas_mangrovi
otu2644	2.032105099	0.000929222	g__Magnetospirillum	s__Magnetospirillum_magneticum
otu403	-3.369496895	0.000984022	g__Alkalihalobacillus	s__Alkalihalobacillus_miscanthi
otu5966	2.652455652	0.001009041	g__Calothrix	s__Calothrix_sp._PCC_6303

otu262	-2.954859736	0.001049428	g__Vagococcus	s__Vagococcus_penaei
otu367	-2.285800276	0.001071887	g__Bacillus	s__Bacillus_sp._NP247
otu5757	2.075142717	0.001078705	g__Microbacterium	s__Microbacterium_chocolatum
otu534	-2.483837413	0.001111537	g__Paenisporosarcina	s__Paenisporosarcina_antarctica
otu2942	1.97901139	0.001148742	g__Hymenobacter	s__Hymenobacter_sp._S2-20-2
otu6239	2.822686221	0.001207161	g__Shewanella	s__Shewanella_glacialimarina
otu431	-3.632353272	0.001267097	g__Heyndrickxia	s__Heyndrickxia_oleronia
otu3059	-2.883127324	0.001267097	g__Tautonia	s__Tautonia_plasticadhaerens
otu514	-2.77127002	0.001267097	g__Listeria	s__Listeria_welshimeri
otu6054	2.058526803	0.001425615	g__Brucella	s__Brucella_ceti
otu99	1.935914827	0.001582466	g__Blautia	s__Blautia_obeum
otu443	-1.973127631	0.001746203	g__Neobacillus	s__Neobacillus_mesonae
otu4370	2.1765323	0.00176117	g__Flavobacterium	s__Flavobacterium_inviolabile
otu324	-3.296324836	0.001803918	g__Aerococcus	s__Aerococcus_urinaehominis
otu419	-2.124171223	0.001896205	g__Priestia	s__Priestia_filamentosa
otu1073	-1.898073169	0.001929532	g__Nesterenkonia	s__Nesterenkonia_sp._NBAIMH1
otu2732	-2.174902444	0.002021656	g__Aliarcobacter	s__Aliarcobacter_cryaerophilus
otu3078	-2.261187913	0.002062644	g__Brachyspira	s__Brachyspira_hampsonii
otu846	-1.719392518	0.002062644	g__Streptomyces	s__Streptomyces_sp._ICC1
otu2782	1.601342655	0.002062644	g__Bacteroides	s__Bacteroides_thetaiotaomicron
otu45	-3.019942165	0.002238911	g__Clostridium	s__Clostridium_tyrobutyricum
otu196	1.62637814	0.002238911	g__Lactobacillus	s__Lactobacillus_amylolyticus
otu39	-1.591997198	0.002238911	g__Clostridium	s__Clostridium_tetani
otu2235	1.590989648	0.002238911	g__Massilia	s__Massilia_sp._NP310
otu3344	-2.328236743	0.002265323	g__Pediococcus	s__Pediococcus_damnosus
otu1400	-1.62410867	0.002290008	g__Pseudomonas	s__Pseudomonas_sp._St29
otu3770	2.009326434	0.002347388	g__Pseudomonas	s__Pseudomonas_zarinae
otu562	1.686507638	0.002347388	g__Selenomonas	s__Selenomonas_sputigena
otu504	-1.582505246	0.002376011	g__Saccharibacillus	s__Saccharibacillus_brassicae
otu253	-2.184537504	0.002391341	g__Enterococcus	s__Enterococcus_durans
otu573	-2.393679408	0.002447286	g__Anaerococcus	s__Anaerococcus_vaginalis
otu756	-2.141629917	0.002490083	g__Gordonia	s__Gordonia_sp._JH63
otu1214	1.575816554	0.002490083	g__Nakamurella	s__Nakamurella_multipartita
otu4220	2.112862226	0.002516969	g__Polynucleobacter	s__Polynucleobacter_wuianus
otu368	-2.003657196	0.002608232	g__Bacillus	s__Bacillus_sp._OxB-1
otu207	2.252216262	0.002627408	g__Lactobacillus	s__Lactobacillus_gallinarum
otu3820	2.25255451	0.002662525	g__Arsenophonus	s__Arsenophonus_endosymbiont_of_Apis_mellifera
otu1345	-4.252166367	0.002680794	g__Acholeplasma	s__Acholeplasma_hippikon
otu2784	1.664625735	0.002726218	g__Bacteroides	s__Bacteroides_heparinolyticus
otu58	-2.778786526	0.002928417	g__Crassaminicella	s__Crassaminicella_profunda

otu421	-2.348880972	0.002934075	g__Cytobacillus	s__Cytobacillus_kochii
otu381	1.554247749	0.002968967	g__Bacillus	s__Bacillus_cereus
otu213	-2.062473252	0.003028626	g__Ligilactobacillus	s__Ligilactobacillus_agilis
otu95	-2.004117424	0.003093498	g__Blautia	s__Blautia_sp._SC05B48
otu5833	2.471120507	0.003394772	g__Roseococcus	s__Roseococcus_sp._NIBR12
otu3026	-2.919880892	0.003416256	g__Streptobacillus	s__Streptobacillus_moniliformis
otu2765	-3.380580455	0.003588132	g__Acidithiobacillus	g__Acidithiobacillus
otu4291	1.816339617	0.003588132	g__Sandaracinus	s__Sandaracinus_amylolyticus
otu5522	-2.06078418	0.003613031	g__Hymenobacter	s__Hymenobacter_baengnokdamensis
otu4351	2.04591838	0.003613031	g__Prevotella	s__Prevotella_scopos
otu549	1.853127967	0.003613031	g__Erysipelothrix	s__Erysipelothrix_sp._HDW6B
otu2915	-3.974338478	0.003627635	g__Riemerella	s__Riemerella_anatipestifer
otu5333	-3.321915874	0.003808636	g__Micrococcus	s__Micrococcus_sp._V7
otu4740	-2.15005926	0.003817063	g__Pseudoalteromonas	s__Pseudoalteromonas_sp._A41-2
otu407	-1.753548748	0.003817063	g__Lysinibacillus	s__Lysinibacillus_sp._2017
otu4298	1.737323839	0.003839249	g__Maridesulfovibrio	s__Maridesulfovibrio_salexigens
otu418	-1.554996521	0.003839249	g__Priestia	s__Priestia_megaterium
otu2833	1.660616155	0.003891764	g__Proteiniphilum	s__Proteiniphilum_saccharofermentans
otu2756	-2.062878938	0.003923321	g__Nitratiruptor	s__Nitratiruptor_sp._SB155-2
otu198	1.774388806	0.003923321	g__Lactobacillus	s__Lactobacillus_acetotolerans
otu339	-2.867167871	0.00429154	g__Staphylococcus	s__Staphylococcus_argenteus
otu59	-3.027827591	0.004335769	g__Alkaliphilus	s__Alkaliphilus_sp._B6464
otu5797	2.408645528	0.004357339	g__Shewanella	s__Shewanella_halifaxensis
otu512	-1.756308459	0.0045659	g__Listeria	s__Listeria_ivanovii
otu424	-1.672289512	0.004741962	g__Oceanobacillus	s__Oceanobacillus_kimchii

Table S3.8. Log fold-change and adjusted *p*-values for the differential abundance of significant bacteria between GAD85 and buffer bacteriomes. Provided at the genus and species level.

GAD85-Buffer (Bact.)	logFC	adj.P.Val	genus	species
otu192	9.465471158	4.90E-120	g__Lactobacillus	s__Lactobacillus_acidophilus
otu3375	6.25592548	2.49E-40	g__Lactococcus	s__Lactococcus_lactis
otu3331	5.022333416	5.94E-33	g__Lactobacillus	s__Lactobacillus_helveticus
otu206	4.574432839	2.67E-27	g__Lactobacillus	s__Lactobacillus_amylovorus
otu252	4.087792671	1.40E-18	g__Enterococcus	s__Enterococcus_faecalis
otu768	2.623511208	4.73E-08	g__Bifidobacterium	s__Bifidobacterium_pseudolongum
otu420	-3.060032074	4.75E-08	g__Priestia	s__Priestia_flexa
otu4068	-8.064259745	4.75E-08	g__Haematobacter	s__Haematobacter_massiliensis
otu371	-3.234008866	7.41E-07	g__Bacillus	s__Bacillus_sp._M4U3P1
otu2406	-2.401327748	9.93E-07	g__Mesorhizobium	s__Mesorhizobium_sp._Pch-S
otu37	-2.607421631	9.93E-07	g__Clostridium	s__Clostridium_beijerinckii

otu310	-3.931344996	1.42E-06	g__Carnobacterium	s__Carnobacterium_inhibens
otu5773	4.774996844	1.84E-06	g__Synechococcus	s__Synechococcus_sp._JA-2-3B'a(2-13)
otu519	-2.383253463	2.85E-06	g__Exiguobacterium	s__Exiguobacterium_sp._N4-1P
otu526	-3.700722187	2.85E-06	g__Sporosarcina	s__Sporosarcina_ureilytica
otu2047	-2.944345009	4.23E-06	g__Methylomonas	s__Methylomonas_methanica
otu2801	2.565908659	4.23E-06	g__Phocaeicola	s__Phocaeicola_coprophilus
otu412	-2.906669922	2.21E-05	g__Virgibacillus	s__Virgibacillus_necropolis
otu32	-2.201270239	3.13E-05	g__Clostridium	s__Clostridium_bornimense
otu6106	2.540765572	3.74E-05	g__Mucilaginibacter	s__Mucilaginibacter_sp._14171R-50
otu330	-2.519196567	4.10E-05	g__Staphylococcus	s__Staphylococcus_lugdunensis
otu439	-2.273907588	4.10E-05	g__Niallia	s__Niallia_circulans
otu69	-2.995482761	5.37E-05	g__Acetivibrio	s__Acetivibrio_saccincola
otu5506	-2.792714504	5.37E-05	g__Candidatus_Methylopumilus	s__Candidatus_Methylopumilus_planktonicus
otu5836	2.908930893	5.78E-05	g__Ehrlichia	s__Ehrlichia_chaffeensis
otu333	-2.158767471	7.75E-05	g__Staphylococcus	s__Staphylococcus_saccharolyticus
otu346	2.351762317	0.000144718	g__Staphylococcus	s__Staphylococcus_arlettae
otu311	-3.00230524	0.000150268	g__Carnobacterium	s__Carnobacterium_viridans
otu2705	-2.576730485	0.000282641	g__Pelobacter	s__Pelobacter_propionicus
otu425	-2.535229666	0.000326965	g__Oceanobacillus	s__Oceanobacillus_zhaokaii
otu3694	3.270922058	0.000352401	g__Koinonema	s__[Phormidium]_sp._ETS-05
otu3329	2.381794208	0.000473116	g__Lactobacillus	s__Lactobacillus_kefiranofaciens
otu520	-2.558466163	0.000497347	g__Exiguobacterium	s__Exiguobacterium_alkaliphilum
otu1348	-3.32620153	0.000520261	g__Candidatus_Phytoplasma	s__Candidatus_Phytoplasma_australiense
otu356	-3.377354488	0.000622908	g__Macrococcus	s__Macrococcus_canis
otu3475	2.083676253	0.000622908	g__Bifidobacterium	s__Bifidobacterium_animalis
otu6475	2.28102159	0.001076628	g__Flavobacterium	s__Flavobacterium_alkalisoli
otu5364	2.141646155	0.001076628	g__Deinococcus	s__Deinococcus_deserti
otu314	-2.217603376	0.001082907	g__Marinilactibacillus	s__Marinilactibacillus_sp._15R
otu267	-3.36349122	0.001207319	g__Tetragenococcus	s__Tetragenococcus_koreensis
otu456	-2.131844928	0.001447604	g__Psychrobacillus	s__Psychrobacillus_sp._INOP01
otu513	-2.078853169	0.001579621	g__Listeria	s__Listeria_grayi
otu1210	-1.987677381	0.001623241	g__Modestobacter	s__Modestobacter_marinus
otu308	2.036180199	0.001681109	g__Lactococcus	s__Lactococcus_cremoris
otu5763	2.045408797	0.001681109	g__Arthrobacter	s__Arthrobacter_sp._PAMC25564
otu2835	1.860189927	0.001681109	g__Odoribacter	s__Odoribacter_splanchnicus
otu208	-1.790372334	0.001822812	g__Ligilactobacillus	s__Ligilactobacillus_salivarius
otu1234	1.844238388	0.002080487	g__Gordonibacter	s__Gordonibacter_urolithinfaciens
otu5959	2.427546448	0.002506713	g__Olsenella	s__Olsenella_sp._GAM18
otu5751	2.487058059	0.002506713	g__Bifidobacterium	s__Bifidobacterium_eulemuris
otu367	-2.30146082	0.002506713	g__Bacillus	s__Bacillus_sp._NP247

otu2560	-2.049723841	0.002506713	g__Sphingomonas	s__Sphingomonas_sanxanigenens
otu421	-2.436008864	0.002557834	g__Cytobacillus	s__Cytobacillus_kochii
otu342	-2.276415221	0.002557834	g__Staphylococcus	s__Staphylococcus_debuckii
otu5809	2.174718168	0.002557834	g__Limnohabitans	s__Limnohabitans_sp._63ED37-2
otu4889	-3.149569451	0.002788833	g__Comamonas	s__Comamonas_kerstersii
otu462	-1.958147764	0.002788833	g__Radiobacillus	s__Radiobacillus_deserti
otu4398	1.795958644	0.003001309	g__Psychroflexus	s__Psychroflexus_torquis
otu409	-3.190609037	0.003052739	g__Lysinibacillus	s__Lysinibacillus_parviboronicapiens
otu57	-2.057686731	0.003052739	g__Crassaminicella	s__Crassaminicella_sp._143-21
otu2514	-1.798198006	0.003052739	g__Brevundimonas	s__Brevundimonas_sp._LM2
otu446	-2.022206089	0.003054495	g__Peribacillus	s__Peribacillus_asahii
otu2795	1.779186344	0.003119177	g__Bacteroides	s__Bacteroides_nordii
otu254	-2.342516471	0.00319867	g__Enterococcus	s__Enterococcus_gilvus
otu419	-2.0805127	0.003244729	g__Priestia	s__Priestia_filamentosa
otu1032	1.980948843	0.003300242	g__Rathayibacter	s__Rathayibacter_sp._VKM_Ac-2804
otu4244	-1.95510497	0.003300242	g__Massilia	s__Massilia_sp._YMA4
otu422	-1.870658537	0.003545366	g__Cytobacillus	s__Cytobacillus_oceanisediminis
otu6520	2.838950921	0.003574696	g__Nostoc	s__Nostoc_piscinale
otu5496	-2.308215872	0.003574696	g__Polynucleobacter	s__Polynucleobacter_sp._MWH-UH2A
otu81	1.810846962	0.003604516	g__Dysosmobacter	s__Dysosmobacter_sp._Marseille-Q4140
otu9	-1.692114862	0.003604516	g__Clostridium	s__Clostridium_perfringens
otu1271	3.969897843	0.0036394	g__Anabaena	s__Anabaena_sp._WA102
otu1322	-2.349584816	0.003915611	g__Mycoplasma	s__Mycoplasma_sp._Mirounga_ES2806-GEN
otu5096	2.691703913	0.004044847	g__Geitlerinema	s__Geitlerinema_sp._PCC_7407
otu2695	-2.340202012	0.004410707	g__Desulfocapsa	s__Desulfocapsa_sulfexigens
otu6051	2.282957422	0.004550238	g__Ancylobacter	s__Ancylobacter_pratisalsi
otu4220	2.021782402	0.004550238	g__Polynucleobacter	s__Polynucleobacter_wuianus
otu2967	-1.603950241	0.004550238	g__Sphingobacterium	s__Sphingobacterium_mizutaii
otu461	-2.142427654	0.004615946	g__Anaerobacillus	s__Anaerobacillus_isosaccharinicus
otu2993	1.894001208	0.004615946	g__Chitinophaga	s__Chitinophaga_sp._KRA15-503
otu3734	-1.808451231	0.004615946	g__Pseudomonas	s__Pseudomonas_sp._Tri1
otu2773	1.709418805	0.004786456	g__Alistipes	s__Alistipes_onderdonkii
otu6068	2.415051511	0.004966341	g__Erythrobacter	s__Erythrobacter_neustonensis

Table S3.9. Log fold-change and adjusted *p*-values for the differential abundance of significant viruses across all groups. Provided at the family level.

NCK56-Buffer (Viruses)	logFC	adj.P.Val	family
otu3270	-5.622	0.000	f__Myoviridae
otu5584	-5.322	0.000	f__Solemoviridae
otu5571	-3.322	0.000	f__Siphoviridae

otu4624	-5.931	0.000	f__Partitiviridae
otu4619	-2.629	0.000	f__Schitoviridae
otu4589	-1.772	0.000	f__Autographiviridae
otu3274	-3.109	0.000	f__Myoviridae
otu4593	-2.394	0.000	f__Autographiviridae
otu3294	-2.211	0.000	f__Potyviridae
otu4587	1.732	0.000	f__Autographiviridae
otu4612	-4.878	0.000	f__Myoviridae
otu3289	-1.570	0.000	f__Podoviridae
otu3249	-1.215	0.001	f__Autographiviridae
otu5572	-2.000	0.002	f__Siphoviridae
otu5273	-2.585	0.002	f__Potyviridae
otu3263	-2.210	0.003	f__Siphoviridae
GAD85-Buffer (Viruses)			
otu3270	-5.791	0.000	f__Myoviridae
otu5584	-5.322	0.000	f__Solemoviridae
otu5571	-3.322	0.000	f__Siphoviridae
otu4624	-5.931	0.000	f__Partitiviridae
otu4619	-2.622	0.000	f__Schitoviridae
otu3201	-1.283	0.000	f__Autographiviridae
otu4589	-1.441	0.001	f__Autographiviridae
otu7014	3.459	0.001	f__Drexlerviridae
otu3274	-2.429	0.002	f__Myoviridae
otu3235	1.176	0.002	f__Autographiviridae
otu5572	-2.000	0.003	f__Siphoviridae
otu5273	-2.585	0.004	f__Potyviridae
GAD85-NCK565 (Viruses)			
otu3294	2.905	0.000	f__Potyviridae
otu7014	3.459	0.000	f__Drexlerviridae
otu5267	3.170	0.000	f__Myoviridae
otu5266	1.983	0.000	f__Myoviridae
otu5270	-1.984	0.000	f__Drexlerviridae
otu6669	3.459	0.000	f__Fimoviridae
otu3230	-1.540	0.000	f__Autographiviridae
otu6302	-3.459	0.001	f__Myoviridae
otu4602	1.955	0.001	f__Autographiviridae
otu3212	-1.218	0.001	f__Autographiviridae
otu3235	1.136	0.002	f__Autographiviridae
otu3201	-1.019	0.003	f__Autographiviridae

Table S3.10. Adjusted Tukey HSD adjusted *p*-values comparing the bacterial β-diversity between all three treatment groups.

Tukey HSD InvSimp	lwr	upr	p.adj
GAD85-Buffer	-8.4135	0.3418	0.0726
NCK56-Buffer	-10.2968	-1.5416	0.0086
NCK56-GAD85	-6.0572	2.2906	0.4831
Tukey HSD Richness			
GAD85-Buffer	-1435.3661	9.1372	0.0532
NCK56-Buffer	-2051.5660	-607.0627	0.0007
NCK56-GAD85	-1304.8398	72.4400	0.0825
Tukey HSD Shannon			
GAD85-Buffer	-2.4120	-0.1277	0.0289
NCK56-Buffer	-3.4519	-1.1675	0.0003
NCK56-GAD85	-2.1289	0.0492	0.0621

Table S3.11. ANOVA indicating no significant differences between the viral α-diversity among treatment groups.

Viruses	Df	Sum Sq	Mean Sq	F value	Pr(>F)
InvSimp	2	0.299695213	0.149847606	0.551784493	0.59106575
Richness	2	53.17693641	26.5884682	0.791819085	0.477227594
Shannon	2	0.029011189	0.014505595	1.816441221	0.20813514

Chapter 4 Supplementary Figures

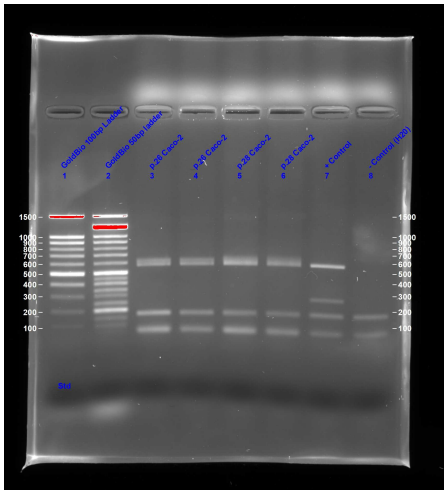

Figure S4.1. Mycoplasma species testing of Caco-2 cells after thawing from liquid nitrogen. PCR performed using the eMyco plus Mycoplasma PCR Detection Kit (LiliF Diagnostics, Seongnam, Kyonggi-do, South Korea). The 2% gel was visualized using the Bio-Rad Chemi-Doc XRS+ system. Lanes were analyzed using Image Lab software (Bio-Rad; v.6.1). There is an approximately 260 base pair (bp) band present in only the positive control included in the kit, and not in either of the cell or negative control samples. Lanes 1: 100bp DNA ladder (GoldBio, St. Louis, MO, USA); 2: 50bp DNA ladder (GoldBio); 3:

passage 26 Caco-2 cells; 4: passage 26 Caco-2 cells; 5: passage 28 Caco-2 cells; 6: passage 28 cells; 7: positive control from kit; 8: nuclease-free water.

Chapter 4 Supplementary Tables

Table S4.1. ANOVA results. Relative change in gene expression (TLR5, TNF-α, MUC2) was compared between PUFA and bacterial treatments. PUFA: polyunsaturated fatty acids.

TLR5 ANOVA table	SS	DF	MS	F (DFn, DFd)	P value
Interaction	0.1992	6	0.0332	F (6, 12) = 0.3939	P=0.8691
PUFA Factor	6.609	3	2.203	F (3, 12) = 26.13	P<0.0001
Bacteria Factor	1.384	2	0.6922	F (2, 12) = 8.212	P=0.0057
Residual	1.012	12	0.08429		
TNF-α ANOVA table	**SS**	**DF**	**MS**	**F (DFn, DFd)**	**P value**
Interaction	3.171	6	0.5285	F (6, 12) = 0.5668	P=0.7494
PUFA Factor	8.401	3	2.8	F (3, 12) = 3.003	P=0.0726
Bacteria Factor	150.7	2	75.36	F (2, 12) = 80.82	P<0.0001
Residual	11.19	12	0.9324		
MUC2 ANOVA table	**SS**	**DF**	**MS**	**F (DFn, DFd)**	**P value**
Interaction	0.5085	6	0.08475	F (6, 12) = 0.6148	P=0.7152
PUFA Factor	45	3	15	F (3, 12) = 108.8	P<0.0001
Bacteria Factor	0.4499	2	0.225	F (2, 12) = 1.632	P=0.2361
Residual	1.654	12	0.1379		

Table S4.2. Tukey's multiple comparisons test for relative change in TLR5 gene expression between bacterial and PUFA treatments.

TLR5 Tukey's multiple comparisons test	95.00% CI of diff.	Summary	Adjusted P Value
None			
NCK56 vs. GAD84	-0.5686 to 0.9805	ns	0.7627
NCK56 vs. GAD85	-0.4329 to 1.116	ns	0.4884
GAD84 vs. GAD85	-0.6389 to 0.9103	ns	0.8877
LNA			
NCK56 vs. GAD84	-0.4381 to 1.111	ns	0.4984
NCK56 vs. GAD85	-0.2353 to 1.314	ns	0.1934
GAD84 vs. GAD85	-0.5718 to 0.9773	ns	0.7689
A-LNA			
NCK56 vs. GAD84	-0.2714 to 1.278	ns	0.2334
NCK56 vs. GAD85	0.1476 to 1.697	*	0.0202
GAD84 vs. GAD85	-0.3556 to 1.194	ns	0.3511
AA			
NCK56 vs. GAD84	-0.6010 to 0.9482	ns	0.8239
NCK56 vs. GAD85	-0.2249 to 1.324	ns	0.1829

GAD84 vs. GAD85	-0.3985 to 1.151	ns	0.4242
NCK56			
None vs. LNA	0.3061 to 2.030	**	0.0079
None vs. A-LNA	-1.072 to 0.6520	ns	0.886
None vs. AA	-0.1418 to 1.582	ns	0.114
LNA vs. A-LNA	-2.240 to -0.5160	**	0.0023
LNA vs. AA	-1.310 to 0.4141	ns	0.4443
A-LNA vs. AA	0.06814 to 1.792	*	0.0333
GAD84			
None vs. LNA	0.4366 to 2.161	**	0.0037
None vs. A-LNA	-0.7747 to 0.9492	ns	0.9901
None vs. AA	-0.1742 to 1.550	ns	0.1366
LNA vs. A-LNA	-2.073 to -0.3494	**	0.0061
LNA vs. AA	-1.473 to 0.2512	ns	0.2067
A-LNA vs. AA	-0.2614 to 1.463	ns	0.2179
GAD85			
None vs. LNA	0.5037 to 2.228	**	0.0025
None vs. A-LNA	-0.4914 to 1.233	ns	0.5938
None vs. AA	0.06620 to 1.790	*	0.0336
LNA vs. A-LNA	-1.857 to -0.1331	*	0.0225
LNA vs. AA	-1.299 to 0.4245	ns	0.4634
A-LNA vs. AA	-0.3044 to 1.420	ns	0.2704

Table S4.3. Tukey's multiple comparisons test for relative change in TNF-α gene expression between bacterial and PUFA treatments.

TNF-α Tukey's multiple comparisons test	95.00% CI of diff.	Summary	Adjusted P Value
None			
NCK56 vs. GAD84	0.3464 to 5.499	*	0.0264
NCK56 vs. GAD85	-4.731 to 0.4207	ns	0.1057
GAD84 vs. GAD85	-7.654 to -2.502	***	0.0005
LNA			
NCK56 vs. GAD84	1.842 to 6.994	**	0.0017
NCK56 vs. GAD85	-4.804 to 0.3482	ns	0.0932
GAD84 vs. GAD85	-9.222 to -4.070	****	<0.0001
A-LNA			
NCK56 vs. GAD84	0.3485 to 5.501	*	0.0263
NCK56 vs. GAD85	-5.567 to -0.4151	*	0.0233
GAD84 vs. GAD85	-8.492 to -3.340	***	0.0001
AA			
NCK56 vs. GAD84	0.7522 to 5.904	*	0.0124

NCK56 vs. GAD85	-6.113 to -0.9609	**	0.0084
GAD84 vs. GAD85	-9.441 to -4.289	****	<0.0001
NCK56			
None vs. LNA	-2.999 to 2.735	ns	0.999
None vs. A-LNA	-2.574 to 3.160	ns	0.9898
None vs. AA	-1.093 to 4.641	ns	0.304
LNA vs. A-LNA	-2.442 to 3.292	ns	0.9702
LNA vs. AA	-0.9609 to 4.773	ns	0.2505
A-LNA vs. AA	-1.386 to 4.347	ns	0.4492
GAD84			
None vs. LNA	-1.503 to 4.230	ns	0.5159
None vs. A-LNA	-2.571 to 3.162	ns	0.9896
None vs. AA	-0.6871 to 5.046	ns	0.1632
LNA vs. A-LNA	-3.935 to 1.799	ns	0.6927
LNA vs. AA	-2.051 to 3.683	ns	0.832
A-LNA vs. AA	-0.9825 to 4.751	ns	0.2588
GAD85			
None vs. LNA	-3.071 to 2.662	ns	0.9965
None vs. A-LNA	-3.409 to 2.324	ns	0.9415
None vs. AA	-2.474 to 3.259	ns	0.9763
LNA vs. A-LNA	-3.205 to 2.529	ns	0.9845
LNA vs. AA	-2.270 to 3.463	ns	0.9244
A-LNA vs. AA	-1.932 to 3.802	ns	0.7696

Table S4.4. Tukey's multiple comparisons test for relative change in MUC2 gene expression between bacterial and PUFA treatments.

MUC2 Tukey's multiple comparisons test	95.00% CI of diff.	Summary	Adjusted P Value
None			
NCK56 vs. GAD84	-0.6993 to 1.282	ns	0.7193
NCK56 vs. GAD85	-0.8577 to 1.123	ns	0.9323
GAD84 vs. GAD85	-1.149 to 0.8321	ns	0.9053
LNA			
NCK56 vs. GAD84	-0.9114 to 1.070	ns	0.9753
NCK56 vs. GAD85	-1.241 to 0.7402	ns	0.7824
GAD84 vs. GAD85	-1.320 to 0.6611	ns	0.6581
A-LNA			
NCK56 vs. GAD84	-1.184 to 0.7966	ns	0.8621
NCK56 vs. GAD85	-1.195 to 0.7856	ns	0.8475
GAD84 vs. GAD85	-1.002 to 0.9795	ns	0.9995
AA			

NCK56 vs. GAD84	-0.6075 to 1.374	ns	0.5721
NCK56 vs. GAD85	-1.444 to 0.5367	ns	0.4632
GAD84 vs. GAD85	-1.827 to 0.1537	ns	0.102
NCK56			
None vs. LNA	-2.243 to -0.03867	*	0.0417
None vs. A-LNA	0.7036 to 2.908	**	0.0019
None vs. AA	1.247 to 3.452	***	0.0002
LNA vs. A-LNA	1.845 to 4.049	****	<0.0001
LNA vs. AA	2.388 to 4.593	****	<0.0001
A-LNA vs. AA	-0.5588 to 1.646	ns	0.487
GAD84			
None vs. LNA	-2.455 to -0.2508	*	0.0154
None vs. A-LNA	0.2185 to 2.423	*	0.0179
None vs. AA	1.339 to 3.543	***	0.0001
LNA vs. A-LNA	1.572 to 3.776	****	<0.0001
LNA vs. AA	2.692 to 4.897	****	<0.0001
A-LNA vs. AA	0.01809 to 2.223	*	0.046
GAD85			
None vs. LNA	-2.626 to -0.4219	**	0.0069
None vs. A-LNA	0.3659 to 2.570	**	0.0089
None vs. AA	0.6605 to 2.865	**	0.0023
LNA vs. A-LNA	1.890 to 4.095	****	<0.0001
LNA vs. AA	2.185 to 4.389	****	<0.0001
A-LNA vs. AA	-0.8077 to 1.397	ns	0.8561

Additional Research, Community Involvement, and Teaching

During my tenure as a Ram, I had the opportunity to contribute to diverse research projects. In lieu of my rotation project in the Dean-Vilander lab, I dipped my feet into the COVID-19 pool during the global pandemic at the start of 2020. Under the tutelage of Dr. Allison Vilander, I streaked (many) MRS plates, ran PCR reactions, and performed flow cytometry and Sanger sequencing to help develop and confirm recombinant *Lactobacillus acidophilus* vaccines expressing a combination of adjuvants and SARS-CoV-2 antigens. This experience provided the template for the remainder of my dissertation work.

In collaboration with Dr. Matt Hopken in the Dr. Zaid Abdo lab, I had the opportunity to contribute as second author to a rabies vaccination microbiome project in wild skunks (*Mephitis mephitis*; Hopken et al. *PLoS One.* 2023. 18(8):e0285852). I presented posters and oral presentations at several conferences, including the Front Range Microbiome Symposium, CVMBS Research Day, and ASM Microbe in Washington, D.C. I was an NIH Infectious Disease Research and Response Network Training Program T32 Fellow (T32AI162691) and received Honorable Mention for my National Science Foundation Graduate Research Fellowship Program application. Finally, I was a Graduate Student Showcase CVMBS Top Scholar Award Recipient in 2021.

As part of curating a well-rounded PhD experience, I prioritized commitment to the Colorado State University (CSU) and Fort Collins communities. I was an active member of the Center for Metabolism of Infectious Diseases (C4MInD), and I greatly appreciated all the opportunities I was given therein. As part of my contribution, I conducted informational interviews from those knowledgeable in the start-up space to inform members of C4MInD about the research to market (R2M) process. I identified, binned, and presented themes from these interviews at a meeting between C4MInD and the Vice President for Research. Thank you to Dr. Nicole Kelp for her advice for interpreting qualitative interview data. I also participated on the C4MInD Training and Guidance Committees. We developed a three-week summer research series to provide trainees additional hands-on lab experience and supported the overall progress of C4MInD. I was co-leader of the C4MInD Trainee Development club which I transitioned to a graduate-level independent study course (described below).

Outside of C4MInD, I participated on the Research Professionals Support Committee to help invest in the professional development and institutional support of non-graduate student trainees (postdoctoral fellows, research associates, and research scientists). I also enjoyed volunteering annually as a Team Captain for the Colorado Science and Engineering Fair Senior Medicine & Heath Division from 2020-2023 and always left in awe of the next generation of scientists. Finally, it was unforgettable volunteering for the Opportunities Unlimited program at Poudre High School and for the Poudre Track & Field team as a distance assistant coach. These volunteer experiences helped me invest in my local community outside of research.

With further interest in R2M, I worked as a Graduate Research Associate and Fund II Analyst for the Fort Collins-based venture capital firm Innosphere Ventures for one and a half years during my graduate training. I assessed deal flow from regional and US-based early-stage companies in B2B Saas, MedTech, and CleanTech – I enjoyed talking to and learning from motivated founders. I also provided due diligence support and visualized deal flow data. I attended the UNMET Founders conference in Denver, Colorado. Thank you to Tim, John, Mike, and the entire team for their patience, support, and instruction.

Finally, thank you to Dr. Gregg Dean for supporting my interest in teaching. I earned my Graduate Teaching Certificate through The Center for Learning and Teaching at CSU. I also had the incredible opportunity to either teach, guest-lecture, or develop course materials for several undergraduate classes (MIP301, MIP381A1, VMBS100). It was also a great learning experience to curate a novel independent study course (MIP795-005) held during the spring 2023 and 2024 semesters. This course provided a semester-long seminar series of professional development for trainees at all levels, including graduate students, postdoctoral fellows, research associates, and research scientists. The white paper written for the 2023 class, which was shared with the Graduate Head of Education for the Microbiology, Immunology, and Pathology department, is provided below along with the 2023 and 2024 semester's syllabi and rubrics. This class was conducted in collaboration with C4MInD. Thank you to Dr. John Belisle for being the sponsoring faculty member and to all the guest lecturers for giving their time and expertise.

Independent Study Course Materials

MIP795-005 SP2023 White Paper

Darby Gilfillan | darbygil@colostate.edu | PhD Candidate

Course Description: This is a graduate-level independent study course for trainees (postdoctoral fellows, graduate students, research associates) encompassing diverse talks from experts across CSU's departments. The purpose of this course is to develop or further enhance student skill set in effective communication, professional development, and dynamic thinking in science. Topics include misinformation, data transparency, the individual development plan, job opportunities post-graduating, and biotech start-ups.

Need: This class provided graduate students credit towards their GS6 for participating in professional development, in addition to giving post-doctoral fellows and research associates a semester-long professional development seminar series to add to their CV's. Professional development is important for general and scientific career progression (e.g., grant applications). Invited speakers were listed as course instructors to ensure they received credit for their talk.

Results: Cohort one of MIP795-005 was taught spring 2023 consisting of seven students and 12 invited speakers. All trainee groups were present (Figure 1), and the invited speakers represented numerous departments across CSU's campus (Figure 2). Dr John Belisle was the supervising faculty.

Fig 1. Class Composition

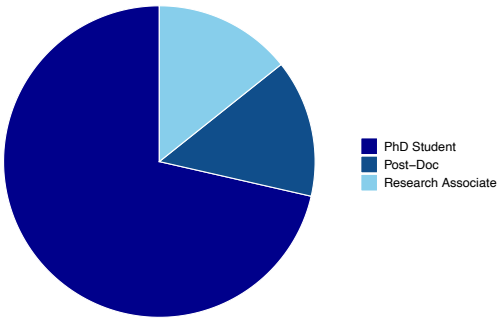

Fig 2. Speakers' Department at CSU

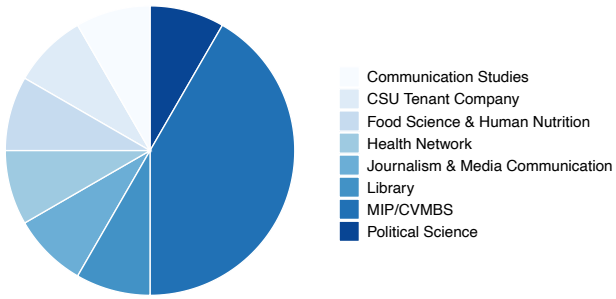

Value: This class helped introduce students to contacts across campus they may otherwise not be familiar with and provided a broad-umbrella approach to professional development (Supplementary File 1 lists the topics covered). Weekly reflection assignments were intended as an active learning approach for students to retain and apply information learned in class (Supplementary File 2).

Future Directions: MIP795-005 is currently scheduled for the SP2024 semester with transition to a new graduate teaching instructor in subsequent years if continued. To increase student registration, advertising is planned for the IDRRTP annual symposium in August, at the weekly MIP department seminar, in common classes such as grant writing and via departmental e-mails.

Supplementary File 1: MIP795-005 Syllabus
Supplementary File 2: MIP795-005 Rubrics & Assignment Examples

MIP795-005 Spring 2023 Syllabus
Instructor Information:

- *Primary Graduate Instructor:* Darby Gilfillan (darbygil@colostate.edu) | pronouns: *she/her/hers*
- *Office Hours:* By appointment virtually (Microsoft Teams) or in-person (Foothills Campus – CVID building)
- *Faculty Supervisor:* Dr. John Belisle (John.Belisle@colostate.edu)

Class Information: Monday 10-10:50AM | Micro C116 | 1 Credit (~1hr/week of work)

- Assignments will be graded, and course information provided on Canvas.

Learning Objectives: This is a graduate-level independent study course for trainees (post-doctoral fellows, graduate students, research associates) encompassing diverse talks from experts across CSU's departments. The purpose of this course is to develop or further enhance student skill set in effective communication, professional development, and dynamic thinking in science.

Grading:

Participation	26%	39 points (3 points weekly)
Weekly Reflection	40%	60 points (5 points weekly)
Final Presentation	34%	51 points
Total	**100%**	**150 points**
Extra Credit Article	NA	5 points

- A: 135-150 points
- B: 120-134 points
- C: 105-133 points
- D: 90-104 points
- F: 0-89 points

Coursework: Assignments are not designed to give you busy work, but to fulfill the independent study course requirements and provide a mechanism for you to process and retain information learned during the week. **What you put into the course will be what you get out of it!** Further details for assignments are described in the "MIP795 Coursework Rubrics-Examples" document on Canvas.

- *Participation:* Please attend weekly. Contact me if something comes up and I will be flexible. Participation requirements are just general contribution to discussion and course engagement.

- *Reflections:* 3-sentence thoughtful reflection on how you applied that week's presentation to your research and/or professional development, or ways you could apply it in the future. Submitted on Canvas by 11:59PM Sunday for a total of 12 throughout the semester. I will be the only one to read your reflections.

- *Final Presentation:* A brief 5-10min presentation on one of the following with an accompanying 3-4 slides. Slides will be submitted on Canvas by 11:59PM on the Sunday before your presentation. Provide constructive feedback for the presentation following yours, or the first presentation if you present last.
    - Option 1: Extended elevator pitch.
    - Option 2: Using a paper from your lab, choose a small section of the methods and suggest ways to improve experimental reproducibility and/or data transparency.
    - Option 3: Providing an example of poor science communication in the media environment and your suggested improvements.

- *Extra Credit Article:* Submit an interesting commentary or research article and include a 1-sentence explanation of which class topic it's related to.

Required Materials: No required materials, everything will be provided during the course.

Semester Schedule:

Semester Week – Date	Speaker	Topic	Assignment
Week 1 – January 17th	No class	Spring semester starts Tuesday, January 18th	None
Week 2 – January 23rd	Darby Gilfillan	Syllabus review & Introductions	None
Week 3 – January 30th	Dr. Dominik Stecuła	Misinformation and the Media Environment	Reflection (Due February 5th)
Week 4 – February 6th	Dr. Andrew West	Elevator Pitch and Presenting Engagingly	Reflection (Due February 12th)
Week 5 – February 13th	Darby Gilfillan	Developing an ABT Thesis	Reflection (Due February 19th)
Week 6 – February 20th	Jaime Jacobsen, M.F.A	Diverse Media in Presentations	Reflection (Due February 26th)
Week 7 – February 27th	Dr. Jeff Wilusz	Confidence in Science and Grad School	Reflection (Due March 5th)
Week 8 – March 6th	Dr. Lyndsey Linke, CEO of SiVEC	Discussing Biotech Start-ups	Reflection (Due March 19th)
Week 9 – March 13th	No Class	Spring Break!	None
Week 10 – March 20th	Dr. Mara Sedlins	Data Management & Reproducibility	Reflection (Due March 26th)
Week 11 – March 27th	CSU Snow Day	None	None
Week 12 – April 3rd	Dr. Ben Curtis Dr. Joe Westrich	Early-Career Panel & Review of Final Project	Reflection (Due April 9th)
Week 13 – April 10th	Dr. Kim Cox-York	Individual Development Plan	Reflection (Due April 16th)
Week 14 – April 17th	Janelle Patrias, MSW	CSUHN Presentation on Burnout & Living a Full Life	Reflection (Due April 23rd)
Week 15 – April 24th	Dr. Martín Carcasson	Public Communication & Decision Making	Reflection & Presentation Slides (Both Due April 30th)
Week 16 – May 1st	You!	Student Presentations	Constructive Feedback (Due May 8th)
Week 17 – May 8th	No Class	Final Exams	None

Course Policies: My expectations for students enrolled in this course center around the following:

- Show others and their ideas respect.
- Give your best that day.
- Be vulnerable and ask questions.

CSU and I take sexual harassment, academic dishonesty, diversity and inclusion, and mental health very seriously. All University guidelines will be followed. Please reach out to me if you have concerns in any of these areas as I am a resource for you. Below are some resources through CSU:

- *Sexual Harassment:* http://policylibrary.colostate.edu/policy.aspx?id=710
- *Academic Dishonesty:* https://resolutioncenter.colostate.edu/wpcontent/uploads/sites/32/2018/08/Student-Conduct-Code-v2018.pdf
- *Diversity & Inclusion:* https://housing.colostate.edu/about/diversity/#:~:text=Diversity%20%26%20Inclusion%20Statement,learning%2C%20development%2C%20and%20actions
- *Mental Health & Security:* https://health.colostate.edu/mental-emotional-health/

Colorado State University Land Acknowledgement: Colorado State University acknowledges, with respect, that the land we are on today is the traditional and ancestral homelands of the Arapaho, Cheyenne, and Ute Nations and peoples. This was also a site of trade, gathering, and healing for numerous other Native tribes. We recognize the Indigenous peoples as original stewards of this land and all the relatives within it. As these words of acknowledgment are spoken and heard, the ties Nations have to their traditional homelands are renewed and reaffirmed. CSU is founded as a land-grant institution, and we accept that our mission must encompass access to education and inclusion. And, significantly, that our founding came at a dire cost to Native Nations and peoples whose land this University was built upon. This acknowledgment is the education and inclusion we must practice in recognizing our institutional history, responsibility, and commitment.

MIP795-005 Spring 2023 Coursework Rubrics & Examples:

Reflection Rubric:

4-5 points	Thoughtful 3 lines written with a clear connection to how you applied/could apply the lecture to your research and/or professional development life.
2-3 points	1-2 lines, minimal attempt to connect the lecture topic to research or professional development.
0-1 points	Not submitted or no effort made.

Reflection Example: Dr. Kim Cox-York discussed making an effective individual development plan, which is a living document designed to establish an attainable and malleable schedule towards professional progress. My PI has encouraged me to make an IDP recently; therefore, I made an account on myIDP through the AAAS website and took the self-reflection quiz. I recognize that IDP's can be used to help evaluate future career goals which is important to do at this stage of my career.

Final Project Rubric:

Verbal presentation (12 points total)	**Visual presentation (10 points total)**	**Answered Prompt (20 points total)**	**Meaningful Connection to Class (9 points total)**
Good cadence and enthusiasm. Flow of presentation is understandable. (9-12 points)	Clear, readable graphics and words. Text and visuals balanced effectively. (8-10 points)	Fulfilled all or majority of required bullet points listed in the final project option description. (16-20 points)	Tied into lessons learned in class well. (9 points)
A bit too fast/slow, somewhat challenging to follow points. (4-8 points)	Text/graphics somewhat hard to read and/or were confusing. (5-7 points)	Missing some important bullet points from the project description. (10-15 points)	No clear relation to the seminar lecture. (6-8 points)
Fatal error in presentation flow. (0-3 points)	Visuals unreadable and lack of effort visible. (0-4 points)	Missing majority of information required. (0-9 points)	Lack of effort visible. (0-5 points)

Option 1 (Elevator Pitch) – Please address the following in your slides/presentation:

- Compelling hook.
- Appropriate but brief background information.
- Methods represented graphically.
- Results.

- Significance of research.

Option 1 Example Slide:

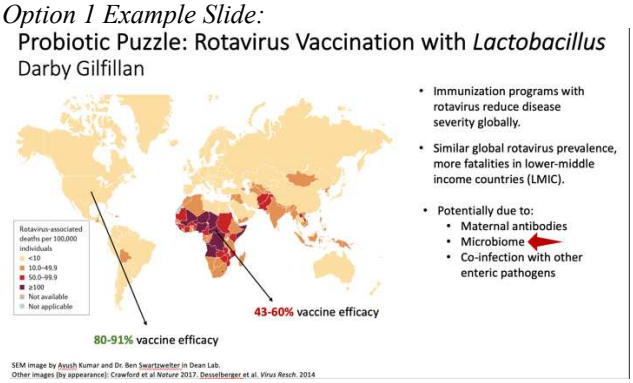

Option 2 (Reproducibility)* – Please address the following in your slides/presentation:

- Choose a short section/sub-section from the methods of a paper from your lab.
- Graphic representation of the methods you chose.
- Provide 3-4 bullet points evaluating how feasible it would be for you to replicate the experiment given just the paper's methods – explain if you would need information exclusively available to lab members.
- Suggested improvements to your paper/lab on how to improve reproducibility/transparency of experiments.

*This assignment was adapted from an RCR training developed by Dr. Candace Mathiason, Dr. Zaid Abdo, and Dr. Gregg Dean.

Option 2 Example Article & Slides:

Paper: https://doi.org/10.1371/journal.pone.0225842

Paragraph Chosen from Methods: "DNA extraction and sequencing"

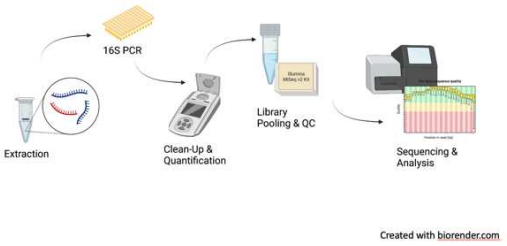

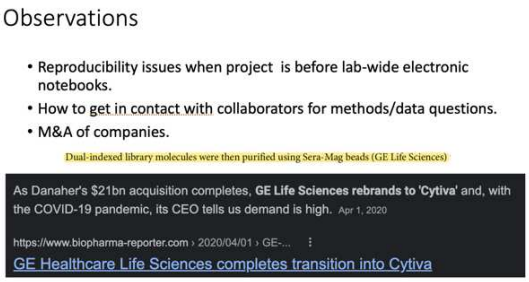

Option 3 (Popular Press) – Please address the following in your slides/presentation:

- Provide brief introduction of the research paper/popular press topic.
- Highlight 1-2 figures you deem important in capturing the primary conclusion of the research paper.
- Compare/contrast 2-3 pieces of information from the popular press piece with the original research article.
- Address what conclusions readers could make from the popular press article about the original research and 1 suggested change to improve effective, accurate science communication.

Method for finding popular press pieces: Find a paper published at least 1 year ago (permits enough time for media release about the research) → Go to the paper's metrics → Look at the mentions in news and blog.

Interesting article on popular press/science: https://www.vox.com/science-and-health/2019/6/11/18652225/hype-science-press-releases

Option 3 Example Articles & Slides:

Popular press article: https://news.umich.edu/common-plant-fiber-gel-doubled-rate-of-tumor-eradication/

Original research article: https://doi.org/10.1038/s41551-021-00749-2

Key Figures

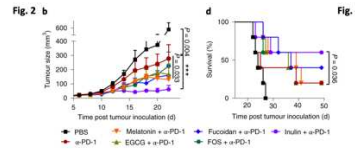

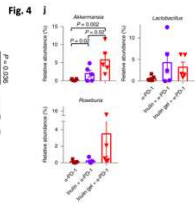

Simplified Compare/Contrast

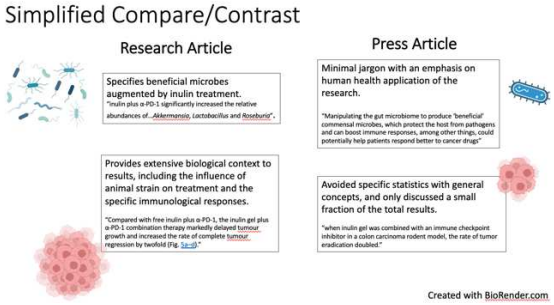

Presentation Constructive Feedback: Provide constructive feedback for the presentation following yours, or the first presentation if you present last. Presentations in alphabetical order by last name. Give a specific example of what you thought worked well and where the presentation had room for improvement, and please e-mail me if you don't want me to share your feedback with the presenter.
Suggestions on effective constructive feedback: https://online.champlain.edu/blog/giving-constructive-feedback

Extra Credit Article Example: https://doi.org/10.1016/j.cell.2022.06.030

- This paper is related to the class discussion on open data and data transparency.

MIP795-005 Spring 2024 Syllabus
Instructor Information:

- *Primary Graduate Instructor:* Darby Gilfillan (darbygil@colostate.edu) | pronouns: *she/her/hers*
- *Office Hours:* By appointment virtually (Microsoft Teams) or in-person (Foothills Campus – CVID building)
- *Faculty Supervisor:* Dr. John Belisle (John.Belisle@colostate.edu)

Class Information: Monday 10-10:50AM | Micro C116 | 1 Credit (~1hr/week of work)

- Assignments will be graded, and course information provided on Canvas.

Learning Objectives: This is a graduate-level independent study course for trainees (post-doctoral fellows, graduate students, research associates) encompassing diverse talks from experts across CSU's departments. The purpose of this course is to develop or further enhance student skill set in effective communication, professional development, and dynamic thinking in science.

Grading:

Participation	11%	14 points (1 point weekly)
Weekly Reflection	50%	65 points (5 points weekly)
Final Presentation	39%	51 points
Total	**100%**	**130 points**
Extra Credit Article	NA	2 points

- A: 117-130 points
- B: 104-116 points
- C: 91-103 points
- D: 78-90 points
- F: 0-77 points

Coursework: Assignments are not designed to give you busy work, but to fulfill the independent study course requirements and provide a mechanism for you to process and retain information learned during the week. **What you put into the course will be what you get out of it!** Further details for assignments are described in the "MIP795 Coursework Rubrics-Examples" document on Canvas.

- *Participation:* Please attend weekly. Contact me if something comes up and I will be flexible. Participation requirements are to simply encourage course engagement.

- *Weekly Assignment:* Thoughtful 3-5 sentence (or graphic/table where applicable) response to the week's prompt as provided on Canvas. Submit on Canvas by 11:59PM Sunday. I will be the only one to read your assignments. Introductions provided by the first day of class (Jan. 22) will not count towards your grade.

- *Final Presentation:* Approximately five-minute presentation on one of the following with an accompanying 2-4 slides. Slides to be submitted on Canvas by 11:59PM the Sunday before your presentation. Provide constructive feedback for the presentation following yours, or the first presentation if you present last.
    - Option 1: Elevator pitch on one aspect of your research.
    - Option 2: Compare/contrast a popular press piece with the original research paper.

- *Extra Credit Article:* Submit a link to a popular press piece or research article you found interesting.

Required Materials: No required materials, everything will be provided during the course.

Semester Schedule:

Semester Week – Date	**Speaker**	**Topic**	**Assignment**
Week 1 – January 15th	No class	Spring semester starts Tuesday, January 16th	Introductions (Due January 21st)
Week 2 – January 22nd	Darby Gilfillan	Syllabus review & Introductions	None
Week 3 – January 29th	Darby Gilfillan	ABT Thesis	Assignment (Due February 4th)
Week 4 – February 5th	Dr. Kristina Quynn	CSU Writes: Semester Projects	Assignment (Due February 11th)
Week 5 – February 12th	Chase Weldon, M.Ed., NCC, LPC	Interviewing tips & Identifying Job Opportunities	Assignment (Due February 18th)
Week 6 – February 19th	Dr. Kim Cox-York	IDP	Assignment (Due February 25th)
Week 7 – February 26th	Dr. Jeff Wilusz	Confidence in Science and Grad School	Assignment (Due March 4th)
Week 8 – March 4th	Dr. Martín Carcasson	Public Engagement	Assignment (Due March 18th)
Week 9 – March 11th	No Class	Spring Break!	None
Week 10 – March 18th	Dr. Andrew West	Effective Presenting	Assignment (Due March 24th)
Week 11 – March 25th	Kahleedah Thomas, M.L.I.S.	Publishing and Copyright	Assignment (Due March 31st)
Week 12 – April 1st	Dr. Gregg Dean	Career in Academia	Assignment (Due April 7th)
Week 13 – April 8th	Janelle Patrias, MSW	CSUHN Presentation on Burnout & Living a Full Life	Assignment (Due April 15th)
Week 14 – April 15th	Dr. Mara Sedlins	Data Reproducibility	Assignment (Due April 21st)
Week 15 – April 22nd	Brad Sparks, M.S.	Successful Financial Planning	Assignment & Presentation Slides (Both Due April 28th)
Week 16 – April 29th	You!	Student Presentations	Constructive Feedback (Due May 5th)

Week 17 – May 6th	No Class	Final Exams	None

Course Policies: My expectations for students enrolled in this course center around the following:

- Show others and their ideas respect.
- Give your best that day.
- Be vulnerable and ask questions.

CSU and I take sexual harassment, academic dishonesty, diversity and inclusion, and mental health very seriously. All University guidelines will be followed. Please reach out to me if you have concerns in any of these areas as I am a resource for you. Below are some resources through CSU:

- *Sexual Harassment:* http://policylibrary.colostate.edu/policy.aspx?id=710
- *Academic Dishonesty:* https://resolutioncenter.colostate.edu/wpcontent/uploads/sites/32/2018/08/Student-Conduct-Code-v2018.pdf
- *Diversity & Inclusion:* https://housing.colostate.edu/about/diversity/#:~:text=Diversity%20%26%20Inclusion%20Statement,learning%2C%20development%2C%20and%20actions
- *Mental Health & Security:* https://health.colostate.edu/mental-emotional-health/

Colorado State University Land Acknowledgement: Colorado State University acknowledges, with respect, that the land we are on today is the traditional and ancestral homelands of the Arapaho, Cheyenne, and Ute Nations and peoples. This was also a site of trade, gathering, and healing for numerous other Native tribes. We recognize the Indigenous peoples as original stewards of this land and all the relatives within it. As these words of acknowledgment are spoken and heard, the ties Nations have to their traditional homelands are renewed and reaffirmed. CSU is founded as a land-grant institution, and we accept that our mission must encompass access to education and inclusion. And, significantly, that our founding came at a dire cost to Native Nations and peoples whose land this University was built upon. This acknowledgment is the education and inclusion we must practice in recognizing our institutional history, responsibility, and commitment.

MIP795-005 Spring 2024 Coursework Rubrics & Examples:

Weekly Assignment Rubric:

4-5 points	Thoughtful response that fulfilled all requirements of the weekly prompt.
2-3 points	Minimal attempt to fulfill requirements of the prompt.
0-1 points	Not submitted or no effort made.

Final Project Rubric:

Verbal presentation (12 points total)	**Visual presentation (10 points total)**	**Answered Prompt (20 points total)**	**Meaningful Connection to Class (9 points total)**
Good cadence and enthusiasm. Flow of presentation is understandable. (9-12 points)	Clear, readable graphics and words. Text and visuals balanced effectively. (8-10 points)	Fulfilled all or majority of required bullet points listed in the final project option description. (16-20 points)	Tied into lessons learned in class well. (9 points)
A bit too fast/slow, somewhat challenging to follow points. (4-8 points)	Text/graphics somewhat hard to read and/or were confusing. (5-7 points)	Missing some important bullet points from the project description. (10-15 points)	No clear relation to the seminar lecture. (6-8 points)
Fatal error in presentation flow. (0-3 points)	Visuals unreadable and lack of effort visible. (0-4 points)	Missing majority of information required. (0-9 points)	Lack of effort visible. (0-5 points)

Option 1 (Elevator Pitch) – include the following:

- Compelling hook or ABT statement.

- Simplified methods represented graphically.
- Significance of one-two of your results.

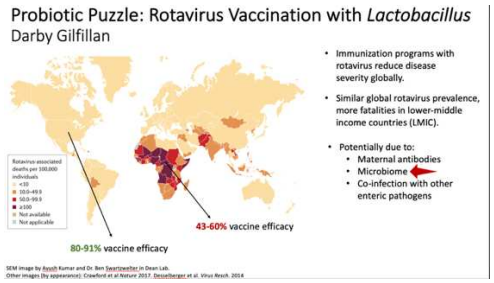

Option 2 (Science Communication) – include the following:

- Explain one-two important figures from the paper.
- Make two-three comparisons between the popular press piece and the original paper.
- Your suggestions for the popular press piece to improve its science communication.

Example:

- Popular press article: https://news.umich.edu/common-plant-fiber-gel-doubled-rate-of-tumor-eradication/
- Original research article: https://doi.org/10.1038/s41551-021-00749-2

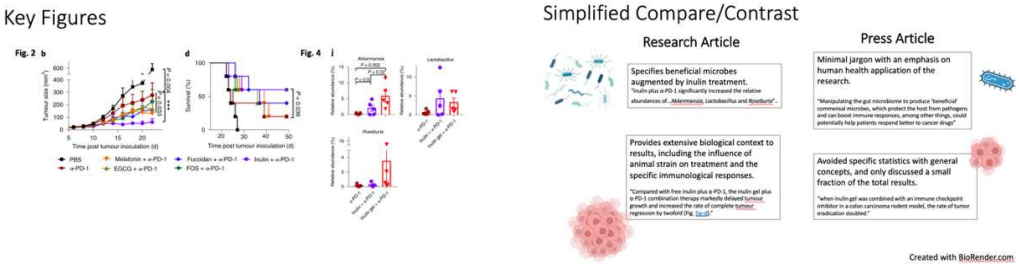

Extra Credit Article Example: https://doi.org/10.1016/j.cell.2022.06.030